

INVESTIGATION ON DETERIORATION MECHANISMS OF THE BASALTS
USED IN THE DİYARBAKIR CITY WALLS

A THESIS SUBMITTED TO
THE GRADUATE SCHOOL OF NATURAL AND APPLIED SCIENCES
OF
MIDDLE EAST TECHNICAL UNIVERSITY

BY
FELAT DURSUN

IN PARTIAL FULFILLMENT OF THE REQUIREMENTS
FOR
THE DEGREE OF DOCTOR OF PHILOSOPHY
IN
GEOLOGICAL ENGINEERING

SEPTEMBER 2017

Approval of the thesis:

**INVESTIGATION ON DETERIORATION MECHANISMS OF THE
BASALTS USED IN
THE DİYARBAKIR CITY WALLS**

submitted by **FELAT DURSUN** in partial fulfillment of the requirements for the degree of **Doctor of Philosophy in Geological Engineering Department, Middle East Technical University** by,

Prof. Dr. Gülbin Dural Ünver
Dean, Graduate School of **Natural and Applied Science**

Prof. Dr. Erdin Bozkurt
Head of Department, **Geological Engineering**

Prof. Dr. Tamer Topal
Supervisor, **Geological Engineering Dept., METU**

Examining Committee Members:

Prof. Dr. Asuman G. Türkmenoğlu
Geological Engineering Dept., METU

Prof. Dr. Tamer Topal
Geological Engineering Dept., METU

Prof. Dr. Ali Bahadır Yavuz
Geological Engineering Dept., DEU

Assoc. Prof. Dr. Ayşe Tavukçuoğlu
Architecture Dept., METU

Assoc. Prof. Dr. Mutluhan Akın
Geological Engineering Dept., NHVU

Date: 08.09.2017

I hereby declare that all information in this document has been obtained and presented in accordance with academic rules and ethical conduct. I also declare that, as required by these rules and conduct, I have fully cited and referenced all material and results that are not original to this work.

Name, Last Name : Felat DURSUN

Signature :

ABSTRACT

INVESTIGATION ON DETERIORATION MECHANISMS OF THE BASALTS USED IN THE DİYARBAKIR CITY WALLS

Dursun, Felat

Ph.D., Department of Geological Engineering

Supervisor: Prof. Dr. Tamer Topal

September 2017, 298 pages

The Diyarbakır City Walls (DCW), which were recently added to UNESCO's World Heritage List, are among the largest and most impressive monuments from ancient times. Basalts having such different textural properties as massive and vesicular were employed as the principal material in the construction of the DCW. Like many other historical structures, the DCW are suffering from stone deterioration. A large variety of weathering forms can be observed on the basalts used in different sections of the DCW.

This dissertation investigated the causes of deterioration in the basalt with which the DCW were constructed. It also ranks the causes of deterioration and indicates proper materials and construction techniques to assist conservation studies.

To accomplish this, fresh (massive and vesicular) and weathered basalts samples were collected from different sections of the study area. Throughout the study, the mineralogical, petrographic, geochemical and physico-mechanical properties of the samples were evaluated. In order to study the physical deterioration of the basalts and to determine their durability, environmental conditions were artificially simulated in

accelerated weathering tests including the wetting-drying, freezing-thawing, and salt crystallization. The durability of the basalts was assessed by determining their average-pore diameters, saturation coefficients and wet-to-dry strength ratio.

The outputs of this study indicate that detachments and material losses are the most common deterioration forms on the DCW. Mineralogical and petrographic analyses highlight that iddingsite is the common secondary mineral developed through the crystal boundaries of olivine. Microfracture studies confirmed that olivine and pyroxene are the most vulnerable minerals with the highest number of microcracks. The microfracture density of the vesicular basalts, as a result of crack propagation originated from the edge of vesicles, is relatively higher than that of the massive basalts. It is found that the salt crystallization is the most effective accelerated weathering test deteriorating the basalt samples most aggressively. It is inferred from the accelerated weathering tests that porosity, water absorption and uniaxial compressive strength (UCS) are the useful parameters for assessing the deterioration of the basalts. Of the durability methods used in this study, the durability of the basalts is best assessed by wet-to-dry strength ratio. The field and laboratory studies show that, although chemical processes trigger the deterioration mechanisms of the basalts, most of the weathering forms on the DCW are controlled by the physical processes. The massive samples yielded better results in the parameters of porosity, water absorption, UCS and wet-to-dry strength ratio. Field observation and laboratory studies indicate that both massive and vesicular basalts are durable; however, the massive basalts are more durable than the vesicular ones.

Keywords: Basalt, city walls, deterioration, durability, physico-mechanical properties, Diyarbakır

ÖZ

DİYARBAKIR KENT SURLARINDA KULLANILAN BAZALTLARIN BOZUNMA MEKANİZMALARININ İNCELENMESİ

Dursun, Felat

Doktora, Jeoloji Mühendisliği Bölümü

Danışman: Prof. Dr. Tamer Topal

Eylül 2017, 298 sayfa

Yakın zamanda UNESCO tarafından Dünya Kültür Mirası Listesi'ne eklenen Diyarbakır Kent Surları, antik dönemlerden günümüze taşınan en etkileyici ve görkemli yapıtlar arasında yer almaktadır. Surların inşasında temel yapı malzemesi olarak masif ve veziküler (gözenekli) dokudaki bazaltlar kullanılmıştır. Diğer birçok tarihi yapıda gözlendiği gibi, Diyarbakır Kent Surları'nda da taş bozunmasından kaynaklı sorunlar ortaya çıkmıştır. Bozunmalar, bazalt malzemesinin kullanıldığı mimari elementlerde ve farklı formlarda kendini göstermektedir.

Bu tez çalışmasında, surlarda kullanılan bazaltlarda meydana gelen bozunmaların tanımlanması, sınıflandırılması ve nedenlerinin belirlenmesi amaçlanmıştır. Çalışma kapsamında elde edilen bulguların, koruma amaçlı çalışmalara, gerek malzeme seçimi, gerekse malzemenin yapıya uygulanması noktasında katkı sağlaması hedeflenmiştir.

Bu amaçla, çalışma sahasının farklı noktalarından taze (masif ve veziküler) ve bozunmuş bazalt numuneleri toplanmış ve çeşitli deneylere tabi tutulmuştur. Çalışma kapsamında numunelerin mineralojik, petrografik, jeokimyasal ve fiziko-mekanik özellikleri incelenmiştir. Masif ve veziküler dokudaki bazaltların uzun dönemdeki fiziksel davranışlarını ve dayanımlarını incelemek amacıyla, malzemenin maruz kaldığı çevresel koşullar laboratuvar ortamında, ıslanma-kuruma, donma-çözülme ve

tuz kristallenmesi deneyleri aracılığıyla incelenmiştir. Numunelerin dayanımı, ortalama gözenek çapı, doygunluk katsayısı ve ıslak-kuru dayanım oranı gibi parametreler üzerinden değerlendirilmiştir.

Tez kapsamında elde edilen bulgular dikkate alındığında, ayrılma ve malzeme kaybı türündeki bozunmaların Diyarbakır Kent Surları'nda çok yaygın olduğu tespit edilmiştir. Yapılan mineralojik ve petrografik analizler neticesinde iddingsitin, olivin ve piroksen kristalleri boyunca gelişen en yaygın ikincil mineral olduğu belirlenmiştir. Mikroçatlak çalışmalarından elde edilen verilere göre, yüksek orandaki mikroçatlak yoğunluğundan dolayı, olivin ve piroksenin en zayıf mineraller olduğu gözlenmiştir. Mikroçatlak yoğunluğu göz önüne alındığında, veziküler numunelerin, gözenek yapılarının da etkisiyle, masif numunelere kıyasla daha fazla mikroçatlak barındırdığı görülmüştür. Yapay bozunma deneyleri içerisinde, bazalt numuneleri en fazla tuz kristallenmesi deneyinden etkilenmiştir. Yapay bozunma deneyleri sonrasında yapılan indeks deneylerin sonuçları incelendiğinde, etkili gözeneklilik, su emme ve tek eksenli basma dayanımı deneylerinin, bazaltın bozunma mekanizması üzerine yürütülecek çalışmalarda kullanışlı olabileceği tespit edilmiştir. Numunelerin dayanıklılık değerlendirmesi kapsamında yürütülen çalışmalar neticesinde, ıslak-kuru dayanım oranı parametresinin en kullanışlı sonuçları verdiği belirlenmiştir. Tez kapsamında yürütülen laboratuvar çalışmaları neticesinde, bazaltların bozunma mekanizmasında her ne kadar kimyasal süreçlerin etkisi olsa da, bozunmayı genellikle fiziksel süreçlerin kontrol ettiği tespit edilmiştir. Etkili gözeneklilik, su emme, tek eksenli basma dayanımı ve ıslak-kuru dayanım oranı gibi parametreler incelendiğinde, masif numunelerin daha iyi sonuçlar verdiği gözlenmiştir. Bu sonuçlar arazi gözlemleriyle birleştirilince, masif ve veziküler numunelerin duraylı olduğu, buna karşın masif numunelerin veziküllere kıyasla daha yüksek dayanıma sahip olduğu tespit edilmiştir.

Anahtar Kelimeler: Bazalt, bozunma, dayanıklılık, fiziko-mekanik özellikler, kent surları, Diyarbakır

*for those who have gone before me,
especially to my mom Hasine, sister Sâide and aunt Miyeser...*

ACKNOWLEDGEMENTS

This dissertation would not have been possible without the priceless contribution from a number of people. I would like to take this opportunity to give my deepest thanks to all these people.

The author would like to express his cordial gratitude to Prof. Dr. Tamer TOPAL, for his kind and restless supervision of the dissertation from the very beginning to the end.

The author is thankful to Prof. Dr. Asuman G. TÜRKMENOĞLU, and Assoc. Prof. Dr. Ayşe TAVUKÇUOĞLU for their valuable contribution to improve the study, through the Thesis Advisory Committee meetings. A special thank goes to Assist. Prof. Dr. Fatma TOKSOY KÖKSAL for her generous advice and assistance throughout the mineralogical and petrographic analyses.

My warm thanks are due to research assistants, Dr. Gökmen ÖZTÜRKMEN, Dr. Yunus GÖNDEN, Dr. Ruşen IŞIK, Dr. Pınar YILDIZ, Dr. Pınar Ç. ÖZTÜRK and Berfin EREN for their constant encouragement from even the sampling stage to the writing phase of this dissertation.

I would like to thank all my friends who helped keep me sane during the process including, Nejdet BULUŞ, Sabri AZİZOĞLU, Dr. Burcu Ertaş, Dr. Engin BOZKURT, Duygu TATAR and Nejla BAYBAŞ.

The author offers his sincere thanks to his colleague at Department of Geological Engineering of METU, especially to Yavuz KAYA, without his guidance and answers to my numerous (and some insane) questions, this dissertation would have never been possible, also my huge gratitude goes out to Mustafa KAPLAN, Alican AKTAĞ,

Faruk BERBER, Levent TOSUN and Çidem ARGUHAN for their patience and kindness in answering my never-ending questions during the lunch breaks. Moreover, to Dr. Hakan TANYAŞ from the University of Twente, the Netherlands.

The financial support from the METU Research Fund Project (Project No: BAP-03-09-2014-02) is gratefully acknowledged. I wish to express my special appreciation to the staff members of the Getty Conservation Institute (GCI) for letting me use their laboratories during my stay in Los Angeles (USA).

I would finally like to express my deepest appreciation and gratitude to my family for their love and support through the study.

TABLE OF CONTENTS

ABSTRACT	v
ÖZ.....	vii
ACKNOWLEDGEMENTS	x
TABLE OF CONTENTS	xii
LIST OF FIGURES.....	xvi
LIST OF TABLES	xxii
LIST OF ABBREVIATIONS	xxiv
CHAPTERS	
1. INTRODUCTION.....	1
1.1 Problem Statement.....	1
1.2 The Aim and Scope of the Study.....	3
1.3 The Study Area.....	4
1.4 Historical Background of Diyarbakır	7
1.5 The Historical and Interventional Background of the Diyarbakır City Walls .	10
1.6 Construction Techniques and Materials	16
1.7 Architectural Features of the Diyarbakır City Walls	27
1.8 Method of the Study.....	37
1.8.1 Sampling.....	39
1.9 Literature Review	44
1.9.1 Previous Works on the Geology of the Site	45
1.9.2 Previous Works on the Weathering Processes of Basalts	46
1.9.3 Previous Works on Basalt Deterioration.....	48

1.9.4 Previous Works on the Engineering Geological Properties of Basalts	53
1.10 Layout of the Dissertation	57
2. GEOLOGY	59
2.1 Regional Geology.....	59
2.2 Geology of the Site Vicinity	62
2.2.1 Yeniköy formation (Tply).....	64
2.2.2 Gölpınar formation (Qplg).....	66
2.2.3 Karacadağ volcanics (K).....	68
2.2.4 Alluvial deposits (Qal)	71
3. PETROGRAPHIC AND GEOCHEMICAL PROPERTIES OF THE BASALTS	75
3.1 Mineralogical and Petrographic Properties of the Basalts	75
3.1.1 Optical Microscopy	76
3.1.2 Methylene Blue Adsorption Test	78
3.1.3 Clay Fraction Determination.....	79
3.1.4 X-Ray Diffraction	80
3.1.5 Scanning Electron Microscopy	82
3.2 Chemical Properties of the Basalts	85
4. PHYSICO-MECHANICAL PROPERTIES OF THE BASALTS	89
4.1 Effective Porosity and Unit Weight	90
4.2 Water Absorption under Atmospheric Pressure.....	91
4.3 Water Absorption under Vacuum Pressure.....	91
4.4 Uniaxial Compressive Strength.....	92
4.5 Indirect (Brazilian) Tensile Strength.....	93
4.6 Sonic Velocity	94
4.7 Pore-size Distribution.....	96

5. THE DETERIORATION OF THE BASALTS	99
5.1 Weathering Forms and State of Deterioration.....	99
5.1.1 Cracks and Deformations	101
5.1.2 Detachments	103
5.1.3 Material Losses	110
5.1.4 Discolorations and Deposits.....	115
5.1.5 Biological Colonization.....	122
5.2 Mapping Visual Decay Forms.....	125
5.3 Accelerated Weathering Tests.....	134
5.3.1 Wetting and Drying Test	135
5.3.2 Freezing and Thawing Test	142
5.3.3 Salt Crystallization Test	149
5.3.4 Correlation of the Physico-mechanical Parameters after the Durability Tests	159
5.4 Petrographic and Chemical Properties of the Weathered Basalts	164
5.4.1 Mineralogical and Petrographic Properties of the Weathered Basalts	164
5.4.2 The Chemical Properties of the Weathered Basalts	169
5.5 Microfracture Properties of the Fresh and Weathered Basalts.....	172
5.5.1 Microfracture Counting.....	183
6. DURABILITY ASSESSMENT	193
6.1 Average Pore Diameter	193
6.2 Saturation Coefficient	195
6.3 Wet-to-dry Strength Ratio	196
7. DISCUSSION	197
7.1 Petrographic and Geochemical Properties of Fresh and Weathered Basalts .	197

7.2 Index Properties of the Basalts.....	200
7.3 Classification of the Decay Forms	203
7.4 Accelerated Weathering Tests.....	209
7.5 Microfracture Properties of the Basalts.....	211
7.6 Assessment of Durability	212
8. CONCLUSIONS AND RECOMMENDATIONS	215
REFERENCES.....	221
APPENDIX	
A. LABORATORY TEST RESULTS OF THE FRESH BASALTS.....	243

LIST OF FIGURES

FIGURES

Figure 1.1 The location map of Diyarbakır	5
Figure 1.2 Map of the Study Area (captured from Google Earth)	5
Figure 1.3 A collection of the inscriptions and reliefs on the DCW	13
Figure 1.4 A Latin inscription on the Dağ Gate	14
Figure 1.5 Ruins of demolished walls	15
Figure 1.6 Dismantled and breached wall sections	16
Figure 1.7 Opus quadratum and opus incertum	19
Figure 1.8 Opus quadratum and opus caementicium	20
Figure 1.9 Opus listatum	21
Figure 1.10 Cylindrical basalt applications	21
Figure 1.11 A Tower façade and wall section	22
Figure 1.12 A collection of the materials used to build the DCW	23
Figure 1.13 The estimated extraction of basalt	24
Figure 1.14 Traces of steepening extraction by the Keçi Tower	25
Figure 1.15 Brick applications on different sections of the DCW	26
Figure 1.16 Limestone applications in the form of inscription and relief	26
Figure 1.17 Limestone and metal applications	27
Figure 1.18 An aerial view of the DCW and the Hevsel Gardens	28
Figure 1.19 East section of the DCW from the Hevsel Gardens	29
Figure 1.20 Plan view of the DCW	30
Figure 1.21 Aqueduct and Pre-wall	31
Figure 1.22 The demolished part of the DCW associated to the earthquake	33
Figure 1.23 A collection of towers on the DCW	35
Figure 1.24 Buttresses at the south section of the DCW	35

Figure 1.25 Four principal gates on the DCW	36
Figure 1.26 Flowchart of the study	39
Figure 1.27 Location map for the fresh samples.....	42
Figure 1.28 The massive and vesicular basalt samples used in experimental studies	43
Figure 1.29 Location map for the weathered samples	44
Figure 2.1 Generalized columnar section of the study area.....	60
Figure 2.2 Geological map of the study area	63
Figure 2.3 A view of Yeniköy formation over the Kırklardağı Mt.....	64
Figure 2.4 Contact relation of Yeniköy formation and Gölpınar formation at the north of the study area	65
Figure 2.5 Contact relation of Yeniköy formation and Karacadağ volcanics near the Citadel	66
Figure 2.6 A view of Gölpınar formation at the north of the study area.....	67
Figure 2.7 Lenticular sand body within in the Gölpınar formation	67
Figure 2.8 A general view of Karacadağ volcanics at the north of the study area....	69
Figure 2.9 A cliff of columnar basalt at the northeastern section of the DCW.....	71
Figure 2.10 A view of the old alluvium from the Kırklardağı Mt.	72
Figure 2.11 A general view of the recent alluvium depositions at the Tigris River ..	73
Figure 3.1 Photomicrograph illustrating overall mineralogical and textural features of fresh massive and vesicular basalt samples	77
Figure 3.2 Hand specimen and photomicrograph view of a vesicular sample displaying calcite replacement.....	77
Figure 3.3 Opaque minerals in the massive sample.....	78
Figure 3.4 X-ray diffraction patterns of the massive and vesicular basalt samples ...	81
Figure 3.5 SEM micrographs and EDX analyses of a fresh massive basalt	83
Figure 3.6 SEM micrographs and EDX analyses of a fresh vesicular basalt.....	84
Figure 3.7 Total Alkali-Silica (TAS) diagram of Le Bas et al. (1986) for the studied basalts.....	88
Figure 4.1 Histogram depicting the pore-size distribution of a massive basalt sample	98

Figure 4.2 Histogram depicting the pore-size distribution of a vesicular basalt sample.....	98
Figure 5.1 Vertical cracks and fractures on sections of the DCW	102
Figure 5.2 Horizontal cracks and fractures on sections of the DCW	102
Figure 5.3 Crack networks on basalt blocks of the DCW	103
Figure 5.4 Blistering patterns at the lower parts of the walls.....	104
Figure 5.5 Delamination of basalt along the flow directions	105
Figure 5.6 Crumbling and spheroidal weathering forms on the DCW	106
Figure 5.7 Spheroidal weathering forms on basalt blocks	106
Figure 5.8 Splintering on the DCW	107
Figure 5.9 Chipping on sections of the DCW	108
Figure 5.10 Flaking on sections of the DCW.....	108
Figure 5.11 Scaling on sections of the DCW	109
Figure 5.12 Alveolization on sections of the DCW	111
Figure 5.13 Erosion in the loss of components form on the DCW	111
Figure 5.14 Erosion of the iconic reliefs on the Selçuklu Tower.....	112
Figure 5.15 Mechanical damages on sections of the DCW	113
Figure 5.16 Dismantled stone blocks and a breach in the DCW.....	114
Figure 5.17 Demolished segments of the north section of the DCW.....	114
Figure 5.18 The missing parts of reliefs carved on the Ulu Beden Tower	115
Figure 5.19 Crust formations on the DCW	116
Figure 5.20 Deposits on the sections of the DCW	117
Figure 5.21 Bleaching and staining on sections of the DCW	118
Figure 5.22 Discoloration of the stone surface due to human-induced activities ...	119
Figure 5.23 Moist areas on sections of the DCW	120
Figure 5.24 Efflorescence patterns on the DCW.....	121
Figure 5.25 Paintings on the DCW	122
Figure 5.26 Plants growing on sections of the DCW	123
Figure 5.27 Lichens on sections of the DCW	124
Figure 5.28 Paint and illegal housing on the east section of the DCW.....	125
Figure 5.29 The material map of the inner section of the Dağ Gate	129

Figure 5.30 The map of visual decay forms on the inner section of the Dağ Gate..	130
Figure 5.31 The material map of the tower 52.....	132
Figure 5.32 The map of visual decay forms on the tower 52.....	133
Figure 5.33 Variations in the physical and mechanical properties of the massive and vesicular basalts after wetting-drying cycles	140
Figure 5.34 Variations in the physico-mechanical properties of the massive and the vesicular basalt samples at the end of the wetting-drying cycles.....	141
Figure 5.35 Variations in the physical and mechanical properties of the massive and vesicular basalts after the freezing-thawing cycles	147
Figure 5.36 Variations in the physico-mechanical properties of the massive and vesicular basalt samples at the end of the freezing-thawing cycles	148
Figure 5.37 Variations in the physical and mechanical properties of the massive and vesicular basalts after the salt crystallization cycles	155
Figure 5.38 Variations in the physico-mechanical properties of the massive and vesicular basalt samples at the end of the salt crystallization cycles	156
Figure 5.39 Patterns of deterioration on the massive basalt samples after 30 th cycle of the salt crystallization test	157
Figure 5.40 Disintegration of some of the vesicular basalt samples after 16 th cycle of the salt crystallization test	158
Figure 5.41 Effect of durability tests on the physico-mechanical properties of the massive basalt samples.....	162
Figure 5.42 Effect of durability tests on the physico-mechanical properties of the vesicular basalt samples	163
Figure 5.43 Photomicrographs of the weathered basalt samples	165
Figure 5.44 X-ray diffraction patterns of the weathered basalt samples.....	168
Figure 5.45 Sampling paths through a spheroidally weathered basalt block.....	170
Figure 5.46 Back-scattered images displaying the microfracture morphology of the fresh massive and fresh vesicular basalt samples	173
Figure 5.47 Back-scattered images displaying the microfracture morphology of the massive and vesicular basalt samples after the wetting-drying cycles	174

Figure 5.48 Back-scattered image showing change in crack direction and partial loss of pyroxene crystal after the wetting-drying test	175
Figure 5.49 Back-scattered image displaying microfracture propagation that initiated from a vesicle after the wetting-drying test.....	176
Figure 5.50 Back-scattered images displaying the microfracture morphology of the massive and vesicular basalt samples after the freezing-thawing cycles	177
Figure 5.51 An image displaying flaking pattern on a massive sample after the freezing-thawing test and a back-scattered view of the flaked sample displaying micropore growth along the flow layer	178
Figure 5.52 Back-scattered images indicating remnants of the olivine and the pyroxene crystals after the freezing thawing cycles	178
Figure 5.53 Back-scattered images displaying the microfracture morphology of the massive and vesicular basalt samples after the salt crystallization cycles	179
Figure 5.54 Photomicrograph and back-scattered views of an olivine mineral displaying weathering microcracks at the end of the salt crystallization test	180
Figure 5.55 Back-scattered images showing spongy microfabrics on the pore-edge of a vesicular sample after the salt crystallization test	180
Figure 5.56 Back-scattered images showing vesicle-associated crack propagation in a naturally weathered basalt sample.....	181
Figure 5.57 A back-scattered image of a naturally weathered basalt sample showing microfracture sets	182
Figure 5.58 A back-scattered image displaying microfracture propagation along the rim of a naturally weathered olivine phenocryst	182
Figure 5.59 Back-scattered image of a naturally weathered basalt sample indicating a microfracture-associated detachment	183
Figure 5.60 Gridded back-scattered images used in microfracture counting of massive basalts samples	185
Figure 5.61 Gridded back-scattered images used in microfracture counting of vesicular basalts samples	186
Figure 5.62 Gridded back-scattered image used in microfracture counting of a naturally weathered basalt sample.....	187

Figure 5.63 Histograms depicting the microfracture density of the examined samples.....	189
Figure 5.64 Thematic map of the microfracture density of the massive basalt samples	190
Figure 5.65 Thematic map of the microfracture density of the vesicular basalt samples	191
Figure 5.66 Thematic map of the microfracture density of a naturally weathered basalt sample	192
Figure 6.1 Durability assessment of the massive and vesicular basalt samples based on the wet-to-dry strength ratio proposed by Winkler (1986)	196
Figure 7.1 Different surface finishes on the DCW	205
Figure 7.2 A surface finish that caused material loss and biological colonization on the surface of the basalt blocks	206

LIST OF TABLES

TABLES

Table 1.1 Long-term climate data for Diyarbakır	6
Table 1.2 Historical timeline of Diyarbakır	9
Table 1.3 The main gates of the DCW	37
Table 1.4 Distribution and number of the fresh samples	41
Table 1.5 Physico-mechanical properties of basalts based on the reviewed studies..	56
Table 3.1 Clay fraction of the massive and vesicular basalt samples	79
Table 3.2 Weight percentages of common oxides of the massive and vesicular basalt samples	86
Table 3.3 Trace element contents of the massive and vesicular basalt samples (in ppm)	87
Table 5.1 Averages and normalized averages of the index properties of the massive basalts after the wetting-drying cycles	138
Table 5.2 Averages and normalized averages of the index properties of the vesicular basalts after the wetting-drying cycles	139
Table 5.3 Averages and normalized averages of the index properties of the massive basalts after the freezing-thawing cycles	145
Table 5.4 Averages and normalized averages of the index properties of the vesicular basalts after the freezing-thawing cycles	146
Table 5.5 Averages and normalized averages of the index properties of the massive basalts after the salt crystallization cycles.....	153
Table 5.6 Averages and normalized averages of the index properties of the vesicular basalts after the salt crystallization cycles.....	154
Table 5.7 Clay fractions of the weathered basalt samples	167
Table 5.8 Weight percentages of common oxides of the weathered basalt samples	170
Table 5.9 Trace element contents of the weathered samples (in ppm)	171

Table 5.10 Microfracture index of the massive, vesicular and naturally weathered basalt samples.....	188
Table 5.11 Microfracture density of the massive, vesicular and naturally weathered basalt samples.....	188
Table 6.1 Descriptive table for pore-size distribution of the massive and vesicular basalts after the MIP test.....	194
Table 7.1 Relative rating of the deterioration forms developed on the massive and vesicular basalts of the DCW.....	207
Table 7.2 Material properties of the massive and vesicular basalts based on the laboratory studies.....	214

LIST OF ABBREVIATIONS

µm	Micrometer
AD	Anno Domini / Air-Dried
ANN	Annual
ASTM	American Society for Testing and Materials
BC	Before Christ
c. , ca.	Circa
CEC	Cation Exchange Capacity
DCW	Diyarbakır City Walls
e.g.	Exempli gratia
EDS/EDX	Energy Dispersive X-ray Spectroscopy
EG	Ethylene Glycolated
FT	Freezing-Thawing
ICOMOS	International Council on Monuments and Sites
I _f	Microfracture Index
ISRM	The International Society for Rock Mechanics
i.e.	Id est
kN	Kilonewton
Ma.	Mega Annus, Million Years

MBA	Methylene Blue Adsorption
meq	Milliequivalents
MIP	Mercury Intrusion Porosimetry
MPa	Megapascal
Mt.	Mountain
ppl	Plane Polarised Light
psi	Pounds per Square Inch
RILEM	Réunion Internationale des Laboratoires et Experts des Matériaux, systèmes de construction et Ouvrages
SC	Salt Crystallization
SEM	Scanning Electron Microscopy
UCS	Uniaxial Compressive Strength
V_v	Volume of Void
WD	Wetting-Drying
wt	Weight
xpl	Cross Polarised Light
XRD	X-Ray Diffraction
ρ_{mf}	Microfracture Density
σ_t	Tensile Strength

CHAPTER 1

INTRODUCTION

1.1 Problem Statement

Adobe, wood, and stone are the oldest building materials in human history. While adobe and wood have been mainly used for domestic and ordinary dwelling structures, stone has been used for such impressive structures as temples, tombs, cathedrals, mosques, churches and city walls.

Stone is known as the oldest material employed for constructions. Stone has been valued as a building material especially, for its long-term performance. Today, for instance, numerous historical structures spread across the world are still standing thanks to the durability and performance of stone. Considering the monuments erected by different civilizations in different regions, one can go so far as to claim that “the history of civilization has been captured in stone” (Chacon, 1999).

Contrary to common sense, stone has a limited service life. Like other construction materials, stone is also affected by weathering in the course of time. All naturally occurring materials on the earth's surface are subject to destructive weathering processes, whether in their natural settings or in construction. Weathering is a slow, continuous and destructive process that changes the characteristic properties of stone.

The weathering of stone may result in the loss of integrity, aesthetic value and structural stability of the historical structures. Even a small amount of surface weathering may deteriorate priceless pieces of monuments (Bristow, 1990; Vincente et al., 1993; Siegesmund et al., 2002).

From a geological point of view, the nature of stone deterioration is associated with intrinsic factors (mineralogical, chemical or structural characteristic) and extrinsic ones (environmental conditions, weathering agents or interventions). Moreover, rates of deterioration can change in response to changes in environmental conditions or interventions. For instance, extensive exposure of the stone to weathering episodes (e.g., freezing and thawing; wetting and drying) or inappropriate repair techniques can accelerate the process of stone deterioration (Warke et al., 2006).

Stone monuments are the most visible and essential structures of our cultural heritage; however, many of the historical structures around the world are now suffering from above-mentioned weathering and associated deterioration (Pope et al., 2002; Fitzner, 2004). Although numerous studies and projects have been conducted to preserve cultural heritages, the long-term activity of stone material and its deterioration mechanisms are not yet well understood (Winkler, 1997; Bell, 2007). In order to preserve our cultural heritages, it is essential to investigate the damaging deterioration mechanisms of stone and to propose remedies that can protect stone structures.

The Diyarbakır City Walls (DCW), which were recently added to UNESCO's World Heritage List, are among the most gigantic surviving structures from ancient times. The history of the DCW stretches back more than four thousand years, therefore making the extant City Walls a combination and reflection of influences of the various civilizations that settled in the region. The reflections of these civilizations can be identified in the City Walls' architectural elements, construction techniques and material applications.

Basalt is the main construction material of the City Walls. It has been employed in almost all of their architectural elements. Like many other historical structures, the DCW are also suffering from stone deterioration.

A large variety of types of deterioration, including cracks, detachments, material losses, discolorations and biological colonization can be observed in different sections of the City Walls. This deterioration of the City Walls damages their integrity, aesthetic value and structural stability.

The City Walls have been the subject of many different studies, including architecture, historic, archaeologic, art history and to some extent, engineering. Nevertheless, the long-term performance, characterization and deterioration mechanism of the materials employed in the City Walls have yet to be studied. Additionally, there are numerous studies available in the literature detailing the material properties and deterioration mechanisms of different types of the building stones, including limestone, marble or tuff; however, as a review of previous studies (see Section 1.9) also revealed a very limited number of studies have focused on basalt as a building material. The lack of such studies has adversely affected the interventions, particularly in selection and application of the materials employed on the City Walls. Repair materials, for instance, if not chosen and applied properly can also become causes of deterioration (Siegesmund et al., 2002). To put it differently, especially repairs applied without identifying the characterization and long-term performance of the materials in their natural conditions, may accelerate the deterioration process and cause new and irreversible damages to the structure. This undesirable situation can also be observed on different architectural elements of the DCW. Thus, some structural and deterioration problems have emerged as a consequence of improper conservation interventions.

1.2 The Aim and Scope of the Study

The major aim of this dissertation is to investigate some of the causes of deterioration in the basalt with which the DCW were constructed. This study also ranks the causes of deterioration on the basis of their importance and suggests proper materials and construction techniques to assist conservation studies. It aims to help save the DCW, as a cultural heritage, from further deterioration and preserve them for the future

generations. In order to understand the effects of the intrinsic and extrinsic factors that may be responsible for the deterioration of the material of the DCW, the present study aims to investigate mineralogical, petrographic and engineering geological studies of the basalt.

The results will enable us to evaluate the factors in deterioration, weathering agents and the character of the material. They will also help us to better understand the behavior of the material under different cyclic environmental factors.

Although basalt is used as the principal construction material, brick, mortar, limestone and metal are also used to some extent in the DCW. Considering the scope, since basalt is used in almost every architectural element of the DCW, this dissertation will focus mainly on the basalt and will not examine the deterioration mechanisms of the brick, mortar or limestone employed in the construction of the DCW.

1.3 The Study Area

This section will briefly describe the location and climate of the study area. The DCW are the study area, and they are located in the province of Diyarbakır in southeastern Turkey (Figure 1.1). The province is surrounded by Elazığ (150 kilometers) and Bingöl (144 kilometers) in the north, Batman (100 kilometers) and Muş (270 kilometers) in the east, Mardin (95 kilometers) in the south, and by Şanlıurfa (180 kilometers), Adıyaman (205 kilometers) and Malatya (230 kilometers) in the west.

The study area is seated above the west bank of the Tigris (Dicle) River. The DCW's elevation from the river is *ca.* 70 meters (Figure 1.2). The elevation of the study area ranges from 650 meters to 666 meters above the sea level. With an elevation of 666 meters, The Great Mosque inside the northwest section of the City Walls, is the most elevated point of the study area. The study area extends from 40° 13' 39.46" E longitudes and 37° 54' 38.60" N latitudes, and occupies an area of some 1.57 square kilometers (Dalkılıç and Nabikoğlu, 2012; Toprak, 2012).



Figure 1.1 The location map of Diyarbakır



Figure 1.2 Areal view of the Study Area (captured from Google Earth)

The severe continental climate features of Southeast Anatolia dominate Diyarbakır. Summers are dry and very hot, while winters are cold and wet with some frosty nights. The long-term meteorological data for 90 years (1926-2016) are shown in Table 1.1 (MGM, 2017). The annual mean temperature of the province is 15.8°C. The hottest months are July and August. The average high temperatures recorded for July and August are 38.4°C and 38.2°C, respectively. The highest temperature recorded was in

July, 1937 at 46.2°C. The coldest months are January and February, and the average low temperatures recorded for January and February are -2.4°C and -1.0°C, respectively. Based on the collected meteorological data in the last 90 years, the lowest temperature recorded was in January, 1933 at -24.2°C.

Most of Diyarbakır's precipitation occurs in winter in the form of rain, snow and hail, though rarely. The maximum snow depth was measured in January, 1973 at 65 centimeters. Diyarbakır has an average of 485.7 millimeters of precipitation per year, or 40.4 millimeters per month. On average, January has the most rainy days, whereas August has the fewest. The mean number of rainy days for January and August are 12.5 and 0.3, respectively (MGM, 2017). The relative humidity is much higher in winter than in summer. The highest mean relative humidity was recorded in January at 76% and the lowest in August at 25%. The annual mean relative humidity of Diyarbakır is 53%.

Table 1.1 Long-term climate data for Diyarbakır (1926-2016) (MGM, 2017)

DIYARBAKIR	JAN.	FEB.	MAR.	APR.	MAY	JUN.	JUL.	AUG.	SEP.	OCT.	NOV.	DEC.	ANN.
Monthly Mean Temp. (°C)	1.6	3.6	8.3	13.8	19.2	26.2	31.1	30.4	24.9	17.2	9.5	3.9	15.8
Average High Temperature (°C)	6.6	9.0	14.4	20.4	26.6	33.5	38.4	38.2	33.3	25.3	16.3	9.1	22.6
Average Low Temp. (°C)	-2.4	-1.0	2.4	7.0	11.2	16.5	21.6	21.0	15.9	10.0	4.1	-0.3	8.8
Mean Sunshine Hours	3.8	4.8	5.6	7.1	9.6	12.2	12.4	11.7	10.0	7.5	5.6	3.9	94.2
Average Rainy Days	12.5	11.7	11.9	11.4	8.9	2.7	0.5	0.3	1.1	5.9	8.3	11.7	86.9
Mean of Monthly Precipitation (mm)	70.7	68.6	65.5	68.2	42.9	8.1	0.7	0.4	3.9	31.8	54.1	70.8	485.7
Highest Recorded Temp. (°C)	16.9	21.3	28.3	35.3	39.8	42	46.2	45.9	42	35.7	28.4	22.5	46.2
Lowest Recorded Temperature (°C)	-24.2	-21.0	-14	-6.1	0.8	3.5	9.9	11.4	4.0	-1.8	-12.9	-23.4	-24.2
Average Relative Humidity (%)*	76	72	65	63	55	35	26	25	30	47	66	75	53.0

*Between 1932-2014

1.4 Historical Background of Diyarbakır

Advantageously situated on the west bank of the Tigris (Dicle) River, Diyarbakır is a characteristic example of a geographical region that bears the traces of many civilizations from prehistoric to modern times. Since the city has been dominated by a variety of civilizations, it has been known by a variety of names such as Amid(i), Amed(i), Amida, Amidav, Augusta, Kara-Amid, Dikranagert, Diyar-Bekr, and Diyarbekir (Gabriel, 1940; Bruinessen and Boeschoten, 1988; Beysanoğlu, 2003; Parla, 2004; Jongerden and Verheij, 2012). The city, however, has been referred to as Diyarbakır since the 1900s, and the name of the city was formally changed to Diyarbakır by a governmental decree in 1937 (Government Gazette, 1937).

Concerning its geographical position, Diyarbakır was founded in the northern part of Upper Mesopotamia. The region lies between the Euphrates and the Tigris Rivers (modern northeastern Syria, northern Iraq, southeastern Turkey), where many cultures and civilizations originated and spread over the centuries. This region, known as the *Fertile Crescent*¹, is regarded as the birthplace of history, religion, trade, science, agriculture, writing and urbanization.

The city occupies a remarkable position at the midpoint of geo-strategically important locations. During its long history, the city was seized many times and ruled by more than thirty tribes, states and Imperials. Therefore, civilization in Diyarbakır has never been interrupted. Not only because of its ancient history, but also because of its geographical location, social life and unique architectural importance, many authors, (e.g., Garden, 1867; Gabriel, 1940; Hüsrev, 1950; Marcellinus, 1963; Braidwood and Braidwood, 1982; Bruinessen and Boeschoten, 1988; Beysanoğlu, 2003; Parla, 2004, 2005; Dumper and Bruce, 2007; Ahunbay, 2012; Jongerden and Verheij, 2012)

¹ The term of “Fertile Crescent” was first mentioned in 1916 by an archaeologist, James Henry Breasted in his study, namely *Ancient Times, A History of the Early World*, where he wrote, “There is no name, either geographical or political, which includes all of this great semicircle. Hence we are obliged to coin a term and can it Fertile Crescent. (...) This fertile crescent is approximately a semicircle, with the open side toward the south, having the west end at the southeast corner of the Mediterranean, the center directly north of Arabia, and the east end at the north end of the Persian Gulf.” (Breasted, 1916).

including voyagers, historians, archaeologists, architects and art historians have studied the city and region. Based on their writings, Table 1.2 shows a historical timeline of the activity of civilizations in Diyarbakır from ancient to modern times.

Although it is unclear when the city was first inhabited, archeological excavations some 50 kilometers north of the city in Çayönü have found traces of human habitation that date back to *ca.* 7,000 BC (Braidwood and Braidwood, 1982). It is reported that the Subartu (an early name for Assyrians) inhabited the region during 3,000 BC and that the Hurrians began to control the region during their ascendancy in 2,000 BC. Mound Amida, where there is now a tumulus in the core of the old city was the first place where the Hurrians settled and encircled the city with walls (Parla, 2004).

Limited information is available on the city during the pre-Roman period. However, it is known that the city first appears in early historical records of the Assyrians as the capital of the Bit-Zamani, a tribe of the Aramean Kingdom, around the ninth century BC (Parla, 2005; Jongerden and Verheij, 2012). The city was captured by the Persians in *ca.* 518 BC, and then it became an important node on the Royal Road that connected Asia Minor to Cappadocia, Babylon and Persia along the Tigris. The Romans later colonized the city in *ca.* 69 BC, and called it Amida. Roman expansion into the region during the first two centuries AD elevated the city to a new level of regional power and authority (Dumper and Bruce, 2007). Amida suffered successive sieges and occupations by Romans, Parthians and Sassanians over the centuries. Subsequently, Amida became a Roman city and was fortified for defense against besiegers (Pollard, 2000; Parla, 2004).

In 638 AD, at the end of a five-month of siege, Arab armies conquered Amida, and Islam was introduced to the city. During that period, the city maintained its role by becoming an Islamic frontier fortress. Ever since, the city has periodically been conquered and ruled by autonomous dynasties and states.

Table 1.2 Historical timeline of Diyarbakır

PERIOD	CIVILIZATION	PERIOD	CIVILIZATION
c. 7,000 BC	Initial occupation of the region	869-898	Shaybanids
3,000 BC	Subartu	898-930	Abbasids
2,000 BC	Hurrians & Mittanis	930-978	Hamdanids
1400 BC	Uartians & Assyrians	978-982	Buyids
900 BC	Bit Zamani	984-1085	Merwanids
653-612 BC	Scythians	1086-1097	Seljuks
612-518 BC	Medes	1097-1183	Inalids & Nisanids
518-322 BC	Persians	1183-1232	Artuqids
322-160 BC	Seleucids	1232-1240	Ayyubids
160-139 BC	Parthians	1240-1277	Seljuks
80-69 BC	Armenian Kingdom	1277-1298	Ilkhanids
69 BC	Romans	1298-1393	Artuqids
63-164	Romans & Parthians	1394-1404	Mongols
c.224-365	Romans & Sasanians	1404-1508	Akkoyuns
c. 365-638	Byzantine	1508-1515	Safavids
638-661	Arabs	1515-1923	Ottomans
661-750	Umayyads	1923	Republic of Turkey
750-896	Abbasids		

With the Ottoman conquest in 1515, Diyarbakır was elevated to the capital of a newly established *eyalet* (province). This large province contained the southern and eastern parts of the Ottoman Empire.

As an administrative district, Diyarbakır also served as a military base to defend the region against the Persians. Finally, in 1923, with the proclamation of the republic, Diyarbakır became a province of Turkey (Gabriel, 1940; Bruinessen and Boeschoten, 1988; Beysanoğlu, 2003; Parla, 2004; Dumper and Bruce, 2007).

This old city kept its commercial, cultural, military and administrative importance over the centuries. Diyarbakır has been part of a wide variety of kingdoms and states. Each civilization that reigned in the city, from the Hurrians to the present has left powerful imprints on Diyarbakır. Their remains and artifacts can be found all around the city. There are over one hundred registered monumental cultural properties located within the Sur District, the old town of Diyarbakır, including the castle, the palace, churches, mosques, madrasahs (educational institutions for teaching Islamic law), caravanserais

(roadside inns), fountains, tombs, baths and as a masterpiece, encircling all these monuments, the City Walls.

1.5 The Historical and Interventional Background of the Diyarbakır City Walls

The need for protection is a basic concern for humans and the spaces they inhabit. In this respect, fortresses fulfill a human need. For ancient settlements, defensive structures were a vital necessity for the inhabitants to protect themselves against enemies. The term fortress is used here in a broad sense to refer all military structures built for defensive purposes. It was assumed that, especially in the early Medieval period, communities depended on their fortified sites.

The positioning of fortresses was influenced by a variety of factors such as visibility, topography and proximity to stone quarries, roads and water. Therefore, fortresses in the Medieval periods were mostly built on cliff tops, slopes, hillsides or river banks, especially to monitor and control their surroundings. These structures were primarily erected to protect the site against the incursions of enemies and to dominate the land (Hogg, 1975).

Strategically positioned above the west bank of the Tigris River and in close proximity to underlying stone quarries, water resources and trade roads, the DCW have the features of a typical medieval defensive artifact.

The City Walls of Diyarbakır are among the most extensive surviving structures from ancient times and also one of the most frequently mentioned fortifications in ancient texts. As a unique landscape, cultural feature and crossroad of the trade roads, Diyarbakır and its City Walls have attracted the attention of numerous travelers, who have set their appreciations down in words for the centuries. Of them, a description of the DCW by a Persian traveler and poet, Nasir Khusraw, who visited Diyarbakır in 1046, is worth quoting. Here is how Khusraw describes the City Walls in his *Safarnama*:

“I have seen many cities and fortresses around the world in the lands of the Arabs, Persians, Hindus and Turks, and yet I have never seen anything comparable to Amid on the face of the earth nor have I never heard anyone claim that he had seen any place equal to this glorious city.” (Hüsrev, 1950)

Although the exact construction date of the DCW is still obscure, it is known that the Hurrians encircled the city with the walls in 2,000 BC. It is also reported by researchers that the City Walls were expanded and strengthened by the Romans to defend against Persian attacks in the early third century AD (Marcellinus, 1963). Therefore, it can be assumed that the City Walls were nearly completed in the fourth century. However, the walls are a combination of the efforts of the various civilizations that reigned in the city (Gabriel, 1940; Beysanoğlu, 2003; Parla, 2004; Ahunbay, 2012). The city has changed hands frequently and suffered severely from endless wars as a consequence of its geographical position and its natural landscape. During its more than four millennia of existence, the city has been besieged, captured, recaptured, ruined and rebuilt many times. It is reported, for instance, that in the late 1300s, a considerable part of the walls and monuments settled in the city were ravaged during the Mongol invasion (Parla, 2005).

The surviving city walls were largely built by the Romans and Byzantines; however, the walls were gradually built and repaired in their current position with minor modifications of morphology by the civilizations that have occupied the city. The walls, therefore, have been subject to numerous interventions during their long history. We know about these interventions from inscriptions carved in different sections such as gates, towers, and walls. The location, intensity and techniques of past interventions play a crucial role in how the DCW have been conserved to this day. It is important to evaluate the overall impact of past interventions on the performance and integrity of the stone. Such studies are necessary to categorize the causes and forms of the deterioration observed in the site and determine whether they are a result of the former

interventions or occurred as a result of external factors (Ema et al., 2013; Fort et al., 2013). However, we have limited information about these interventions.

Since the repairs were not recorded properly and we lack published studies of the archaeological evidence and the walls' construction techniques, inscriptions and historical evidences are the only available sources for dating and documenting past interventions. Meanwhile, many of the inscriptions are worn, have crumbled away or been damaged over the centuries, meaning that inscriptions are a limited resource for such studies. Nevertheless, inscriptions remain the primary reference for tracing the evolution of the city and its walls over the centuries.

As forms of writing, records of temporally remote events and cultural symbols, as well as the inscriptions and reliefs on the DCW enhance their historical and cultural character. Moreover, those epigraphical remains turn the city into a museum of inscriptions, which distinguishes it from other walled cities. Figure 1.3 shows a set of inscriptions and reliefs from the walls. Of the 63 existing inscriptions on the walls, towers and gates, six date to the period of the Byzantines (four in Greek and one in Latin), and the rest date to their Islamic successors (Berchem and Strzygowski, 1910; Gabriel, 1940, 2014; Sourdel-Thomine, 1965; Blair, 2000; Pollard, 2000; Gierlichs, 2009; Parla, 2012).

The inscriptions partially record the history of the walls' construction and modifications. The Latin inscription, for instance, embedded on the Dağ Gate section (Figure 1.4) is unique thanks to its commemoration of the extension of the DCW in the fourth century (Gabriel, 1940, 2014; Parla, 2012). The carved inscriptions also reveal some basic information on the architects, rulers or persons who ordered work on the walls. In addition to the inscriptions, some parts of the walls, gates and towers have been decorated with magnificent reliefs of humans, flowers and animals such as birds, lions, scorpions, bulls and horses (Figure 1.3).

Inscriptions and historical evidence indicate that especially during the dominance of the Abbasids, Merwanids, Seljuks, Ayyubids, Artuqids, Akkoyuns and Ottomans, many repair and reconstruction works were conducted on different sections of the DCW, mostly to increase the strength of the walls of the fortified city (Beysanoğlu, 2003; Parla, 2004, 2012).



Figure 1.3 A collection of the inscriptions and reliefs on the DCW (a) Detail of Yedi Kardeş Tower, showing part of reliefs and inscription; (b) Some eroded limestone reliefs on the Artuqid Arch in Citadel; (c) Some iconic reliefs with an inscription on Dağ Gate; (d) A close view of Evli/Ulu Beden Tower, showing part of inscription and reliefs



Figure 1.4 A Latin inscription on the Dağ Gate (After Gabriel, 1940, 2014)

Since the proclamation of the republic in 1923 until recently, the destruction and demolition of the DCW have continued without respite. Between 1930 and 1932, for example, considerable parts of the walls located in the Dağ Gate section were systematically dynamited (Gabriel, 1933), demolishing three towers and some 200 meters of the northern section of the DCW (Figure 1.5).

The demolition of the walls and towers was ordered by the then-governor for the sake of improving air circulation in the city (Gabriel, 1940, 2014). Fortunately, Albert Gabriel, an architect and archaeologist who was doing archaeological investigations in the region, prevented further demolitions to some extent by sending a letter to the Minister of Education of the period urging him to stop the destruction immediately (Gabriel, 1933).

Although Gabriel's effort suspended the demolition of the walls this time, it would then be continued in the following years in different sections of the walls for reasons such as constructing new roads, widening the streets, opening new gates or modernizing and expanding the city. On the other hand, especially since 1940, many repair campaigns have been conducted in an attempt not to increase the strength of the walls against external attacks, but to preserve them as a cultural heritage.

However, some sections of the walls have been adversely affected by inappropriate contemporary interventions as a result of the employment of incompatible stone materials, cement-based mortars and improper construction techniques.

Different sections of the walls have been breached and large stone blocks, especially at the base and corners of the walls, have been removed by the city's inhabitants for squatting purposes. As an evidence of this thoughtless intervention, the dismantled stone blocks can still be seen on the façades of some houses in the vicinity (Figure 1.6).



Figure 1.5 Ruins of demolished walls (northern section of the DCW; Tower 4 and vicinity) (Gabriel, 1940, 2014)

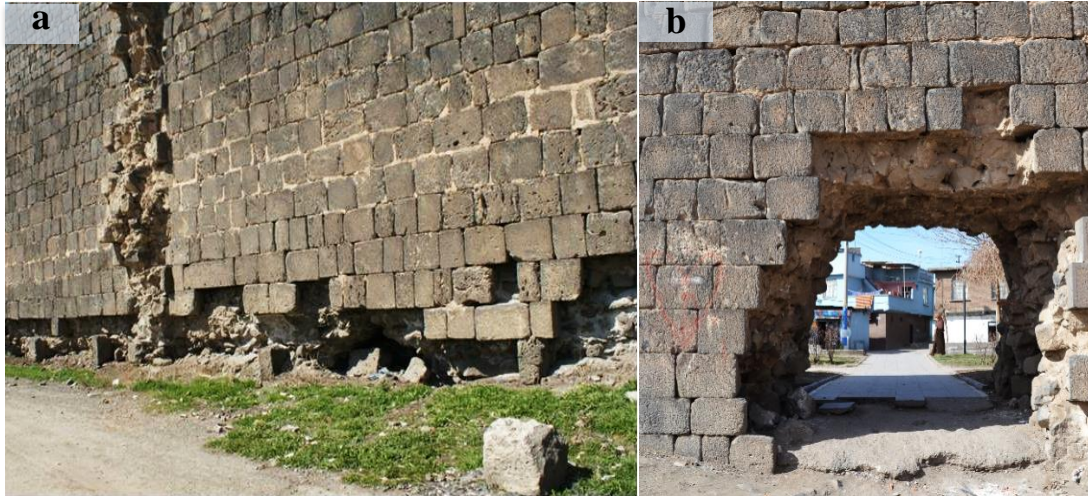


Figure 1.6 Dismantled and breached wall sections (a) Dismantled wall base; (b) A gateway opened by breaching the wall

1.6 Construction Techniques and Materials

The selection and use of construction materials characterize civilizations, and there is a close relationship between the nature of building materials and knowledge behind construction techniques. In other words, construction techniques are not only derived from the functional aspects and availability of materials, but largely from cultural aspects and interpretation of knowledge (Dietler and Herbich, 1998; Baltali, 2007).

The Romans established and built numerous cities throughout the Imperial period and fortified most of them for defensive purposes. As a physical result of building structures with different and locally available materials in various regions, conditions and cultures, the Romans mastered a number of construction techniques, including roads, arches, vaults, aqueducts, and fortification walls (Sherwood, 2000).

Inscriptional, historical and architectural researches investigated in the study area have determined that the Romans constructed and shaped the present form of the DCW in the fourth century AD.

Although the city is a combination of the heritage of the various civilizations that occupied it over the centuries, the Romans left a strong mark on the city, and the Roman influence can still be traced in the construction techniques, materials, the orientation of the streets and the overall layout of the DCW. Here, some of their construction techniques, particularly for those applied to the masonry walls will be discussed. Masonry wall-related deterioration problems will be discussed in the following chapters. The Romans developed and improved various masonry wall methods. Those methods are generally classified according to the type of material and facing (Ward-Perkins, 1992). Most of them are explained by Vitruvius, a Roman architect, in his *De Architectura*, including *opus incertum* (masonry wall faced with irregular stone blocks), *opus quadratum* (masonry wall faced with regular stone blocks), *opus reticulatum* (masonry wall faced with pyramidal stones) or *opus listatum* (masonry wall faced with brick and stone).

The Romans also developed *opus caementicium*, filling the core of masonry walls with irregular stone or brick pieces and mortar (Vitruvius, 1960; Ward-Perkins, 1992; Curl, 2003).

Construction techniques have an important effect on the durability of materials. Restoration and repair work performed without understanding what the stone type is and how it functions in a wall system can seriously damage a masonry wall. Masonry walls are exposed to a variety of such complex forces as rising damp, efflorescence and seismic activity. These forces act simultaneously on walls, and errors in design and construction cause walls to deteriorate over time. For instance, during the construction of the wall, a stone block may not be correctly placed on its natural face, and this may increase the decay rate of the material (Grimmer, 1984; Honeyborne, 1998; Hendry and Khalaf, 2001).

The DCW have been subjected to numerous interventions, a considerable number of which failed to conserve them properly. Material selection and construction techniques are the outstanding factors usually blamed for inappropriate contemporary interventions (Güçhan et al., 2005; Dalkılıç and Nabikoğlu, 2012).

The construction of the DCW was not the result of a specific civilization or period. They are the reflection of different civilizations and historical periods. Differences in construction throughout the fortifications, including the gates and tower designs, the size of the stone blocks and the masonry techniques support this view. Previous studies and field surveys have noted that masonry wall construction was widely used in the DCW.

The most common masonry wall facing techniques in the DCW are classified as *opus incertum* and *opus quadratum*. There are also some composite walls in the form of *opus listatum*, and wall cores in the form of *opus caementicium*. *Opus incertum* is a wall facing form of rubble masonry work formed of oddly shaped stone blocks and set irregularly in mortar.

Opus quadratum is a form of ashlar masonry work in which squared and finished stone blocks are set in continuous and parallel courses, usually without the use of mortar. In addition, *opus listatum* masonry in which the stone alternates with brick courses was also used to some extent in the construction of the DCW (Figures 1.7, 1.8, 1.9 and 1.11).

Preparing the foundation is the initial step in wall and tower construction. Although there is no specific evidence of the precise form of the foundations of the DCW, they lie on the basalt bedrock. In order to form the internal and external faces of the masonry, two parallel walls were constructed, and the spaces between them were filled with rubble and mortar (Figures 1.8 and 1.11).

The erected masonry walls were commonly faced with *opus incertum*, *opus quadratum*, and *opus listatum*. In order to fill their cores, *opus caementicium* was most commonly used. *Opus caementicium*, is a mixture of irregular basalt and brick fragments with mortar and is found in many sections of the DCW (Figure 1.8). In order to create a friction with mortar, the interior faces of the basalt blocks were intentionally left undressed.

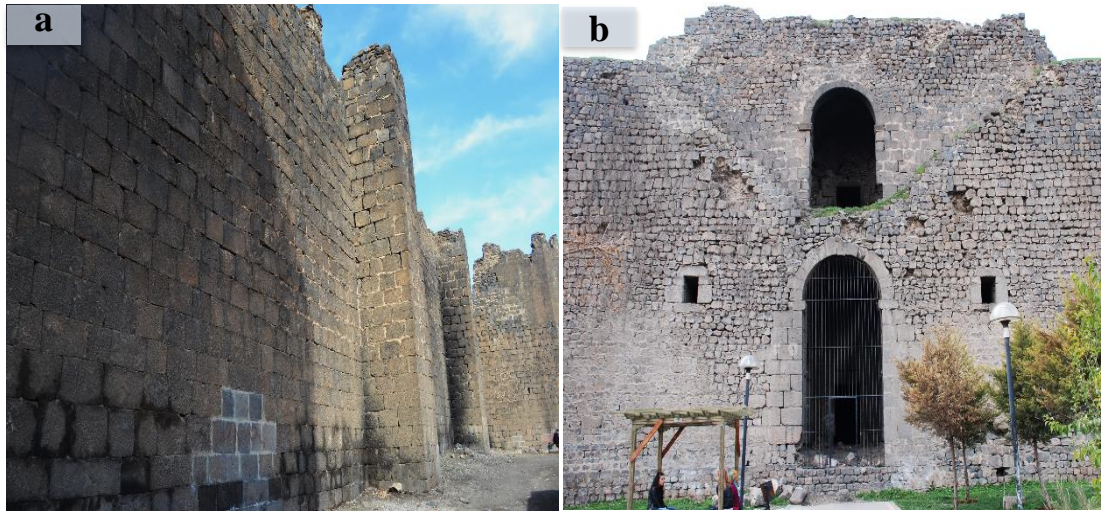


Figure 1.7 Opus quadratum and opus incertum (a) Exterior of the wall, opus quadratum; (b) Interior of the wall, opus incertum (north and east section of the DCW)

The undressed faces of the basalt blocks were then installed to that mixture. The installed blocks were set by rotating and pushing them to fit the leveled wall surface smoothly (Tuncer, 2012b).

In some sections, cylindrical or squared basalt blocks were placed perpendicularly to the face of the walls and towers. These embedded columns were probably intended to increase the strength of the walls (Figure 1.10).

The above-mentioned construction techniques were used in different sections of the DCW as a reflection of priorities, conditions or functions. In other words, the construction technique used to erect the wall depends on various factors, but largely depends on its function. For instance, the interior faces of the DCW are mostly rubble masonry work, or *opus incertum*, with relatively small, oddly shaped basalt blocks. The exterior walls were constructed with courses of accurately cut, large and dressed basalt blocks, or *opus quadratum* (Figure 1.7).

The interior walls, as a result of priorities and functions, were constructed with less care than the exterior walls where large ashlar basalt blocks were used with great care. The large basalt blocks on the exterior walls not only increased the grandeur of the fortified city, they also had defensive purposes. The large basalt blocks were also employed in a similar fashion to erect the towers.

The largest basalt blocks were used at the base of the walls and towers, especially for load-bearing purposes. The dimensions of the basalt blocks used in the exterior walls range from 40 to 70 centimeters wide, 30 to 50 centimeters high and 15 to 45 centimeters deep (Dalkılıç and Nabikoğlu, 2012).

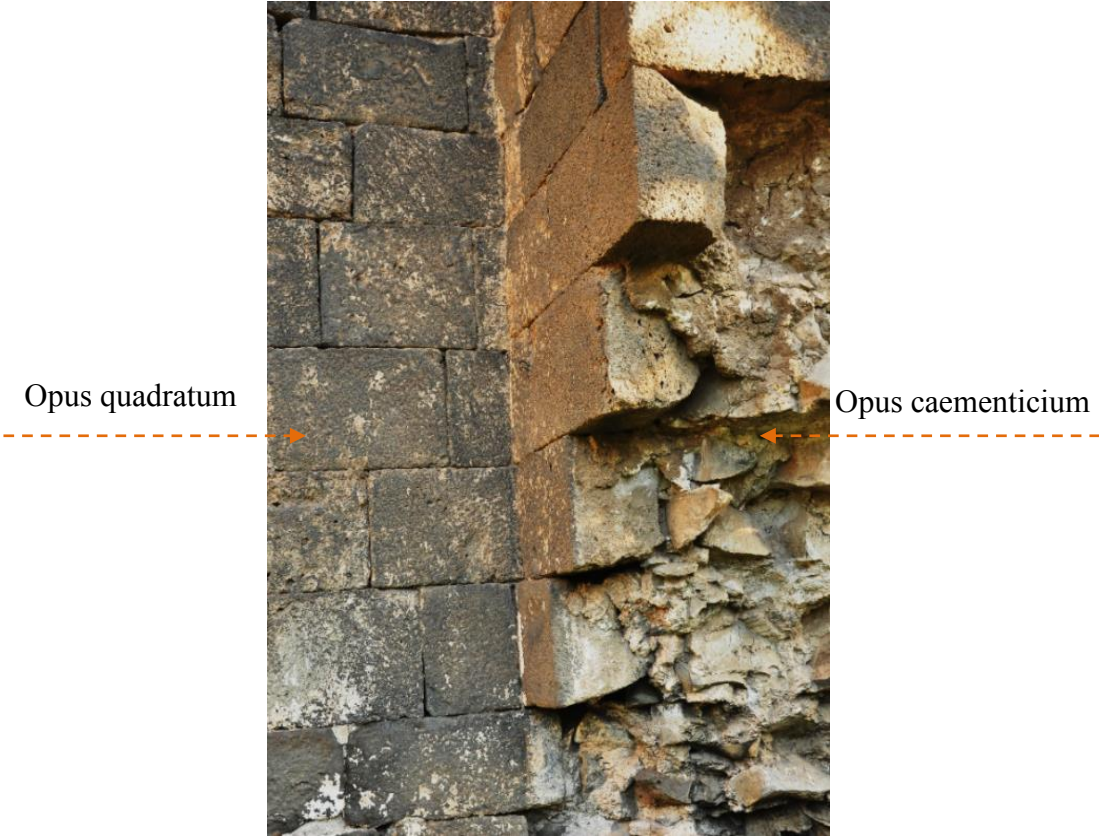


Figure 1.8 Opus quadratum and opus caementicium (north Section of the DCW)



Figure 1.9 Opus listatum (east section of the DCW)



Figure 1.10 Cylindrical basalt applications (south and north section of the DCW)

Morphology had a great effect on the construction path, development and overall shape of the DCW. The ancient DCW is located on the west bank of the Tigris River since their east and south sections are naturally protected by cliffs. The southern section of the walls, for example, has the most elevated, (*ca.* 70 meters) part of the morphology. Due to morphological limitations, the north and west sections of the DCW were expanded. For instance, all sections of the walls except those in the north were erected so as to be in harmony with the existing morphology. The current form of the DCW can thus be evaluated as the dictate of morphology.



Figure 1.11 A Tower façade and wall section

Although the city has been continuously occupied for ages and the walls have been subjected to numerous interventions, the principal geological material employed in their construction has not changed at all. Basalt is their principal construction material. In addition to the basalt, brick, mortar, limestone and a limited amount of metal are employed in the structures (Figure 1.12).

Considering the scope and motivation of this dissertation, the origin and composition of the brick, mortar, limestone and metal used in the construction of the structures will not be dealt with in detail. This section is a brief review of some of the basic construction materials with a particular emphasis on their use. As the focus of this dissertation, basalt will be explained in detail. It is the principal construction material used in the DCW and is used in almost all of their architectural elements, including masonry walls, towers, buttresses, gates, arches and even in decorative elements.

Several field surveys were performed in the study area. Some of those surveys were conducted to assess the origin of the basalt and locate ancient quarries near the city walls. Field surveys and previous studies carried out at the site have shown that the locally available basalt material originated from the lava eruptions of Karacadağ Volcano *ca.* 40 kilometers southwest of the city.

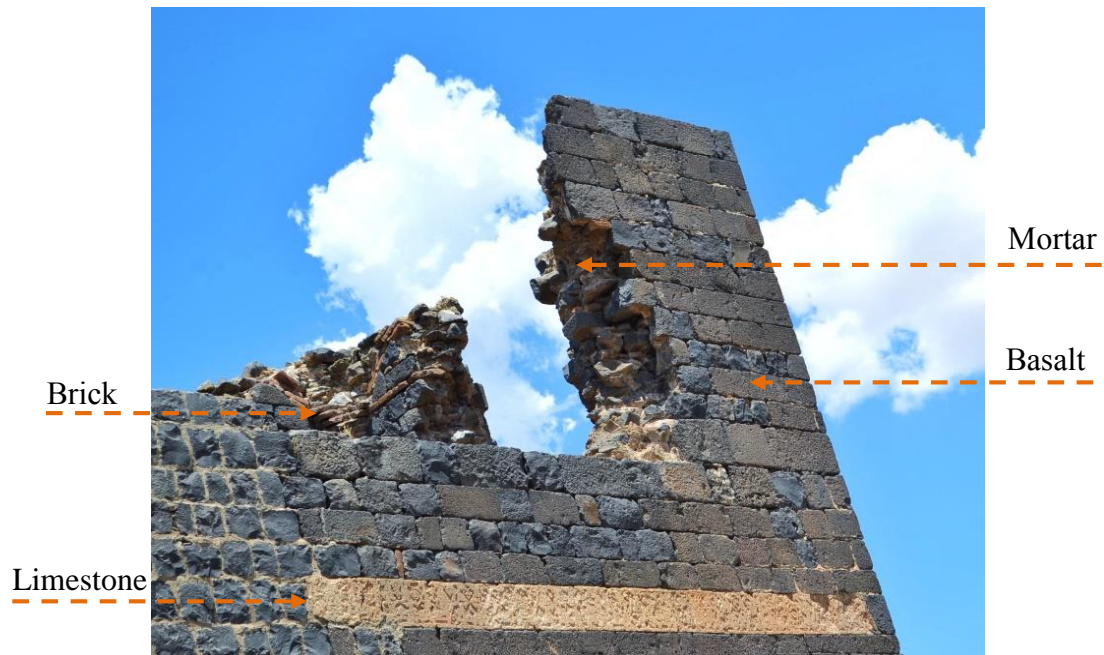


Figure 1.12 A collection of the materials used to build the DCW (east section of the DCW)

It is assumed by some researchers (Assenat, 2012; Toprak, 2012) that the basalt blocks were excavated by means of special carving tools from the recently abandoned quarries, especially those located on the steep slope facing the river. This means that the steep slopes along the south and east sections of the City Walls are not natural, but were made much steeper by artificial escarpments.

Toprak (2012) claims that the extracted blocks were transferred to the site and employed in the construction of the walls immediately above the quarries. This was visually confirmed in some sections of the wall by comparing the texture of the basalt outcrops with those used in the wall; however, since the walls have been repaired and rebuilt various times over the centuries, such *in situ* observations need to be confirmed by additional fieldwork and laboratory research.

As Figure 1.13 illustrates, removing basalt blocks from the face of the natural cliffs not only reduced the cost of transportation and the duration of the construction, but also enhanced the defensive function of the walls by creating artificially steepened slopes (Toprak, 2012).

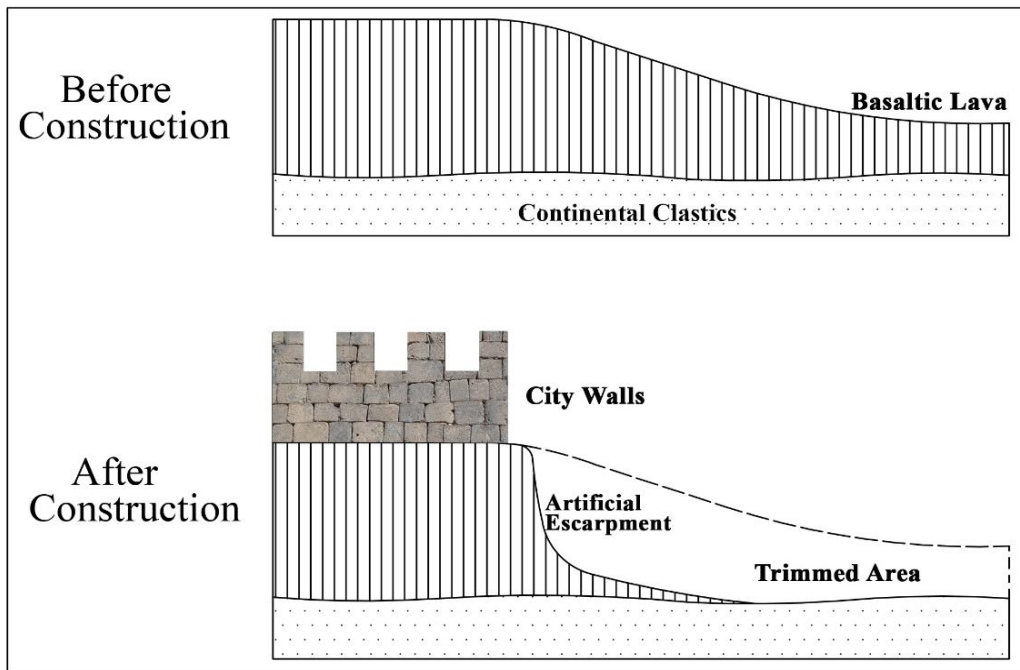


Figure 1.13 The estimated extraction of basalt (Modified from Toprak, 2012)

Although the evidence of hillside extraction still can be traced to some extent, most of the ancient quarries have been destroyed or covered with debris. A 1909 photograph, credited to an English traveler, Gertrude Bell, shows visible evidences of the extraction (Bell, 1924; NUGBA, 2014). In it, traces of some 10 m of extraction on the south section of the DCW can be seen (Figure 1.14).



Figure 1.14 Traces of steepening extraction by the Keçi Tower (NUGBA, 2014)

Brick, as another construction material, was used in different sections of the city walls. It was the primary construction material for the domes, vaults and arches of the towers. (Figures 1.9 and 1.15).

As a composite material, mortar was used extensively in the DCW. Mortar was applied to stone and brick, especially for bedding, pointing and repairing the walls, towers, gates and any other structural elements. Based on the observations, it can be stated that plaster was not applied to any original architectural elements of the City Walls (Güçhan et al., 2005).

Limestone was also used in the DCW, particularly, in some of the inscriptions and decorative elements (Figure 1.16). Limestone was not used as a principal construction material for the different historical structures in the study area. It was mostly used for decorative purposes; especially on the façades of some structures to produce an aesthetic contrast with the basalt (Figure 1.17a). Limestone, however, was not available on site. It is assumed that the limestone used in the DCW and other structures within them probably derived from quarries at some distance both to the north and south of the city.



Figure 1.15 Brick applications on different sections of the DCW (a) Brick courses; (b) Brick domes and arches (Melikşah Tower); (c) Brick vault (Melikşah Tower); (d) Brick dome (Keçi Tower)



Figure 1.16 Limestone applications in the form of inscription and relief

Finally, metal was also employed in the City Walls, only used in the doors of some principal gates and as clamps to hold stone blocks (Halifeoğlu, 2012). Particularly, the doors of the Mardin and Urfa Gate were cast in metal (Figure 1.17b).



Figure 1.17 Limestone and metal applications (a) Alternation of limestone and basalt at Behram Pasha Mosque; (b) A metal door at Mardin Gate (Governorship of Diyarbakır, 2016)

1.7 Architectural Features of the Diyarbakır City Walls

Considering their scale, structural elements, construction and material applications, the DCW are symbolizing the architectural characters of over thirty ruling civilizations in the region. It is, therefore, the masterpiece of the skills of the people of the ancient and modern era. Here is a brief overview of the architectural elements and their basic features.

The City Walls are located on an elevated terrace of the Tigris Valley and overlooking a vast alluvial fan spreads out in that valley, known as Hevsel Gardens (Figures 1.18 and 1.19). As a cultivation land, Hevsel Gardens are carrying a significant role in the history of the city, regarding their historical background, cultural aspect and also agricultural productivity.



Figure 1.18 An aerial view of the DCW and the Hevsel Gardens (captured from Google Earth)

Therefore, the City Walls and Hevsel Gardens were jointly nominated for UNESCO's World Heritage List. Eventually, as "an outstanding example of a type of building or architectural landscape which illustrates significant stages in human history," *Diyarbakır Fortress and Hevsel Gardens Cultural Landscape* were officially acknowledged the status of World Heritage Site by UNESCO in 2015 (UNESCO, 2015).

The DCW are roughly oval in plan and elongated on the north and west sides. The current form of the walls, towers and gates shaped by the Romans in the fourth century is mostly the result of topography and morphology.

The existing topography is shared not only with the DCW, but also over one hundred registered monumental cultural properties, including mosques, churches, baths, fountains and inns.



Figure 1.19 East section of the DCW from the Hevsel Gardens (DMM, 2014)

The city walls consist of two sections: The Citadel, or *İçkale*, and the Outer Castle, which will be referred to in this section as the enceinte. (Figure 1.20). The term, enceinte, is used here to refer to the walls, towers and gates that surrounded the fortress, including the citadel (Kaufmann et al., 2004). Since the exact date of its construction is still obscure, it is assumed that the citadel, located in the northeast corner of the fortress, was surrounded within walls during the period of the Hurrians (Beysanoğlu, 2003; Parla, 2005; Ahunbay, 2012; Gabriel, 2014). The citadel is the core of the city, and served as an administrative and residential function for centuries. In addition to the residential and administrative buildings, inside, there is a mound, surrounded with fragments of walls, called as the Mound Amida (Parla, 2005; Halifeoğlu, 2012; Gabriel, 2014).

The most comprehensive investigation on architectural features of the DCW is that of the French architect, Albert Gabriel. His outstanding plans, drawings and detailed descriptions of the DCW are still used as a reference and were published in his *Voyages archéologiques dans la Turquie Orientale* (Gabriel, 1940, 2014). Gabriel identified 18 towers on the citadel, and 82 on the enceinte. He designated letters and Roman numerals to identify the towers. This dissertation will refer to the towers with the numbering system devised by Gabriel (1940) (Figure 1.20).

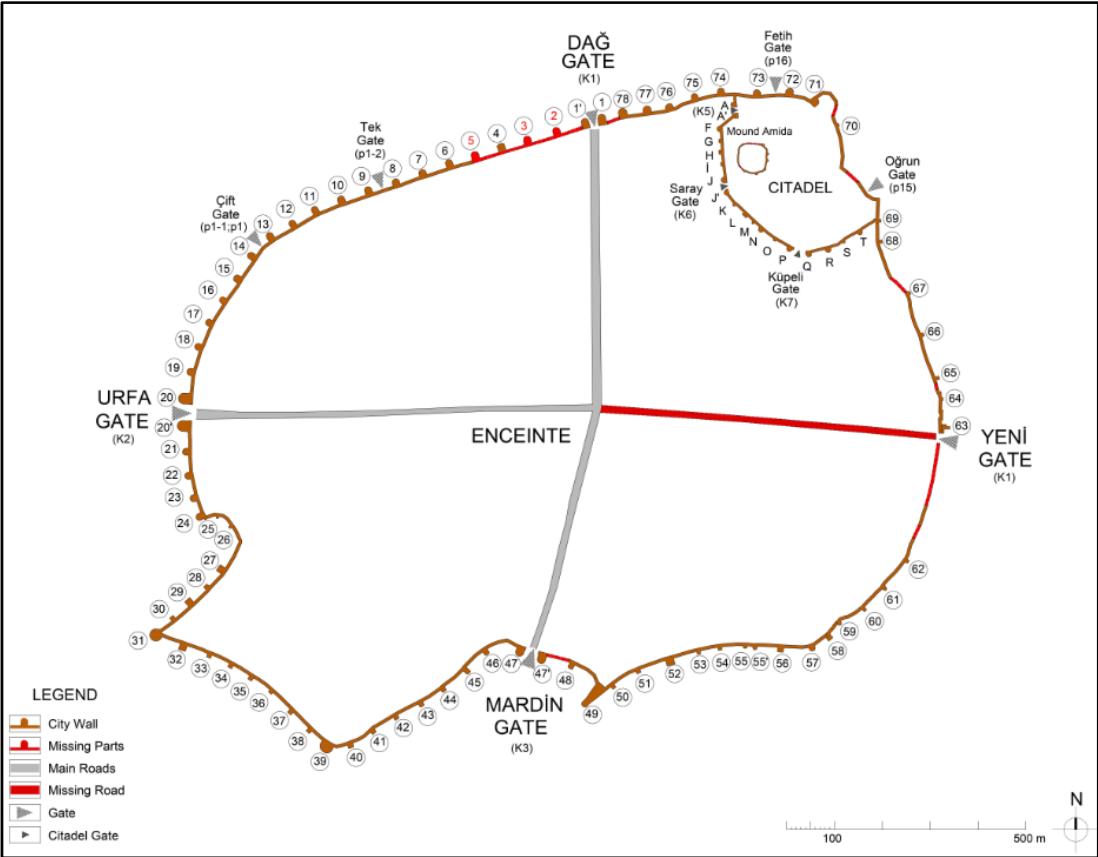


Figure 1.20 Plan view of the DCW (Modified from Gabriel, 1940; 2014)

Gabriel (1940; 2014) also mention an aqueduct on the north section, and a pre-wall surrounding the walls themselves (Figure 1.21). Although the aqueduct and pre-wall have now almost entirely vanished, especially, traces of pre-wall can still be seen at the northern and western sections of the DCW.

As an initial defense phase of the fortress, the pre-wall was erected just in front of the walls with a lower height. There was a rubble-filled ditch between the walls and pre-walls. The width of this ditch reaches to *ca.* 15 meters at some points (Ahunbay, 2012; Gabriel, 2014).

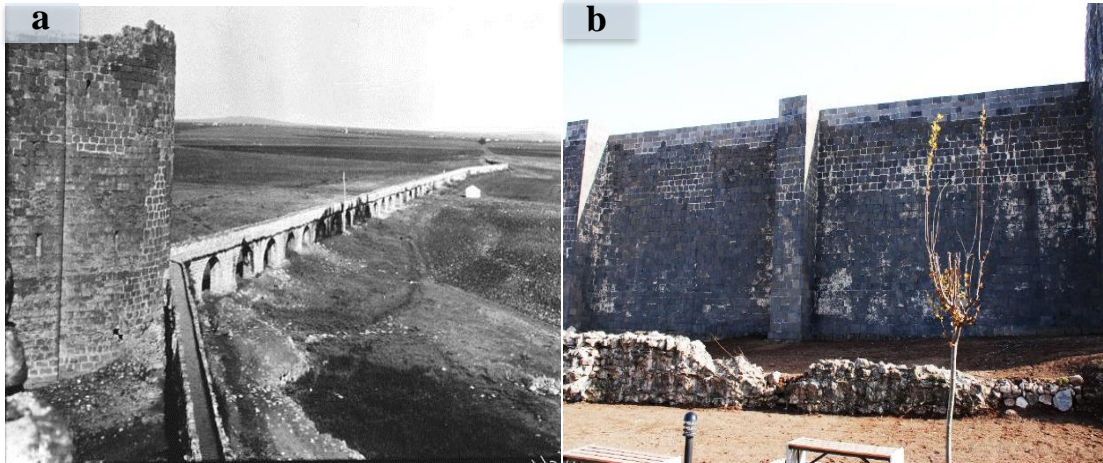


Figure 1.21 Aqueduct and Pre-wall (a) Recently vanished aqueduct (Bell, 1924); (b) Remains of the Pre-wall at the north section of the DCW

The walls have been subjected to numerous destructions, reconstructions, restorations and modifications over the centuries, and as a result, the original form has changed to such an extent that it is difficult to measure it precisely. There exist a few studies (e.g., Gabriel, 1940, 2014; Dalkılıç and Nabikoğlu, 2012; Halifeoğlu, 2012; Nabikoğlu and Dalkılıç, 2013) that focus on the dimensions of the fortress of architectural elements. These studies indicate that the citadel and the enceinte have peripheral lengths of 599 meters and 5,200 meters, respectively.

Hence, the overall length of the DCW is roughly 5,800 meters. The citadel encloses an area of *ca.* 0.074 square kilometers, and the overall area occupied by the citadel and the enceinte is approximately 1.57 square kilometers (Dalkılıç and Nabikoğlu, 2012).

There are many descriptions of the thickness and height of the DCW, especially by scholars and travelers who visited the region. Many of them reported that the thickness of the walls is 3 to 5 meters and that their height is 8 to 12 meters (Gabriel, 1940, 2014; Hüsrev, 1950; Sourdel-Thomine, 1965). Nevertheless, most of these estimates are far from accurate and fail to define the dimensions of the components precisely. A recent study was performed by Dalkılıç and Nabikoğlu (2012) to obtain precise measurements of the walls' architectural components. Unlike earlier reports, the authors found that the walls and towers have a width ranging between *ca.* 1.4 and 5 meters. The wall thickness, as a result of topography and defensive concerns, decreases in their east section where the measured width ranges between 1.4 to 2.6 meters.

In the north and the west sections, on the other hand, the wall thickness increases up to 5.25 meters. The heights of the walls and towers also contrast prior assumptions. Here, it should be taken into account that most of the towers were erected to the same height as that of the walls. Thus, the measured height of the walls from ground level ranges from 7.6 to 22 meters in height. Considering the earthen fill at the base sections and demolished portions of the upper sections, it should be noted that the walls and towers were probably once taller than they are now.

In addition, more than ten percent of the walls have been dynamited, destroyed or demolished. In other words, a total of *ca.* 650 meters of the walls and towers are now missing (Nabikoğlu and Dalkılıç, 2013). Most of the missing parts are in the north and east sections. In the north section, for instance, immediately after the Dağ Gate, there is a gap of some 220 meters where the walls and 3 towers were dynamited and removed for the sake of air circulation in the city (see missing parts on Figure 1.20).

There is only one tower, now called Tek (Single) Tower, left in this dynamited sector of the DCW. There are also 250 meters of missing parts spread unevenly throughout the walls' east section. Some damages can be associated with natural events, as earthquake (Gabriel, 1940, 2014; Toprak, 2012), but most are due to human interventions such as building housing, opening new gates or the idea of ventilating the city (Figure 1.22).

Finally, in the south section, next to the Mardin Gate, some 50 meters of the walls were removed in the early 1930s to make room for vehicle traffic (Dalkılıç and Nabikoğlu, 2012; Tuncer, 2012b).

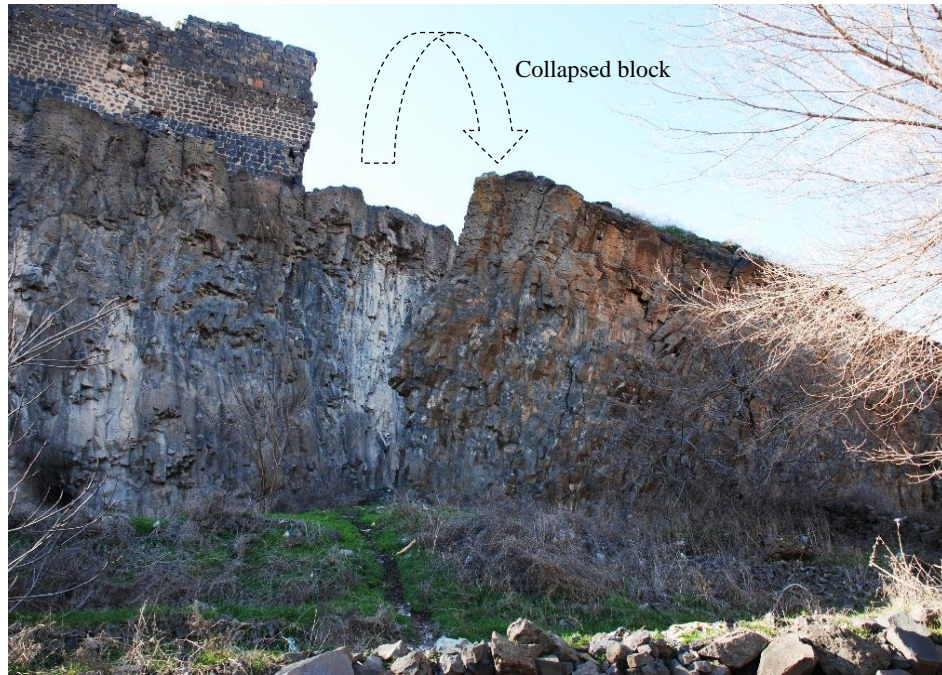


Figure 1.22 The demolished part of the DCW associated to the earthquake

The DCW are heavily fortified with walls, towers and buttresses. The towers along the walls of the citadel and the enceinte are situated to fulfill defensive functions appropriate to the terrain and the choices of their builders. In other words, the orientation, size, shape and spacing of the towers reflect defensive and morphological concerns. For instance, the south and the east sections of the walls follow the upper shoulders of the valley for some 2.5 kilometers. Here, the fortress was naturally protected by cliffs and the Tigris River. In contrast, the north and the west sections of the walls lie on a flat area where the fortress was more vulnerable to attack.

Therefore, the towers, especially those on the south and the east sections were mostly placed at large intervals of *ca.* 125 meters, whereas, the towers on the north and the west sections were placed at somewhat more regular and close intervals of *ca.* 50 meters (Dalkılıç and Nabikoğlu, 2012; Tuncer, 2012b; Nabikoğlu and Dalkılıç, 2013). This is, as has been noted, a consequence of morphology on the construction and development path of the DCW.

The projecting towers were shaped in different forms. The citadel's 18 towers are circular, triangular, square or polygonal in form. The 82 towers on the enceinte are mostly circular, polygonal or square. The towers have 2, 3 or 4 stories with staircases and domes or vaults (Güçhan et al., 2005; Dalkılıç and Nabikoğlu, 2012; Halifeoğlu, 2012; Gabriel, 2014). Of the towers on the DCW, the Melikşah, Ulu Beden, Yedi Kardeş, Nur and Keçi Towers are the most significant ones regarding their decoration, inscription, plan, size or construction techniques (Figure 1.23). These towers have attracted the attention of various researchers, including historians, archaeologists, architects, art historians and engineers. However, considering the scope of this dissertation, the towers' remarkable features will not be discussed here. In addition to the towers, more than 120 buttresses (Tuncer, 2012b) were constructed against the exterior walls to provide them with additional support (Figure 1.24).

Like so many medieval cities, the enceinte is traversed by the classic forms of perpendicularly intersecting Roman roads (Figure 1.20). In Roman city planning, the road running north to south is called the *cardo*, and the road from east to west is called the *decumanus* (Sear, 1998). The *cardo* at the DCW has a length of 1,120 meters, and the *decumanus* has a length of 1,610 meters (Dalkılıç and Nabikoğlu, 2012). These roads are still in existence and connect the four main gates positioned at the cardinal points of the DCW (Figure 1.20).

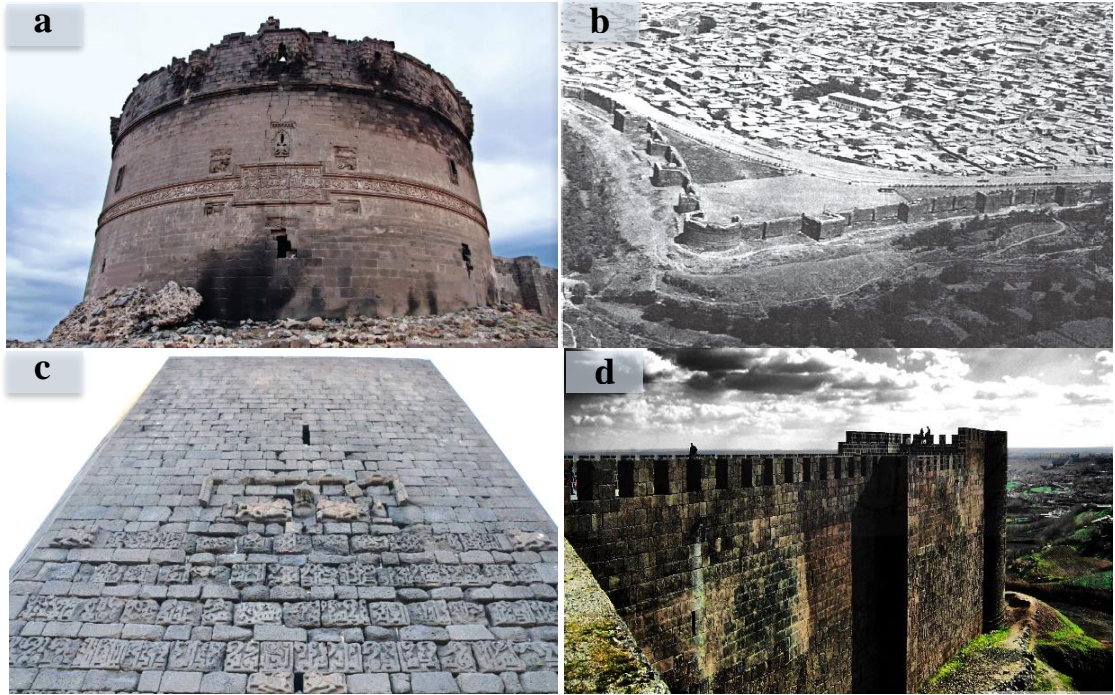


Figure 1.23 A collection of towers on the DCW (a) Evli Beden Tower; (b) Yedi Kardeş Tower; (c) Nur Tower; (d) Keçi Tower (Governorship of Diyarbakır, 2016; Tuncer, 2012a)



Figure 1.24 Butresses at the south section of the DCW

Another architectural element of the fortress is its gates. The DCW are interrupted by several monumental gates. Four main gates open to the four cardinal directions: Dağ Gate, to the north, Urfa Gate to the west, Mardin Gate to the south and Yeni Gate to the east (Figure 1.25).



Figure 1.25 Four principal gates on the DCW (a) Dağ Gate; (b) Urfa Gate; (c) Mardin Gate; (d) Yeni Gate

The Dağ Gate is located on the north section of the DCW. It was used as a principal entrance until the destruction of the walls in the 1930s. The Urfa Gate to the west has three entrances, and the one in the middle was enlarged in 1940 to ease the traffic flow (Beysanoğlu, 2003; Tuncer, 2012b). One of the entrances is employed for pedestrian access and the rest for vehicle traffic. The Mardin Gate to the south is principally employed for pedestrian access; however, in the 1930s it was employed for vehicle access as well after removing a 50-meter section of the walls next to it. Finally, the Yeni Gate to the east opens to the Tigris River and the Hevsel Gardens.

In addition to these gates, there are some other gates that were pierced on the DCW in different periods. The Çift and Tek Gates on the northwest section were opened in 1950 and 1959, respectively. The citadel has also been pierced by the gates. Its four main gates are still in existence. Its Saray and Küpeli Gates open to the enceinte, and the Oğrun and Fetih Gates open to outside the fortress. The main gates through different sections of the DCW are listed in the following table counterclockwise from the north of the citadel (Table 1.3). Apart from these 8 principal gates, there are 25 small ports through different sections of the DCW (Gabriel, 1940, 2014; Beysanoğlu, 2003; Tuncer, 2012a, 2012b; Nabikoğlu and Dalkılıç, 2013; DMM, 2014).

Table 1.3 The main gates of the DCW

Gates	Historical Names	Location	
		(On the Map / City Walls)	
Dağ Kapı	Armenian Gate ; Harput Gate	K1	North
Tek Kapı	Single Gate	P1-2	Northwest
Çift Kapı	Double Gate ; Hindibaba Gate	P1 ; P1-1	Northwest
Urfa Kapı	Greek Gate ; Bab-el Rum ; Aleppo Gate	K2	West
Mardin Kapı	Bab-el Tell	K3	South
Yeni Kapı	Dicle Gate ; Su Gate	K4	East
Oğrun Kapı*	Oğrun Gate	P15	Northeast
Fetih Kapı*	Fetih (Conquest) Gate	P16	Northeast
Saray Kapı*	Palace Gate	K6	Northeast
Küpeli Kapı*	Küpeli Gate	K7	Northeast

(*) Citadel Gates

1.8 Method of the Study

This study was carried out in three main stages: preliminary studies, field studies and laboratory research. The objective of the preliminary studies was to investigate the available references relating to the study area. For this purpose, the relevant documents, including topographical and geological maps, plans, aerial photographs of

the study area and its vicinity, together with published and unpublished reports, papers and theses were collected and reviewed.

The second stage (field studies) consists of site observation and sampling. Site observation was done in different periods and for different motivations. The observation began in April 2014 and continued through August 2016. During the site observation, the geological formations, their boundaries and characteristics were identified. The accessible sections of the DCW were examined to evaluate the sources of the construction material, construction techniques and morphology. The general state of conservation of the site was also examined during this stage. Special emphasis was given to the forms of stone weathering on the walls. The data for the forms of the weathering were then used to produce maps of the weathering forms of the walls.

For sampling, oriented basalt blocks were collected from several locations, mostly from the outcrops along the DCW and from the quarries in their vicinity. The samples were then prepared for the laboratory studies in different sizes specified by the international standards. The detail of the sampling stage is explained in the following section (see Section 1.8.1).

The third stage was laboratory studies. The laboratory stage included physico-mechanical studies, mineralogical and petrographic studies, chemical studies, and accelerated weathering tests. The data obtained from the field studies were combined with the results of the laboratory studies to determine and rank the main causes of the deterioration. Figure 1.26 shows a flowchart of this study. The standards and procedures adopted for the stages of the methodology will be detailed with the results in the relevant chapters.

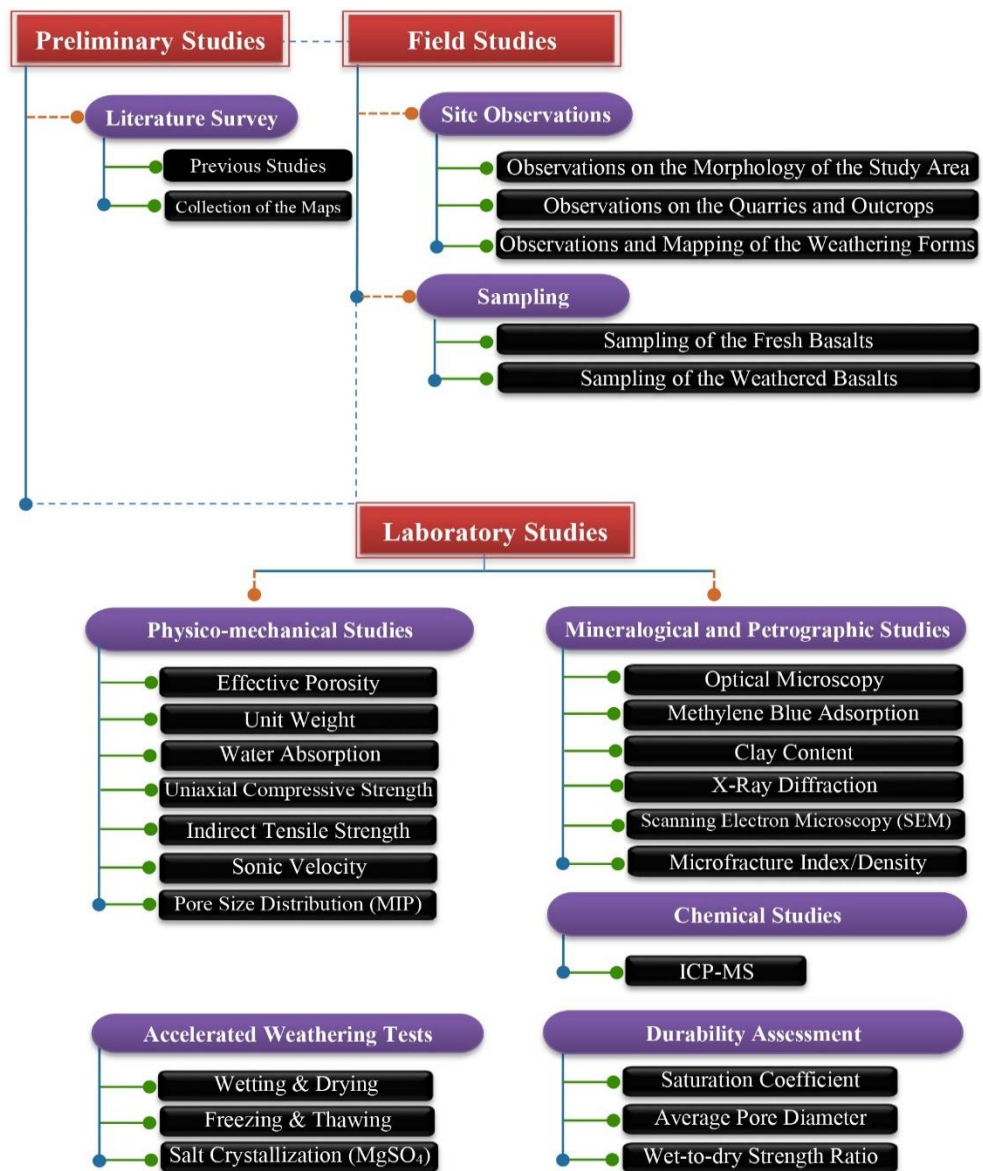


Figure 1.26 Flowchart of the study

1.8.1 Sampling

Based on the field and previous studies, it can be understood that the basalts beneath the DCW are derived from the lava eruptions of Karacadağ Volcano and are classified as Karacadağ volcanics. Basalts with different types of textures were commonly used in the construction of the DCW.

These are classified as massive and vesicular basalts. Some basalts locally display amygdaloidal texture were also employed in the DCW.

For the accelerated weathering and proposed experiments, several field surveys were performed in the study area to determine sampling spots. Based on the types of the basalts, six representative locations were chosen for sampling. They are listed in Table 1.4, and shown in Figure 1.27. Fresh basalt blocks were taken from the outcrops along the City Walls and from quarries in the vicinity of the site. Oriented samples were extracted from the surface, using jackhammers. The oriented block samples were collected and cut into slabs in accordance with the ASTM D5121–15 standard and ISRM suggestion (ISRM, 1981; ASTM, 2017a). A description of each sample site and the blocks were recorded, including information pertaining to the location, alignment, texture, color, secondary minerals and other observable features. For the sample preparation stage, the oriented (normal to the flow direction) block samples were cut with 7 centimeters sides and 30 centimeters height parallel sets. Those parallel sets were then cut into 7 centimeters (and some into 6 centimeters) cubic samples for the laboratory studies (Figure 1.28). A total of 390 massive and vesicular fresh cubic basalt samples were prepared, packed, and then transferred from Diyarbakır to the Engineering Geology Laboratory of Geological Engineering Department of METU for the laboratory studies. Here, the cubic samples were sorted as massive and vesicular, and were defined by their provenances and textures (e.g., 1M-10: the first character is the sampling location; the second is the texture of the sample, whether massive or vesicular, and the number is the specific sample number for that sample location).

Table 1.4 Distribution and number of the fresh samples

Location on the Map	Location Description	# of Fresh Samples		
		Massive	Vesicular	Total
L1	Fiskaya (Ferit Köşk Dist.)	42-11*	68	121
L2	University Bridge (İç Kale St.)	23-5*	•	28
L3	Hasırlı Dist. (Bardakçı St.)	•	72	72
L4	Evli (Ulu) Tower	15-15*	•	30
L5	Northwest of the site	•	77	77
L6	Northwest of the site	62	•	62
Total		173	210	390

(*) 6x6x6 cm Cubes (31 samples)

In addition to the fresh samples, during the field survey special emphasis was given to collecting weathered samples. However, due to the ongoing emergency conditions in the region, it is difficult to investigate and to sample all the sections of the DCW. However, it was possible to collect weathered basalt samples from some relatively secure sections of the DCW. A total of 35 weathered samples were collected from different sections of the DCW. The weathered samples from the DCW were collected with the permission of the Diyarbakır Cultural Heritage Preservation Board. The distribution of the weathered sample locations is shown in Figure 1.29.

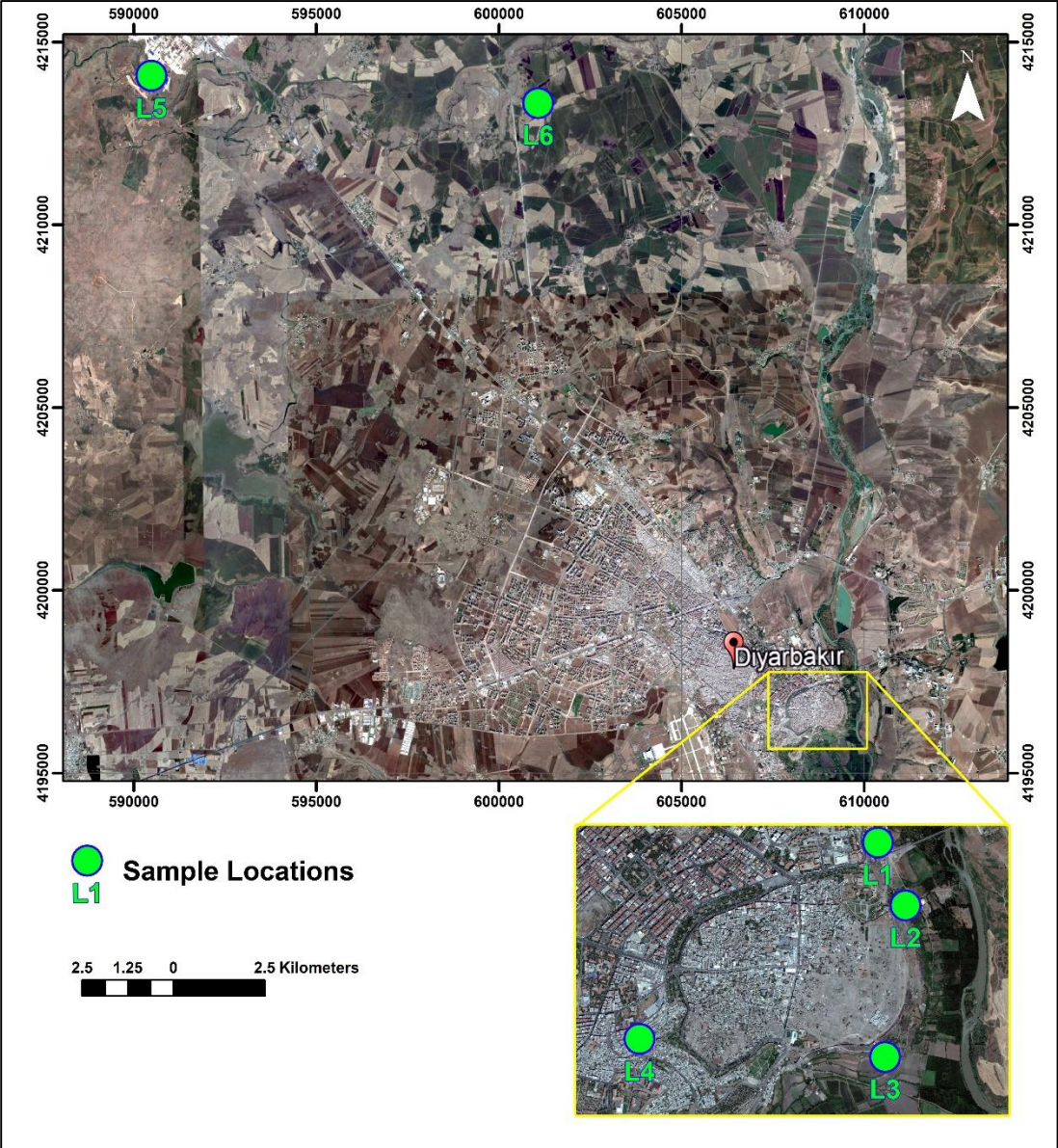


Figure 1.27 Location map for the fresh samples



Figure 1.28 The massive and vesicular basalt samples used in the experimental studies

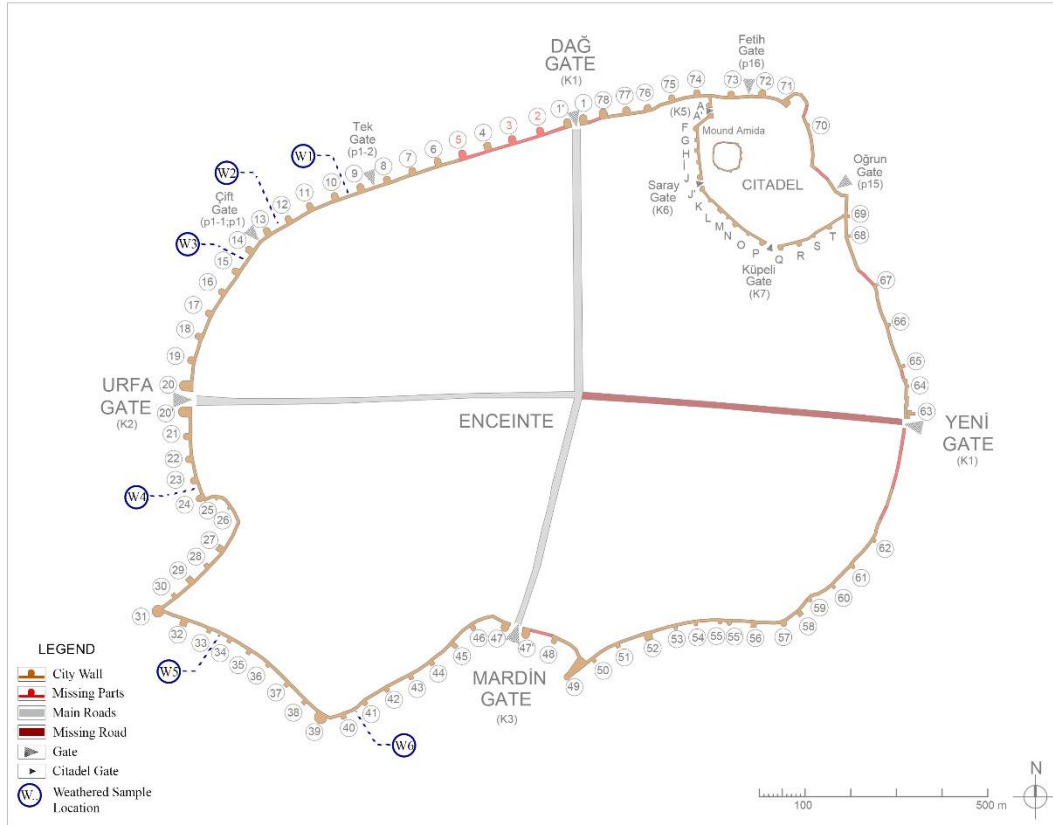


Figure 1.29 Location map for the weathered samples

1.9 Literature Review

This section summarizes the major studies related to the aim and scope of this dissertation. The literature review begins with the studies of the geology of the study area and vicinity, with a focus on the Karacadağ Volcanism. It will go on to discuss the weathering process and deterioration mechanisms of basalt and end with an overview of the engineering geological properties of basalt.

1.9.1 Previous Works on the Geology of the Site

Various authors have conducted studies to understand the geology of the region (e.g., İçerler, 1981; Şaroğlu and Emre, 1987; Perinçek et al., 1987; Ercan et al., 1990, 1991; Yılmaz and Duran, 1997; İmamoğlu and Çetin, 2007). Duran et al. (1988) investigated the Late Paleocene-Early Miocene deposits of the Silvan Group in the southeastern Anatolia. Bağırşakçı et al. (1995) conducted a comprehensive study to describe the geological units of Diyarbakır, Ergani and Çınar. The authors defined the lithologies, including the units outcropping in the study area by considering their age, thickness, contact relationships and depositional environments. Osmançelebioğlu et al. (2000) prepared a report for General Directorate of the Mineral Research and Exploration of Turkey (MTA) to investigate the land use dynamics of the city of Diyarbakır. The study defines proper sites for the urban development, landfills and industrial enterprises by evaluating the engineering geological properties of the proposed sites. In order to do so, the authors produced engineering geological, geomorphological and hydrogeological maps.

The DCW are built over the basalt of the Karacadağ Quaternary volcanic field. The Karacadağ Volcanism is the source of the basalt in the study area and has been described in the literature by different studies. There are plenty of discussions of the mineralogical, petrographic and geochemical properties of the Karacadağ Volcanism. The volcanic products of Karacadağ have been distinguished by different authors (e.g., Haksal, 1981; Şaroğlu and Emre, 1987; Ercan et al., 1990, 1991; Lustrino et al., 2010).

The work by Ercan et al. (1991) has subsequently been largely confirmed by other authors. The volcano-stratigraphic scheme proposed by Ercan et al. (1991) divides the activity of the Karacadağ Volcanism into three main phases. Pearce et al. (1990) conducted geochemical studies to understand the genesis of the Karacadağ Volcanism and proposed a model for foreland volcanism. In addition to these, there are many discussions available in the literature on the geochronological dating of the Karacadağ Volcanism.

Many studies (e.g., Sanver, 1968; Haksal, 1981; Pearce et al., 1990; Ercan et al., 1991; Notsu et al., 1995; Arger et al., 2000; Sen et al., 2004; Bridgland et al., 2007; Westaway et al., 2009; Lustrino et al., 2010) have been conducted to determine the age of the Karacadağ Volcanic rocks. The reported ages range from ~11 to ~0.1 Ma.

1.9.2 Previous Works on the Weathering Processes of Basalts

Weathering processes of the rocks and their products have often been reviewed in the literature. One of the early attempts to understand rock weathering was proposed by Goldich (1938) with an interest in the weathering of common rock-forming minerals. In his comprehensive study, the author established a mineral-stability series of weathering in the following order: olivine > augite > hornblende > biotite > plagioclase > K-Feldspar > quartz. Many of the researchers (e.g., Aomine and Wada, 1962; Craig and Loughnan, 1964; Humphris and Thompson, 1978; Chesworth et al., 1981; Colman, 1982; Bennett et al., 2001; Wilson, 2004; Carroll, 2012) have confirmed the stability principle of Goldich.

Basalt weathering and susceptibility to weathering have been widely discussed in the literature. The earlier studies on basalt weathering were summarized by Loughnan (1969), and many other authors have conducted studies to understand the weathering mechanisms of basalt. They studied basalts of different compositions in a variety of environments. The relevant literature is presented here with a brief review of their main results.

In order to determine the mineralogy of the sequences and to describe the secondary and alteration minerals, the authors used mineralogical, petrographic and chemical techniques, including thin-section examination, XRD, XRF, SEM/EDX, differential thermal analysis, methylene blue and electron probe microanalysis.

Craig and Loughnan (1964) found the weathering susceptibility order for basalt to be olivine > pyroxene > plagioclase > sanidine.

Another comprehensive study was conducted by Colman (1982) for the weathering characteristic of basalt and andesite, finding a susceptibility of the minerals in the order glass > olivine > pyroxene > plagioclase > amphibole > K-Feldspar > opaque minerals. According to Eggleton et al. (1987), the minerals of basalt have weathering susceptibility in the order glass ~ olivine > plagioclase > pyroxene > opaque minerals. According to Banfield et al. (1991), the order is glass, olivine > laihunite > clinopyroxene > orthopyroxene > plagioclase > K-Feldspar > magnetite > apatite > rutile > quartz, and according to Nesbitt and Wilson (1992), it is olivine > glass > plagioclase > clinopyroxene > Fe-Ti-oxides.

Based on these weathering sequences, volcanic glass and olivine are the most susceptible components of basalt. Pyroxene and plagioclase have intermediate stabilities, whereas quartz and opaque minerals are the least susceptible to weathering. Therefore, the influence of quartz and opaque minerals on weathering processes is assumed to be very small (Goldich, 1938; Smith, 1962; Craig and Loughnan, 1964). The studies reviewed indicate that the predominant weathering products of basalt are smectite, montmorillonite, vermiculite, iddingsite, kaolinite and chlorite.

Considering the dominant rock-forming minerals of basalt, many different products of weathering have been reported. These products may vary by the degree of weathering. Olivine, for instance, as the least stable component, most commonly altered to iddingsite (Gay and LeMaitre, 1961; Craig and Loughnan, 1964; Colman, 1982; Smith et al., 1987), vermiculite (Smith, 1957), serpentine and montmorillonite (Bell and Haskins, 1997).

The weathering products of pyroxene are reported to be montmorillonite (Craig and Loughnan, 1964; Bell and Haskins, 1997), smectite (Glasmann and Simonson, 1985; Banfield et al., 1991), vermiculite (Basham, 1974), kaolinite (Craig and Loughnan, 1964), goethite (Glasmann and Simonson, 1985) and chlorite (Colman, 1982). Plagioclase, another component that has an intermediate stability, weathers to montmorillonite (Craig and Loughnan, 1964), kaolinite (Craig and Loughnan, 1964;

Basham, 1974; Colman, 1982; Nesbitt and Wilson, 1992; Tugrul, 1995; Rasmussen et al., 2010), beidellite (Glasmann and Simonson, 1985), smectite (Basham, 1974; Eggleton et al., 1987; Banfield et al., 1991), and zeolite (Bell et al., 2000).

The weathering of amphibole is also reviewed in the literature and its main products are chlorite and vermiculite (Cawsey and Mellon, 1983; Kelsall et al., 1986). As a relatively stable component, the weathering products of feldspar are reported to be kaolinite (Tiller, 1958; Basham, 1974; Cawsey and Mellon, 1983; Helmi, 1994; Rasmussen et al., 2010), vermiculite (Smith, 1962; Cawsey and Mellon, 1983) and smectite (Banfield et al., 1991).

1.9.3 Previous Works on Basalt Deterioration

Although basalt has been extensively used in construction of various structures, there are still few studies of its deterioration mechanisms. Compared to other types of stone, little information about igneous rocks has been reported in the stone conservation literature. Grissom (1994) reviewed the literature and collected the studies on the deterioration of volcanic stones. Her comprehensive review mentions that only eight percent of the published papers on stone conservation refers to igneous rocks. Of the papers on the deterioration of igneous rocks, most focus on the deterioration of tuff (Grissom, 1994). Two comprehensive studies of the conservation of stone were published in very recent years. The first, published by the Getty Conservation Institute, is a literature overview on stone conservation, and the second, published by Documentation Center of the International Council on Monuments and Sites (ICOMOS), is a current bibliography on stone heritage. These studies were examined in detail and confirm the lack of studies on basalt deterioration (Price and Doehne, 2011; ICOMOS, 2015).

A literature review was performed to collect and review studies of basalt deterioration. Here, the main deterioration types and causes are discussed based on the studies reviewed. Caner and Türkmenoğlu (1985) studied the deterioration mechanisms of the

basalts used in reliefs at the Hittite site of Karatepe, Turkey. The Karatepe basalts are classified as olivine basalts with porphyritic texture. The authors reported exfoliations and cracks as the main deterioration forms on the reliefs. In order to simulate deterioration, the authors investigated cyclic wetting and drying, freezing and thawing and salt crystallization tests in the laboratory on fresh basalt samples collected from the site. Moreover, XRD, Transmission Electron Microscopy (TEM), infrared spectroscopy and thin section analysis were performed to identify clay fraction, mineralogical composition and the petrography of the Karatepe basalts. Five cubic samples were used for each cyclic test, and Na₂SO₄ solution was used for the salt crystallization test. The authors reported no visible decay after ninety-one wetting and drying cycles and eighty-six freezing and thawing cycles. However, authors reported the following observations at the end of the fiftieth cycle of salt crystallization test: crack development, rounding of corners and an almost ten percent weight loss from the initial weight of the tested samples.

Helmi (1994) investigated the deterioration mechanisms of some volcanic rocks in Egypt. Basalt was mainly employed there for making vessels, statues, paving roads and for the construction of temples. Helmi reported that, water, variations of temperature and ultraviolet (UV) radiation exposure are the main agents of the deterioration of volcanic rocks in Egypt. The author collected different volcanic rocks from the temples, including fresh and weathered basalt samples, and investigated XRD, SEM, atomic absorption and thin section analyses to identify the deterioration mechanism. Artificial weathering tests were performed on cubic samples for sixty cycles of exposure to UV radiation and immersion in distilled water. The author concluded that the fresh basalt samples have fine-grained textures and are black in color. Their mineralogical composition consists of augite (a mineral in pyroxene group) and grunerite (a mineral in amphibole group). The weathered basalt samples are pale grey, very friable, and their mineralogical composition consists of augite. Artificial weathering revealed that the basalt cubes became pitted, and the pits were filled with hematite and goethite. Finally, SEM examination of the artificially weathered basalt showed mineral alterations, crack formations and again pits.

Ismail (2004) has also studied the deterioration mechanisms of weathered basalts in Egypt, with a special emphasis on those used for the pavements and walls of mortuary temples. This study identified water and variations in daily temperature as the principal agents of deterioration, and observed deterioration forms on the structures such as flaking, granular disintegration, discoloration, biological colonization and efflorescence. The author collected weathered basalt samples from different temples to analyze the mineralogical and petrographic properties using SEM/EDX, XRD, thin section examination, and to investigate index properties such as porosity, bulk density and water absorption. Cyclic tests were also performed on fresh basalts to understand the long-term performance of the material. These tests were wetting and drying, chemical attack with H₂SO₄ and salt crystallization.

Unlike Caner and Türkmenoğlu (1985), the author used NaCl solution for the salt crystallization test. Cubic samples (the number of samples for each test was not mentioned) were subjected to salt crystallization and chemical attack tests for thirty cycles, and wetting and drying for forty cycles. However, the results and observations on the material's behavior under the cyclic loads were not mentioned in the study. On the other hand, the author did summarize the petrographic results of weathered basalts. Plagioclase was partially weathered and replaced by secondary clay minerals along the fractures Olivine was replaced by its common forms of iddingsite and serpentine. Pyroxene was replaced by iron-rich kaolinite, whereas clinopyroxene was partially weathered to smectite. Finally, the study reported that the opaque minerals remained undisturbed and unaltered in the basalt.

El-Gohary and Al-Shorman (2010) investigated the effect of climate on the decay process of the basalts used in the Greco-Roman structures located at the Umm Qeis archaeological site in Jordan. Exfoliation was reported as the major deterioration form observed on the site. Material loss, crust formations and salt crystallization were also observed. The authors reported that climatic conditions are the principal factors of the decay process, and that thermal dilatation, microbiological infection, vibration and ice pressure were other aggressive factors of the decay mechanisms that affect basalt artifacts. Twenty-four samples were collected to represent different forms of

exfoliation in the study area. To analyze the samples, the authors used SEM/EDX, XRD and polarized microscope. The authors concluded that the exfoliation observed on the structures were mostly due to factors such as climatic conditions, cooling and heating cycles, solubility and crystallization effects, expansion and contraction, and microbiological effects.

There are some other studies that partially reported basalt deterioration. Nishiura et al. (1996) conducted a conservation study of the basalts used in the reliefs of the Ain Dara Temple in Aleppo, Syria. The authors observed exfoliations, detachments, cracks and biological growth on the temple. The main agents and causes of the deterioration were specified by the authors as water, freezing and thawing, precipitation, uneven topography and human vandalism. The authors proposed different methods to overcome these problems such as filling the cracks with the proper type and viscosity of epoxy resin and providing a tent-like shelter to stop interaction of water with the reliefs. Bell and Haskins (1997); Bell et al. (2000); and Sumner et al. (2009) studied the durability and deterioration of the basalt employed for the Katse Dam in Lesotho, South Africa. The authors noted that crazing, an extensive microfracturing, develops in some basalts. Bell and Haskins (1997) reported that these microfractures in basalt expand with time and cause the material to disintegrate into gravel-sized fragments. They also cause to further mineralogical alteration and structural weaknesses in the rock. They emphasized, “while basalt is exposed, clay minerals which are at or near the surface either absorb or lose moisture and in so doing swell or shrink, respectively. Repeated hydration and dehydration results in mechanical disruption of small portions of the rock close to the surface, causing flaking and surface cracking. The process is self-perpetuating as the formation of these cracks allowing access of water into the basalt, causing an increase in the degree and rate of breakdown” (Bell and Haskins, 1997).

The principle deterioration factors in this study area were reported by Sumner et al. (2009) as the expansion of the swelling montmorillonite and active zeolites occurring within the rock mass. The authors linked the presence and influence of the active minerals to the texture and permeability of the parent rocks.

Wedekind et al. (2011) investigated the weathering of the different stone types including vesicular basalts in the Valley of Mexico. Basalts were mostly used there for basements. The authors mentioned that two major deterioration forms on the basalt as scaling, up to one centimeter, and rounding by sanding and splitting.

Graue et al. (2011) studied the decay of different stone types used in the Cologne Cathedral. Various stone deteriorations were reported, including scaling, crumbling and flaking for sandstones and trachyte. Basalt was used in the cathedral to a very small extent, and the authors reported that it is highly resistant against weathering, but susceptible to microbiological activity due to its large pores.

Similar to the Graue et al. (2011), many authors have reported biodeterioration for basalt. Jackson and Keller (1970) studied the effect of lichen colonization on the intensity of chemical weathering. The authors reported that the rate of the chemical weathering on basalt is “considerably more intense in the presence than the absence of the lichen.” Jones et al. (1980) analyzed lichen weathering on basalt using SEM, XRD and thin sections. They reported that lichen colonization causes the decomposition of the minerals that form basalt and observed extensive surface corrosions, round edges and etch marks on the primary rock-forming minerals, especially on labradorite. Warscheid and Braams (2000) reported patina formation on basalt used as building stone. Chen et al. (2000) studied lichen colonization and its effect on different rock materials. Based on their studies, it has been experimentally demonstrated that pyroxene, olivine and feldspar, the main rock-forming minerals of basalt, are all susceptible to the attack of organic acids.

Etienne and Dupont (2002) studied biochemical weathering on basalts in a cold environment (Iceland) using SEM/EDS and XRD. Their study focused on the effects and types of fungal communities in the development of weathering rinds on basaltic deposits.

The authors reported ribbing patterns on feldspars and flaking on plagioclases. Aghamiri and Schwartzman (2002); Gordon and Dorn (2005); and Scheerer et al. (2009) reported that lichen growth causes mechanical damage and increases the weathering rate of basalt.

1.9.4 Previous Works on the Engineering Geological Properties of Basalts

Over the years, many studies have investigated the engineering geological properties of basalt. Many different approaches and methods have been used to calculate the physico-mechanical properties of basalts. The tests mostly measure such material properties as unit weight, porosity, water absorption, uniaxial compressive strength, point load index, P-wave velocity, modulus of elasticity, Poisson's ratio and internal friction angle.

Even rocks with the same composition and pore structure can have significant variations in material properties (DeLan and QiaoLin, 2014). In other words, as Kühnel et al. (1994) mentioned in their study on the role of the clay minerals on the durability of basaltic rocks, the quality of basalt varies from region to region. This is due to the heterogeneity of the rock itself, more specifically “to the heterogeneity of conditions in which the rock was formed and cooled down.” The authors emphasize that “the scale of such variability is a matter of meters” (Kühnel et al., 1994). Therefore, it is essential to correlate basalts from different regions, compositions and textures. In order to do so, a large amount of paper, reports and books has been reviewed to understand and evaluate the variability of basalts, especially regarding their material properties.

Aggistalis et al. (1996) studied amygdaloidal basalts in northern Greece to correlate their material properties. The basalt in this study had some secondary minerals, and the amygdales (microcavities) were mostly filled with calcite, which affects their index properties. Tuğrul and Gürpınar (1997) investigated the Eocene basalts in the Niksar region to determine the effect of weathering on their engineering properties.

The authors proposed a weathering classification for basalts based on the following criteria: the color of the rock mass, the color of discontinuous surfaces, rock and soil ratio, rock hardness, and the existence of core stones and their identity.

In addition to the cited works, the following works were also conducted to determine the engineering geological properties of the basalts from various regions. Özsan and Akın (2002) studied the basalts employed in construction of Uruş Dam, Ankara; Gürocak and Kılıç (2005) investigated basalts of Toprakkale, Adana; Koçbay and Kılıç (2006) examined basalt used in Obruk Dam, Çorum. Gomes and Rodrigues (2007) dealt with massive and columnar basalts of southern Brazils; Graue et al. (2011) surveyed decay forms and mechanical properties of the basalts used in the Cologne Cathedral, Germany. DeLan and QiaoLin (2014) carried out a study on mechanical properties of the vesicular basalts in Hainan, China; Engidasew and Barbieri (2014) conducted a research on basalts with fluidal and porphyritic textures from Central Ethiopia to identify their engineering geological properties, and Endait and Juneja (2015) experimentally measured physico-mechanical properties of the Eocene basalt in Mumbai, India.

Many other authors focus on the importance of fractures and porosity on the mechanical properties of basalts. (e.g., Brace et al., 1972; Kranz, 1983; Al-Harathi et al., 1999; Tuğrul, 2004; Stanchits et al., 2006; Atzeni et al., 2008; Leyland et al., 2015; Hasancebi, 2016). Kelsall et al. (1986), for instance, claimed that “a rock with a porosity of five percent will generally have a compressive strength less than seventy percent of the same rock with zero porosity.” The porosity of vesicular basalts that have porphyritic texture was discussed by Al-Harathi et al. (1999). This study claimed that conventional tests for measuring porosity are unsuitable if the pores are non-connected. To overcome this problem, they suggest an image analysis technique, which estimates the porosity of vesicular basalts. In her study, on the weathering grade and engineering properties of different rocks, Tuğrul (2004) correlated some physico-mechanical properties with basalts of different weathering grades, i.e., from fresh to highly weathered. According to the results, unit weight, average pore diameter and uniaxial compressive strength of the rock fall as weathering grades rise. She also

observed that water absorption, total porosity and effective porosity rise with weathering grade. Karakuş and Akatay (2013) conducted a study of the physico-mechanical properties of basalt outcrops in Diyarbakır.

The authors, found an empirical relationship between P-wave velocity and the index properties of the rock material. Hasançebi (2016) investigated vesicular basalts from Diyarbakır to determine the impact of porosity on uniaxial compressive strength. This study's results are in accordance with the other studies, and she concluded that the uniaxial compressive strength of the rock falls as porosity increases.

A summary of the results from the selected studies on the basalt is shown in Table 1.5.

Table 1.5 Physico-mechanical properties of basalts based on the reviewed studies

References	Engineering Properties					
	Unit Weight	Porosity	Water Absorption	Uniaxial Compr. Strength	Elastic Modulus	Tensile Strength
	(kN/m ³)	(%)	(%)	(MPa)	(GPa)	(MPa)
Aggitalis et al. (1996)	•	•	•	17.1-91.2* (46.65)†	•	•
Tuğrul and Gürpınar (1997)	25.2-26.4* (25.4)†	0.3-2.9* (1.4)†	•	88.4-129* (106.1)†	44-71* (56)†	8.8-9.5* (8.79)†
Özsan and Akın (2002)	22.1-25.7* (24)†	3.0-3.5* (3.2)†	•	64-249* (142.0)†	40	6.2-8.3* (7.25)†
Kılıç et al. (2003)	•	1.7	1.2	86.2	•	13.5
Yaşar and Erdoğan (2004)	26.67	1.37	•	111.5	•	•
Tuğrul (2004)	25.7-28.4*	0.3-3.4*	3.5-5.5*	86.0-136.0*	•	•
Dinçer et al. (2004)	25.3-26.5* (25.7)†	•	•	65-108* (86.4)†	21.7-21.1* (16)†	•
Korkanç and Tuğrul (2004)	25.1-28.4*	1.86-10.87*	0.3-1.2*	125.8-262.5*	•	•
Gürocağ and Kılıç (2005)	23.1-28.1* (25.5)†	0.71-13.39* (6.35)†	0.4-8.8* (3.53)†	8.7-76.4* (40.6)†	•	•
Justo et al (2006)	27.4	•	•	20-150* (69.0)†	44-80* (60.9)†	•
Koçbay and Kılıç (2006)	22.5-28.3* (25.7)†	2.1-14.9* (7.17)†	0.14-5.3* (1.2)†	9.8-130.2* (52.5)†	8.9-89* (39.25)†	•
Gomes and Rodrigues (2007)	28.7-28.9*	0.6-1.5*	0.2-0.5*	86.0-290.0*	•	•
González De Vallejo et al. (2008)	23-28*	•	•	40-80*	15.0-30.0*	•
Graue et al. (2011)	24.71	13.3	•	63.1-72.1*	•	5.0-5.9*
Karakuş and Akatay (2013)	16.8-26.5*	0.9-12.9*	•	17.2-145.1*	5.2-66.4*	•
DeLan and QiaoLin (2014)	•	12.0-27.1*	•	28-140.5*	9.7-20.5*	•
Engidasew and Barbieri (2014)	•	0.9-3* (1.9)†	0.3-1* (0.6)†	130-351* (249)†	64-129* (99)†	•
Endait and Juneja (2015)	20.7-28.1* (25.6)†	1.3-19.6* (7.1)†	0.5-9.1* (2.8)†	2.2-181.7*	22-75*	•
Hasançebi (2016)	20-28.1* (24.5)†	3.6-6* (4.8)†	•	23.9-172.8* (55.3)†	•	•

* Minimum and maximum values of test results; † Mean values; • Not measured

1.10 Layout of the Dissertation

This dissertation has eight chapters. This introductory chapter (Chapter 1) has ten sections which discuss the aim and scope of the study, the geographic and historical settings of the DCW, the history of interventions, construction techniques and architectural features of the DCW. The chapter then describes the research methods, sampling stage and reviews the literature on the geology of the study area, weathering processes, deterioration mechanisms and engineering geological properties of basalts. It ends with the layout of the study.

The second chapter mainly focuses on the geology of the site and its vicinity, with particular emphasis on its geological units.

The petrographic and geochemical properties of the fresh basalts are examined in Chapter 3.

Chapter 4 examines the physico-mechanical properties of the fresh basalts in various experimental studies.

Chapter 5 gives a comprehensive account of the deterioration of the basalts used in the DCW. It has five sections. The first section documents the common weathering forms on the DCW. The next section presents weathering maps of two selected sections. The following section examines the durability of the massive and vesicular basalts in wetting-drying, freezing-thawing and salt crystallization accelerated weathering tests. The next two sections of this chapter concentrate on the petrographic and geochemical properties of weathered basalts and their microfracture properties.

Chapter 6 assesses the basalts' durability by average pore diameter, saturation coefficient and wet-to-dry strength ratio.

The experimental results of this study are summed up and discussed in Chapter 7. Finally, concluding remarks with some recommendations are outlined in Chapter 8.

CHAPTER 2

GEOLOGY

This chapter describes the geological setting of the study area and its vicinity. It discusses the lithostratigraphic units of the region (from older to younger) with special emphasis on the exposed units in the study area.

2.1 Regional Geology

In order to specify the distribution of the units, many authors (Perinçek et al., 1987; Şaroğlu and Emre, 1987; Duran et al., 1988; Ercan et al., 1990, 1991; Yılmaz, 1993; Bağırşakçı et al., 1995; Yılmaz and Duran, 1997) have studied the region. The units outcropped in the region have been well identified; however, there are some ongoing discussions on the description and naming of the units, especially those exposed in the study area.

The following stratigraphic summary of the region was compiled from Bağırşakçı et al. (1995) and Yılmaz and Duran (1997). The lithostratigraphic units exposed in and around the study area are characterized by volcanic and sedimentary units of Middle-Late Eocene to Holocene. Based on the previous studies conducted in the region, a generalized stratigraphic column depicting various geological units of the region is presented in Figure 2.1.

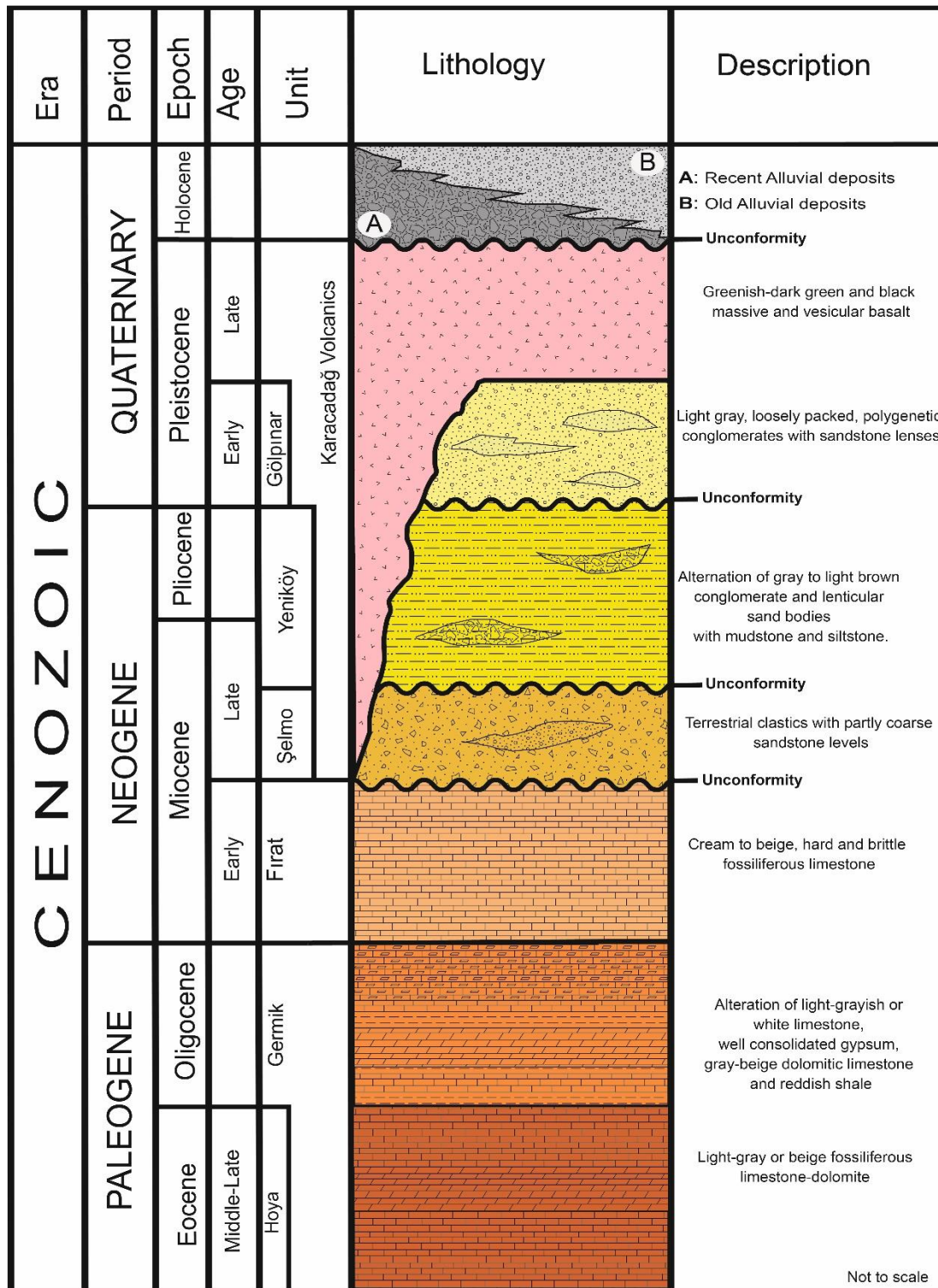


Figure 2.1 Generalized columnar section of the study area (Modified from Bağırşakçı et al., 1995)

The oldest unit cropping out north of the study area was reported by Yılmaz and Duran (1997) as Hoya formation, the lower part of Midyat Group.

This formation is exposed in the village of Hoya near Çüngüş, a district of Diyarbakır. The Hoya formation is characterized by light gray or beige fossiliferous limestone with laminations and poorly sorted dolomite and conglomerate. Although the formation is not exposed in the study area, it has been reported in drillers' logs at a depth of some 200-300 meters in the study area. The unit has been observed at depths of 67 meters at Ergani, 47 to 118 meters between the Dicle and Hani; and at 94 to 352 meters near the Hazro districts (Yılmaz and Duran, 1997). The Eocene-Oligocene aged Hoya formation is overlain conformably by Germik formation (Bağırsakçı et al., 1995; Yılmaz and Duran, 1997).

The Germik formation is the youngest member of the Midyat Group. As Yılmaz and Duran (1997) documented in their study, the formation was first named by Bolgi (1961). The Germik formation can be clearly observed near Çınar, a district of Diyarbakır. The total thickness of the formation ranges between 40 to 220 meters. The formation is composed mainly of light grayish or white limestones, well consolidated gypsum, gray-beige dolomitic limestone and reddish shale. The unit was deposited in a regressive and shallow-marine environment. Similar to the Hoya formation, the Germik formation is not exposed in the study area. The Middle Eocene-Oligocene aged Germik formation is conformably overlain by Fırat formation of Silvan Group (Yılmaz and Duran, 1997).

The Fırat formation, the middle member of the Silvan Group. It is mostly cropping out in the northern parts of Diyarbakır. The formation is composed of cream to beige, hard and brittle fossiliferous limestone. The total thickness of the formation in the region is about 150 meters. The deposition of formation was in the shallowest part of the carbonate platform. The Early Miocene aged Fırat formation is unconformable with the Kapıkaya formation, the lowest member of Silvan Group and Şelmo formation (Figure 2.1).

Consisting of terrestrial clastics and conglomerates with partly coarse sandstone levels, the Şelmo formation was first named by Bolgi (1961) (In Yılmaz and Duran, 1997). The unit, which is not observed in the study area, is exposed near the village of Şelmo in Sason, a district of Batman. The average thickness of the Late Miocene Şelmo formation is 455.53 meters (İmamoğlu et al., 2014). According to İmamoğlu et al. (2014), the thickness of the formation has been measured as 500 meters near Çermik and Çüngüş districts of Diyarbakır. The formation was deposited in a transitional zone of beach sand and tidal-flat environments (Yılmaz and Duran, 1997).

This formation is frequently confused with Yeniköy formation cropping out in the study area (İmamoğlu, 1993; Yılmaz and Duran, 1997). The succeeding units as Yeniköy formation, Gölpınar formation, Karacadağ volcanics and alluvials are exposed in the study area. These units will be discussed in detail in the next section.

2.2 Geology of the Site Vicinity

This section was prepared based on the studies reviewed, field observation and current maps. However, most of the information was compiled from Bağırşakçı et al. (1995) who gives detailed geological information about Diyarbakır and its vicinity.

Based on the previous studies conducted in the study area, a simplified geological map was prepared on the 1/25.000 scale topographical map of the study area. The distribution of these units is represented in the geological map of the study area (Figure 2.2). In the following sections, the geological units cropping out in the study area will be detailed from older to younger as:

- a) Late Miocene-Pleistocene aged Yeniköy formation
- b) Quaternary aged Gölpınar formation and Karacadağ volcanics
- c) Quaternary aged alluviums

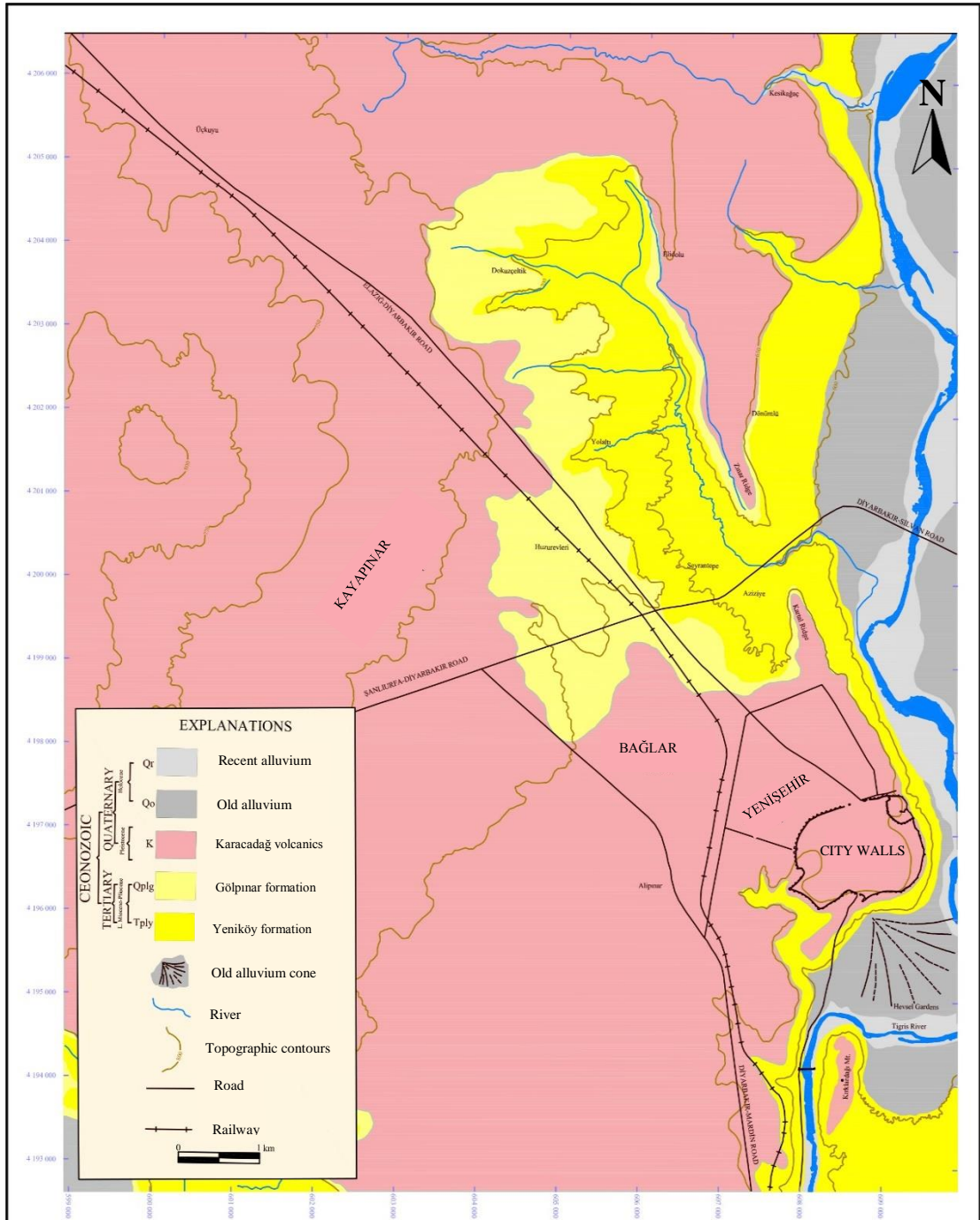


Figure 2.2 Geological map of the study area (Modified from Osmañelebioğlu et al., 2000)

2.2.1 Yeniköy formation (Tply)

This formation, the oldest unit in the study area, was defined by Ercan et al. (1991). The Yeniköy formation is exposed in the east and the south parts of the study area. It is best exposed at the west of the village of Yeniköy on the south bank of the Tigris River and along the northern foothills of Kırklardağı Mountain (Figure 2.3).



Figure 2.3 A view of the Yeniköy formation over the Kırklardağı Mt.

The bottom contact of the formation is not observed in the study area; however, the top contact is clearly observed in the north part of the study area near the village of Şilbe (Yolaltı) (Dursun, 2008). Here, the formation is overlain unconformably by Gölpınar formation on an erosional surface (Figure 2.4). However, in the study area, the formation is overlaid by the Karacadağ volcanics (Figure 2.5).

Yeniköy formation is characterized by the alternation of conglomerate and sandstone lenses with mudstone and siltstone. The gray to light brown conglomerate and sandstone observed in the formation are medium to thick-bedded, polygenetic, graded and well sorted. They have a grain size ranging from 1 to 10 centimeters. The conglomerate lenses include sandstone lenses and the voids between the grains are filled with fine sand and silt.

The poorly cemented conglomerate shows no distinct bedding. The thickness of the formation along the Tigris River is 50 meters and 90 meters in the north of the study area (Dursun, 2008). Bağırsakçı et al. (1995) assigned a Late Miocene / Pliocene age for the formation, based on its fossil content. The formation was deposited in a flood plain.



Figure 2.4 Contact relation of the Yeniköy formation and the Gölpınar formation at the north of the study area (the contact is indicated by yellow line)

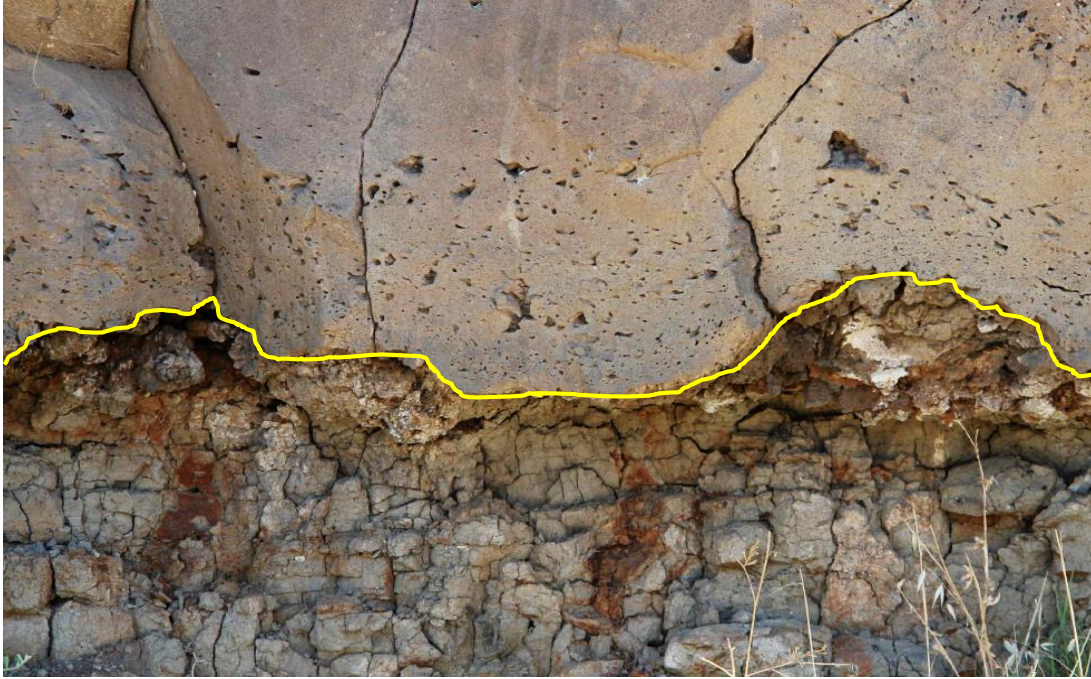


Figure 2.5 Contact relation of the Yeniköy formation and the Karacadağ volcanics near the Citadel (the contact is roughly indicated by yellow line)

2.2.2 Gölpınar formation (Qplg)

The Gölpınar formation is the other unit of the study area and was defined by Ercan et al. (1991). It is exposed mostly in the northwest section and partially in the south section of the study area. The formation is well exposed near the village of Gölpınar on the Diyarbakır-Silvan road. The lower contact of the formation overlies the Yeniköy formation on an erosional surface, whereas the upper contact is overlain by the Karacadağ volcanics. The formation is characterized by light gray, loosely packed, polygenetic conglomerates with lens-shaped sandstone levels (Figure 2.6). The conglomerates have an average grain size of five centimeters in diameter. The voids are mostly filled with fine sand and cemented by carbonate. There are also lenticular sand bodies embedded in the formation (Figure 2.7). The observed thickness of the formation in the study area ranges between 5 to 30 meters.

Although no fossil evidence was found by Bağırşakçı et al. (1995), regarding the age of the Gölpınar formation, the authors assigned a Pleistocene age on the basis of such

properties of formation as overlying the Yeniköy formation, loosely packaged, weakly cemented and less altered. The formation is a braided-river deposit.



Figure 2.6 A view of the Gölpinar formation at the north of the study area

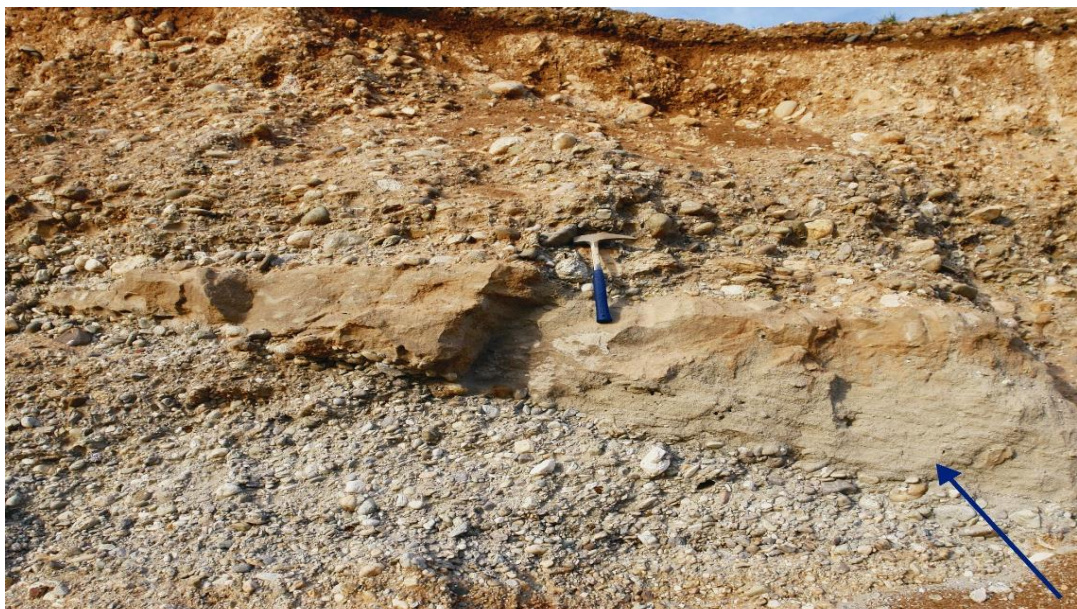


Figure 2.7 Lenticular sand body within in the Gölpinar formation (the lens is indicated by the blue arrow)

2.2.3 Karacadağ volcanics (K)

The Karacadağ volcanics are the dominant lithology employed in the construction of the DCW. They are derived from a typical shield volcano *ca.* forty-five kilometers southwest of the study area. Ercan et al. (1991) divided the volcanic activity of the Karacadağ into three main phases. According to the proposed scheme, the Siverek volcanic complex is defined as the first phase of the activity. The complex covers an area of *ca.* 10,000 square kilometers to the south and west of Diyarbakır and was determined by K-Ar dating to be Late Miocene. The second phase is defined as the Karacadağ volcanics, which resulted in the development of 1,957-meter-high Karacadağ Volcano and includes the basalt beneath the DCW (Figure 2.8). The most recent phase of the Karacadağ Volcanism is defined as the Ovabağ Volcanics. They are spread over the southeastern and eastern edges of the study area. The Ovabağ Volcanics, the youngest volcanics, are fresh looking basalts. It is claimed that the volcanic rocks of Ovabağ erupted during the Quaternary with dates ranging from Middle Pleistocene to Late Pleistocene (Ercan et al., 1991; Bridgland et al., 2007; Westaway et al., 2009; Lustrino et al., 2010).

In order to understand the genesis of the Karacadağ volcanism, Pearce et al. (1990) conducted geochemical studies. They stated that Karacadağ is a low shield volcano and its generation was controlled by N-S compression accompanied by E-W extension tectonic dynamics. Based on the findings, the authors identified the common characteristics of the Karacadağ lavas as predominantly basic and mildly alkaline.

The major, trace and isotope compositions of the Karacadağ volcanics indicate that their parental magmas may have been generated by low degree partial melting of a garnet lherzolite mantle source.

These magmas, which do not have any subduction signatures, may have been exposed somewhat to crustal contamination during their magmatic evolution. This characterization of the Karacadağ Lavas defined by the Pearce et al. (1990) has been widely accepted and enhanced by other studies (Ercan et al., 1991; Notsu et al., 1995; Arger et al., 2000; Sen et al., 2004; Lustrino et al., 2010, 2012).

These studies show that the basalt beneath the DCW belongs to the second phase of activity and are classified as Karacadağ volcanics (Figure 2.8).



Figure 2.8 A general view of the Karacadağ volcanics at the north of the study area

Many studies available in the literature discuss the activity of the Karacadağ Volcanism. These mostly focus on the dating of the volcanic rocks. Here, the geochronological studies, especially of the second phase of the volcanism, are discussed.

Sanver (1968) was among the first to assign an age to the basalts outcropping in Diyarbakır province. He sampled three basaltic flows in the region and dated two of them to 1.45 ± 0.10 and 1.04 ± 0.10 Ma. Research on dating Karacadağ volcanics was also performed by Haksal (1981). In his dissertation, the author geochemically investigated and dated the basalts. Haksal dated the basalts to 10 ± 0.30 and 1.3 ± 0.10 Ma. Pearce et al. (1990) dated the volcanic complex of the study area to 0.94 ± 0.33 and 0.83 ± 0.88 Ma. Notsu et al. (1995) collected eight samples from different phases of the Karacadağ volcanics and determined their K-Ar ages with a range of 1.9 ± 0.14 and 0.10 ± 0.01 Ma.

Bridgland et al. (2007) carried out a geochemical and geochronological study of the basalt outcrops above the Tigris River where the DCW were built. The authors carried out new high-precision Ar-Ar dating for the basalt in Diyarbakır province. The new date of *ca.* 1.2 ± 0.01 Ma assigned to the collected sample is concordant with the results obtained by Sanver (1968). Westaway et al. (2009) investigated a K-Ar dating study on the units of the Karacadağ Volcanism in Diyarbakır province. The authors collected samples along the Tigris River and its vicinity and dated them to 1.22 ± 0.02 and 1.07 ± 0.03 Ma. They also dated the relatively younger basalt outcrops *ca.* 14 kilometers southeast of the DCW to 0.43 ± 0.02 Ma.

The Karacadağ volcanics, exposed in the study area unconformably overlie the Yeniköy formation. The volcanics are mostly composed of basalt. They are characterized by greenish dark green and black, finely grained. They came from generally massive basaltic lava flows and have pyroclastic levels. There are also cliffs of columnar basalt and cooling joints can be seen at the northeastern and eastern sections of the study area (Figure 2.9). In addition to the study area, the unit crops out widely north and west of the DCW. Vesicular texture is common for the basalt exposed in the study area. There is also massive texture basalt with some joints in the study area. The observed thickness of the unit in the study area ranges from 2 to 98 meters (Dursun, 2008). The K-Ar dating conducted on the Karacadağ volcanics by various authors reveals that this second phase began in Pliocene and continued through Pleistocene.



Figure 2.9 A cliff of columnar basalt at the northeastern section of the DCW

2.2.4 Alluvial deposits (Qal)

There are alluvial deposits formed by the Tigris River in the study area. These deposits are classified as Old and Recent Alluvium. The observed outcrop patterns suggest that the alluvial units might be deposited along the abandoned lateral channels of Tigris River or by old alluvial fans. The grain size of the alluvial deposits decreases upwards (Kuzucuoğlu and Karadoğan, 2015).

Although there is no evidence for the age of the unit, an age of Quaternary was suggested by Ercan et al. (1991) and Bağırsakçı et al. (1995).

The alluvium deposited along the banks of the Tigris River is classified as the old alluvium (Figure 2.10). The unit consists of five terraces, and they were formed as a result of the deepening of the Tigris Valley. The thickness of the terrace deposits attains an elevation of more than 50 meters (Kuzucuoğlu and Karadoğan, 2015). This unit contains more sand and silt sized materials than the recent alluvium.



Figure 2.10 A view of the old alluvium from the Kırklardağı Mt.

The recent alluvium is also deposited in the study area. The recent alluvium was formed along the Tigris River and is composed of unconsolidated gravel, sand, silt and clay. The recent alluvium can be seen in the east and south of the DCW (Figure 2.11). The unit is mostly derived from the older rocks exposing in the north of the region (Bağırsakçı et al., 1995).



Figure 2.11 A general view of the recent alluvium depositions at the Tigris River

CHAPTER 3

PETROGRAPHIC AND GEOCHEMICAL PROPERTIES OF THE BASALTS

The locally available basalt material originated from the lava eruptions of Karacadağ volcano *ca.* 40 kilometers southwest of the DCW. Ercan et al. (1991) have divided the volcanic activity of the Karacadağ into the three main phases. The basalts employed in the construction of the DCW belong the second phase of the activity and are classified as Karacadağ Volcanics. The petrographic and geochemical properties of the Karacadağ Volcanics basalts will be assessed based on fresh samples collected during field studies. Since the field observation and sampling stage have been discussed in the previous chapters, this chapter will discuss the mineralogical, petrographic and geochemical properties of the massive and vesicular basalts as determined by laboratory studies.

3.1 Mineralogical and Petrographic Properties of the Basalts

Mineralogical composition, texture and structure are the main factors controlling the physico-mechanical properties of rock materials. Therefore, it is essential to define mineralogical and petrographic characteristics of rock materials to evaluate their engineering properties accurately (Zaleskii, 1967; Bell, 1992).

This section concerns the mineralogical and petrographic features of the samples collected from the study area. It will discuss studies, including polarizing optical microscopy, SEM, XRD and the methylene blue adsorption test.

3.1.1 Optical Microscopy

The mineralogical and petrographic studies were based on the examination of the basalt samples. For this purpose, more than thirty thin sections were prepared from the fresh massive and vesicular basalt samples, from the samples used in accelerated aging tests and finally, from the weathered samples. For the petrographic examinations of the samples, Nikon microscopes were used, and photomicrographs were acquired using a Nikon camera located in the Department of Geological Engineering of METU.

The sections were examined under a polarizing microscope to determine and quantify their mineral composition, texture and structure. Particular attention was paid to the identification of the rock-forming minerals and the presence of secondary minerals. Grain sizes, grain boundaries, bonding structure, microfractures and type of matrix were also described.

Much attention was devoted to the thin sections made from the weathered samples. The sections of the weathered samples were systematically prepared to provide a continuous view of the weathering depth. The details of the mineralogical and petrographic studies performed on the fresh basalt samples will be discussed in the following section; however, the studies performed on the samples used in the accelerated aging tests and on the weathered samples will be discussed in the subsequent chapter (see Chapter 5).

In hand specimen, basalts are brown, dark grey and black. Some of them contain secondary minerals. The basalts are subdivided by texture into massive and vesicular groups. Thin section views show that the mineral assemblages of the massive and vesicular basalts are similar and characterized by the presence of plagioclase, pyroxene and olivine minerals, which are commonly euhedral to subhedral in shape.

The groundmass is composed largely of plagioclase. The plagioclase microlites are more likely to be lath-shaped, and less pyroxene is found in their groundmass (Figure 3.1). The presence of the secondary minerals can also be seen in the thin sections, and especially easily in some vesicular samples with calcite precipitations (Figure 3.2). Opaque minerals are also observed in the studied samples (Figure 3.3).

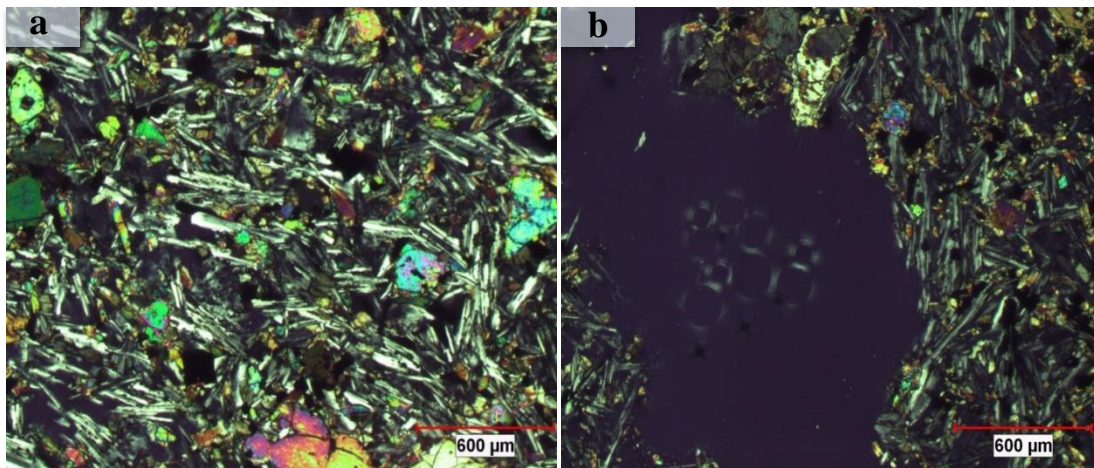


Figure 3.1 Photomicrograph illustrating overall mineralogical and textural features of the fresh (a) massive and (b) vesicular basalt samples

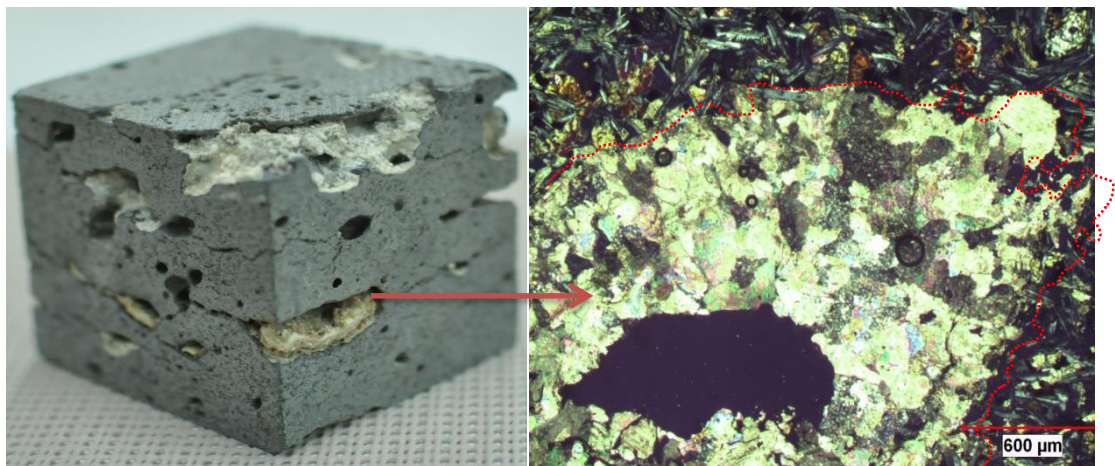


Figure 3.2 Hand specimen and photomicrograph view of a vesicular sample displaying calcite replacement (calcite filling is roughly indicated by the dotted lines)

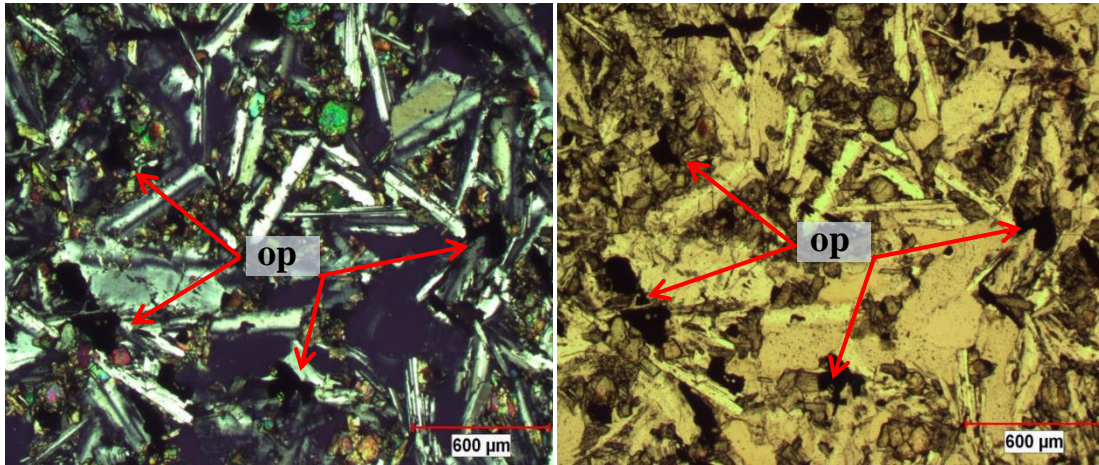


Figure 3.3 Opaque minerals (op) in the massive sample (left: xpl; right: ppl view)

3.1.2 Methylene Blue Adsorption Test

The methylene blue adsorption test was performed to quantify the presence and properties of clay minerals in the basalt samples. The spot method proposed by AFNOR (1980) was used during the test.

Since the methylene blue dye is hygroscopic and the normality of the methylene blue solution is not included in the methylene blue adsorption value (MBA), the MBA was not used for the evaluation of the test results. Instead, the CEC of the samples was used because the normality of the methylene blue solution was included in the calculation of the CEC of the bulk samples (Topal, 1996).

This test was performed on 8 fresh massive and vesicular basalt samples. The CECs of the massive basalt samples range from 0.60 to 1.52 meq/100 g, with an average of 0.85 meq/100 g, whereas the vesicular samples have CECs between 0.30 and 1.21 meq/100 g, with an average of 0.70 meq/100 g. According to the test results, the CECs of the bulk massive and vesicular basalt samples are very low. Therefore, the significant amount of clay is not expected in the bulk samples tested.

3.1.3 Clay Fraction Determination

In order to determine the clay fraction of the basalt, six fresh basalts samples were used. The experiment was conducted based on the procedures suggested by Jackson (1979); and Moore and Reynolds (1989). For the experiment, 10 grams of powdered sample was weighed and transferred to a 1000-ml beaker, which was then filled with distilled water. In order to prevent flocculation a minimal amount of (*ca.* 250 mg) of sodium polyphosphate was also added to the beaker. The beaker was stirred using a mixer for 2 minutes, and by following the Stokes law, the solution was left to stand for eight hours in the laboratory conditions. At the end of the eight hours, the suspension was siphoned from a depth of 200 ml, which corresponds to 10 centimeters, to extract clay size particles (the first siphoned suspension was set aside to use in XRD analysis, which will be discussed in the following section). The siphoning of the clay size particles was repeated every eight hours until the suspension became clear. Afterward, the beaker was oven-dried and weighed to calculate the fraction of the clay. The clay percentages of the massive and vesicular samples are shown in Table 3.1.

Based on the tested samples, the massive samples have a clay fraction ranging between 3.46 and 4.41 %, with an average of 4.20%. On the other hand, the clay fraction of the vesicular samples is between 3.61 and 5.68%, with an average of 4.48%.

Table 3.1 Clay fraction of the massive and vesicular basalt samples

Sample	Clay Fraction (%)
Massive I (1M)	3.46
Massive II (2M)	3.73
Massive III (6M)	5.41
Vesicular I (1V)	3.61
Vesicular II (3V)	4.97
Vesicular III (5V)	5.68

3.1.4 X-Ray Diffraction

The X-ray diffraction (XRD) analyses were performed on both the fresh and weathered samples to assess the abundance of all minerals and types of clay minerals in the basalts. For the XRD analyses, the fresh massive and vesicular samples were obtained from the collected block samples at the site, and weathered samples were obtained from the deteriorated sections of the DCW by scratching and collecting the detached pieces. The selected samples were then powdered in an agate mortar to pass through the #200-mesh sieve (75 μ m openings). The samples used for XRD were prepared by following the combined procedures of Carroll (1970), Jackson (1979) and Moore and Reynolds (1989). The XRD analyses were carried out using Siemens D5000 X-ray diffractometer located in the Building Material Laboratory of Getty Conservation Institute in Los Angeles/California (USA) and a Rigaku Miniflex II diffractometer with Cu K α radiation in the Department of Geological Engineering of METU. Two kinds of samples, namely oriented and unoriented were prepared for the analyses. The oriented samples were tested for each fraction in following states: air-dried (AD), ethylene-glycolated (EG), heated at 300, and 550 °C.

The XRD analyses of the weathered samples will be discussed in the subsequent chapter (see Chapter 5).

As it was discussed in the previous section, one massive and one vesicular sample having a clay content somewhat higher than 5% were used in the XRD analyses. The XRD patterns of the massive and vesicular basalt samples are shown in Figure 3.4. Based on the patterns of the oriented samples, no significant amount clay was detected in both the massive and the vesicular samples. However, some peaks of the x-rayed vesicular sample can be attributed to the trace amount of smectite. The observed peaks, especially at the right side of the diffractograms, are attributed to the plagioclase minerals that are very abundant in the basalt samples. The peaks obtained from the unoriented samples reveal the presence of plagioclase, clinopyroxene and calcite minerals.

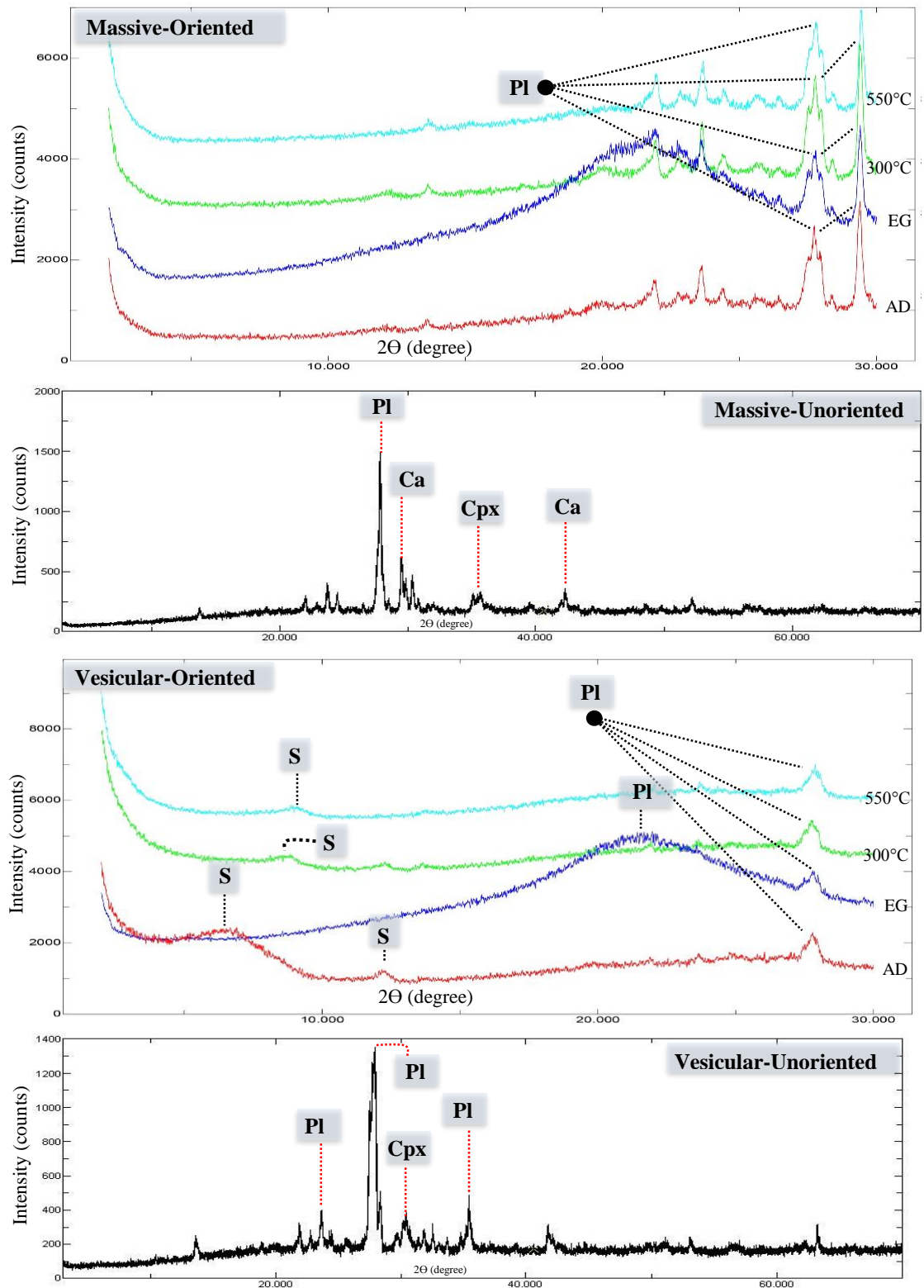


Figure 3.4 X-ray diffraction patterns of the massive and vesicular basalt samples (Pl: Plagioclase, Ca: Calcite; Cpx: Clinopyroxene; S: Smectite)

3.1.5 Scanning Electron Microscopy

Scanning electron microscope (SEM) analyses were performed to gather complementary information on surface morphology, microstructure and the chemical composition of the fresh massive and vesicular basalt samples. The SEM analyses were carried out using a FEI Nova NanoSEM 430 model scanning electron microscope equipped with an energy dispersive x-ray spectroscopy (EDX) unit operated at 20 kV. The instrument is located in METU's Department of Metallurgical and Materials Engineering. Since the samples are non-conductive, the surface of the specimens was coated with a thin gold (Au) layer prior to SEM analysis in order to get sufficient conductivity. The presence of Au peaks in the EDX results is due to this gold coating.

The SEM analyses of the fresh massive basalts reveal the existence of microfractures and the development of some calcite deposits (Figure 3.5-1).

The EDX analysis of the overall surface view demonstrates that the existence of Si, Fe, O, Al, with minor amount of Ca, Mg, K, Ti and C (Figure 3.5 A). On the other hand, the calcite deposition section illustrates that the presence of Ca, O, Fe, Si, Mg, and minor amount of Co and C (Figure 3.5 B).

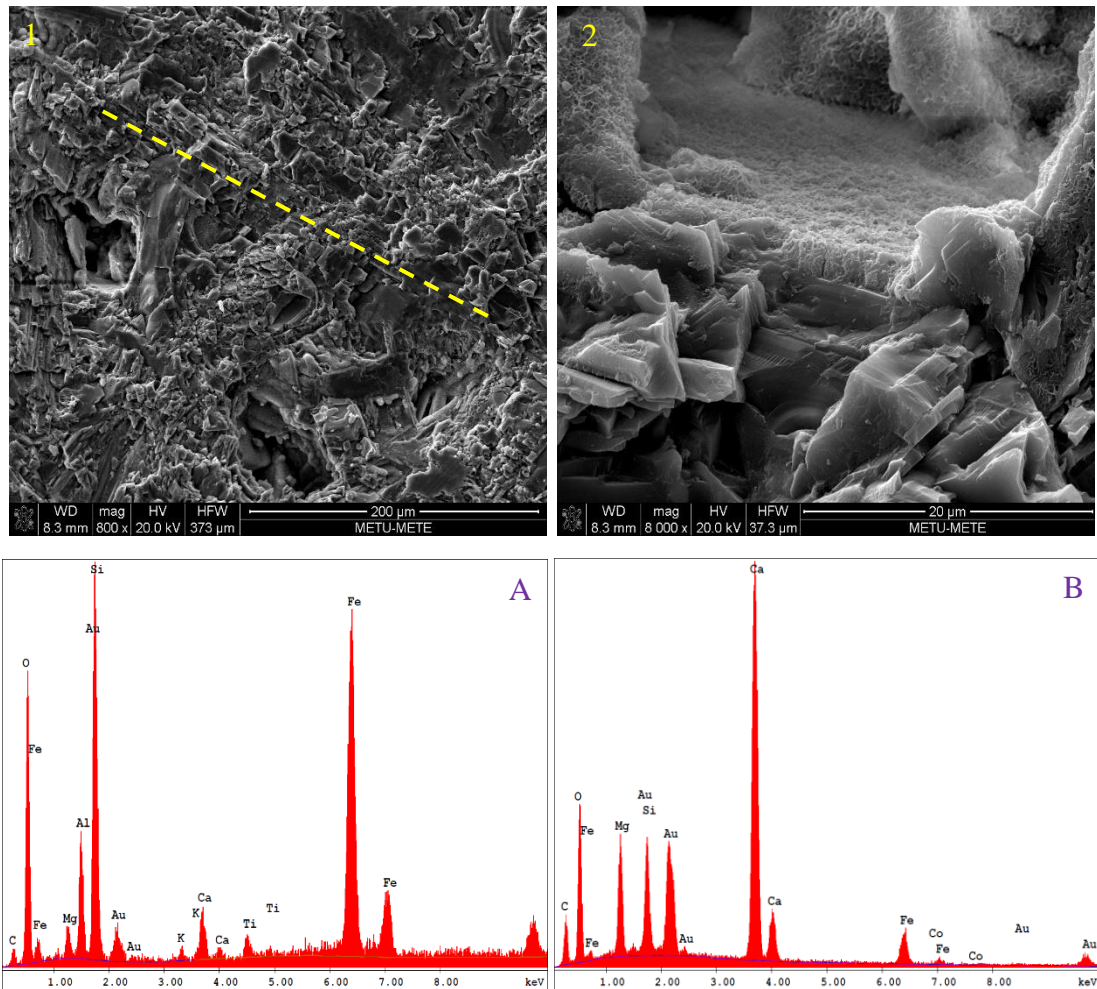


Figure 3.5 SEM micrographs and EDX analyses of a fresh massive basalt (1: microfracture pattern; 2: calcite deposition; A: EDX analyses of the overall surface; B: EDX analyses of the calcite deposition section) (microfracture pattern is indicated by yellowish dashed line)

The SEM analyses performed on vesicular basalts indicate that all samples contain vesicles. Secondary minerals are also observed in the pores of some vesicular samples. The enhanced magnification of the view illustrates some needle-like textures developed in the vesicular basalt sample (Figure 3.6-2). The EDX analysis of the overall surface view reveals that the presence of Si, O, Fe, Ca, Mg, and minor amount of Al (Figure 3.6 A).

On the other hand, the EDX analyses of the needle-like structure illustrate the existence of Si, O, Fe, Ca, Al, P, K with minor amount of Mn, Mg, Ti and C (Figure 3.6 B).

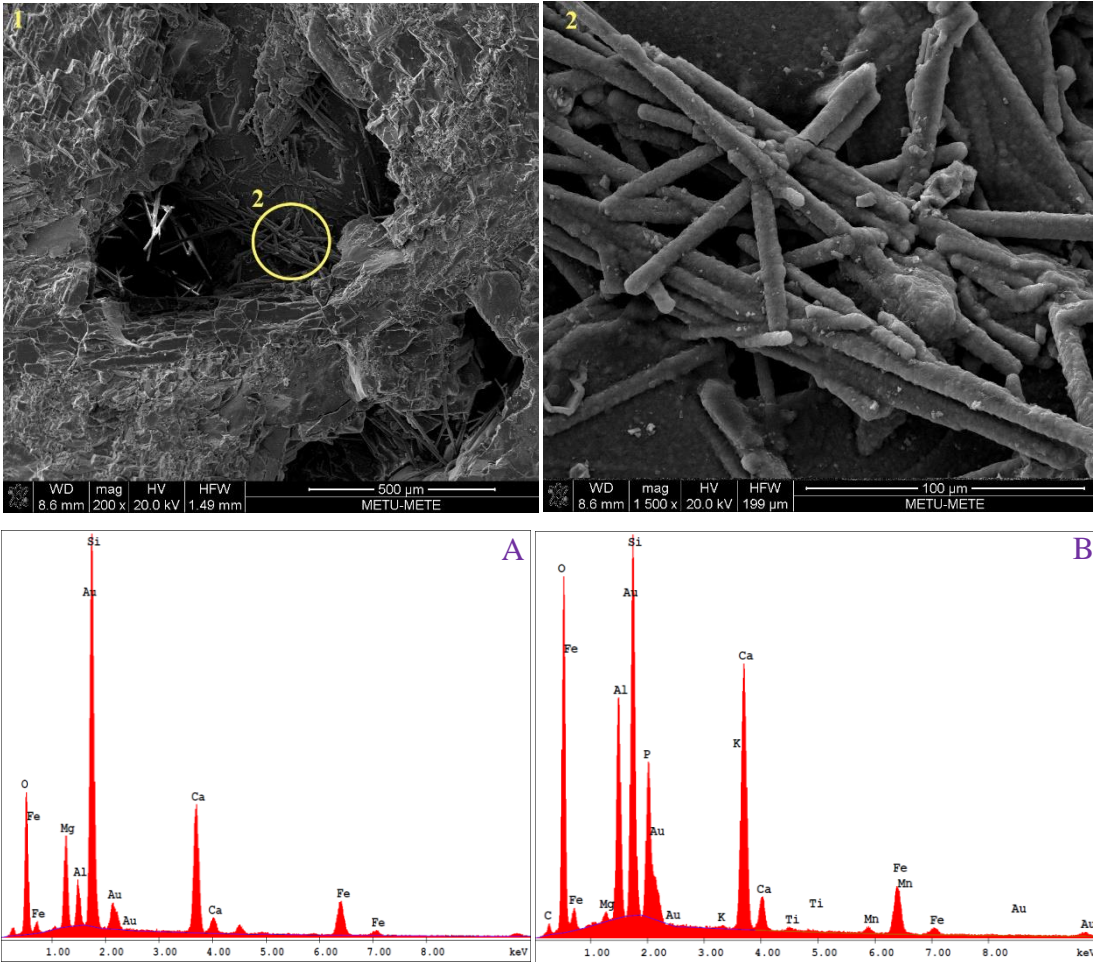


Figure 3.6 SEM micrographs and EDX analyses of a fresh vesicular basalt (1: overall morphology; 2: needle-like textures; A: EDX analyses of the overall surface; B: EDX analyses of the needle-like structure)

3.2 Chemical Properties of the Basalts

In order to examine the major and trace element characteristics of the massive and vesicular basalts, 8 fresh or relatively less altered samples were selected for the analysis after petrographic examination. The fresh rock samples selected were crushed and ground at the Department of Geological Engineering of METU, and then were put into 20 gram packages to send for the analysis. The abundances of the major oxides and trace elements were determined using Inductively Coupled Plasma Mass Spectrometry (ICP-MS) at ACME Analytical Laboratories Ltd. in Vancouver, Canada. The analyses were conducted based on the commercial litho geochemistry package named as LF202 “Total Whole Rock Characterization.”

The results of the whole-rock geochemical analysis of the massive and vesicular basalts are tabulated in Tables 3.2 and 3.3. The contents of the major and trace elements are given in weight percentages and in parts per million, respectively.

As Table 3.2 shows, the relative content variations of major elements of the massive and vesicular basalts indicate abundance of SiO₂ concentration. The concentration of SiO₂ for the basalt samples range from 46.33 to 49.73 wt%, with an average of 47.18 wt%. Relatively higher amount of oxides is observed for Fe₂O₃, Al₂O₃, MgO, and CaO contents. The Fe₂O₃ contents range from 12.85 to 15.45 wt%, averaging 14.04 wt%. The concentration of Al₂O₃ ranges between 13.17 and 14.95 wt% and averages 13.72 wt%, whereas MgO and CaO contents vary from 3.49 to 9.94 wt%, and 7.33 to 9.08 wt%, respectively. The concentration of Na₂O and K₂O range from 2.86 to 4.27 wt%, and 0.91 to 1.93 wt%. The average concentrations of the TiO₂, P₂O₅, MnO, and Cr₂O₃ are 2.54, 0.39, 0.18, and 0.05 wt%, respectively.

The analytical results of the selected trace elements are shown in Table 3.3. Similar to the results for the major elements, variations of the trace element composition showed no significant differences between the massive and vesicular basalt samples apart from the relatively higher Ba and Sr contents. According to the results, the Sr, V, Ni, Ba, and Zr contents are high compared to the other elements. The Sr concentrations of the tested samples vary from 376.30 to 706.20 ppm, with an average of 563.16 ppm.

The average concentrations of V, Ni, Ba, and Zr are 221.75, 194.96, 184.00 and 176.70 ppm, respectively. The other trace elements have very low proportions in the composition of the massive and vesicular basalt samples.

When the studied samples are plotted on the total alkali-silica (TAS) diagram proposed by Le Bas et al. (1986), it can be seen that most of the samples are basalt. Only one sample falls in the trachybasalt field with a 49.73 wt% of SiO₂. The samples are characterized by alkaline composition (Figure 3.7).

Table 3.2 Weight percentages of common oxides of the massive and vesicular basalt samples

Major Oxides	Massive Samples					Vesicular Samples		
	1M-A	1M-C	2M	4M	6M	1V	3V	5V
SiO ₂	46.50	46.33	46.73	46.53	48.43	46.71	46.45	49.73
Al ₂ O ₃	13.54	13.66	13.70	13.41	14.95	13.43	13.86	13.17
Fe ₂ O ₃ Total	14.41	13.85	14.25	13.59	12.85	13.75	14.17	15.45
MgO	9.63	9.19	9.94	9.57	7.38	9.49	9.60	3.49
CaO	8.63	8.75	8.65	8.70	9.08	8.63	8.41	7.33
Na ₂ O	3.06	2.86	2.94	3.12	3.31	3.18	2.89	4.27
K ₂ O	1.06	0.91	0.94	1.32	1.07	1.29	1.09	1.93
TiO ₂	2.32	2.29	2.31	2.50	2.32	2.49	2.30	3.81
P ₂ O ₅	0.34	0.34	0.33	0.42	0.29	0.44	0.35	0.63
MnO	0.19	0.17	0.17	0.17	0.17	0.17	0.17	0.20
Cr ₂ O ₃	0.057	0.053	0.054	0.068	0.050	0.058	0.055	0.031
LoI	-0.1	1.2	-0.4	0.2	-0.2	0.0	0.3	-0.3
Sum	99.67	99.66	99.67	99.65	99.72	99.65	99.66	99.73

Table 3.3 Trace element contents of the massive and vesicular basalt samples (in ppm)

Element	Massive Samples					Vesicular Samples		
	1M-A	1M-C	2M	4M	6M	1V	3V	5V
Ba	153	152	150	187	160	198	203	269
Be	2	2	4	1	2	1	3	4
Co	59.0	60.0	60.5	58.5	48.5	60.3	58.6	32.1
Cs	0.2	0.4	<0.1	0.1	0.1	0.1	<0.1	<0.1
Ga	20.4	21.0	20.3	21.9	20.6	21.9	21.7	26.6
Hf	3.5	3.6	3.8	4.6	3.6	4.6	3.7	7.8
Nb	21.1	21.6	19.2	26.3	16.5	27.3	20.7	35.0
Rb	10.3	9.2	8.5	15.6	14.5	15.8	10.2	24.3
Sn	2	2	2	2	1	2	1	4
Sr	560.9	706.2	563.7	626.4	477.5	650.1	544.2	376.3
Ta	1.3	1.4	1.3	1.6	1.1	1.7	1.2	2.2
Th	1.9	2.0	1.9	2.7	2.2	2.8	1.9	4.7
U	0.5	0.3	0.4	0.9	0.5	0.9	0.3	0.4
V	212	209	214	215	231	216	211	266
W	0.8	3.2	<0.5	7.5	1.1	3.3	1.1	9.0
Zr	148.7	151.7	141.4	186.7	145.3	191.0	150.0	298.8
Y	17.2	17.7	17.8	20.1	19.5	18.9	17.6	37.5
La	19.6	18.9	17.7	25.5	17.0	25.3	19.2	33.5
Ce	40.1	39.9	37.5	51.3	37.5	54.1	39.8	72.0
Pr	4.84	5.03	4.70	6.24	4.49	6.46	4.94	9.03
Nd	21.4	21.6	19.7	25.7	19.5	26.4	20.9	38.4
Sm	4.88	5.08	4.79	6.11	4.53	5.95	4.66	9.08
Eu	1.75	1.79	1.74	1.93	1.60	1.91	1.68	2.77
Gd	4.81	4.92	4.71	5.51	4.84	5.56	4.85	9.58
Tb	0.73	0.73	0.69	0.81	0.72	0.81	0.72	1.46
Dy	3.76	3.74	3.65	4.44	4.06	4.08	3.83	8.08
Ho	0.69	0.69	0.65	0.74	0.71	0.75	0.76	1.38
Er	1.66	1.68	1.70	1.83	1.92	1.86	1.67	3.86
Tm	0.22	0.22	0.22	0.25	0.27	0.23	0.21	0.53
Yb	1.21	1.35	1.41	1.39	1.65	1.39	1.37	3.16
Lu	0.20	0.20	0.19	0.20	0.25	0.19	0.18	0.46
Mo	3.2	2.7	2.7	5.0	2.6	4.2	2.3	7.1
Cu	83.1	79.2	77.9	72.9	49.9	71.1	69.4	73.2
Zn	101	88	98	90	71	90	91	113
Ni	248.7	258.7	246.8	219.0	107.5	219.9	231.1	28.0

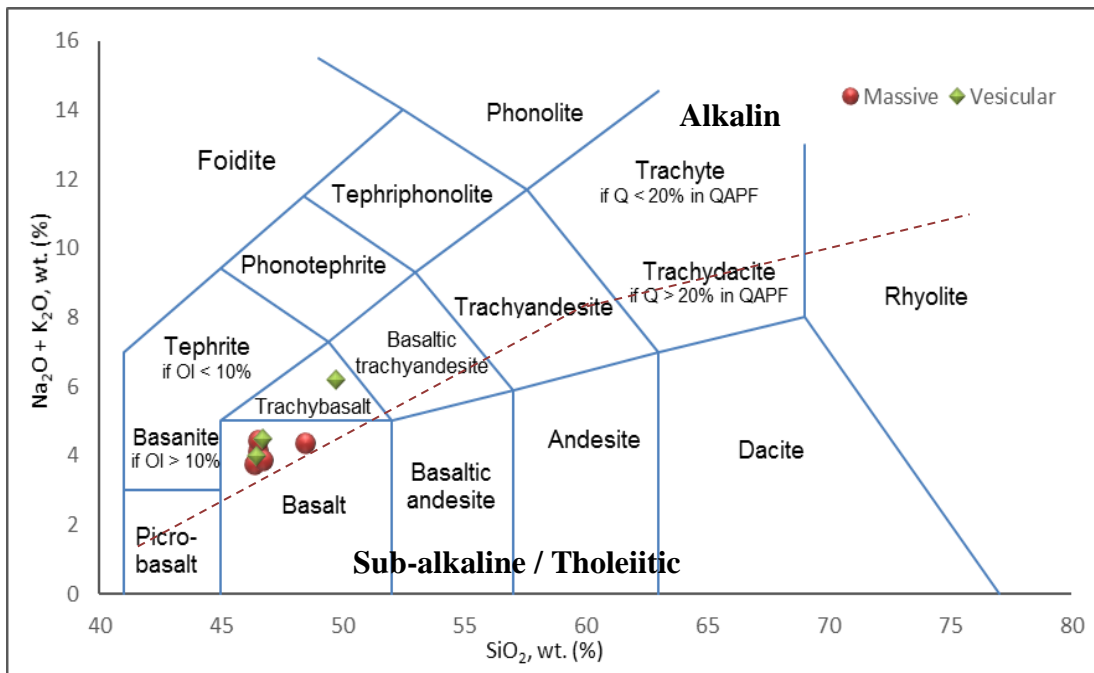


Figure 3.7. Total Alkali-Silica (TAS) diagram of Le Bas et al. (1986) for the studied basalts

CHAPTER 4

PHYSICO-MECHANICAL PROPERTIES OF THE BASALTS

Physico-mechanical properties mainly affect the durability of rock material. In order to characterize the physical and mechanical properties of rock material, it is essential to analyze their index properties. This chapter presents and discusses the laboratory studies performed on the fresh massive and vesicular basalt samples.

A total of 310 (155 massive and 155 vesicular) cubic samples with 7 centimeter edge lengths were used to determine the physico-mechanical properties of the massive and vesicular basalts. Basalt, especially those having massive texture does not show a distinct flow layer; however, those with vesicular texture show relatively a distinct flow layer. Therefore, oriented block samples were taken in the vertical and horizontal directions to assess anisotropy. These orientations are expected to represent the material characteristics of the basalts parallel or normal to the flow layering.

Several laboratory tests of the physico-mechanical properties of the fresh basalts were conducted in this study. The laboratory tests were performed in accordance with the standards and suggestions proposed by TSE (1978), RILEM (1980) ISRM (1981) and TS 699 (1987).

This section presents some of the index and mechanical properties of massive and vesicular basalts. The ranges and average values of the obtained results will be described in the text; however, the details of the test results are shown in Appendix A.

4.1 Effective Porosity and Unit Weight

Effective porosity and unit weight are both fundamental index properties of rock material that can affect its durability. The presence of pores in the fabric of a rock material decreases its strength and increases its deformability (ISRM, 1981). Unit weight is another important indicator for interpreting the physical properties of rock material and correlates well with porosity, strength and mineral composition (Anon, 1979). Those two index properties can be measured by the same test. The effective porosity and the dry and saturated unit weights of the massive and vesicular basalts were determined using the saturation and buoyancy techniques suggested by ISRM (1981). The details of the test results are shown in Appendix A.

Based on measurements of 130 samples, the massive basalts have effective porosities varying from 3.76% to 9.10%, with an average of 6.39%. The majority of the effective porosity values for the massive samples are less than 7% (Appendix A: Table A.1). The ranges of dry and saturated unit weights of the massive samples are 25.88-28.40 kN/m³ (with an average of 27.28 kN/m³) and 26.56-29.07 kN/m³ (with an average of 27.91 kN/m³), respectively.

The vesicular basalts, on the other hand, have effective porosities ranging between 7.96% and 14.20% with an average of 10.96%. Based on the results obtained from 130 vesicular samples, half of the values are greater than 11% (Appendix A: Table A.2). The dry and saturated unit weights of the vesicular samples are between 23.26-26.19 kN/m³ (with an average of 24.73 kN/m³) and 24.44-27.50 kN/m³ (with an average of 25.80 kN/m³), respectively.

According to Anon (1979), massive basalts have a medium porosity and a high unit weight, whereas vesicular basalts have a medium porosity, and a moderate unit weight.

4.2 Water Absorption under Atmospheric Pressure

Water absorption is an important parameter that affects the durability of rock material. This test was performed to measure the amount of water that rock can absorb under atmospheric pressure, and the results are expressed as percentages. The test was conducted using the procedures suggested by RILEM (1980) and TS 699 (1987). During the tests, water absorptions by weight and by volume were determined for 130 massive and 130 vesicular basalt samples. The details of the test results are shown in Appendix A: Tables A.3 and A.4.

The water absorption by weight and by volume of the massive basalts vary from 0.33% to 1.65% and from 0.95% to 4.35%, respectively. The average water absorption by weight and water absorption by volume values for massive samples are 0.89% and 2.46%, respectively.

The ranges of water absorption by weight and water absorption by volume of the vesicular basalts are 0.58% to 3.53% and 1.53% to 8.67%, respectively. The average water absorption by weight and by volume results for vesicular samples are 2.30% and 5.78%, respectively.

4.3 Water Absorption under Vacuum Pressure

The water absorption under vacuum pressure test is also intended to measure the amount of water that rock can absorb. Unlike the test performed under atmospheric pressure, this test is intended to measure the water absorption capacity of a rock material in a vacuum vessel under a certain pressure. The results are expressed as percentages.

The test was performed on the same 130 massive and 130 vesicular basalt samples used for the water absorption under atmospheric pressure test. The tests were conducted in accordance with the RILEM (1980) and TS 699 (1987) standards. The details of the test results are shown in Appendix A: Tables A.5 and A.6.

The water absorption by weight and by volume of the massive basalts lie between 1.34%, 3.37% and 3.75%, 9.10%, respectively. The average water absorption by weight and by volume values for massive samples are 2.30% and 6.39%, respectively.

The water absorption by weight and by volume of the vesicular basalts are in the range of 3.16% to 5.80% and 7.96% to 14.20%, respectively. The average water absorption by weight and water absorption by volume results for the vesicular samples are measured as 4.35% and 10.96%, respectively.

4.4 Uniaxial Compressive Strength

The uniaxial compressive strength (UCS) of a rock material is the highest stress that a specimen can bear under unidirectional stress (Bell, 1992). The test is mainly used for strength classification and the characterization of intact rock. The UCS of the massive and vesicular basalts was determined using the procedure described in ISRM (1981). Basalt samples in cubic shapes were prepared both in vertical and horizontal directions (especially for those with vesicular texture). The test was performed on 18 dry and 18 saturated (a total of 36 massive and 36 vesicular) cubic basalt samples. Most of the cubic samples had edge lengths of 7 centimeters, with some exceptions. During the tests, the load was applied by a motorized hydraulic compression machine with a loading capacity of 1,500 kN. The pace rate of the hydraulic compression machine was adjusted to 0.1 kN/s. The details of the test results are shown in Appendix A: Tables A.7, A.8, A.9 and A.10.

The average UCS values of massive samples for dry and saturated states are 143.75 and 117.91 MPa, respectively. The average UCS values of vesicular samples for dry and saturated states are 63.30 and 34.99 MPa, respectively.

According to the rock classification for the strength of rocks proposed by Anon, (1979) and BSI (2015), the massive and vesicular basalts are classified as very strong and strong, respectively.

In an attempt to check the isotropy, a total of 20 basalt samples having distinct flow layers were used. The massive basalts do not show distinct layering. Therefore, the vesicular samples were tested only based on their flow directions (i.e., parallel and perpendicular to the flow direction). The details of the test results are shown in Appendix A: Tables A.17 and A.18. The average uniaxial compressive strengths of the samples in the parallel and perpendicular to the flow directions are 79.10 and 51.26 MPa, respectively. Although higher UCS values were expected for the basalts tested perpendicular to flow direction, lower UCS values were obtained. This might be explained by the presence of incipient cracks within the samples in the other direction of the flow layering.

4.5 Indirect (Brazilian) Tensile Strength

Tensile strength of the rock materials is among the most important engineering properties. It can be experimentally determined through either direct or indirect methods (ISRM, 1981). In this study, the tensile strength of the massive and vesicular basalt samples was measured indirectly by the Brazilian test. The principle of this test is to apply a compressive load across the diameter of the specimen and then a tensile strength is induced in the sample perpendicular to the direction of loading (Carneiro, 1943; Li and Wong, 2013).

Indirect (Brazilian) tensile strength of the massive and vesicular basalt samples was determined using the procedures explained in ISRM (1981). For this test, two steel loading jaws designed so as to contact a disc-shaped rock sample (NX size) are used. The core samples obtained in vertical direction were cut in such a way that the thicknesses of the specimens are not less than the radius of the specimens. The tests were performed on 10 massive and 10 vesicular basalt samples.

The indirect tensile strength measurements were carried out using MTS 815 Rock Mechanics Test System located in the Department of Mining Engineering at METU. The pace rate of the compression machine is set to 0.1 kN/s. The details of the test results are shown in Appendix A: Tables A.11 and A.12.

The indirect tensile strength of the samples is calculated by the following equation proposed by ISRM (1981)

$$\sigma_t = \frac{0.636xP}{Dxt} \quad (4.1)$$

Where, “ σ_t ” is the indirect tensile strength; “ P ” is the load at failure; “ D ” is the diameter of the sample; and “ t ” is the thickness of the sample.

Based on the measurements, the tensile strength of the massive basalts ranges from 14.50 to 18.52 MPa, with an average of 16.60 MPa, whereas the tensile strength of the vesicular basalts is between 5.54 to 12.1 MPa, with an average of 8.76 MPa.

4.6 Sonic Velocity

As a non-destructive test method, sonic velocity is a parameter commonly used to evaluate rock materials in terms of their elasticity, anisotropy, degree of fissuring, porosity and state of deterioration. Moreover, this test can be used to monitor the degradation mechanisms of rock material under such different cyclic loads as wetting and drying, freezing and thawing, and salt crystallization.

The sonic velocity measurements of the massive and vesicular basalts were carried out according to the recommendations of ISRM (1981). Before the measurements, the faces of the cubic samples were made flat and smooth. A thin film of vaseline was applied to surface of the transmitter and receiver.

As suggested in ISRM (1981), the pulse transmission technique was applied so that the transmitter and receiver were positioned on two opposite faces of the cubic samples. During the test, the measurements were performed on the three different pairs of faces of the cubic samples. The sonic velocity measurements were conducted using the PUNDIT-PLUS (Portable Ultrasonic Non Destructive Digital Indication Tester)

equipment with a 54 kHz transducer located in the Department of Geological Engineering at METU. The details of the test results are shown in Appendix A: Tables A.13, A.14, A.15 and A.16.

Based on the measurements, the sonic velocity of the 130 dry massive basalts ranges from 2123.05 to 5608.13 m/sec., with an average of 4599.68 m/s, whereas the sonic velocity of the 130 saturated massive basalt samples is between 3510.40 and 5690.40 m/s, with an average of 4981.06 m/s.

The sonic velocity measurements for the 130 dry vesicular basalt samples vary from 3306.67 to 5179.22 m/s, with an average of 4157.58 m/s, whereas the sonic velocity measurements of the 130 saturated vesicular basalt samples range from 3861.11 to 5401.53 m/s., with an average of 4609.15 m/s.

According to the rock classification based on sonic velocity proposed by Anon (1979), the massive and vesicular basalts are classified as high sonic velocity for both dry and saturated states.

The isotropy of some vesicular samples having distinct flow layers were also evaluated during the sonic velocity measurements. A total of 20 vesicular basalt samples were used. The samples were tested based on their flow directions (i.e., parallel and perpendicular to the flow direction) and on their dry and saturated conditions. The details of the test results are shown in Appendix A: Tables A.19, A.20, A.22 and A.23.

The average dry sonic velocities of the samples in the parallel and perpendicular to the flow directions are 4206.66 and 3754.79 m/s, respectively; whereas the average saturated sonic velocities of the samples in the parallel and perpendicular to the flow directions are 4497.57 and 4081.62 m/s, respectively. Slightly lower sonic velocity values suggest that there exists anisotropy validated by reduction in sonic velocities of the vesicular basalts in the perpendicular to flow direction.

4.7 Pore-size Distribution

Pore-size distribution is among the important parameters in the investigation of the physico-mechanical properties of the rock materials. There are various methods, including optical microscopy, scanning electron microscope (SEM), gas adsorption, and more recently developed X-ray computed tomography and nuclear magnetic resonance imaging microscopy, for measuring pore-size distribution.

In addition, mercury intrusion porosimetry (MIP) has been extensively employed to assess the pore-size distribution of rocks (Van Brakel et al., 1981; Meng, 1992; Fitzner, 1993; Topal et al., 1998; Weishauptová and Pfikryl, 2004). The range of all the methods mentioned, more or less, overlaps with that of mercury porosimetry. The principle of the mercury intrusion technique is based on forcing mercury under increasing pressure to penetrate the pores of a sample. In this technique, mercury behaves as a non-wetting liquid against most substances, including rocks. This means mercury does not penetrate into the openings and cracks within the material unless sufficient pressure is applied to intrude the mercury into the porous material. The volume of mercury that penetrates into the material is measured as a function of the applied pressure, as described in the following equation proposed by Washburn (1921)

$$r = \frac{-2\gamma \cos\theta}{P} \quad (4.2)$$

Where, “ r ” is pore radius; “ γ ” is the surface tension of mercury in the pore; “ θ ” is the contact angle between mercury and pore wall; and “ P ” is the applied pressure.

The pore-size distributions of the samples discussed through this study were determined by means of the mercury intrusion technique. The measurements were carried out using the Quantachrome Corporation, Poremaster 60 device located in the Central Laboratory at METU. The samples were analyzed with an injection pressure up to 55,000 psi.

A total of 9 fresh basalt samples (6 massive and 3 vesicular) were used to determine pore-size distribution. The results from the MIP analysis are plotted on a histogram. This section will discuss the pore-size distribution of the selected massive and vesicular samples.

Based on the obtained results, the both massive and vesicular basalt samples exhibit bimodal pore-size distribution. Figure 4.1 is a histogram representing the pore-size distribution of a massive basalt sample. As it shows, the pore-size distribution of the sample is bimodal with one maximum in the range of micropores and macropores. In other words, the size distribution varies from 0.003 to 0.1 μm , and from 5 to 200 μm . The small pores are clustered at 0.006 μm and the large pores at 15 μm . The sample has no pores between 0.01 and 5 μm as determined by mercury porosimetry.

The pore-size distribution histogram of a vesicular basalt is shown in Figure 4.2. It seems that this sample also exhibits bimodal pore-size distribution. The tested vesicular sample has large pores in between 7 to 100 μm clustered at 40 μm . In other words, the pore-size distribution of the vesicular sample reaches its highest value around 30 and 50 μm . The tested sample has no pores smaller than 0.1 μm as determined by mercury porosimetry.

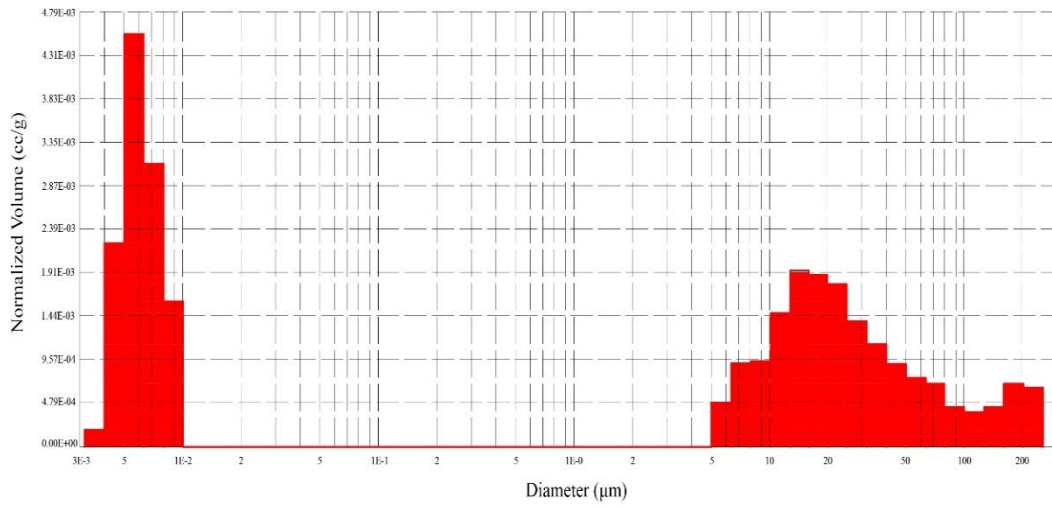


Figure 4.1 Histogram depicting the pore-size distribution of a massive sample

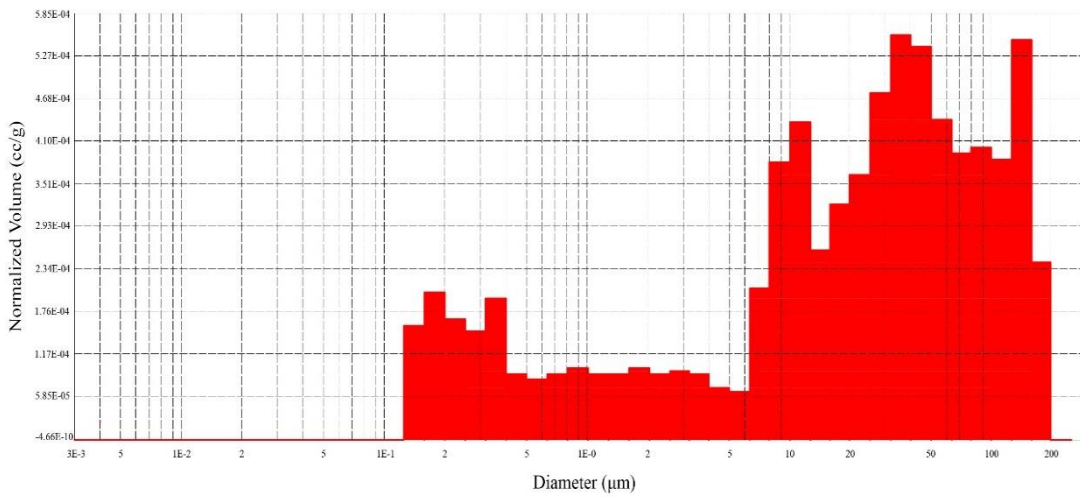


Figure 4.2 Histogram depicting the pore-size distribution of a vesicular sample

CHAPTER 5

THE DETERIORATION OF THE BASALTS

This chapter is based heavily on the deterioration of the basalt employed in the DCW. The first sections document the field studies performed on the DCW. In this context, in the first two sections of this chapter, the common weathering forms developed on the DCW are defined, and weathering maps of the selected two sections are produced to visualize their dominant weathering patterns. The following two sections of this chapter detail the petrographic and geochemical properties of weathered basalts and the accelerated weathering tests. Finally, the microfracture properties of the fresh and weathered basalts are evaluated in the last section of the present chapter.

5.1 Weathering Forms and State of Deterioration

Weathering forms on historical structures occur due to weathering processes. These forms are initiated and determined by the combination of various weathering factors (Fitzner et al., 1997). The documentation of lithologies and weathering forms is a widely used technique for diagnostic studies that not only assess the types, depth, degree and distribution of weathering forms, but also monitor the progress of deterioration and plan further analyses. (Fitzner and Heinrichs, 2001; Török and Přikryl, 2010).

Many different approaches (Winkler, 1966; Bell and Coulthard, 1988; Fitzner et al., 1997; Honeyborne, 1998; Fitzner et al., 2002; Warke et al., 2003; Charola, 2004) have been reported in the literature to define terminologically and to classify weathering forms.

However, too many different approaches increase misunderstandings of weathering forms. Of weathering classifications, the one proposed by Fitzner et al. (1995) is well-recognized. The authors divided weathering forms into four main groups (i) loss of stone material, (ii) detachment, (iii) cracks and deformations and (iv) discoloration and deposits.

The authors divided these main groups into subgroups and individual weathering forms. Discussions of the classification of weathering forms are still ongoing.

In order to overcome terminological confusion and to harmonize all the existing standards, glossaries and classification approaches, ICOMOS published an illustrated glossary (Siedel and Siegesmund, 2014). In their short glossary, the committee reviewed seven documents on stone decay, including the classification proposed by Fitzner et al. (1995), and produced a document to clarify some terms and to propose an updated classification of weathering forms (ICOMOS-ISCS, 2008).

Several field surveys were conducted to examine the influence of weathering on the DCW. Field surveys permit to identify the construction materials employed in structures and to distinguish the main weathering forms and the state of deterioration. Based on the field surveys, it is observed that there are numerous weathering forms of various sizes on the DCW, which are evidence of the destruction and deterioration in progress.

The degradation features of stone are described in the following sections based on the classification scheme proposed by ICOMOS (ICOMOS-ISCS, 2008). The most common forms of weathering that are affecting the basalts of the DCW are:

1. *Cracks* in the form of vertical and horizontal cracks, fractures and crack networks;
2. *Detachments* in the form of blistering, delamination, crumbling, splintering, chipping, flaking and contour scaling;
3. *Material loss* in the form of alveolization, erosion, mechanical damage and missing part;
4. *Discolorations and deposits* in the form of crusts, deposits, discoloration, efflorescence and graffiti;
5. *Biological colonization* in the form of lichen, plant, alga and moss.

5.1.1 Cracks and Deformations

The term, *crack*, is used here to describe narrow and clearly visible fissures. Other glossaries also use the terms, fissure, fault and joint. Cracks may result from a variety of factors such as structural instability, vibration, frost, mortar repointing, mechanical impact or inherent masonry character (Grimmer, 1984; ICOMOS-ISCS, 2008).

Cracks are one of the common weathering forms observed on the DCW. They are mostly in the form of fractures or networks. The cracks on the DCW have mostly developed vertically and horizontally along the flow layer (Figures 5.1 and 5.2).

Fractures are another crack form found on the DCW. They have also developed vertically and horizontally on the DCW (Figures 5.1 and 5.2). Unlike cracks, fractures completely cross the stone block. Thermal stresses or cyclic freezing/thawing of water are most probably causes of fractures along flow layers.

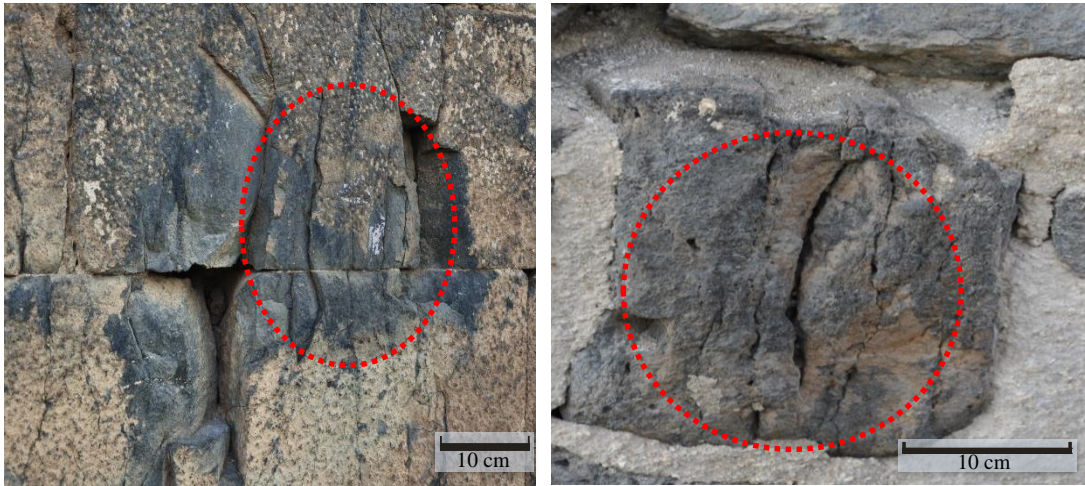


Figure 5.1 Vertical cracks and fractures on sections of the DCW (cracks and fractures are indicated by the dashed circles)

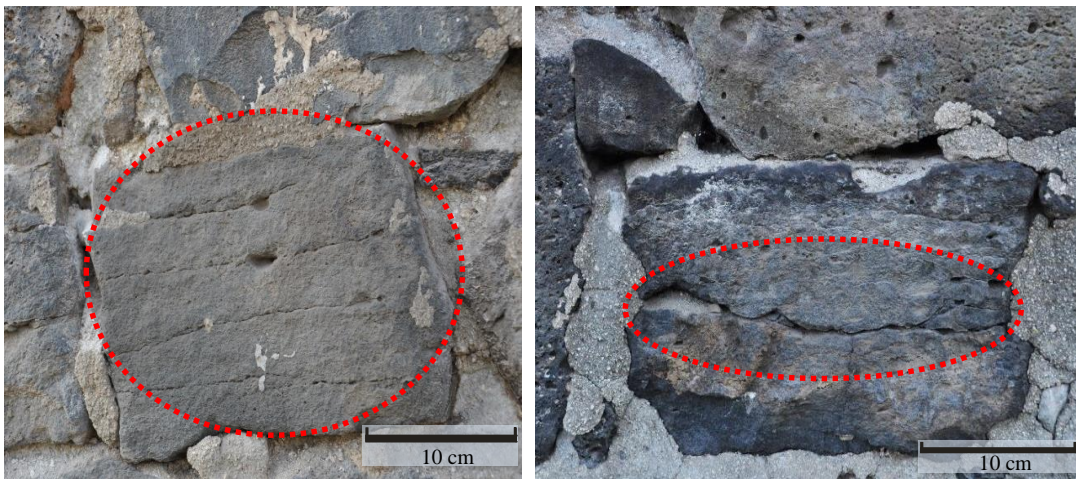


Figure 5.2 Horizontal cracks and fractures on sections of the DCW (cracks and fractures are indicated by the dashed circles)

There are also crack networks on the DCW. Those networks, observed on the lower part of the walls, may partially cross the basalt blocks (Figure 5.3). Crack networks on the walls can be attributed to the overloading or differential settlement. As the various examples, most of the cracks and fractures that developed on DCW are oriented parallel to the flow direction (Figures 5.1 and 5.2). Therefore, such weathering forms are strongly associated with flow direction.

Cracks on the other hand, cause leakages, moisture and thermal bridges, where they may accelerate the degree of weathering. Therefore, especially those relatively wider, should be monitored and examined in terms of persistence, aperture, spacing, direction and depth for a period of time to understand whether they are stable or active (Sowden, 1990).

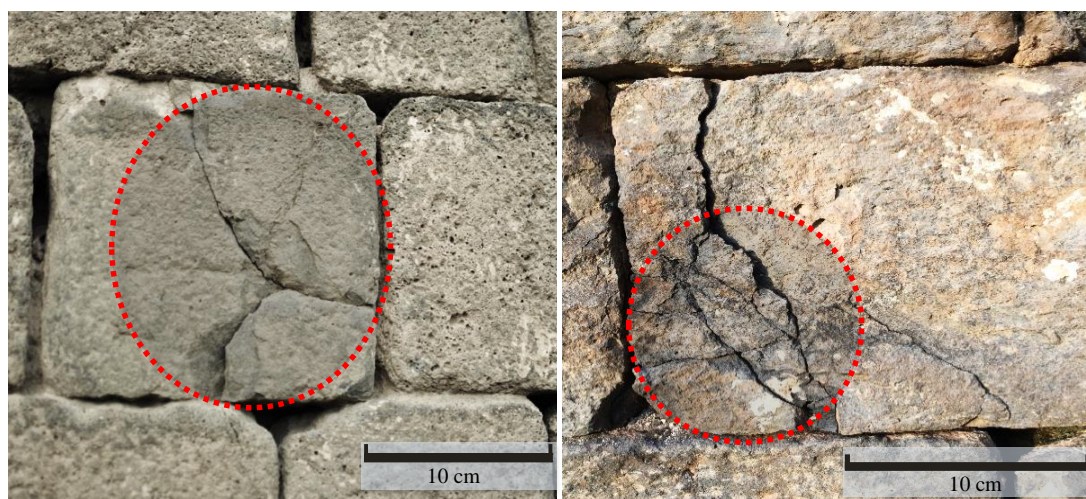


Figure 5.3 Crack networks on basalt blocks of the DCW (crack networks are indicated by dashed circles)

5.1.2 Detachments

The term, *detachment*, is used here to categorize weathering forms representing disintegration of stone structures both at the microscopic and macroscopic scales (Siedel and Siegesmund, 2014). ICOMOS-ISCS (2008) divided the detachments into the subgroups of blistering, bursting, delamination (exfoliation), disintegration (crumbling or granular disintegration), fragmentation (splintering or chipping), peeling and scaling (flaking or contour scaling).

Of weathering forms, detachments are the most common deterioration pattern on the DCW. The detachments are mostly in the form of blistering, delamination, disintegration, fragmentation and scaling. There are also many visible signs of transitional weathering forms, especially blistering, crumbling and scaling.

Blistering patterns are found on the DCW (Figure 5.4). Blistering is defined as swelling and detachment of a thin uniform layer (Grimmer, 1984). Blistering can be caused by salt action, entrapped air or ground moisture.

It is frequently observed on the lower parts of the walls. It is considered that blistering triggers spalling or delamination of the stone and finally results in loss of material (ICOMOS-ISCS, 2008).



Figure 5.4 Blistering patterns at the lower parts of the walls (blistering patterns are indicated by dashed circles)

Delamination is another form of weathering that is detected on the basalt surfaces in places. Delamination is a detachment process in which the outer surface of stone separates into laminae or thin layers. It takes place parallel to the natural bedding plane of stone, particularly when they are placed vertically (Grimmer, 1984; ICOMOS-ISCS, 2008). Although delamination is more common in sedimentary and metamorphic rocks, it is also observed on the basalt surfaces.

The delamination patterns on the DCW mostly developed parallel to the flow direction (Figure 5.5). There are also some elongated vesicles arranged in rows on the delaminated surfaces. Such weathering patterns are visible on the lower and middle part of the masonry and towers of the DCW. This weathering form is mostly associated with the improper placing of the basalt on the masonry.

To put it differently, since the direction of flow layer was not properly oriented during the construction of the walls and towers, delamination patterns developed on the basalt blocks.

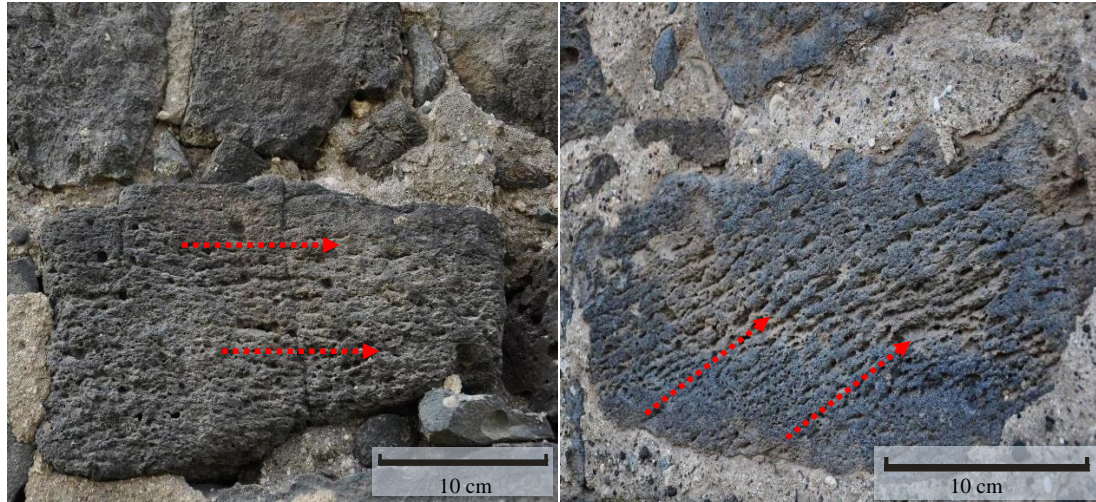


Figure 5.5 Delamination of basalt along the flow directions (flow directions are indicated by dashed arrows)

The disintegrations identified on basalt surfaces of the DCW are commonly in the form of crumbling (Figure 5.6). Crumbling can be caused by the penetration of moisture or salt in the masonry or by gradual disintegration of binder (Grimmer, 1984). Crumbling can also develop in a spheroidal form. Spheroidal weathering is a “form of chemical weathering in which concentric or spherical shells of decayed rock (ranging in diameter from 2 centimeters to 2 meters) are successively loosened and separated from a block of rock by water penetrating the bounding joints or other fractures and attacking the block from all sides” (Neuendorf et al., 2005). It is also called concentric weathering, onion-skin weathering or spherical weathering.

Ollier (1971) lists the causes of spheroidal weathering: unloading, temperature change, frost, salt, absorption of water, micro cracks and the chemical decay of minerals. This type of weathering occurs not only on the dressed basalt used in the DCW, it is also common on basalt blocks spread over road alignments and on single stone blocks (Figure 5.7).

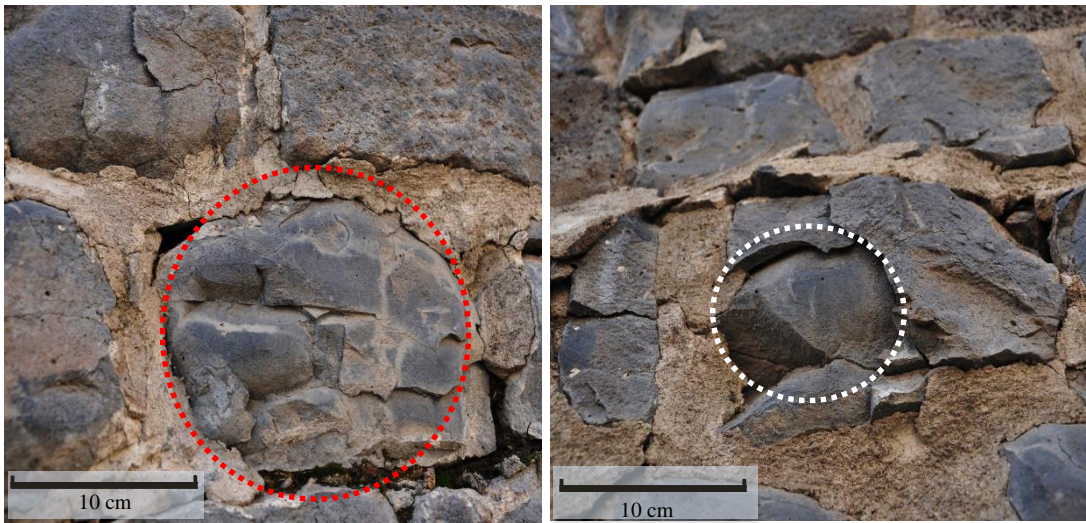


Figure 5.6 Crumbling and spheroidal weathering forms on the DCW (crumbling is indicated by reddish dashed circle, and spheroidal weathering is indicated by whitish dashed circle)



Figure 5.7 Spheroidal weathering on basalt blocks (north section of the study area)

In addition to disintegration, the DCW have suffered from fragmentations, commonly in the form of splintering (Figure 5.8) and chipping (Figure. 5.9). The patterns of splintering and chipping can be observed on both the lower and middle parts of the walls and towers. Splintering is the detachment of stone pieces from the main body in the form of splinters, whereas chipping is the breaking off the stone pieces from the masonry unit often at the corner of a block or in mortar joints.

The causes of the splintering and chipping are associated with overloading; however, improper repairs such as the absence of pointing or the use hard mortar, or impact damages such as vandalism may also cause them (Grimmer, 1984; ICOMOS-ISCS, 2008).

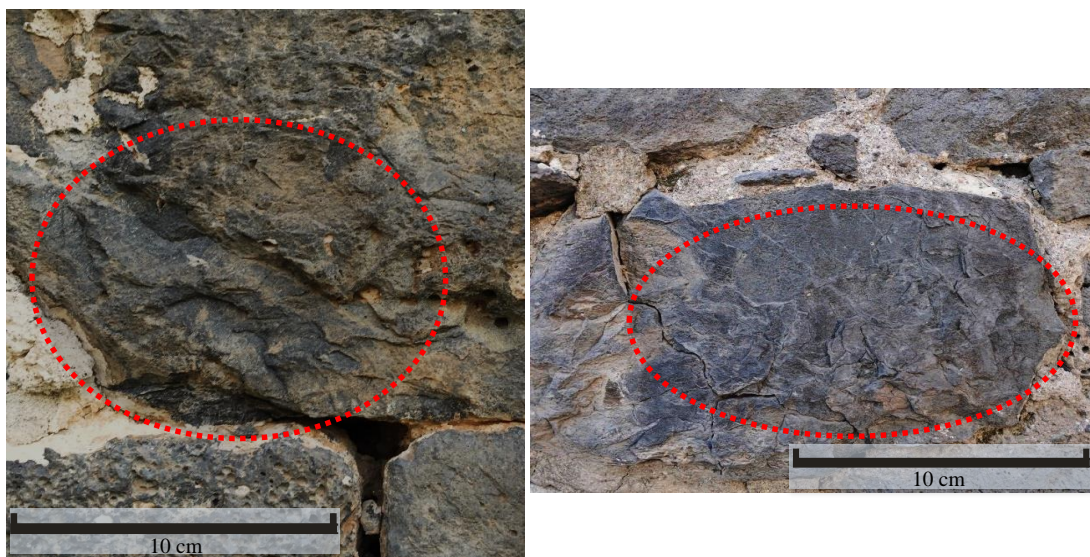


Figure 5.8 Splintering on the DCW (splintering is indicated by dashed circles)

Scaling is another frequently observed detachment form on the DCW. It is described as a deterioration pattern in which the outer layer or layers of the stone unevenly break off from the larger stone block (Grimmer, 1984). Scaling of the stone can be like fish scales or parallel to the stone surface (ICOMOS-ISCS, 2008). Scaling is usually divided into the subgroups of flaking and contour scaling. Flaking is the detachment of small, thin and flat pieces parallel to the stone surface. It usually caused by freezing-thawing cycles or masonry capillary action (Grimmer, 1984). On the other hand, contour scaling is the detachment of relatively larger pieces that parallel the sound part of the stone surface. Contour scaling may be called spalling when it involves the detachment of flat surfaces (ICOMOS-ISCS, 2008). The causes of contour scaling and spalling are freezing-thawing cycles, salt, moisture trapped under the surface, improper laying of stone and improper repointing (Grimmer, 1984).

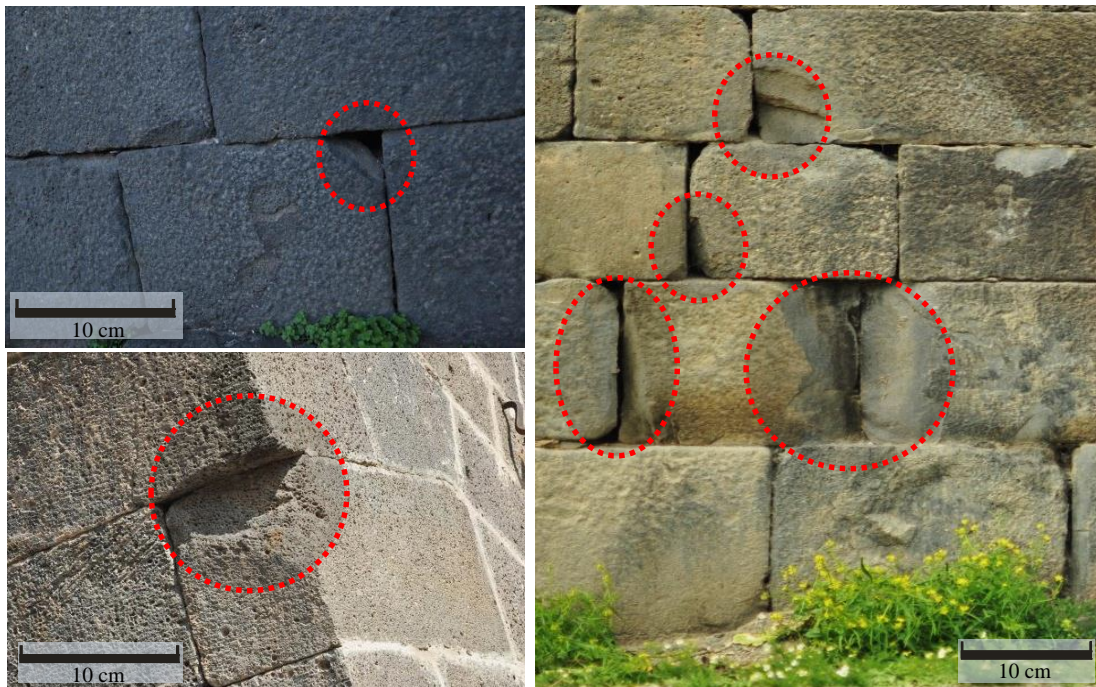


Figure 5.9 Chipping on sections of the DCW (chipping is indicated by dashed circles)

Scaling patterns have developed on various sections of the DCW. As an early stage of delamination or spalling, flaking is witnessed on some sections of the DCW (Figure 5.10).

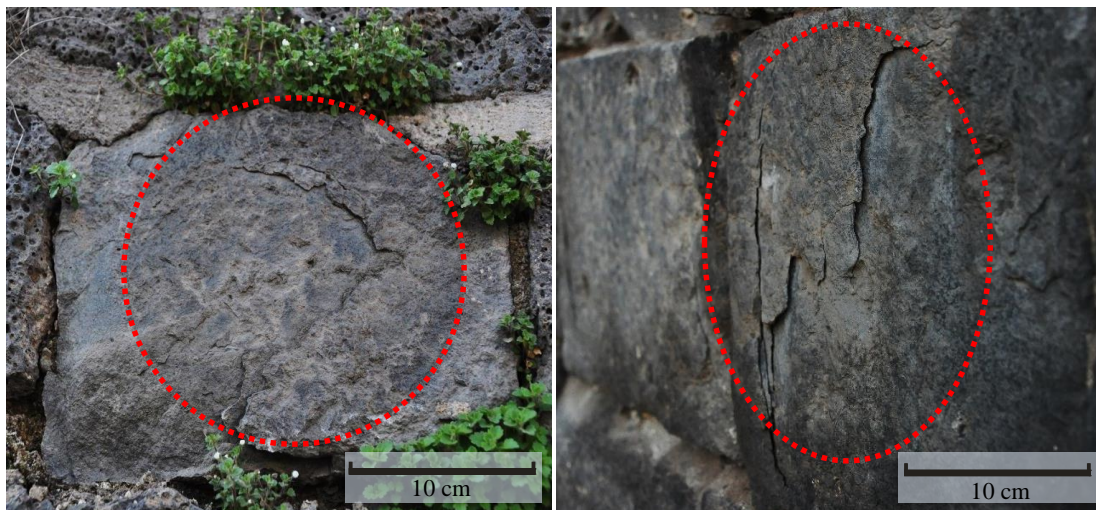


Figure 5.10 Flaking on sections of the DCW (flaking is indicated by dashed circles)

As one of the most common weathering forms, contour scaling and spalling can be observed almost at any level of the DCW (Figure 5.11). The thickness of the scaling on the DCW ranges from millimeters to centimeters, and most of them result in loss of material through detachments.



Figure 5.11 Scaling on sections of the DCW (scaling is indicated by dashed circles)

5.1.3 Material Losses

The features induced by loss of material cover all the weathering forms that cause a loss of stone material. In its glossary, ICOMOS (2008) subdivided them into alveolization (coving), erosion (differential erosion, loss of components, loss of matrix, rounding and roughening), mechanical damage (impact damage, cut, scratch, abrasion and keying), microkarst, missing parts (gaps), perforation and pitting. Material loss on the DCW is in the form of alveolization, erosion, mechanical damage and missing parts.

As a form of material loss, alveolization or coving (as a single alveole) patterns are found on the DCW (Figure 5.12). Alveolization is described as the formation of closely spaced cavities that may have different shapes and sizes. It may develop with such other weathering patterns as scaling and/or granular disintegration (ICOMOS-ISCS, 2008).

It is also known as honeycomb weathering and alveolar erosion (Rodriguez-Navarro et al., 1999; ICOMOS-ISCS, 2008). Although the mechanism and causes of the alveolization are still not well understood, many authors (e.g., Mustoe, 1982; Rodriguez-Navarro et al., 1999; Siedel, 2010; Bilén et al., 2016) have proposed that salt crystallization and wind exposure probably play a key role, especially in the initial formation of alveolization.

Erosion is another form of material loss that observed on the DCW. It is broadly described as the loss of original surface or edge of stones leading to smoothed forms (ICOMOS-ISCS, 2008).

Erosion on the DCW commonly takes the form of differential erosion, rounding and roughening (Figure 5.13). Differential erosion is found in the loss of components form, defined as partial or selective loss of stone components. According to ICOMOS-ISCS, differential erosion “occurs when erosion does not proceed at the same rate from one area of the stone to the other.”

As a result, stone material deteriorates irregularly (ICOMOS-ISCS, 2008). Erosion is also found on the iconic reliefs engraved on the towers. As it can be seen in Figure 5.14, erosion on the reliefs results in the loss of engraved details.

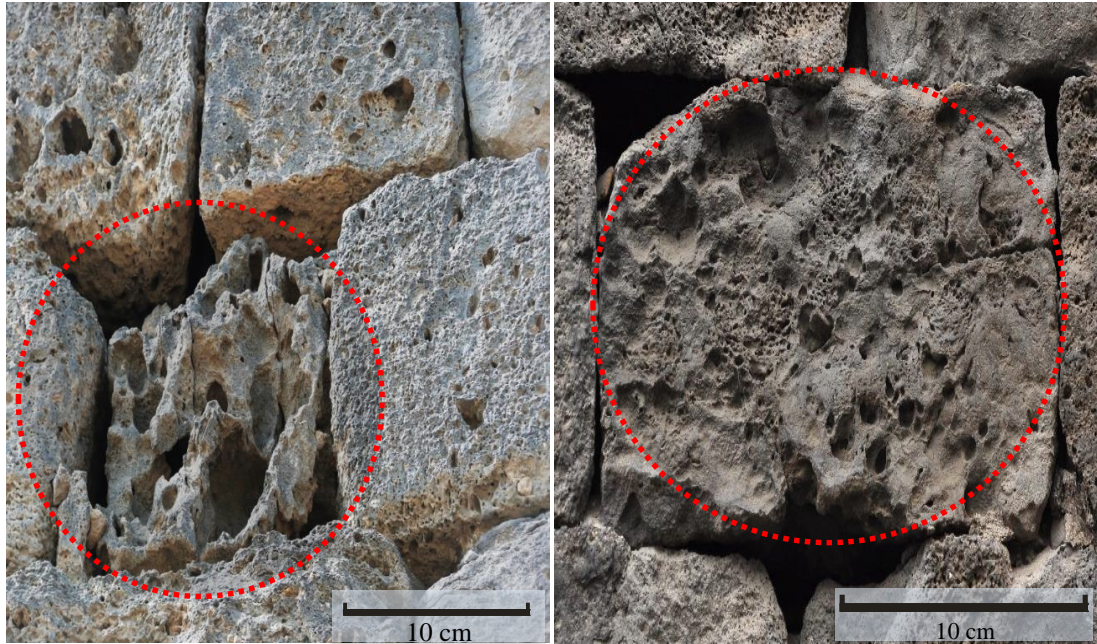


Figure 5.12 Alveolization on sections of the DCW (alveolization is indicated by dashed circles)

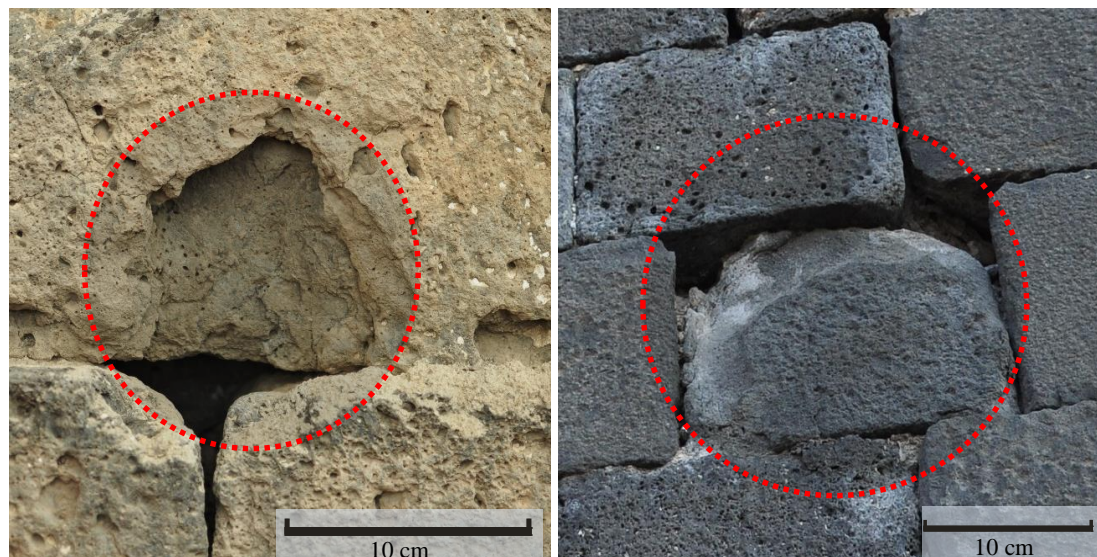


Figure 5.13 Erosion in the loss of components form on the DCW (loss of component is indicated by dashed circles)

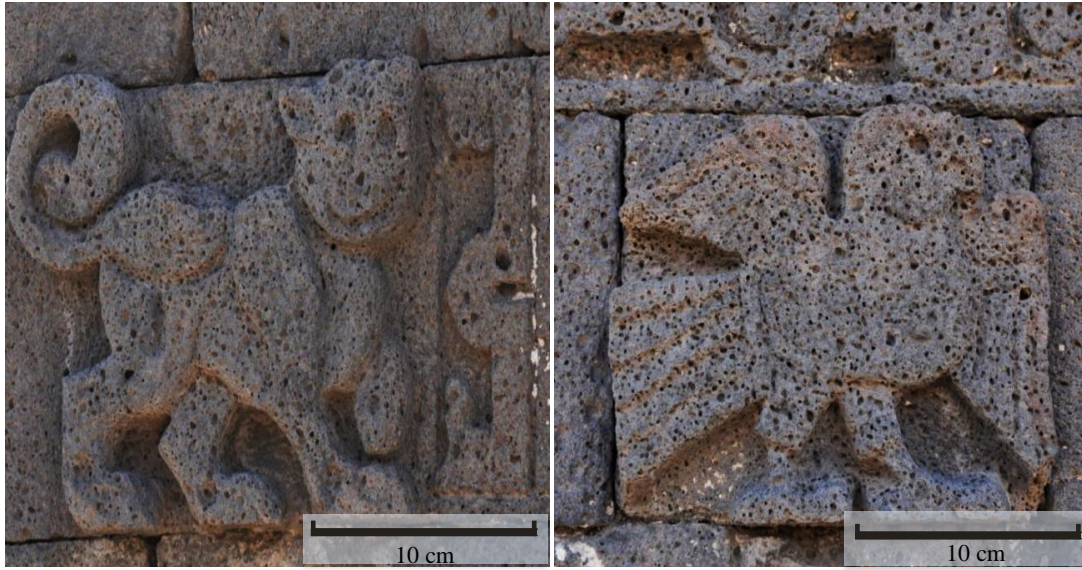


Figure 5.14 Erosion of the iconic reliefs on the Selçuklu Tower (image credit: Governorship of Diyarbakır, 2017)

The DCW have suffered from different kinds of mechanical damage (Figure 5.15), including impact damage, due to the impact of a bullet or a hard tool; cuts in the appearance of excavated cavities; scratches and engraving, as a form of material loss due to the action of sharp points; and pecking or keying. Pecking or keying can be defined as hitting and marking the stone surface with a pointed tool during construction to get an irregular surface and to facilitate adhesion (ICOMOS-ISCS, 2008; Odgers and Henry, 2012).

Missing parts are another forms of damage to the DCW. The missing parts are not small-scale gaps or holes, they are also in large-scale forms such as demolishing entire wall sections and towers. Currently, a total of *ca.* 650 meters of the DCW are missing. Although some damage occurred due to natural events, most of them are due to human interventions. For instance, different sections of the walls have been breached, and large stone blocks, especially at the base of the walls, have been dismantled (Figures 5.16 and 5.17). Loss of stone material is observed on the iconic reliefs as well. As Figure 5.18 shows, the missing parts of the lion reliefs on the Ulu Beden Tower are mostly the loss of heads, legs or tails.

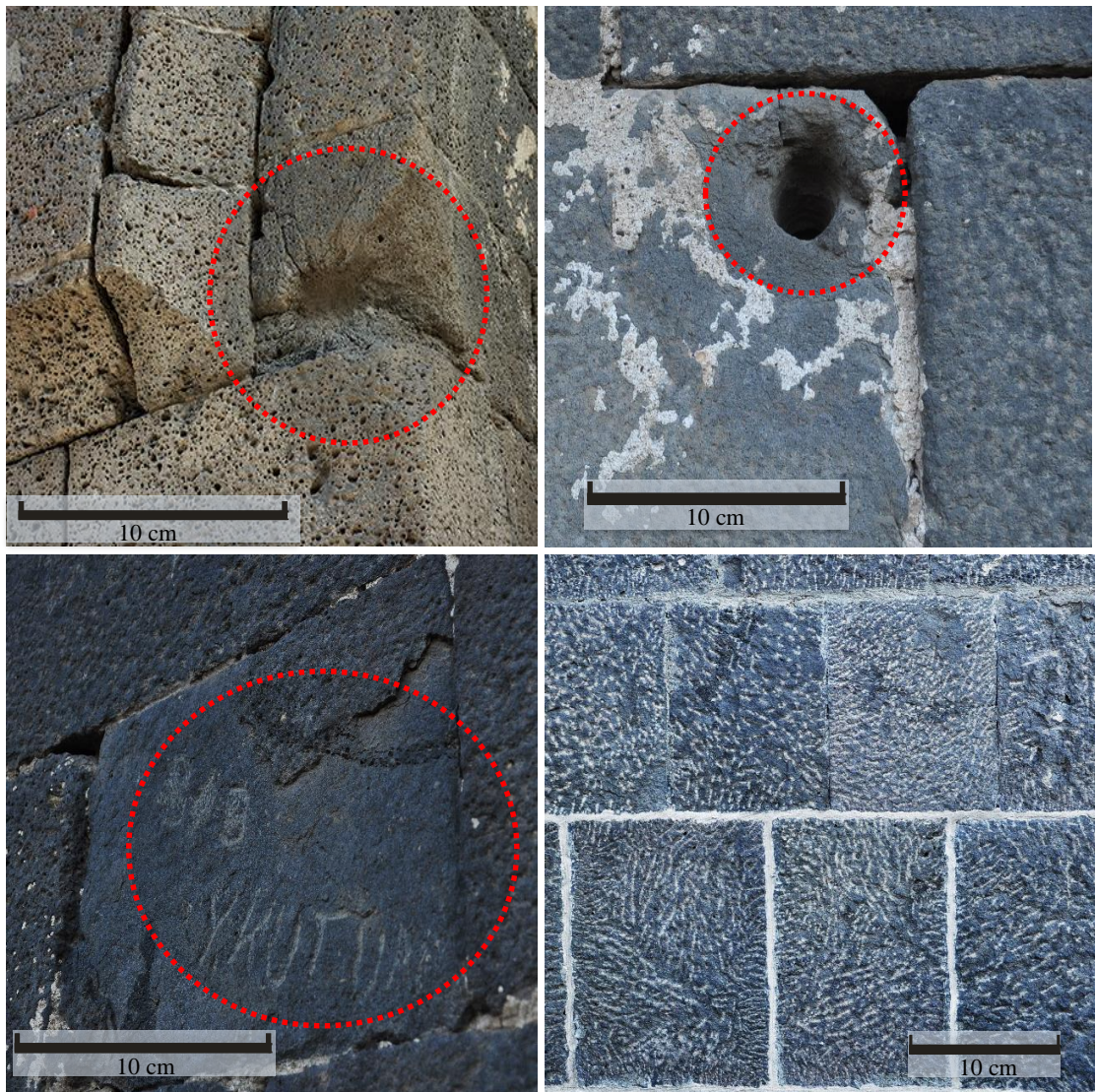


Figure 5.15 Mechanical damages on sections of the DCW (clockwise from top left: impact damage; cavity; scratch/engrave; keying) (damages are indicated by dashed circles)



Figure 5.16. Dismantled stone blocks and a breach in the DCW (dismantled sections are indicated by dashed circles)



Figure 5.17 Demolished segments of the north section of the DCW (demolished parts are indicated by reddish dashed lines)

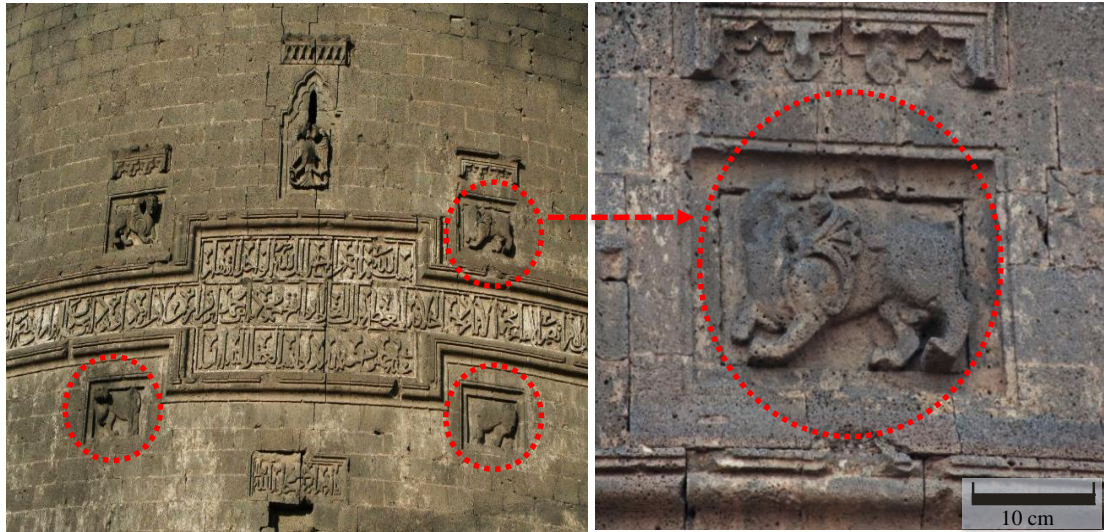


Figure 5.18 The missing parts of reliefs carved on the Ulu Beden Tower (the reliefs have missing parts are indicated by dashed circles) (image credit: Governorship of Diyarbakır, 2017)

5.1.4 Discolorations and Deposits

The weathering forms categorized as discoloration and deposits include all forms of color modification and deposits on stone surfaces. ICOMOS subdivided these forms into crusts (black crust, salt crust), deposit, discoloration (coloration, bleaching, moist area and staining), efflorescence, encrustation (concretion), film, glossy aspect, graffiti, patina (iron-rich, oxalate patina), soiling, and subfluorescence.

The discolorations and deposits on the DCW are mainly in the form of crusts, deposits, discoloration, efflorescence and graffiti.

Crust formation is found on some specific sections of the DCW (Figure 5.19). Crust is defined as the accumulation of materials on the stone surface, and it may include deposits with a combination of materials derived from the stone (ICOMOS-ISCS, 2008). A crust is usually characterized by a dark color (black crust); however, it can also have a light color.

The development of salt crust is associated with the concentration of salt on the stone surface. As a result of wetting and drying cycles, the soluble salts form a layer of salt crust on the stone surface. (ICOMOS-ISCS, 2008).

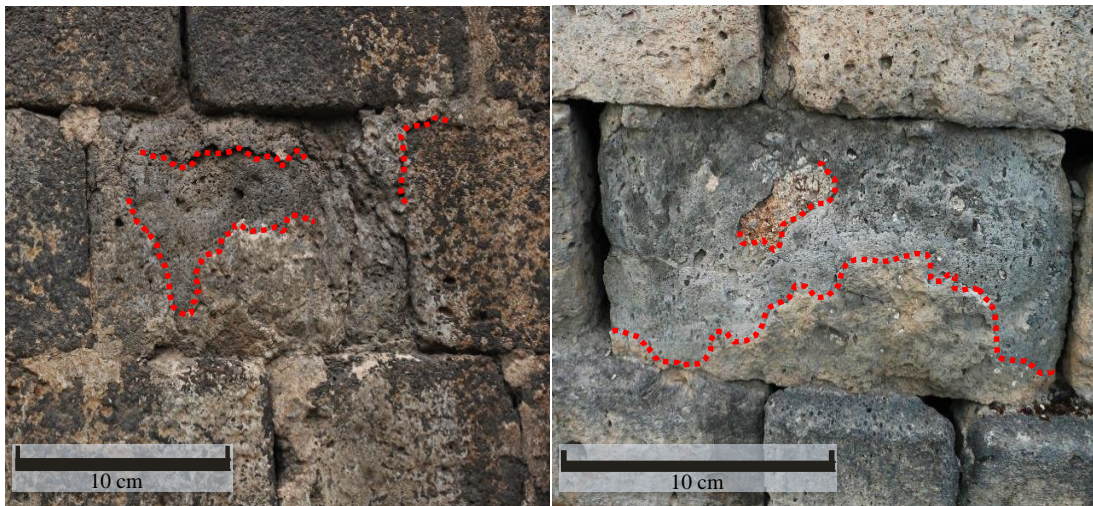


Figure 5.19 Crust formations on the DCW (the crust layers are roughly indicated by reddish dashed lines)

Deposit is another common weathering form found on various sections of the DCW. Deposits refer to the accumulation of exogenic material on the stone surface. Deposits vary in thickness, color, morphology and origin. Deposits can be splashes of mortar or paint, bird droppings, black soot or dust. The remains of conservation materials or housing are also categorized as deposits through the present study (Figures 5.20 and 5.22).

The DCW have suffered from discoloration-associated problems. These can be observed at all levels of the walls and towers. Discoloration is described as color change of the stone material in color parameters such as hue, value and chroma (ICOMOS-ISCS, 2008).



Figure 5.20 Deposits on the sections of the DCW (deposits are indicated by dashed circles)

The DCW are particularly susceptible to bleaching/fading and staining (Figure 5.21) forms of discoloration. The discoloration of the stone material affects the aesthetic appeal of the DCW.

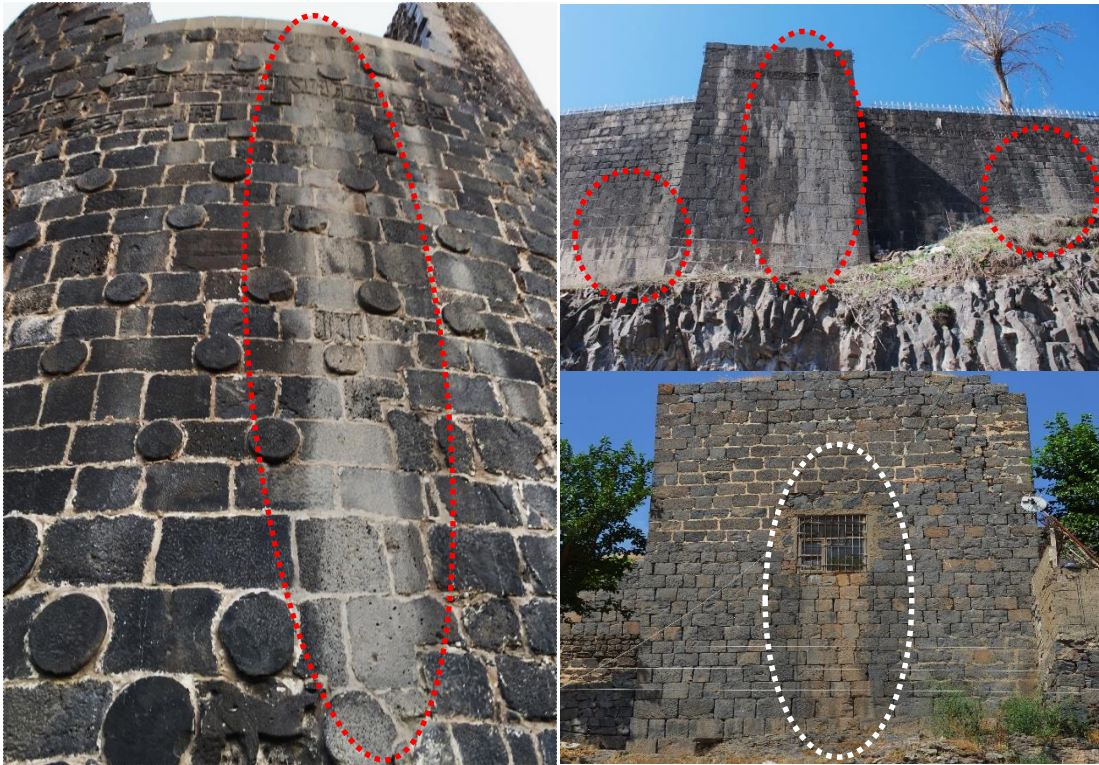


Figure 5.21 Bleaching and staining on sections of the DCW (bleaching is indicated by reddish dashed circles and staining is indicated by whitish dashed circle)

In addition, firing is a common cause of discoloration of the basalt material used in the DCW. For instance, in order to bake bread, tandoors are located at the corners of the walls, resulting in discoloration due to black soot.

Some abandoned portions of the DCW, especially the inner sides of some towers, are used for shelter by the homeless. Here, the walls are discolored due to unconscious human-induced activities (Figure 5.22).

Firing activities may induce stress and differentiations in the surface temperature of the stone material. Hence, fires may modify the physical properties of stone, and finally, such damages may increase the susceptibility of stone to deterioration (Steiger et al., 2011).



Figure 5.22 Discoloration of the stone surface due to human-induced activities (left: A tandoor located just under the Yedi Kardeş Tower; right: Inside part of an abandoned tower) (left image credit: Aşılı, 2010)

Moist areas cause another form of discoloration on the DCW. Moist areas found on the DCW can be characterized as a general weathering form that corresponds to the darkening of stone surfaces due to dampness (Figure 5.23).

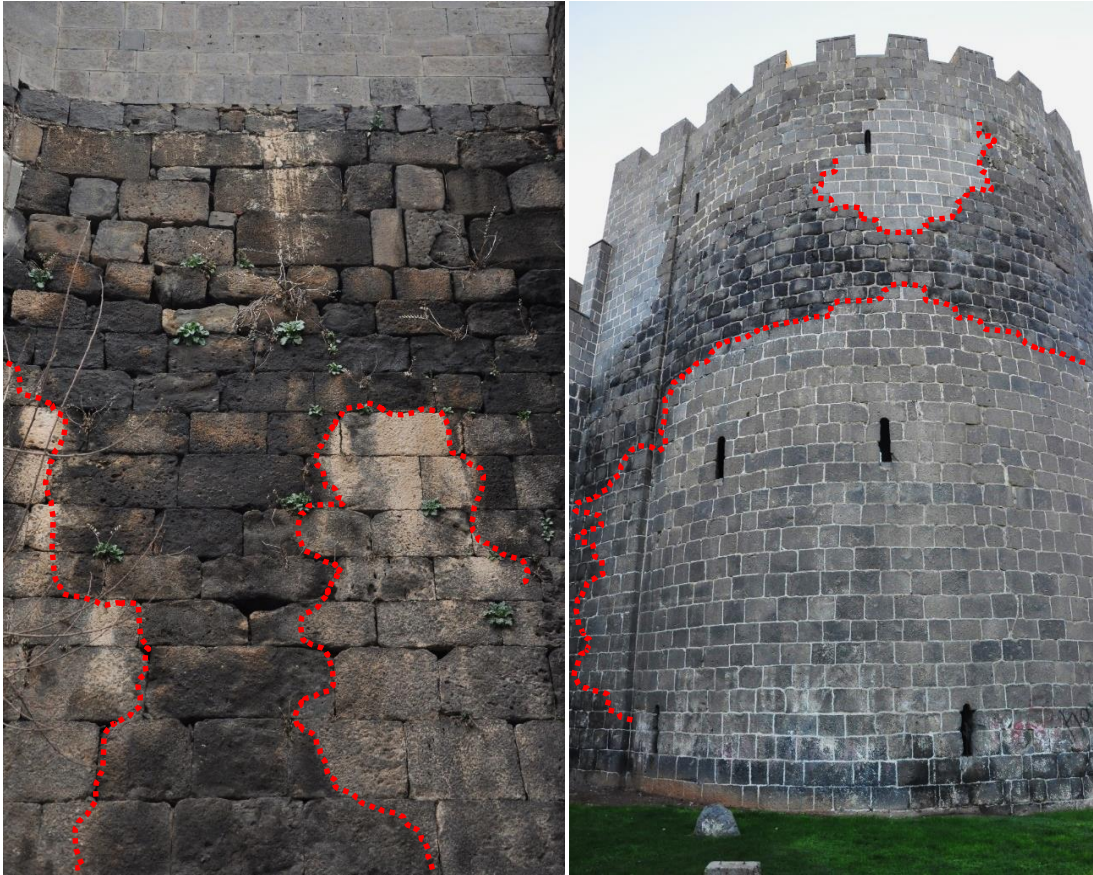


Figure 5.23 Moist areas on sections of the DCW (the moist area boundaries are roughly indicated by reddish dashed lines)

Efflorescence patterns are also detected on the stone surfaces of the DCW (Figure 5.24). The term, efflorescence, broadly refers to any occurrence of light-colored, powdery or whisker-like salt crystals on the stone surface (ICOMOS-ISCS, 2008).

Unlike deposits, the constituents of efflorescence may come from the stone itself and it may originate from such soluble salts as NaCl , Na_2SO_4 , $\text{MgSO}_4 \cdot 7\text{H}_2\text{O}$, CaCO_3 , BaSO_4 or $\text{SiO}_2 \cdot n\text{H}_2\text{O}$ (ICOMOS-ISCS, 2008).



Figure 5.24 Efflorescence patterns on the DCW (the whitish patterns on the stone surface are considered as efflorescence)

Graffiti is another form of discoloration and deposits found on many sections of the DCW (Figure 5.25). Graffiti can be writing, scratching, cutting or engraving. It can also be paint, ink or similar materials applied to the stone surface (ICOMOS-ISCS, 2008).



Figure 5.25 Paintings on the DCW

5.1.5 Biological Colonization

Living organisms also have a contribution to the deterioration of stone materials, and their actions on decay of the stone are somewhat considered less important than the other weathering agents (Schaffer, 1972).

Biological colonization refers to the colonization of rock material by plants and such micro-organisms as algae, bacteria, cyanobacteria, lichens and fungi. Bio-colonization also points to the influences that induced by different organisms such as animals nesting on and in the rock material (ICOMOS, 2008). Biological weathering is considered as a combination of physical and chemical activities, as an interaction of stone surfaces and living organisms.

Tree roots, for instance, can exert pressure on stone and then lift large blocks up as they grow. On the other hand, lichens produce acid that can deteriorate even the most durable stone materials. Biological colonizations as fungi, algae and plants affect the aesthetic appeal of the stone material (Siegesmund and Török, 2011).

The biological colonization on the DCW is commonly in the form of plants (Figure 5.26) and lichens (Figure 5.27), but alga and moss development are also found on some specific sections of the DCW. The higher plants frequently grow through the open joints, cracks and the missing parts on the walls and towers.



Figure 5.26 Plants growing on sections of the DCW



Figure 5.27 Lichens on sections of the DCW (lichens are indicated by dashed circles)

In addition to the above-mentioned weathering forms, the DCW are significantly affected from the damages caused by human activities. Those activities can be classified as environmental pollution, illegal housing, painting, vibrations caused by traffic, fires, the dismantling of stone blocks and so forth (Figure 5.28).



Figure 5.28 Paint and illegal housing on the east section of the DCW (the houses no longer exist, however, traces of them can be found on the walls)

5.2 Mapping Visual Decay Forms

The weathering forms on the DCW were also mapped in this study. Many field surveys were conducted to examine the state of deterioration on the sections of the DCW. The proper description of problems and detailed information on the state of stone deterioration are essential for further studies. In order to describe the state of stone deterioration, mapping weathering forms is an important approach (Galán and Aparicio, 2009).

Weathering maps document the deterioration forms on the surface of a structure. It can be prepared for a façade, a stone surface or for all the façades of a structure (Fitzner et al., 1995). The purpose of mapping of weathering forms is to visualize the distribution, intensity and extent of weathering forms. As a nondestructive method, mapping the weathering forms provides information for monitoring the deterioration patterns and predicting their future outcomes (Fitzner et al., 1992; Fitzner et al., 1995; Fitzner, 2004).

The DCW have been subjected to interventions such as destruction, reconstruction, restoration and modification over the centuries. The information on past interventions plays a crucial role in how the DCW has been conserved to this day. It is also important to assess the overall impact of past interventions on the performance and integrity of the stone material. It is especially necessary to categorize the causes and forms of the deterioration observed at the site and determine whether they are a result of interventions or occurred as a result of external factors (Ema et al., 2013; Fort et al., 2013).

Since the repairs on the DCW were not recorded properly it is hardly possible to produce weathering maps of the original forms of the DCW. In addition, since the overall length of the DCW is *ca.* 6,000 meters, it is also hard to map entire segments. In order to select the most appropriate sections and map their weathering forms, several field surveys were conducted in the study area. Two specific sections of the DCW were selected for mapping the visual decay forms.

One is the inner façade of the Dağ Gate located on the north section, and the other is a tower located on the south section of the DCW (see Figure 1.20).

The former is selected to document the deterioration state of a recently restored section, and the latter to document the deterioration state of a relatively original section. The weathering maps of these sections (Figures 5.30 and 5.32) are produced in accordance with the method suggested by Fitzner et al. (1995). However, in order to overcome the terminological confusion, the glossary published by ICOMOS were followed for the description of the weathering forms.

During the field surveys, photographs of the sections from different perspectives were taken, and some sketches were drawn to assess the state of weathering.

The collected data were then used to draw the maps. Moreover, in order to reveal the type and distribution of the construction materials, the sections were systematically investigated; and the results are illustrated in the material maps of the studied sections (Figure 5.29 and 5.31). Mapping of the visual decay forms are produced by using computer aided design software, AutoCAD (2014), and image processing software, PhotoShop (CS6; Adobe Systems).

The documented weathering patterns on the first section (Figure 5.30) are classified into the categories of deposits, material loss, delamination, fragmentation, cracks and fractures, scaling, discoloration and moist areas. Here, the category of deposits includes crusts, efflorescence, splashes of mortar or paint, bird droppings, soot, dust and plaster. The cracks and fractures category includes vertical, horizontal or network cracks on the façade. Since the detachments observed on the façade developed in different forms, they were represented separately as delamination, fragmentation and scaling. The features induced by loss of stone material include erosion, mechanical damage and missing parts. Those weathering forms were represented in the material loss category. The discoloration category includes color changes in the form of bleaching or fading; and finally, the darkening of the stone surface due to dampness is represented in the category of moist areas.

Figure 5.29 reveals the materials employed in the construction of the inner section of the Dağ Gate. The types of materials used in the structure are classified as massive and vesicular basalt, limestone and brick. As Figure 5.30 shows, the external façade of the inner side of the Dağ Gate is examined, and the common weathering patterns are compared to the relatively original condition of the stone material. The uppermost part of the façade (see the upper section of the dashed line) was recently restored and is characterized by weathering forms such as deposits and moist areas. However, the lower parts (see the lower section of the dashed line) are relatively original and characterized by common weathering forms such as scaling, material loss,

discoloration, cracks and fractures, delamination and fragmentation. Like the upper part, deposits and moist areas are also found on the lower part of the façade.

The documented weathering patterns on the second section (Figure 5.32) are classified into such categories as material loss, discoloration, detachment, biological colonization, crust and alveolization. Here, the category of material loss includes mechanical damages and material losses. The observed mechanical damages on the tower in question are mainly in the form of missing parts and some impact damages. Bleaching, moist area and staining of the material are categorized in the discoloration. The detachments are here categorized to represent blistering, delamination, crumbling, chippings and scaling forms of the deterioration. The deterioration forms induced by the biological colonization include particularly the higher plants and animals nesting. Since the crust and alveolization formations are commonly observed on the tower façade, they did not include to their main groups (i.e., discoloration and material loss) and indicate on the map as separate forms of deterioration.

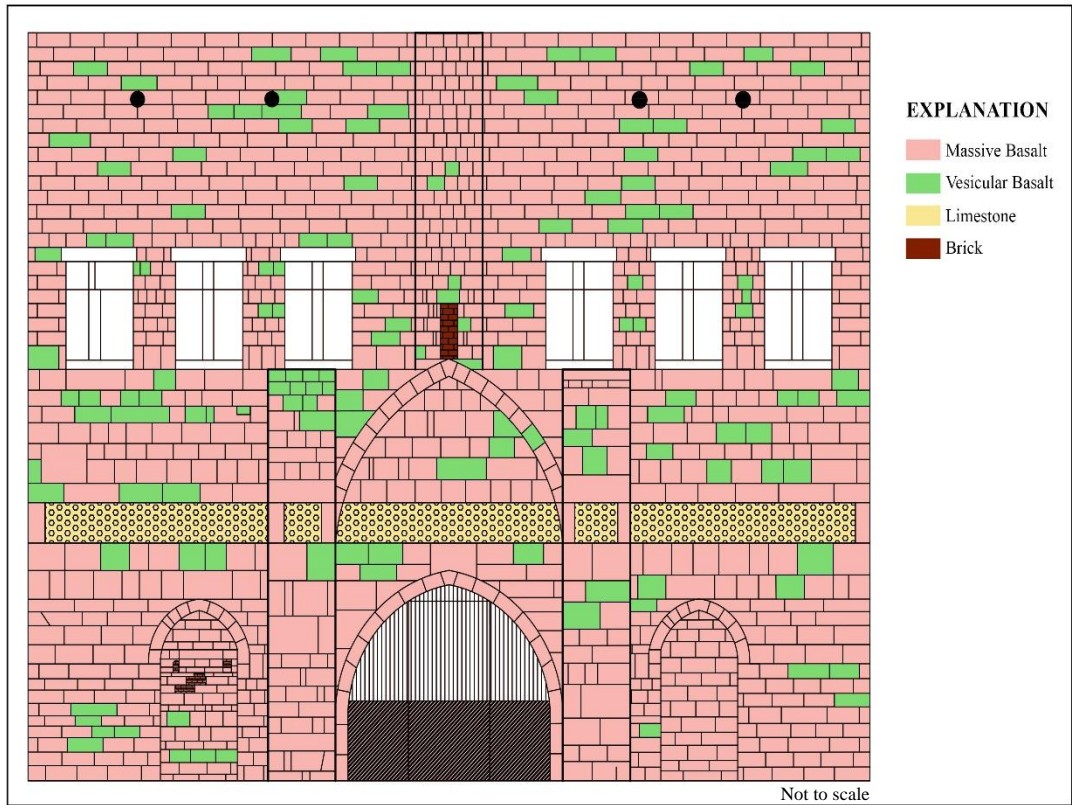


Figure 5.29 The material map of the inner section of the Dağ Gate

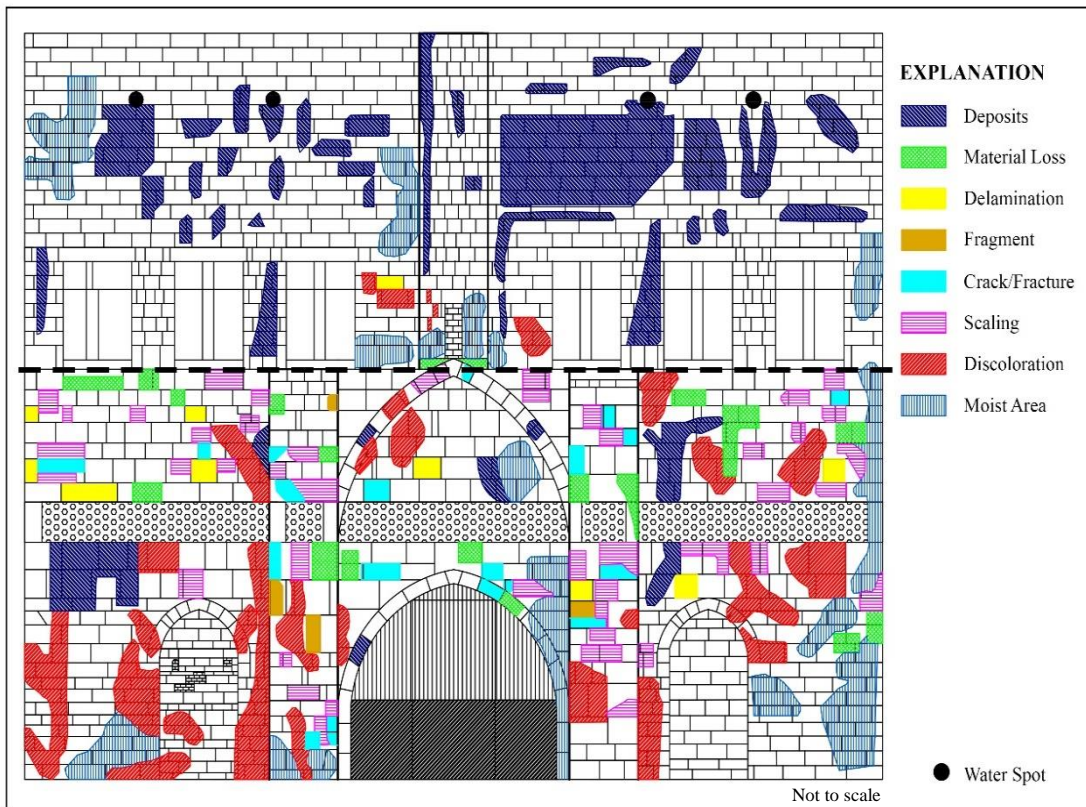


Figure 5.30 The map of visual decay forms on the inner section of the Dağ Gate

Figure 5.31 indicates the materials employed in the construction of the tower façade. The materials used in the construction are classified as massive and vesicular basalt and limestone. As Figure 5.32 shows, the external façade of the tower is examined, and the common weathering patterns are represented by means of the decay map. As it can be followed from the decay map, especially, missing parts are located in the upper parts of the tower and most of the higher plants grew through those missing parts. Considering the large basalt blocks, carvings and decorations, it can be inferred that especially the lower part of the tower retains its original state. Therefore, the weathering has a more pronounced effect on the lower parts.

Unlike to the former one, here the crust and alveolization formations are commonly witnessed. Such types of deterioration are also unusual for the DCW. The formation of crust and alveolization can be attributed to the tower location. In other words, since the tower is seated on the steep slope facing the Tigris River, it might become more vulnerable to moisture, salt, wind and solar exposure. The weathering forms on the tower façade partially differ from those of the gate façade. Although formations of crust and alveolization are unusual weathering forms for the DCW, they are common on the lower part of the tower façade. This can be attributed to the location of the tower on a steep slope facing the Tigris River, making it more vulnerable to moisture, salt, wind and solar exposure.

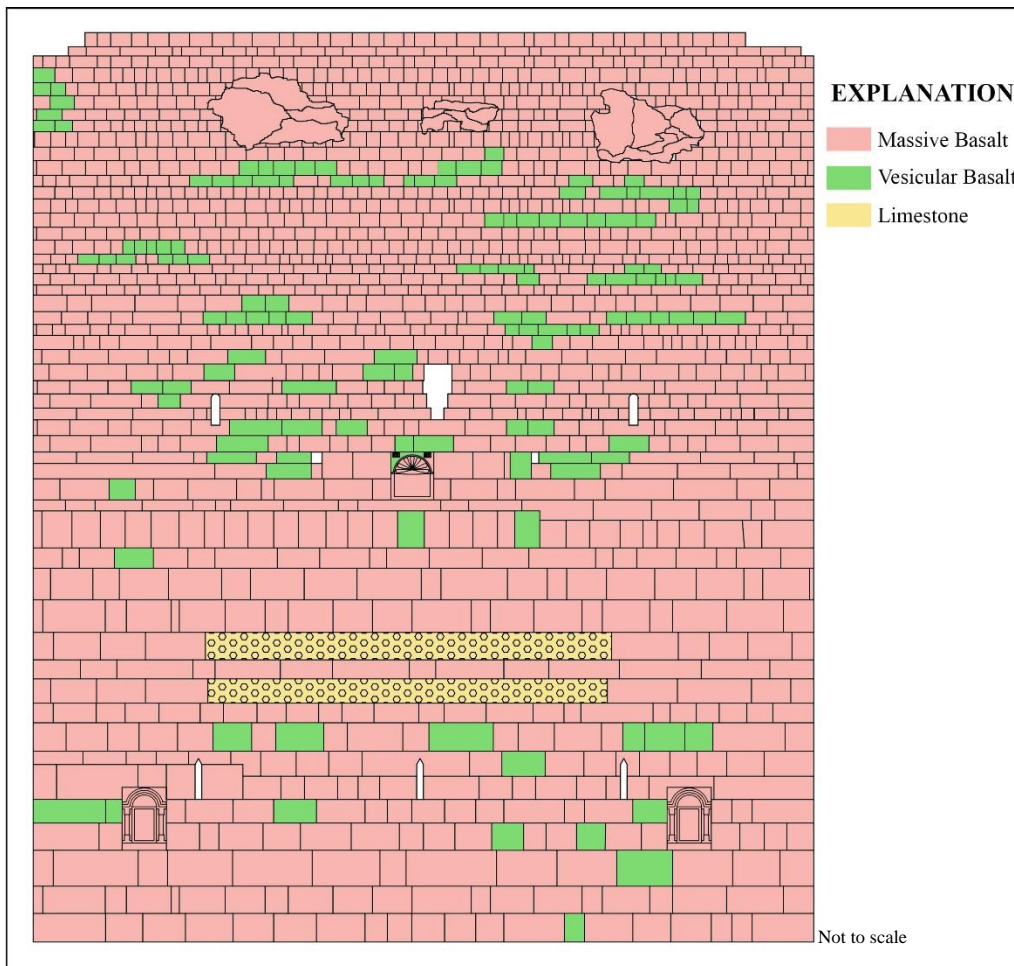
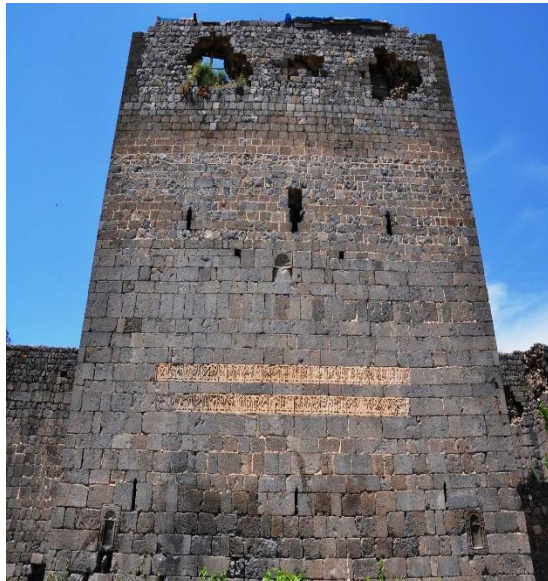


Figure 5.31 The material map of the tower 52

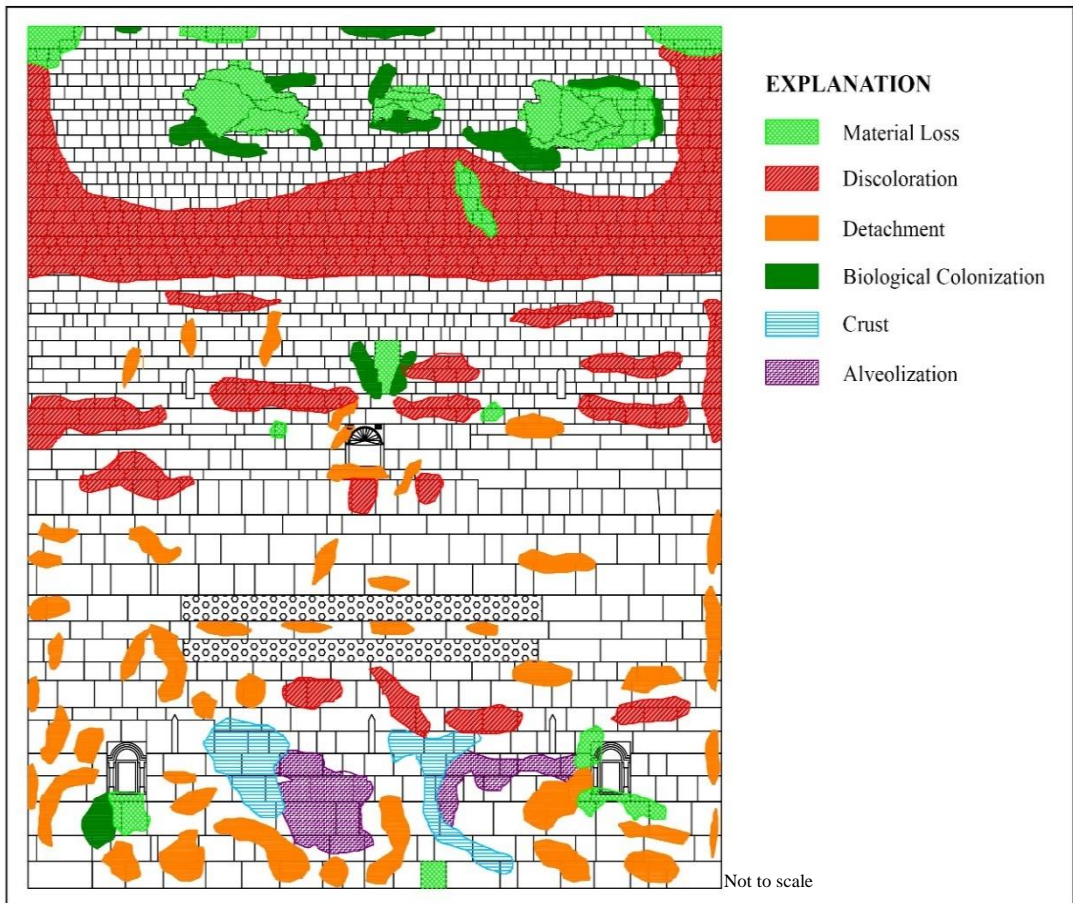
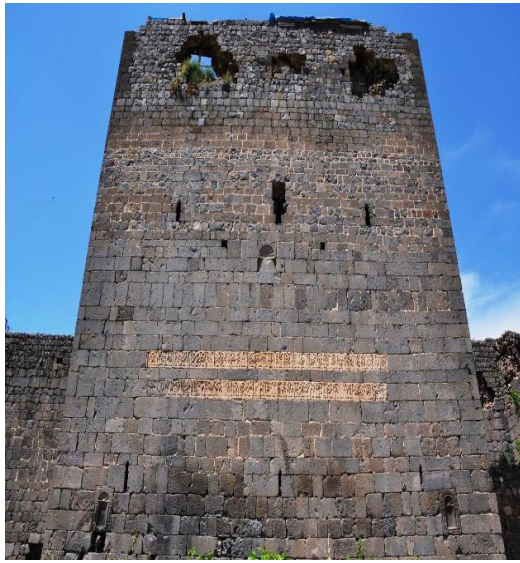


Figure 5.32 The map of visual decay forms on the tower 52

5.3 Accelerated Weathering Tests

The ultimate goal of science is to predict the behavior of the entire geosystem. Considering the deterioration of the building stones, making predictions on their behavior will not only improve our understanding of decay mechanisms, it will also provide a projection for assessing the behavior of the similar systems (Trofimov and Phillips, 1992; Warke et al., 2003). Many testing procedures for measuring the physical properties that are directly relevant to the durability of rock material or for simulating natural decay mechanisms have been reported in the literature (Price, 1987). In order to study the physical deterioration of stones and to determine their durability, environmental conditions are artificially simulated through various accelerated weathering tests (Knöfel et al., 1987). The most commonly used durability tests include wetting-drying, freezing-thawing, salt crystallization, thermal cycles, acid dissolution, ultraviolet radiation exposure and ethylene glycol saturation (Sleater, 1978; Cawsey and Mellon, 1983; Fookes et al., 1988; Ross and Butlin, 1989; Fitzner and Kalde, 1991). Durability tests in accelerated conditions are performed to evaluate the suitability of various stone materials as a function of time of exposure to the various agents of deterioration. In other words, these tests are useful for (i) monitoring and predicting the medium- to long-term behavior of stone materials, (ii) assessing the weathering mechanisms that cause deterioration and (iii) determining the tests that provide the most reliable results for evaluating the degradation of stone materials (Rossi-Doria, 1985; Pfikryl et al., 2003).

Selecting the most suitable tests is based on the climatic and environmental conditions of the study area. The severe continental climate conditions of Southeast Anatolia dominate the province of Diyarbakır. The long-term meteorological data for Diyarbakır indicate that summers are dry and very hot, while winters are cold and wet with some frosty nights. Thus, weathering processes such as wetting-drying and freezing-thawing have an effect on the study area. During the field investigations, it is also observed that there are some deterioration patterns associated with salt attack. Soluble salts that originate from sources such as soils, road de-icers, biological matter, pollution and from the ordinary cement that is frequently used for construction

purposes make it essential to conduct salt crystallization tests (Topal and Doyuran, 1998; Odgers and Henry, 2012). Based on the environmental characteristics of the site where the stone is exposed and field observation, wetting-drying, freezing-thawing and salt crystallization tests were performed in this study to assess the durability of the massive and vesicular basalts.

Block samples collected from the basalt outcrops along the DCW and from the quarries in their vicinity were cut into cubes and used for these durability tests. Most of the cubic samples have edge lengths of 7 centimeters with a few exceptions. The ends of the specimens were flattened in accordance with the ISRM and ASTM standards (ISRM, 1981; ASTM, 2017a). A total of 180 fresh basalt specimens (90 massive and 90 vesicular) from different outcrops and quarries were used for the accelerated weathering tests. For each experimental set (i.e., wetting-drying, freezing-thawing and salt crystallization) 30 massive and 30 vesicular basalt specimens were tested.

The durability tests were performed in accordance with the recommendations and standards suggested by RILEM (1980), TSE (2011) and ASTM (2013, 2017b, 2017c, 2017d). In addition to visual examination, the weight loss, effective porosity, dry and saturated unit weights, water absorption under atmospheric pressure and under pressure, the sonic velocity and the uniaxial compressive strength of the samples were measured at different test cycles and compared with those of the fresh samples. For the uniaxial compressive strength measurements, at the end of each certain test cycles, 10 samples (5 massive and 5 vesicular) were excluded from the sample sets of the tests. The excluded samples were then used to determine the index parameters in question.

5.3.1 Wetting and Drying Test

Wetting-drying tests were performed to understand the effects of wetting and drying cycles on the massive and vesicular basalt samples for their resistance to deterioration. As Fookes et al. (1988) note, wetting and drying affects the engineering and

petrographic parameters of rocks, specifically, their porosity, texture, secondary mineral content and microfractures.

The wetting-drying cycles of the basalt samples were determined using the procedure described in ASTM (2017d). For the wetting-drying tests, the cubic samples were fully immersed for at least 18 hours in distilled water at 15-20 °C. The samples were dried in an oven at 65 °C for 20 hours and then allowed to cool to ambient room temperature. The completion of this sequence constituted one wetting-drying cycle and was repeated for a total of 80 cycles.

The test was conducted on two sets of 30 massive and 30 vesicular basalt samples with edge lengths of 7 centimeters. The index properties of the massive and vesicular basalt samples were determined after 10, 30, 50, 60, 70 and 80 test cycles and compared with the index properties of the fresh basalt samples. The average and normalized average values of these parameters of the massive and vesicular basalt samples after specific numbers of wetting-drying test cycles are shown in Tables 5.1 and 5.2, respectively. Since the original data have different units and values, the average results were normalized for meaningful comparisons between the different parameters. The average values were normalized by dividing each of the results with the corresponding initial result of the fresh samples. It gives weight percent of each parameter. Thus, the fresh samples are represented by 100% for all variables. Variations in the physical and mechanical properties of the massive and vesicular basalts after wetting-drying test cycles are shown in Figures 5.33 and 5.34. In order to plot these figures, the normalized values shown in Tables 5.1 and 5.2 were used.

At the end of 80 wetting-drying tests, no remarkable change in weight is observed (Figure 5.33-a). The total weight losses of the massive and vesicular basalt samples are measured as 0.72% and 0.98%, respectively.

Apart from some discoloration, the morphology of the samples remains unchanged. The color of the massive and vesicular samples became lighter and yellowish after the thirtieth wetting-drying cycle.

The effective porosity of the basalt samples increases considerably at the end of the wetting-drying cycles. The effective porosity of the massive and vesicular basalt samples increases by 30.25% and 37.75%, respectively (Figure 5.33-b). There are slight changes in the dry unit weight of the samples. The reduction in the dry unit weight of the massive and vesicular basalt samples is almost equal at 2.74% and 2.93%, respectively, at the end of 80 wetting-drying cycles (Figure 5.33-c). The water absorption capacity of the samples under atmospheric pressure increases progressively at the end of the cycles. The water absorption under atmospheric pressure of the massive and vesicular basalt samples is 37.70% and 44.97%, respectively (Figure 5.33-d). The sonic velocity of the dry massive and vesicular samples decreases by 6.39% and 16.72%, respectively, at the end of 80 wetting-drying cycles (Figure 5.33-e). The uniaxial compressive strength of the samples is also reduced at the end of the wetting-drying cycles. The massive and vesicular basalt samples' reduction in compressive strength is measured as 24.98% and 31.32%, respectively (Figure 5.33-f).

Table 5.1 Averages and normalized averages of the index properties of the massive basalts after the wetting-drying cycles

Cycles	Weight (g)	Normalized Weight (%)	Effective Porosity (%)	Normalized Porosity (%)	Dry Unit Weight (kN/m ³)	Normalized Dry Unit Weight (%)	Water Abs. by Weight (atm. press.) (%)	Normalized Water Abs. by Weight (atm. press.) (%)	Dry Sonic Velocity (m/s)	Normalized Dry Sonic Velocity (%)	UCS (MPa)	Normalized UCS (%)
0	860.97	100.00	4.11	100.00	27.51	100.00	1.07	100.00	4911.11	100.00	145.49	100.00
10	860.11	99.90	4.18	101.70	27.50	99.96	1.08	101.05	4904.54	99.87	139.42	95.83
30	858.48	99.71	4.25	103.38	27.48	99.90	1.11	104.22	4882.89	99.43	135.67	93.25
50	857.49	99.60	4.54	110.41	27.43	99.70	1.20	112.85	4778.13	97.29	129.56	89.05
60	856.75	99.51	5.00	121.60	27.12	98.58	1.27	119.62	4697.21	95.64	121.91	83.79
70	855.55	99.37	5.28	128.49	26.98	98.09	1.32	124.12	4603.36	93.73	115.72	79.54
80	854.79	99.28	5.35	130.25	26.84	97.56	1.47	137.70	4597.44	93.61	109.15	75.02

Table 5.2 Averages and normalized averages of the index properties of the vesicular basalts after the wetting-drying cycles

Cycles	Weight (g)	Normalized Weight (%)	Effective Porosity (%)	Normalized Porosity (%)	Dry Unit Weight (kN/m ³)	Normalized Dry Unit Weight (%)	Water Abs. by Weight (atm. press.) (%)	Normalized Water Abs. by Weight (atm. press.) (%)	Dry Sonic Velocity (m/s)	Normalized Dry Sonic Velocity (%)	UCS (MPa)	Normalized UCS (%)
0	847.62	100.00	9.91	100.00	24.50	100.00	2.18	100.00	3931.15	100.00	63.30	100.00
10	846.80	99.90	10.13	102.25	24.34	99.33	2.19	100.47	3893.58	99.04	58.92	93.08
30	845.60	99.76	10.84	109.42	24.26	99.02	2.23	102.31	3642.46	92.66	55.61	87.85
50	843.78	99.55	11.85	119.62	24.23	98.88	2.41	110.51	3440.35	87.52	52.82	83.46
60	841.97	99.33	12.28	124.00	23.88	97.45	2.66	122.07	3352.27	85.27	49.74	78.59
70	840.31	99.14	12.92	130.41	23.85	97.33	2.83	129.76	3332.07	84.76	45.96	72.62
80	839.29	99.02	13.65	137.75	23.78	97.07	3.16	144.97	3274.05	83.28	43.47	68.68

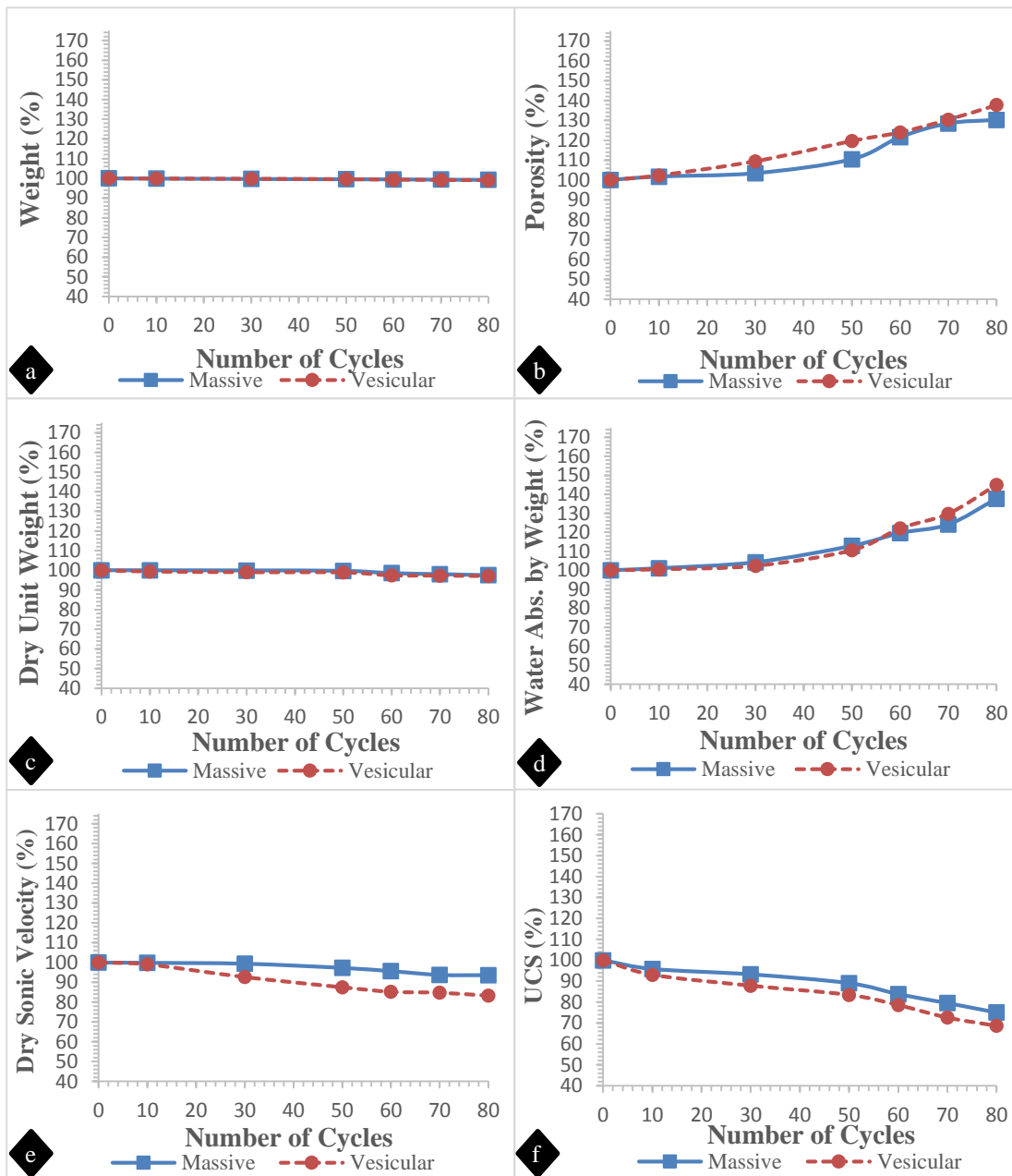
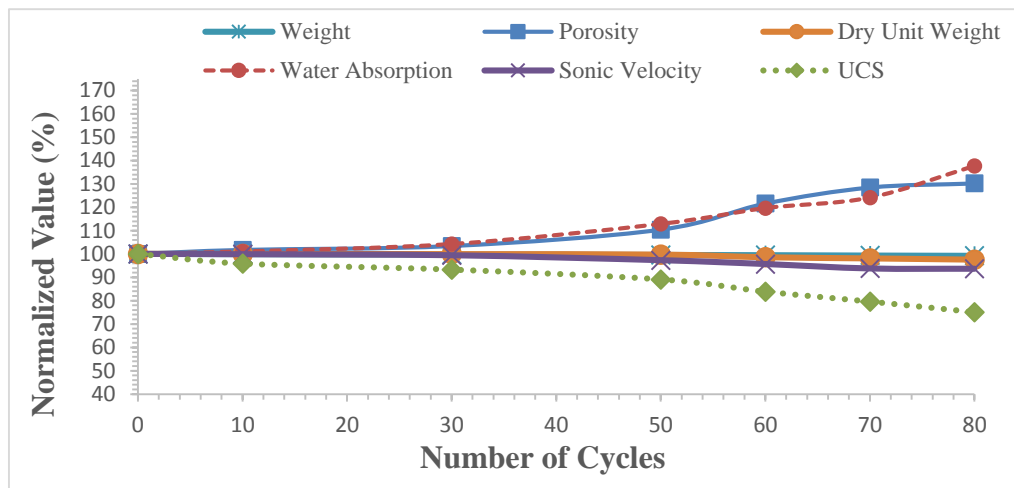
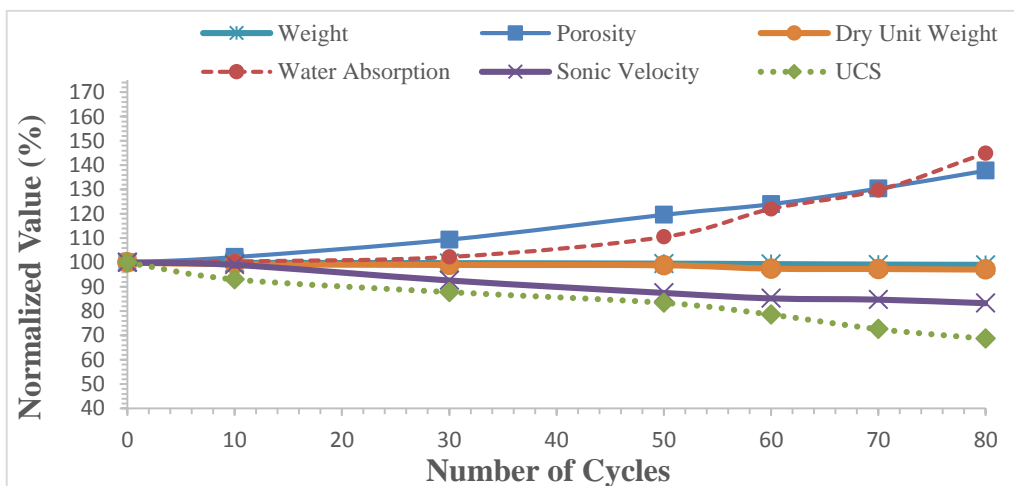


Figure 5.33 Variations in the physical and mechanical properties of the massive and vesicular basalts after the wetting-drying cycles

As Figure 5.34 shows, the wetting-drying cycles result in no significant changes in the weight loss and dry unit weight of the massive and vesicular basalt samples. However, the cycles affect parameters such as porosity, water absorption, sonic velocity and uniaxial compressive strength. The porosity and water absorption of the samples increase greatly, whereas the sonic velocity and uniaxial compressive strength decrease throughout the cycles. In general, wetting and drying has an effect on both the massive and vesicular samples. However, the massive basalt samples are more resistant to this test than the vesicular basalt samples.



(a)



(b)

Figure 5.34 Variations in the physico-mechanical properties of (a) the massive and (b) the vesicular basalt samples at the end of the wetting-drying cycles

5.3.2 Freezing and Thawing Test

The expansion of water when it freezes in the pores of rocks is a major cause of their deterioration, especially those employed as dimensional stones (Robertson, 1987; Ruedrich and Siegesmund, 2007). Freezing-thawing tests attempt to reproduce the stresses that can arise inside rock material when ice crystals form. These effects are generally obtained by varying the temperature of samples containing a known amount of water to higher and lower than 0 °C (Rossi-Doria, 1985; Topal and Sözmen, 2000). The effect of freezing and thawing on some of the engineering and petrographic properties of the rocks was reported by Fookes et al. (1988) who noted that freezing and thawing affects parameters such as compactness, porosity, texture, moisture content and microfractures.

In order to understand the frost resistance of the material, the freezing-thawing test was conducted following the procedure described in TSE (2011) and ASTM (2017c). The test was conducted on two sets of 30 massive and 30 vesicular basalt samples with edge lengths of 7 centimeters. For the freezing-thawing test, the cubic samples were fully immersed in a special solution of a 0.5% isopropyl alcohol/water for 24 hours at 15 °C to 20 °C. As ASTM (2017c) suggests, this solution is used to lower the viscosity of water and facilitate its penetration into the micropores of the samples prior to freezing. To initiate the freezing-thawing test, the samples immersed in the solution were placed in the freezing-thawing chamber located in the Department of Geological Engineering at METU. The chamber runs automatically within the limits suggested by TSE (2011). The freezing-thawing chamber was programmed to gradually fluctuate the temperature from +2 °C to -15° C for 13 hours. The completion of this sequence constituted one freezing-thawing cycle and was repeated for a total of 100 cycles. Although 100 cycles of freezing and thawing is too much for the study location, the number of cycles were intentionally increased to observe excessive damages of the frost action on the samples in question. The index properties of the massive and vesicular basalts were determined after 10, 20, 70, 80, 90 and 100 test cycles. The measurements performed for the wetting-drying tests were also conducted for the freezing-thawing test cycles, and the normalization of the results followed the same

procedure as the wetting-drying results. The average and normalized average values of the index parameters of the massive and vesicular basalt samples after specific numbers of freezing-thawing cycles are shown in Tables 5.3 and 5.4, respectively.

The variations in the physical and mechanical properties of the massive and vesicular basalts after the freezing-thawing test cycles are shown in Figure 5.35 and 5.36. In order to plot these figures, the normalized results in Tables 5.3 and 5.4 were used.

At the end of 100 freezing-thawing tests, no remarkable change in weight is observed for the massive basalt samples. However, the vesicular basalt samples have a relatively higher weight loss (Figure 5.35-a). The massive and vesicular basalt samples' total weight losses are measured as 0.74% and 3.06%, respectively.

The morphology of the samples reveals some degree of deterioration. The freezing-thawing cycles cause the vesicular basalt samples to become lighter in color, and grainy in feel and appearance at the end of 30th cycle. There are some signs of spalling and flaking at the edges of the massive basalt samples after the cycle 70.

The effective porosity of the massive and vesicular basalt samples is considerably increased at the end of the freezing-thawing cycles. The effective porosity of the massive and vesicular basalt samples is increased by 38.50% and 49.51%, respectively at the end of the 100 freezing-thawing cycles (Figure 5.35-b). There are minor variations observed in dry unit weight of the massive samples. The reduction in dry unit weight of the massive and vesicular basalt samples is 2.26% and 3.08%, respectively at the end of the 100 freezing-thawing cycles (Figure 5.35-c). Effect of freezing-thawing tests on water absorption capacity of the samples under atmospheric are increased progressively at the end of the cycles. The increase in water absorption under atmospheric pressure for massive and vesicular basalt samples are measured as 40.46% and 48.40%, respectively at the end of the 100 freezing-thawing cycles (Figure 5.35-d). The sonic velocity of the dry sample decreases as the number of test cycle increases. The reduction of the sonic velocity for vesicular basalt samples is higher than the massive basalt samples.

The reductions in the sonic velocity values of the massive and vesicular basalt samples are measured as 7.5% and 16.83%, respectively at the end of the 100 freezing-thawing cycles (Figure 5.35-e). The uniaxial compressive strength of the samples is also significantly reduced at the end of freezing-thawing cycles. The loss in UCS is more pronounced after the 70 test cycles. UCS is dropped 24.06% in the massive samples and 27.14% in vesicular sample at the end of 70 test cycles. At the end of the 100 freezing-thawing cycles, the reduction of the compressive strength is measured for massive and vesicular basalt samples as 36.07% and 37.48%, respectively (Figure 5.35-f).

Table 5.3 Averages and normalized averages of the index properties of the massive basalts after the freezing-thawing cycles

Cycles	Weight (g)	Normalized Weight (%)	Effective Porosity (%)	Normalized Porosity (%)	Dry Unit Weight (kN/m ³)	Normalized Dry Unit Weight (%)	Water Abs. by Weight (atm. press.) (%)	Normalized Water Abs. by Weight (atm. press.) (%)	Dry Sonic Velocity (m/s)	Normalized Dry Sonic Velocity (%)	UCS (MPa)	Normalized UCS (%)
0	904.35	100.00	5.31	100.00	27.01	100.00	1.03	100.00	4446.95	100.00	145.49	100.00
10	901.76	99.71	5.79	108.94	26.94	99.74	1.08	105.28	4438.40	99.81	128.77	88.51
20	901.04	99.63	6.28	118.30	26.73	98.97	1.18	114.88	4338.24	97.56	124.70	85.71
70	900.43	99.57	6.38	120.04	26.64	98.64	1.29	125.76	4317.26	97.08	110.49	75.94
80	899.70	99.49	6.40	120.48	26.64	98.64	1.34	130.92	4285.36	96.37	103.88	71.40
90	899.03	99.41	6.72	126.41	26.44	97.87	1.39	135.71	4184.96	94.11	98.39	67.63
100	897.65	99.26	7.36	138.50	26.40	97.74	1.44	140.46	4113.56	92.50	93.01	63.93

Table 5.4 Averages and normalized averages of the index properties of the vesicular basalts after the freezing-thawing cycles

Cycles	Weight (g)	Normalized Weight (%)	Effective Porosity (%)	Normalized Porosity (%)	Dry Unit Weight (kN/m ³)	Normalized Dry Unit Weight (%)	Water Abs. by Weight (atm. press.) (%)	Normalized Water Abs. by Weight (atm. press.) (%)	Dry Sonic Velocity (m/s)	Normalized Dry Sonic Velocity (%)	UCS (MPa)	Normalized UCS (%)
0	847.19	100.00	9.81	100.00	24.72	100.00	2.11	100.00	4095.50	100.00	63.30	100.00
10	845.19	99.76	10.21	104.14	24.62	99.58	2.45	116.15	3979.46	97.17	59.16	93.46
20	842.95	99.50	11.40	116.21	24.36	98.53	2.67	126.92	3886.59	94.90	56.01	88.49
70	838.42	98.96	12.32	125.63	24.27	98.19	2.76	131.04	3632.79	88.70	46.12	72.86
80	828.73	97.82	12.38	126.21	24.18	97.81	2.83	134.55	3580.58	87.43	43.62	68.91
90	823.90	97.25	13.81	140.81	24.03	97.22	3.04	144.23	3473.76	84.82	41.03	64.82
100	821.29	96.94	14.66	149.51	23.96	96.92	3.12	148.40	3406.03	83.17	39.60	62.52

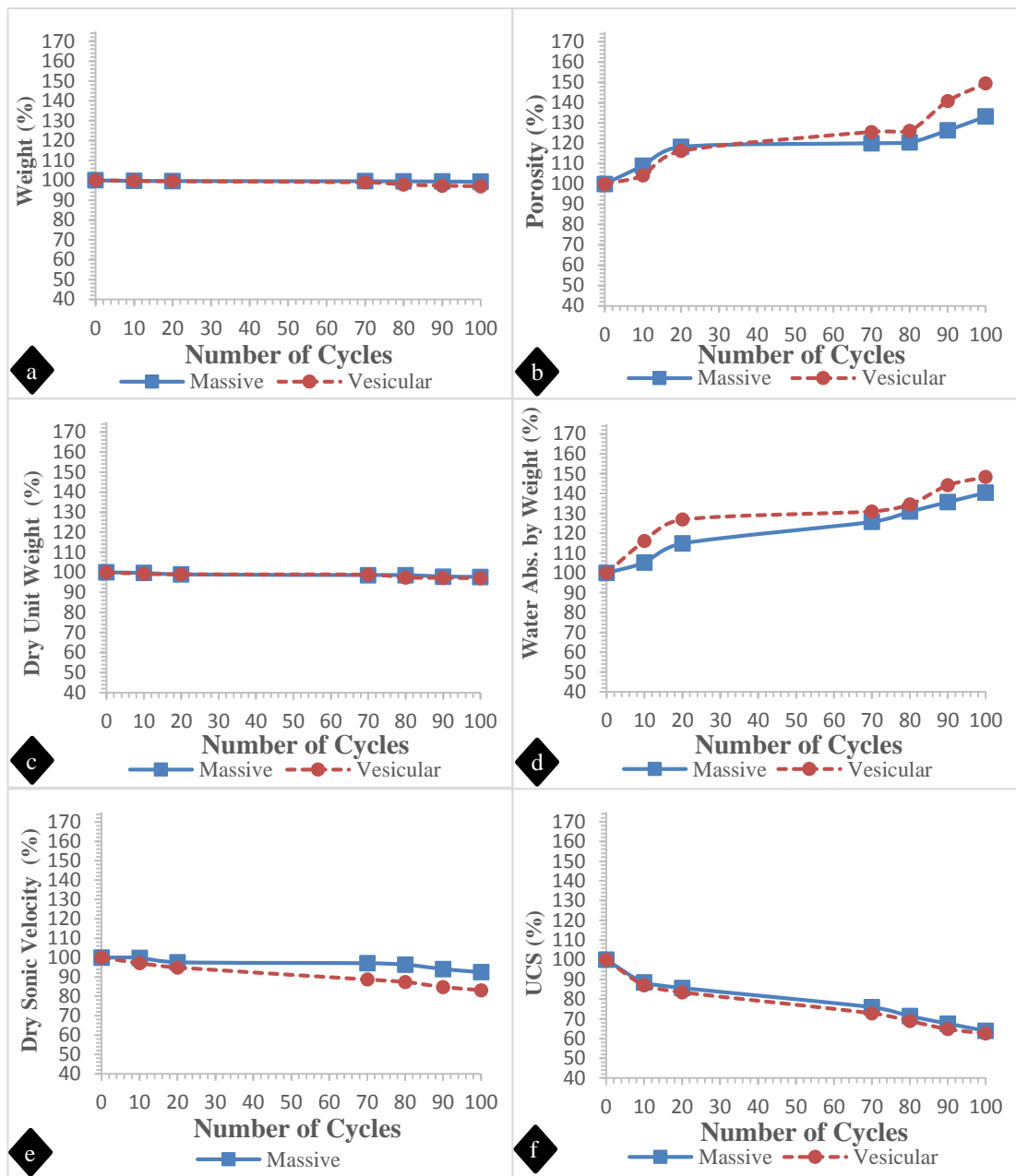
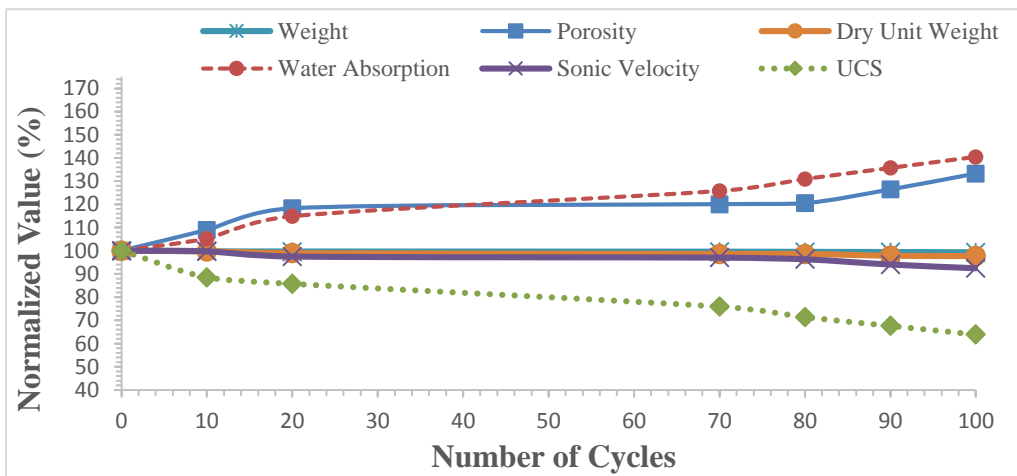
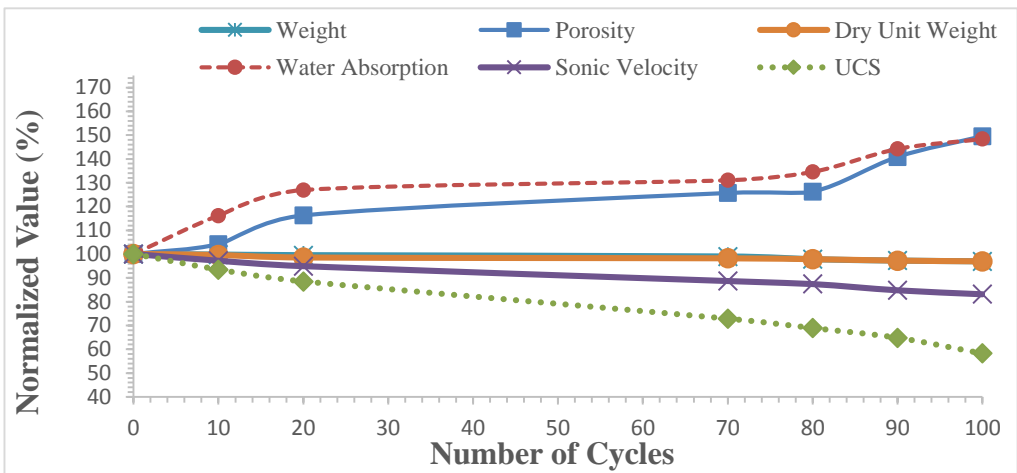


Figure 5.35 Variations in the physical and mechanical properties of the massive and vesicular basalts after the freezing-thawing cycles

As the freezing-thawing test cycles increase the effective porosity and water absorption of the samples increase, and their sonic velocity and uniaxial compressive strength decrease (Figure 5.36). The change in the physico-mechanical properties of the vesicular basalt samples is greater than that of the massive basalt samples. In general, freezing and thawing has a more pronounced effect on the vesicular basalt samples, and the massive basalt samples have relatively better resistance to freezing and thawing.



(a)



(b)

Figure 5.36 Variations in the physico-mechanical properties of (a) the massive and (b) the vesicular basalt samples at the end of the freezing-thawing cycles

5.3.3 Salt Crystallization Test

Salt weathering is recognized as one of the most important mechanisms in the deterioration of stone materials employed in historical structures (Doehne, 2002). Stone material can be contaminated by salts in various ways, including: air pollution as a major source of nitrates and sulfates, soil (via rising damp), salt blown by the wind, bird droppings, improper conservation practices, incompatible building materials and inappropriate cleaning materials (Torraca, 1982; Topal and Sözmen, 2003; Price and Doehne, 2011; Steiger et al., 2011).

Salt can deteriorate stone material in several ways; however, salt alone does not damage stone. The presence of water is essential for it to do so (Steiger et al., 2011). For instance, after the evaporation of water from a stone surface, salts within its pores can generate stresses by means of crystallization, hydration, osmosis and differential thermal expansion, which are sufficient to overcome the tensile strength of the stone and turn it into powder like material (Winkler, 1997; Price and Doehne, 2011). In other words, if the crystallization pressure exceeds the tensile strength of the rock material, the existing microfractures tend become deeper and wider. Moreover, the crystallization pressure can cause new microfractures within the rock material (Jamshidi et al., 2013). Textural characteristics an important property for determining crystallization pressure in rock materials. It is commonly accepted that the damage mechanisms induced by salt crystallization are higher in materials that have larger proportions of micropores (Schaffer, 1972; Winkler, 1975; La Iglesia et al., 1997; Rodriguez-Navarro and Doehne, 1999).

It is reported in the literature that magnesium sulfate is among the most deleterious salts. It is known to be more severe when used in salt crystallization tests (Goudie et al., 1970; Juling et al., 2004; Steiger et al., 2007; Balboni et al., 2011; ASTM, 2013). This is mainly associated with its ability to hydrate and dehydrate (Siedel, 2013). The effects of sulfate soundness on some of the engineering and petrographic properties of rocks were investigated by Fookes et al. (1988). As the authors reported, sulfate

soundness affects parameters such as compactness, porosity, shape, anisotropy, secondary mineral content and microfractures.

The resistance of basalt samples with massive and vesicular textures to salt crystallization was investigated to evaluate these effects of salt. In order to do so, salt crystallization tests were conducted as an accelerated weathering test. This test was performed to reproduce the effect of salt crystallization occurring in natural environments (RILEM, 1980; Rossi-Doria, 1985; ASTM,2013; ASTM,2017b).

The salt crystallization test was carried out using magnesium sulphate (epsomite: $\text{MgSO}_4 \cdot 7\text{H}_2\text{O}$) by following the procedure described in ASTM (2013) and ASTM (2017b). The test was conducted on two sets, comprised of 30 massive and 30 vesicular basalt samples, having edge lengths of 7 centimeters. For the salt crystallization tests, a solution of 350g crystalline $\text{MgSO}_4 \cdot 7\text{H}_2\text{O}$ per liter of water (with a specific gravity of 1.295 to 1.308) was used. The cubic samples were fully immersed in this solution for 18 hours at a temperature of 21 ± 1 °C (ASTM, 2017b). The samples were dried in an oven, at 65 °C for 20 hours. They were then allowed to cool to ambient room temperature. The completion of this sequence constituted one salt crystallization cycle and was repeated for a total of 50 cycles. The index properties of the massive and vesicular basalts were determined after 10, 20, 30, 40 and 50 test cycles. Before the measurements of index properties, the samples were washed with distilled water every day for 1.5-2 months to remove the remaining salt. To ensure that the remaining salt was washed away, the conductivity of the samples was periodically measured using a portable conductivity meter.

The measurements performed for the wetting-drying and freezing-thawing tests are also conducted for the salt crystallization test cycles. The normalization of the results was done by following the same procedure conducted for those tests. The massive and vesicular basalt samples' average and normalized average values of the index parameters after specific numbers salt crystallization cycles are shown in the Tables 5.5 and 5.6, respectively.

The variations in the physical and mechanical properties of the massive and vesicular basalts after salt crystallization cycles are shown in Figures 5.37 and 5.38. In order to plot these figures, the normalized results from Tables 5.5 and 5.6 were used.

At the end of the salt crystallization tests, no remarkable change in weight is observed in the massive and vesicular basalt samples. However, the massive basalt samples have a relatively higher weight loss (Figure 5.37-a). The massive and vesicular basalt samples' total weight losses at the end of 50 salt crystallization cycles are measured as 2.25% and 1.13%, respectively.

The morphology of the samples shows different degrees of deterioration. Most of the deterioration patterns are in the form of detachment and loss of material. There are some signs of initial flaking patterns observed along the edges of some massive basalt samples during the first 20 cycles of the test. As the number of cycles increases, these flaking patterns grow larger, and the corners of samples become rounded (Figure 5.39).

At the end of 30th cycle, cavities developed on the surface of some samples, and small fragments along the edges came off, mostly in the form of chipping (Figure 5.39). As a result of crystallization pressure, some of the massive samples are broken through their structural cracks (Figure 5.39). The salt crystallization test drastically weathered some of the vesicular samples. The vesicular basalt samples began to have forms of flaking, efflorescence and discoloration after the first 5 cycles of the crystallization test. As the cycles increase in number, especially at the end of the tenth cycle of the salt crystallization test, some of the vesicular samples take on highly globular shapes and their surfaces become sponge-like in feel and appearance. These samples then totally disintegrated at the end of the sixteenth cycle of the test, causing 13 of the 30 vesicular basalt samples to be excluded from the vesicular sample set at the end of the 16th cycle of salt crystallization test (Figure 5.40).

The effective porosity of the massive and vesicular basalt samples is considerably increased by the salt crystallization cycles. The effective porosity of the massive and vesicular basalt samples increases by 39.80% and 61.24%, respectively, at the end of 50 salt crystallization cycles (Figure 5.37-b). There are minor variations in the dry unit weight of the massive samples. The reduction in the dry unit weight of the massive and vesicular basalt samples is 2.95% and 1.79%, respectively, at the end of 50 salt crystallization cycles (Figure 5.37-c). The water absorption capacity of the samples under atmospheric pressure increases progressively throughout the salt crystallization cycles. The massive and vesicular basalt samples' increases in water absorption under atmospheric pressure are measured as 49.36% and 64.33%, respectively, at the end of 50 salt crystallization cycles (Figure 5.37-d). After 50 cycles, the sonic velocities of the dry massive samples decrease by 4.96%. On the other hand, the sonic velocities of the dry vesicular samples increased by 13.03% (Figure 5.37-e). The uniaxial compressive strengths of the samples are significantly reduced at the end of salt crystallization cycles. The reduction of the compressive strengths of the massive and vesicular basalt samples is measured as 40.92% and 41.84%, respectively (Figure 5.37-f).

Table 5.5 Averages and normalized averages of the index properties of the massive basalts after the salt crystallization cycles

Cycles	Weight (g)	Normalized Weight (%)	Effective Porosity (%)	Normalized Porosity (%)	Dry Unit Weight (KN/m ³)	Normalized Dry Unit Weight (%)	Water Abs. by Weight (atm. press.) (%)	Normalized Water Abs. by Weight (atm. press.) (%)	Dry Sonic Velocity (m/s)	Normalized Dry Sonic Velocity (%)	UCS (MPa)	Normalized UCS (%)
0	969.12	100.00	4.46	100.00	27.32	100.00	0.84	100.00	4767.02	100.00	145.49	100.00
10	961.65	99.23	5.16	115.70	26.84	98.26	0.91	108.90	4690.66	98.40	127.06	87.33
20	958.97	98.95	5.39	120.79	26.74	97.91	1.03	122.58	4624.38	97.01	116.29	79.93
30	957.51	98.80	5.94	133.10	26.64	97.53	1.10	131.47	4587.06	96.22	101.01	69.43
40	953.55	98.39	6.12	137.24	26.58	97.29	1.18	140.83	4564.77	95.76	95.05	65.33
50	947.31	97.75	6.24	139.80	26.51	97.05	1.25	149.36	4530.64	95.04	85.95	59.08

Table 5.6 Averages and normalized averages of the index properties of the vesicular basalts after the salt crystallization cycles

Cycles	Weight (g)	Normalized Weight (%)	Effective Porosity (%)	Normalized Porosity (%)	Dry Unit Weight (kN/m ³)	Normalized Dry Unit Weight (%)	Water Abs. by Weight (atm. press.) (%)	Normalized Water Abs. by Weight (atm. press.) (%)	Dry Sonic Velocity (m/s)	Normalized Dry Sonic Velocity (%)	UCS (MPa)	Normalized UCS (%)
0	861.16	100.00	7.56	100.00	25.04	100.00	1.38	100.00	4393.48	100.00	63.30	100.00
10	858.54	99.70	10.02	132.59	24.84	99.19	1.55	112.25	4580.67	104.26	54.00	85.31
20	855.54	99.35	10.80	142.92	24.70	98.62	1.73	125.14	4650.67	105.85	47.89	75.66
30	854.09	99.18	11.28	149.33	24.65	98.42	1.87	135.76	4731.97	107.70	42.55	67.22
40	852.71	99.02	11.41	151.01	24.62	98.31	2.01	145.64	4869.36	110.83	39.07	61.72
50	851.43	98.87	12.18	161.24	24.60	98.21	2.27	164.33	4966.08	113.03	36.82	58.16

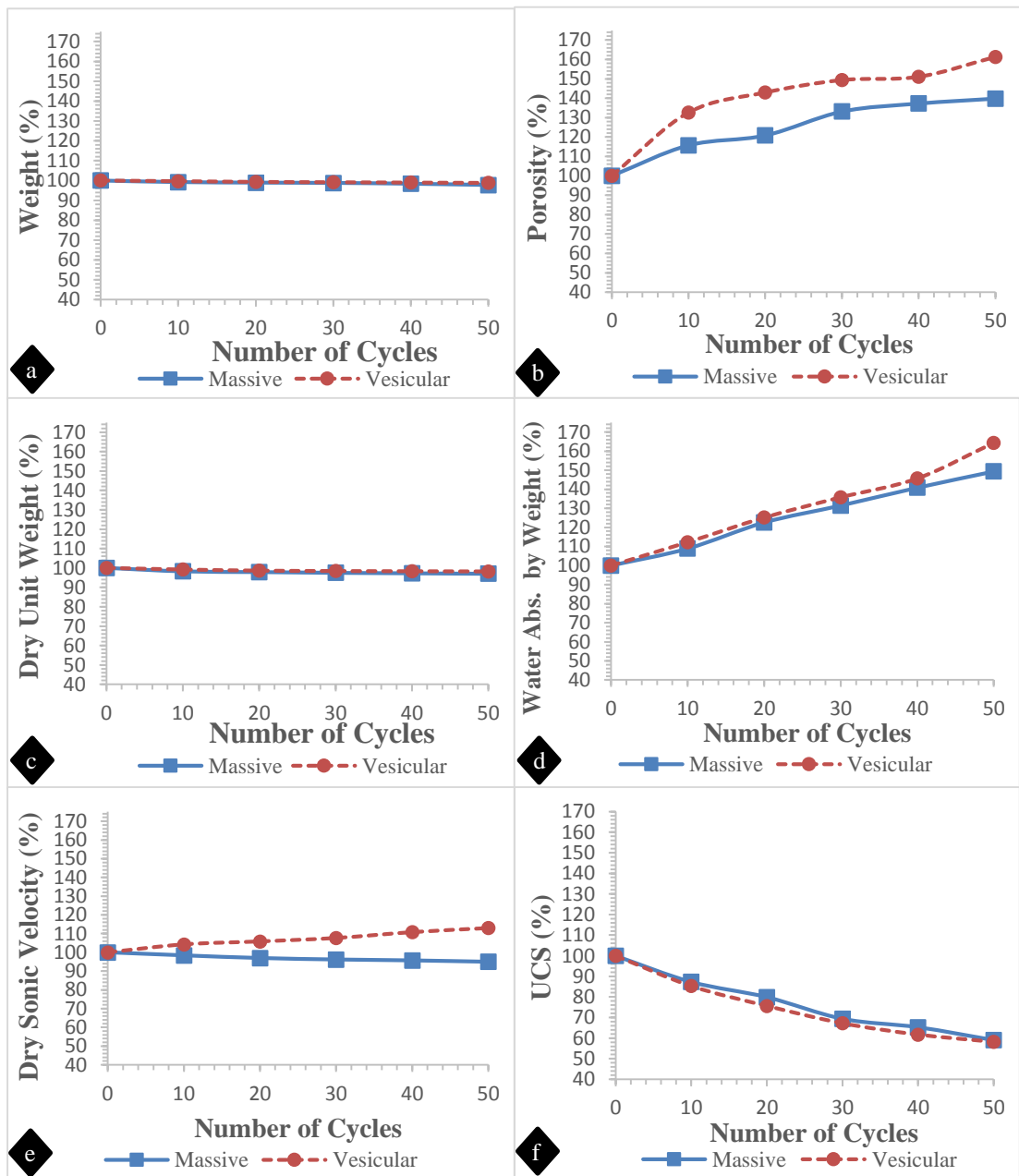
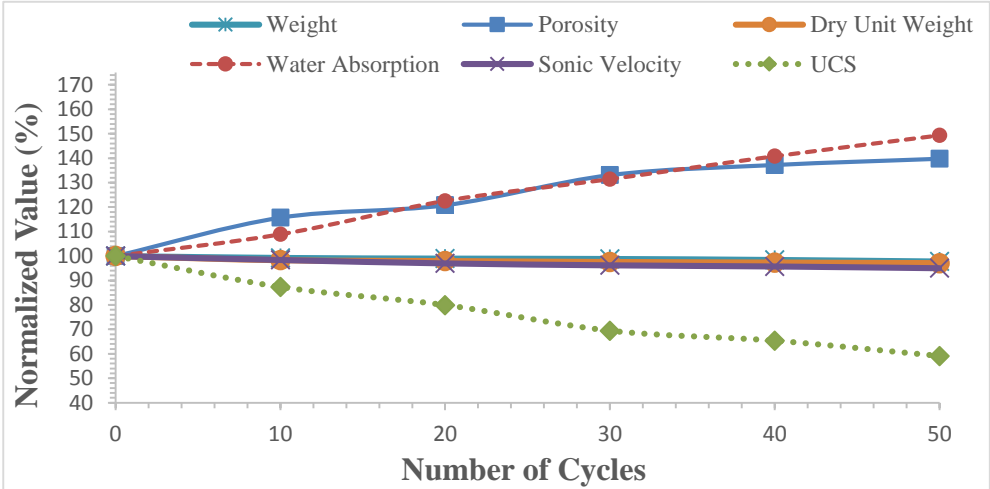
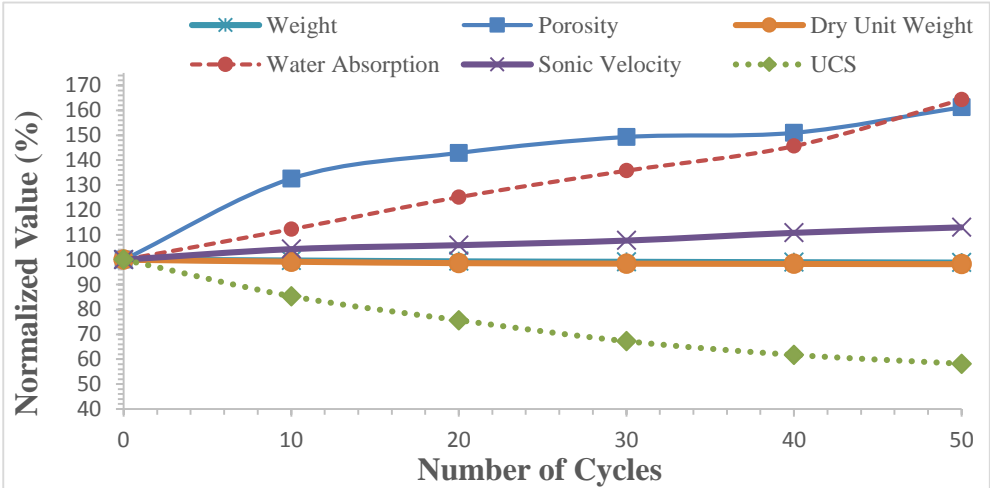


Figure 5.37 Variations in the physical and mechanical properties of the massive and vesicular basalts after the salt crystallization cycles

The salt crystallization test has a more pronounced effect on the physical appearance of the massive and vesicular basalt samples. As Figure 5.38 shows, as the salt crystallization cycles increase so does their effective porosity and water absorption capacity. The sonic velocity of the massive samples decreases, but it increases in the vesicular samples. This increase may be attributed to incomplete removal of salt from the micropores of the vesicular samples. At the end of the test, it is observed that, the uniaxial compressive strengths of the both massive and vesicular samples are significantly reduced.



(a)



(b)

Figure 5.38 Variations in the physico-mechanical properties of (a) the massive and (b) the vesicular basalt samples at the end of the salt crystallization cycles

In general, the salt crystallization test has strongly pronounced effects not only on the vesicular basalt samples, but also on the massive ones. However, the massive samples possess a relatively better resistance to salt attack than the vesicular basalt samples.

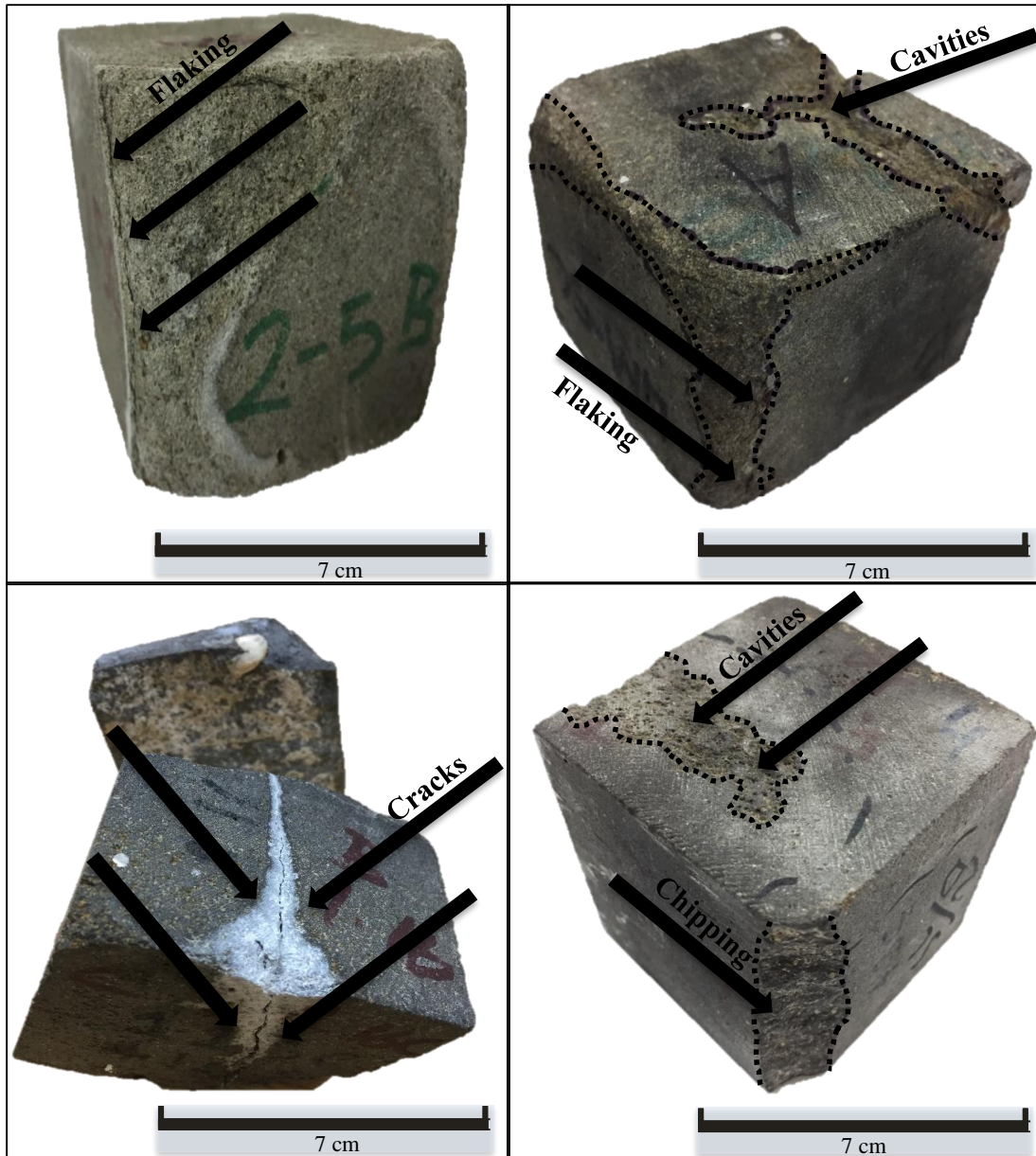


Figure 5.39 Patterns of deterioration on the massive basalt samples after the 30th cycle of the salt crystallization test



Figure 5.40 Disintegration of some of the vesicular basalt samples after 16th cycle of the salt crystallization test

5.3.4 Correlation of the Physico-mechanical Parameters after the Durability Tests

This section describes the effects of the durability tests on the physical and mechanical properties of the basalt samples. The variations in each physico-mechanical property caused by the wetting-drying, freezing-thawing and salt crystallization tests are plotted on graphs in Figures 5.41 and 5.42. These graphs allow for better comparison of the different parameters.

Of the accelerated weathering tests, salt crystallization is considered the test that most aggressively affects the morphology of the basalts. For instance, almost half of the vesicular basalt samples disintegrated in the earlier cycles of the salt crystallization test. While the freezing-thawing test has a moderate influence on the morphology of the massive and vesicular basalt samples, the wetting-drying cycles has the least influence on them.

The total weight losses of the massive samples are slightly changed at the end of the durability tests. Their largest reduction in weight is 2.25% at the end of the salt crystallization test. However, this is not the case with the vesicular samples. Unlike the massive samples, their largest weight loss reduction is 3.06% after the freezing-thawing test (Figures 5.41-a and 5.42-a).

The porosity of the massive and vesicular basalt samples progressively increases as the number of durability tests cycles increase. The largest increase in the porosity of the massive and vesicular basalt samples is observed at the end of the salt crystallization test. The change in the porosity of the massive and vesicular basalt samples is 39.80% and 61.24%, respectively. The smallest increase in the porosity of the massive and vesicular basalt samples is measured at the end of the wetting-drying cycles as 30.25% and 37.75%, respectively (Figures 5.41-b and 5.42-b).

A very slight change is noticed in the dry unit weight of the massive and the vesicular basalt samples at the end of the durability tests. The largest reduction in the dry unit weight of the massive basalt samples is 2.95% at the end of the salt crystallization

cycles. However, the largest reduction in the dry unit weight of the vesicular basalt samples is 3.08% at the end of the freezing-thawing cycles (Figures 5.41-c and 5.42-c).

Like porosity, the samples' water absorption capacity under atmospheric pressure increases progressively as the cycles of durability tests increase in number. Increased water absorption is observed in all the durability tests reported here. The massive and vesicular samples' largest increase in water absorption capacity is 49.36% and 64.33%, respectively, at the end of the salt crystallization cycles. On the other hand, the smallest increase in the massive and vesicular samples' water absorption capacity is measured at the end of the wetting-drying cycles as 37.70% and 44.97%, respectively. Increased water absorption capacity is also observed at the end of the freezing-thawing cycles, 40.46% for the massive samples and 48.40% for the vesicular samples (Figures 5.41-d and 5.42-d).

The sonic velocity of the dry samples reveals different behavior throughout the durability tests. The sonic velocity decreases throughout the wetting-drying and freezing-thawing cycles for both the massive and vesicular samples; however, this shared diminishing trend is not observed during the salt crystallization cycles, especially for the vesicular basalt samples. The largest reduction in the sonic velocity of the massive and vesicular basalt samples is 7.5% and 16.83%, respectively, at the end of the freezing-thawing cycles. This reduction is quite similar to the results obtained from the wetting-drying cycles. The sonic velocity of the massive basalt samples at the end of the salt crystallization cycles also decreases by 4.96%; however, the sonic velocity of the vesicular samples is increased by 13.03% at the end of the salt crystallization cycles.

The dry UCS of the samples progressively decreases in all the durability tests performed in this study. The largest reduction in compressive strength is caused by the salt crystallization cycles. Compared to the average strength values of the fresh samples, the reduction in the UCS of the massive and vesicular basalt samples is measured as 40.92% and 41.84%, respectively, at the end of 50 salt crystallization

tests. This reduction is notably more pronounced than the massive and vesicular samples' reduction in UCS after the freezing-thawing cycles to 36.07% and 37.48%, respectively. Relatively less reduction in UCS is noticed at the end of 80 wetting-drying cycles when the decrease in the UCS of the massive and vesicular basalt samples is 24.98% and 31.32%, respectively.

It can be concluded from these results that salt crystallization is the durability test that most aggressively affected both the massive and vesicular basalt samples. Freezing and thawing has the next most effect on the samples, and wetting and drying has the least effect.

The basalt's physico-mechanical properties are effected to varying degrees by the durability tests. Unit weight is the parameter least affected by the durability tests. Porosity, water absorption and UCS are the parameters most affected by the durability tests. Although sonic velocity tends to fall during the tests, it does not follow a consistent pattern in some cycles of the durability tests. It is worth mentioning that the sonic velocity changes by the degree of the weathering. This is examined by comparing the samples with decay patterns (see Figures 5.39 and 5.40) to those that do not have significant decay patterns. The comparison suggests that the sonic velocity distinctly changes through the deteriorated faces of the samples.

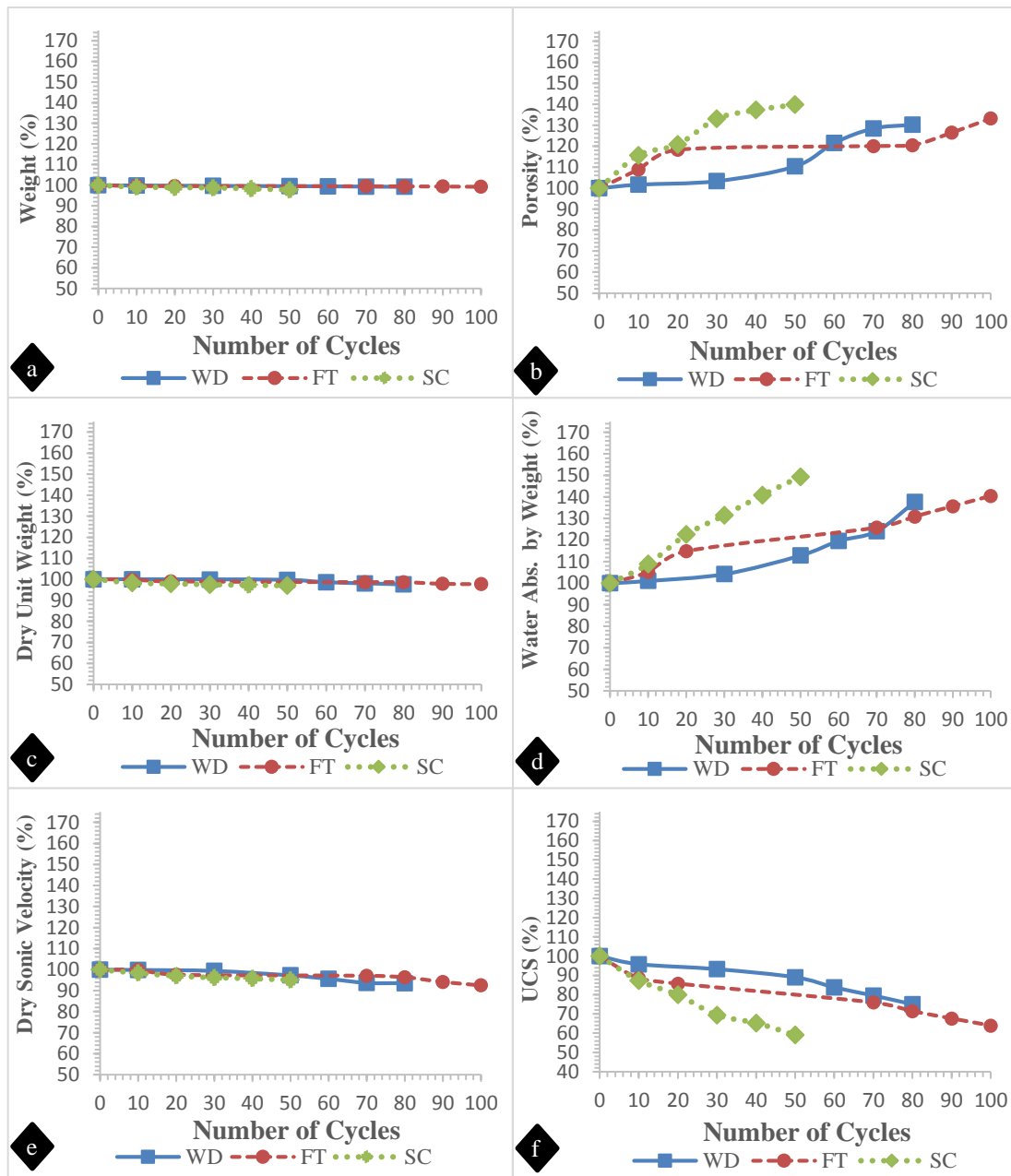


Figure 5.41 Effect of durability tests on the physico-mechanical properties of the massive basalt samples (WD: Wetting-Drying; FT: Freezing-Thawing; SC: Salt Crystallization)

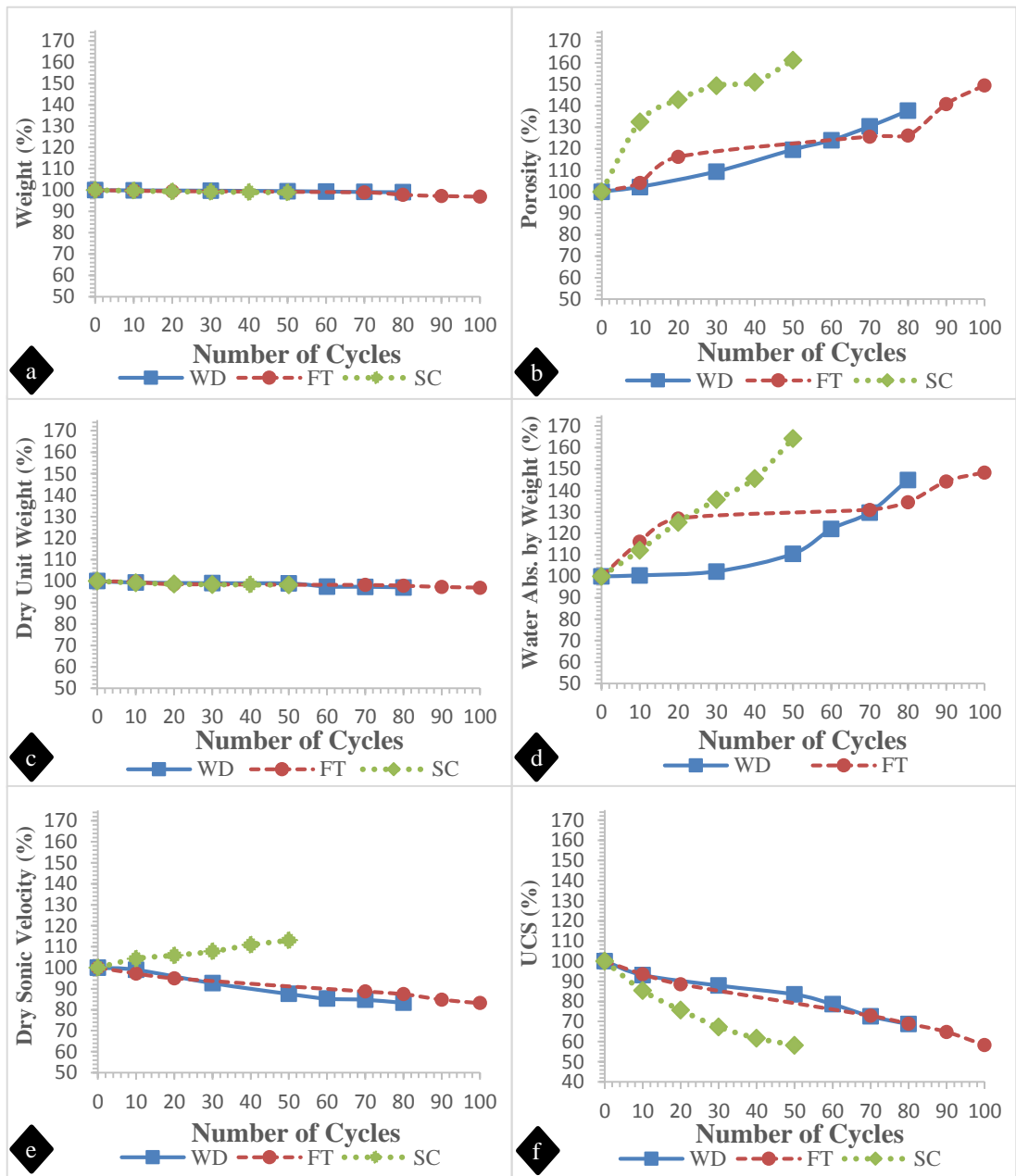


Figure 5.42 Effect of durability tests on the physico-mechanical properties of the vesicular basalt samples (WD: Wetting-Drying; FT: Freezing-Thawing; SC: Salt Crystallization)

5.4 Petrographic and Chemical Properties of the Weathered Basalts

In order to investigate the state and depth of the weathering in the basalts, the mineralogical, petrographic and chemical properties of several basalt samples with different weathering degrees of the basalts were studied and petrographically correlated to those of fresh and naturally weathered samples.

5.4.1 Mineralogical and Petrographic Properties of the Weathered Basalts

This section discusses the mineralogical and petrographic features of the weathered samples collected from the DCW. In this section, the mineralogical and petrographic properties of the samples will be argued by means of such studies as optical microscopy, back-scattered images, the methylene blue adsorption test, clay percentage and XRD.

For the optical and back-scattered image investigations, a total of 18 thin and polished sections were prepared in the thin and polished section laboratories located in the Department of Geological Engineering at METU. The petrographic examinations of the samples were performed using Nikon microscopes and cameras located in the Department of Geological Engineering at METU. The Electron Probe Microanalyser (EPMA) back-scattered images were obtained using the JEOL-JXA-8230 electron microprobe device located in the Central Laboratory at METU.

To the unaided eye, the weathered basalts have a pale brown to yellowish color tending towards red. Their surfaces reveal different forms of weathering, mostly in the form of flaking. Thin section examinations indicate that, like the fresh samples, the weathered samples also contain plagioclase, pyroxene and olivine minerals. Although primary minerals are preserved in most of the weathered samples, olivine phenocrysts were partly replaced by iddingsite (Figure 5.43-a, b and c). As the major secondary mineral, iddingsite is observed frequently in olivine phenocrysts, even in some of the fresh basalt samples. However, compared to the fresh samples, the degree of iddingsitization was distinctly increased in the weathered basalt sections.

Iddingsitization most frequently developed on the edges and cracks of the olivine minerals. The thin section analyses, moreover, reveal different degrees of oxidation. The olivine and pyroxene crystals were discolored due to iron-oxide staining. Iron oxide stained inwards by penetrating the joint faces along the microfractures (Figure 5.43-d).

The crystal boundaries (particularly of olivine and pyroxene) are the weakest zones for microfracture formations. Most of the cracks in the weathered samples originate and propagate through these weak zones. The detail of the microfractures will be discussed in Section 5.5.

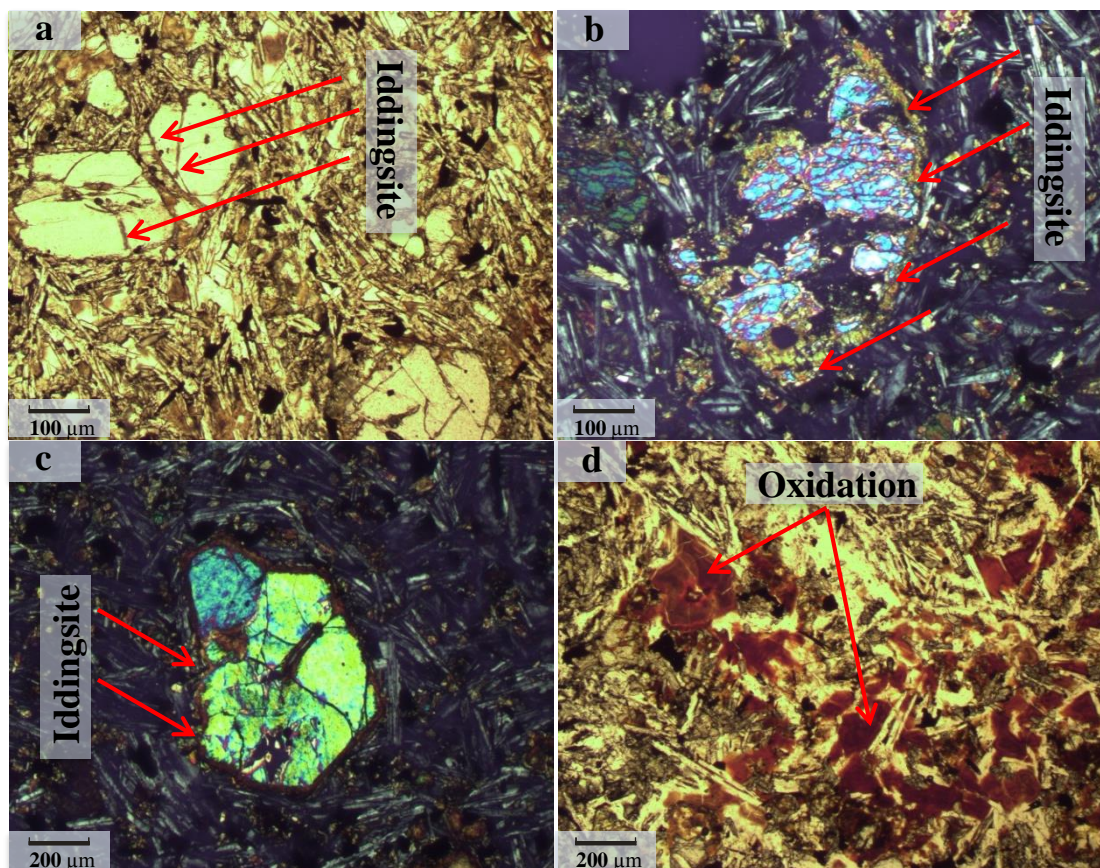


Figure 5.43 Photomicrographs of the weathered basalt samples (a,b,c: iddingsite formations through the mineral boundaries and cracks; d: oxidation)

In order to quantify the presence and types of clay minerals in the weathered basalt samples, methylene blue adsorption, clay content determination and XRD studies were performed. For the methylene blue adsorption test, seven basalt samples with different degrees of weathering were used.

The CECs of the weathered samples are ranged from 0.9 to 2.1 meq/100 g, with an average of 1.3 meq/100 g. According to the test results, the CECs of the weathered basalt samples are very low. Therefore, the significant amount of clay was not observed in the bulk samples tested. Since the methylene blue adsorption test is not enough to quantify the abundance and type of the clay minerals, the samples were also examined for clay fraction and by XRD. For clay fraction determination, a total of ten weathered samples were examined. The clay fractions of the questioned samples are listed in Table 5.7. As the Table indicates, the weathered samples have a clay fraction ranging from 3.2 to 6.22% with an average of 4.58%. The results suggest that most of the weathered samples have a clay fraction close to or below the detection limit (i.e., 5%) of the XRD analysis. Two of the samples with clay fraction near the detection limit was subjected to XRD analysis. The oriented samples were X-rayed in several conditions (e.g., air-dried (AD), ethylene glycolated (EG), heated at 300 and 550 °C). The XRD patterns of two weathered samples are presented in Figure 5.44. The X-ray patterns of the weathered samples reveal that no significant amount of clay was detected. However, some of the peaks can be attributed to the trace amount of smectite and illite. The observed peaks of the oriented samples, especially those at the right side of the diffractograms, are attributed to the plagioclase minerals. In addition to the plagioclase, some of the peaks obtained from the unoriented samples reveal the presence of clinopyroxene minerals.

Table 5.7 Clay fractions of the weathered basalt samples

Sample	Clay Fraction (%)
Weathered 1	4.72
Weathered 2	4.05
Weathered 3	4.7
Weathered 4	6.22
Weathered 5	3.37
Weathered 6	3.2
Weathered 7	5.56
Weathered 8	4.91
Weathered 9	4.97
Weathered 10	4.15

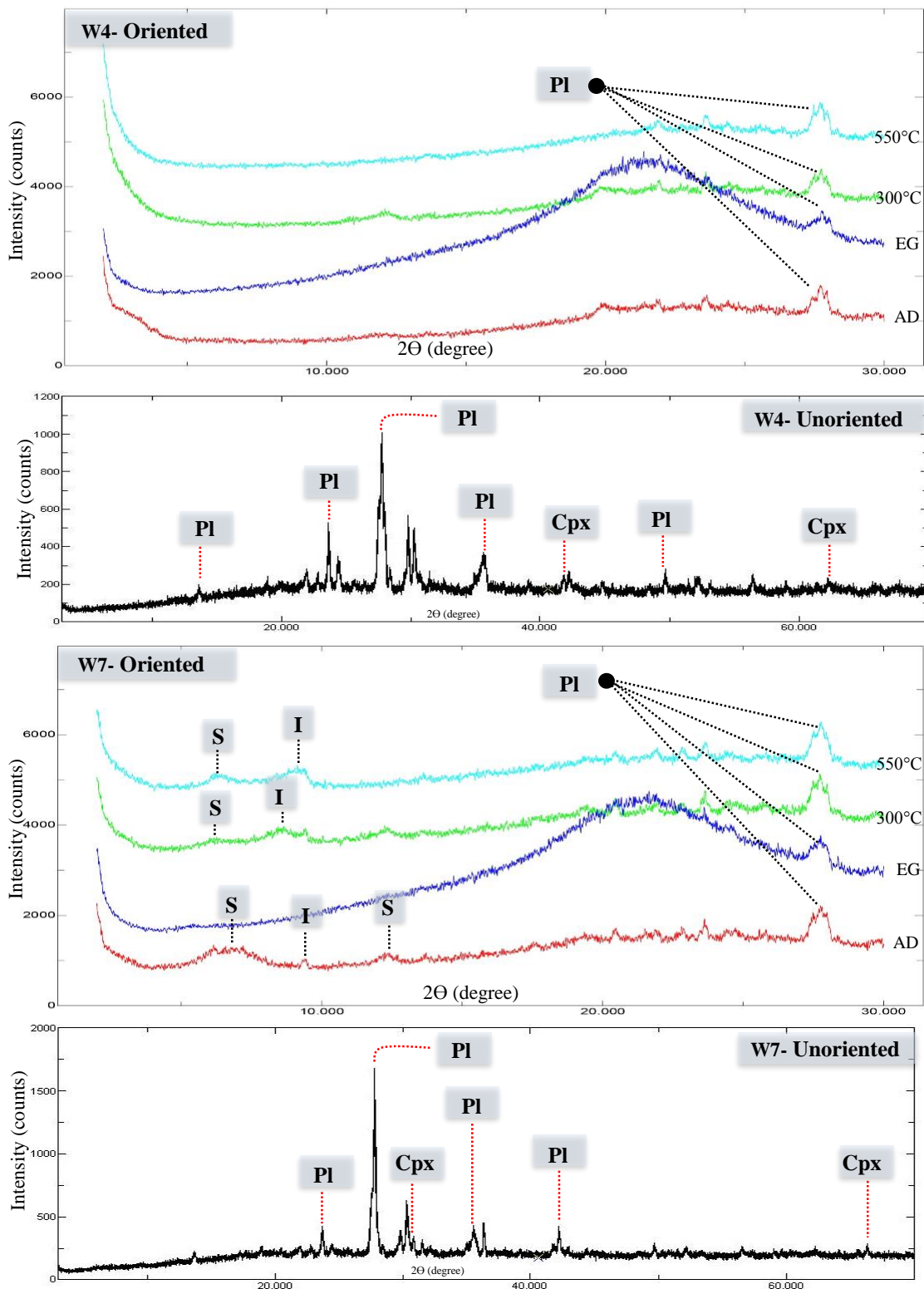


Figure 5.44 X-ray diffraction patterns of the weathered basalt samples (Pl: Plagioclase; Cpx: Clinopyroxene; S: Smectite; I: Illite)

5.4.2 The Chemical Properties of the Weathered Basalts

The chemical weathering of rock materials changes initial elemental abundances by leaching and enrichment (Borchardt and Harward, 1971; Borchardt et al., 1971). It is, therefore, important to assess processes and degrees of weathering using variations in quantities of elements (Colman, 1982).

To understand the effect of chemical weathering and assess its state and depth in the weathered basalts, samples were collected from some sections of the DCW. A basalt block showing spheroidal weathering was evaluated for the depth of chemical weathering in the study area. It was possible to collect samples from the outer to the inner part of the block. The observed effects of mechanical and chemical weathering on the block cease at a depth of 3 cm. Since weathering is expected to be more significant near the source of alteration (Topal, 2002), the outer part of the block (0-1 cm) was considered as weathered and the inner part (3-4 cm) as relatively unweathered. Four samples were scratched from the outer part to the inner, following the path indicated in Figure 5.45.

In order to evaluate the major and trace element characteristics, the scratched samples were then put into 20 gram packages to send for the analysis. The abundance of the major oxides and trace elements of the collected samples were determined using Inductively Coupled Plasma Mass Spectrometry (ICP-MS) at ACME Analytical Laboratories Ltd. in Vancouver, Canada. The major and trace elemental concentrations of the basalts showing variation with depth are listed in Tables 5.8 and 5.9. As Tables 5.8 and 5.9 show, except a minor decrease in SiO₂ concentration and a relative increase in loss on ignition (LoI), the major and trace elements of the weathered samples were not significant to quantify the depth of weathering. The mobility index of LoI is slightly larger than that of the fresh samples, which points to chemical weathering. LoI, defined as the mass loss of a tested sample due to heating (igniting) at a high temperature of *ca.* 1000 °C, (ASTM, 2013b) can be used to determine the weathering of basalt.

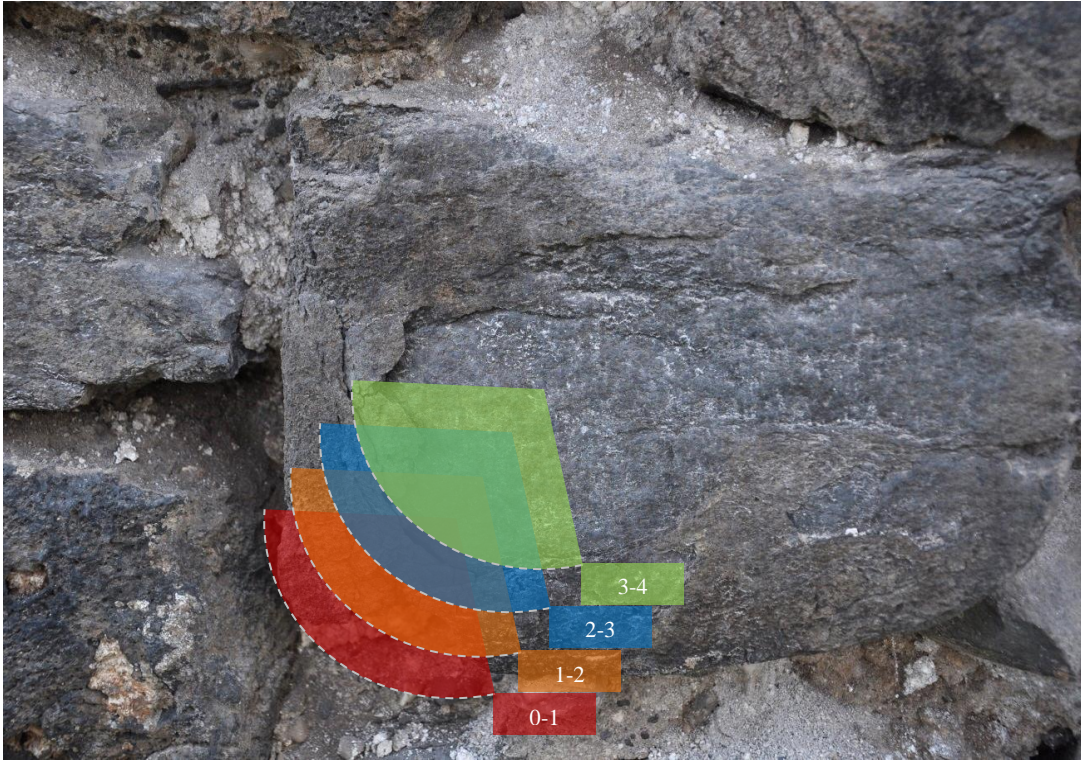


Figure 5.45 Sampling path through a spheroidally weathered basalt block (see Figure 1.29, sample location: W4)

Table 5.8 Weight percentages of common oxides of the weathered basalt samples

Major Oxides	Sample Depth (cm)			
	0-1	1-2	2-3	3-4
SiO ₂	44.44	44.56	44.84	44.88
Al ₂ O ₃	13.02	13.19	13.56	13.52
Fe ₂ O ₃ Total	13.07	13.35	12.77	12.94
MgO	7.82	8.43	8.14	8.25
CaO	9.43	8.83	8.85	8.72
Na ₂ O	2.65	2.71	2.82	2.75
K ₂ O	1.38	1.54	1.57	1.53
TiO ₂	2.38	2.43	2.49	2.50
P ₂ O ₅	0.43	0.43	0.43	0.47
MnO	0.13	0.14	0.14	0.14
Cr ₂ O ₃	0.041	0.042	0.044	0.044
LoI	4.8	4.0	4.0	3.9
Sum	99.70	99.69	99,69	99.69

Table 5.9 Trace element contents of the weathered samples (in ppm)

Element	Sample Depth (cm)			
	0-1	1-2	2-3	3-4
Ba	330	237	212	228
Sc	18	18	19	19
Co	53.7	55.0	58.2	55.9
Cs	0.1	<0.1	0.1	0.1
Ga	20.6	21.0	21.4	21.7
Hf	4.2	4.2	4.3	4.3
Nb	24.0	25.1	25.7	25.2
Rb	12.1	12.8	12.8	12.3
Sn	2	2	2	2
Sr	643.2	606.7	605.2	579.3
Ta	1.5	1.6	1.8	1.5
Th	2.9	2.9	2.7	2.8
U	0.5	0.5	0.4	0.4
V	203	206	208	211
Zr	171.8	179.6	178.5	176.5
Y	19.2	20.1	19.2	21.5
La	24.2	25.7	25.2	26.2
Ce	48.6	51.3	51.9	50.4
Pr	6.08	6.32	6.28	6.22
Nd	25.1	25.7	26.4	25.9
Sm	5.40	5.62	5.75	5.74
Eu	1.85	1.96	1.86	1.84
Gd	5.52	5.55	5.70	5.68
Tb	0.76	0.75	0.80	0.77
Dy	4.29	4.10	4.41	4.10
Ho	0.72	0.72	0.74	0.79
Er	1.85	1.83	1.87	1.89
Tm	0.23	0.24	0.24	0.23
Yb	1.48	1.33	1.43	1.42
Lu	0.21	0.20	0.22	0.22
Mo	2.0	1.4	1.6	1.6
Cu	61.8	64.3	68.2	56.2
Pb	3.8	4.4	4.4	4.7
Zn	84	87	91	91
Ni	187.0	237	212	228
As	1.5	18	19	19

5.5 Microfracture Properties of the Fresh and Weathered Basalts

Petrographic investigations not only provide knowledge on the mineralogical state and provenance of rock materials, they also can be used as a strong tool for evaluating its weathering potential and durability. They help also to understand why the behavior of macroscopically similar rock materials differ with respect to environmental conditions and their weathering potential (Dreesen and Duser, 2004). Weathering is strongly related to the type, amount, dimension, orientation and density of cracks. The chemical agents that cause weathering in rock materials use cracks to penetrate into their depths (Ündül and Tuğrul, 2012). The extending of cracks, for instance, increases stone's surface area and consequently leads to physical, chemical and biological weathering. This makes it important to do microfracture studies of rock materials. Petrographic investigations can also be used to assess the amount, type, direction and density of microfractures (Dearman et al., 1978; Irfan and Dearman, 1978; Ündül and Tuğrul, 2012).

To conduct microfracture studies, a total of nine basalt samples (one fresh massive and one fresh vesicular, three massive and three vesicular samples from the final cycles of the wetting-drying, freezing-thawing and salt crystallization tests, and finally, one naturally weathered basalt sample collected from the DCW) were investigated. Thin and polished sections were prepared and investigated using optical microscopy and back-scattered views obtained from EPMA. The investigation examined microfracture properties of the samples such as type, amount, orientation and density. Special attention was given to the samples used in the accelerated weathering tests to evaluate systematically the effects of wetting-drying freezing-thawing and salt crystallization on microfracture development.

The fresh massive basalt sample has some structural microfractures. These microfractures are commonly tight and frequently intragranular (i.e., occurring within the grains of the mineral). However, the microfractures in the vesicular sample are both intragranular and transgranular (i.e., crossing the grains and grain boundaries).

The intragranular microfractures in the massive and vesicular samples developed within mineral crystals of olivine and pyroxene. The microfractures in the massive sample do not have a specific direction; however, many of them are along the grain boundaries. The microfractures in the vesicular sample have relatively simple branched and dendritic patterns (Figure 5.46). Considering the overall microfracture development, the fresh massive sample is microfractured by hair-like, tight and simple branched microfractures. The vesicular sample has dendritic intragranular and transgranular microfractures. Most of the microfractures in the massive and vesicular samples are fresh and unstained. The distribution of microfractures, especially in the vesicular sample, is random with no specific orientation and developed through the grain boundaries.

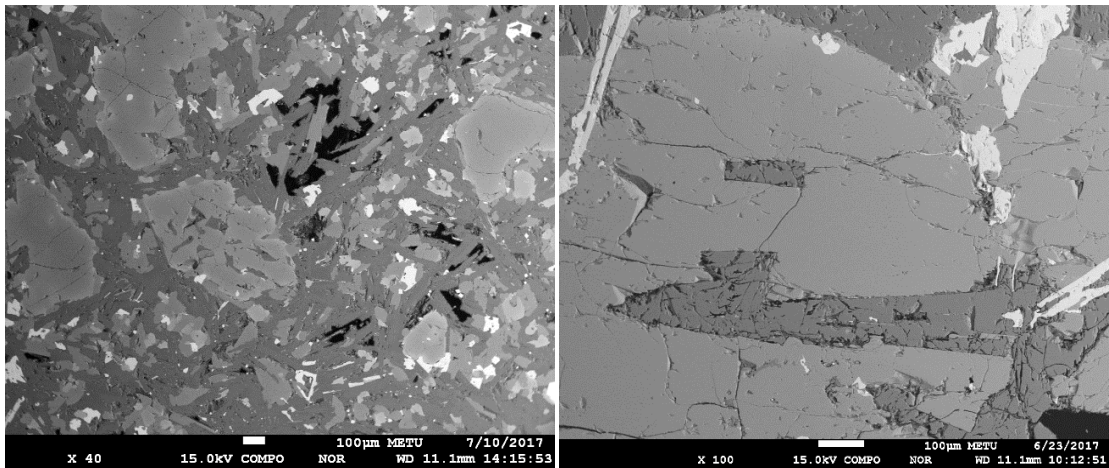


Figure 5.46 Back-scattered images displaying the microfracture morphology of the (left) fresh massive and (right) fresh vesicular basalt samples

Microfracture studies of the massive and vesicular samples were conducted at the end of the wetting-drying test. The density of the hair-like, tight and very short microfractures increase in the massive sample. Most of the branched cracks propagate through a transgranular-unstained microfracture develop in the groundmass, which crosses the entire section of the massive sample (Figure 5.47). The density and behavior of microfractures change slightly in the vesicular samples after the wetting-drying cycles.

Most of the microfractures in the groundmass of the vesicular sample have dendritic forms (Figure 5.47). Although the direction of microfractures does not have a distinct pattern, some of the microfractures change their direction while crossing through a different mineral crystal. As shown in Figure 5.48, a microfracture that originated from the mineral grain of pyroxene changes its direction while passing through the plagioclase. In addition, the initial stage of grain loss is observed in some mineral grains of the vesicular basalt sample. Figure 5.48 shows a partially lost pyroxene grain as a result of physical degradation of the wetting-drying cycles. The investigations found that most of the microfractures initiate at the edges of the vesicles (Figure 5.49).

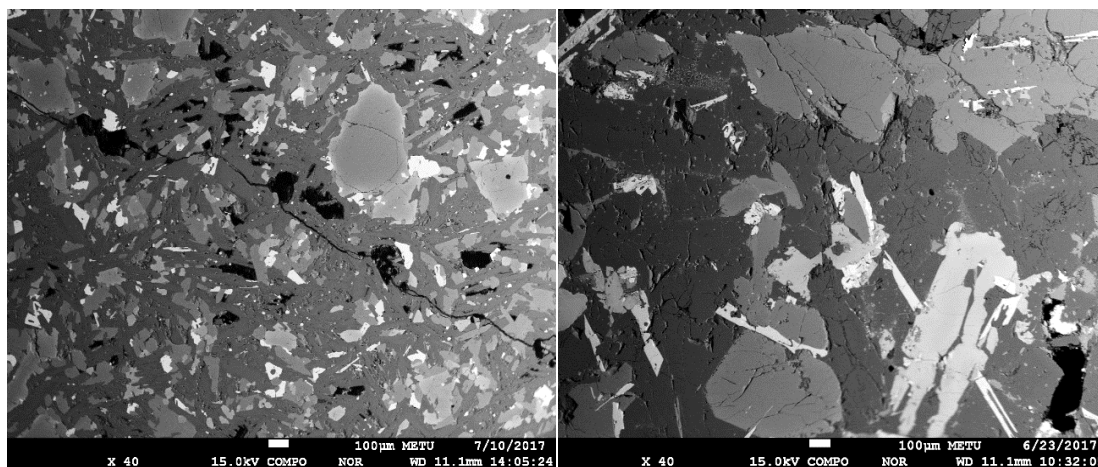


Figure 5.47 Back-scattered images displaying the microfracture morphology of the (left) massive and (right) vesicular basalt samples after the wetting-drying cycles

Considering the overall microfracture development after the wetting-drying test, the massive sample is traversed by a long transgranular microfracture. Various hair-like and tight microcracks developed along this microfracture. The microcracks in the massive sample do not have a dendritic pattern; however, the vesicular sample has branched and dendritic microcrack patterns. Compared to the fresh sample, the massive sample does not have any distinct widening and deepening in microcracks, except for the microfracture across it.

However, the vesicular sample differs from the fresh sample in terms of partial loss of pyroxene grains and widening and deepening of microcracks. Most of the microcracks in the massive and vesicular samples are fresh and unstained. Their distribution does not have a distinct direction in the massive sample, but has a somewhat dendritic pattern in the vesicular sample.

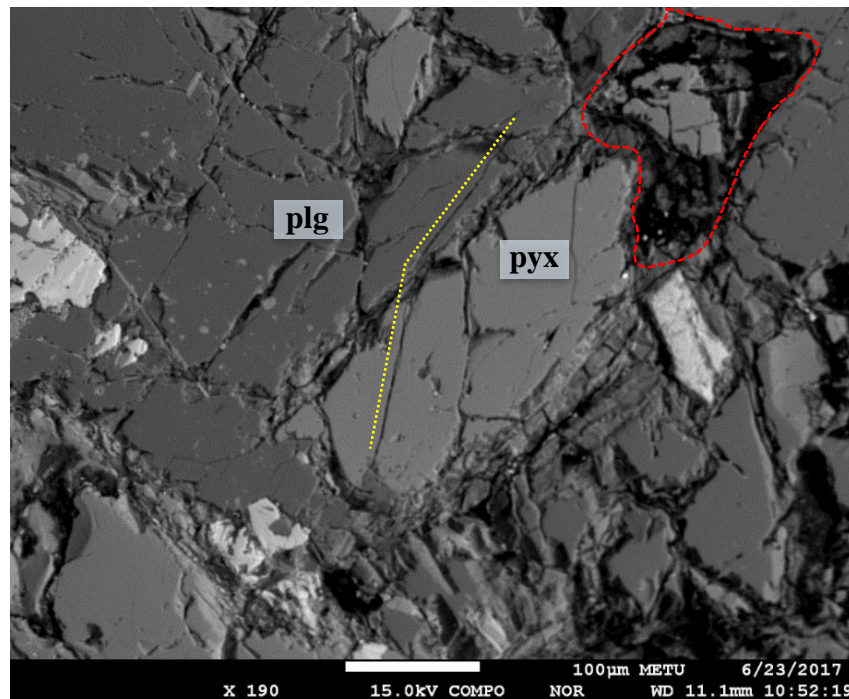


Figure 5.48 Back-scattered image showing change in crack direction and partial loss of pyroxene crystal after the wetting-drying test (the direction change is indicated by the yellow dotted lines, and the mineral remnant is indicated by the red dashed lines)

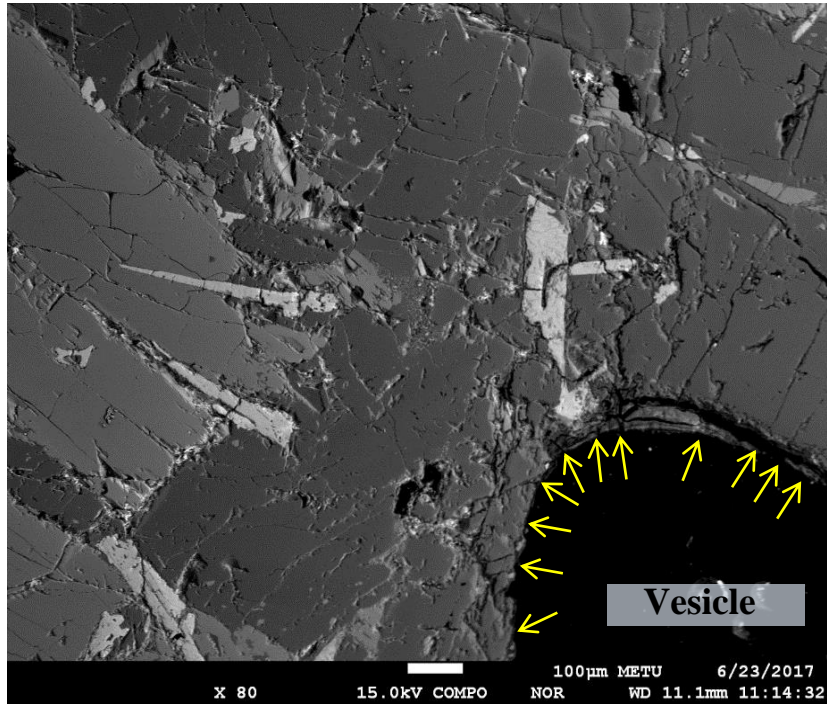


Figure 5.49 Back-scattered image displaying microfracture propagation that initiated from a vesicle after the wetting-drying test (microfractures are indicated by the yellow arrows)

The microfracture properties of the massive and vesicular samples were assessed at the end of the freezing-thawing test, and the freezing and thawing cycles considerably increase the number of intragranular and transgranular microfractures in the massive and vesicular samples (Figure 5.50). Most of the structural microfractures, including cleavages and grain boundaries, are widened. Microfractures not only develop within the phenocrysts, also in the groundmass. However, the microfracture density in the olivine phenocrysts is lower than that of the olivine in the groundmass. Similar observations are made for the plagioclase in the groundmass. As discussed in previous sections, some of the massive samples displayed flaking and scaling patterns during the freezing-thawing cycles. Figure 5.51 shows the growth of micropores in a massive sample, commonly through the flow direction. Such growth behaviors of micropores can be attributed to the flaking patterns that developed during the freezing-thawing test.

The partial loss of crystal grains that began during the wetting-drying test is increased and resulted in the loss of entire grains of some minerals. Figure 5.52 shows the remnants of the olivine and pyroxene crystals after the freezing-thawing test. This loss of mineral grains can be attributed to physical processes that occurred during the accelerated weathering tests. Considering the overall microfracture development after the freezing-thawing test, the number of microcracks in massive and vesicular basalt samples increase remarkably. Compared to the previously investigated samples (i.e., the fresh and the ones used in wetting-drying tests) there is a distinct widening and deepening in the structural and weathering-associated microcracks. The number of intragranular microfractures is increased, especially in the olivine and pyroxene crystals. The microcracks are mostly fresh, intragranular, transgranular, unstained, and present in both the phenocrysts and the groundmass. Most of the microcracks run parallel to the cleavage patterns in the vesicular sample, however, this is not the case for the massive sample.

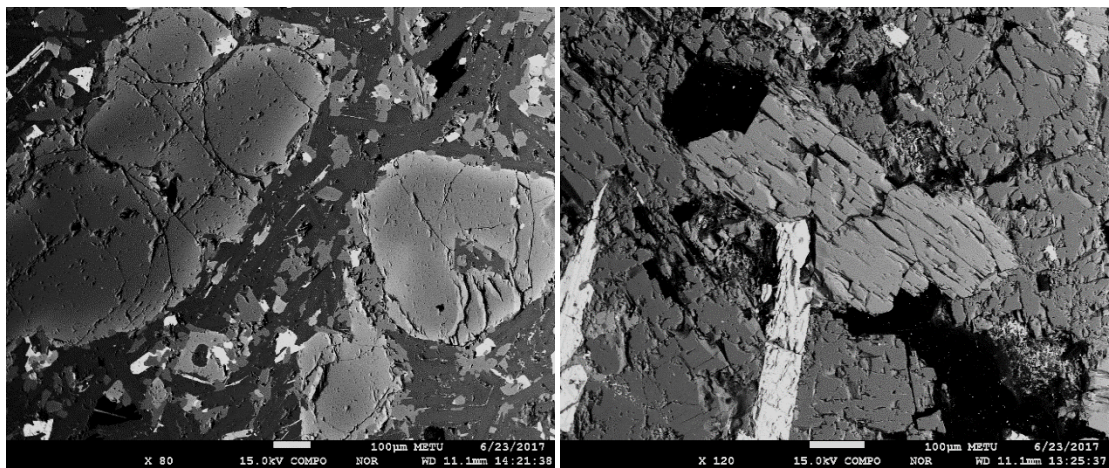


Figure 5.50 Back-scattered images displaying the microfracture morphology of the (left) massive and (right) vesicular basalt samples after the freezing-thawing cycles

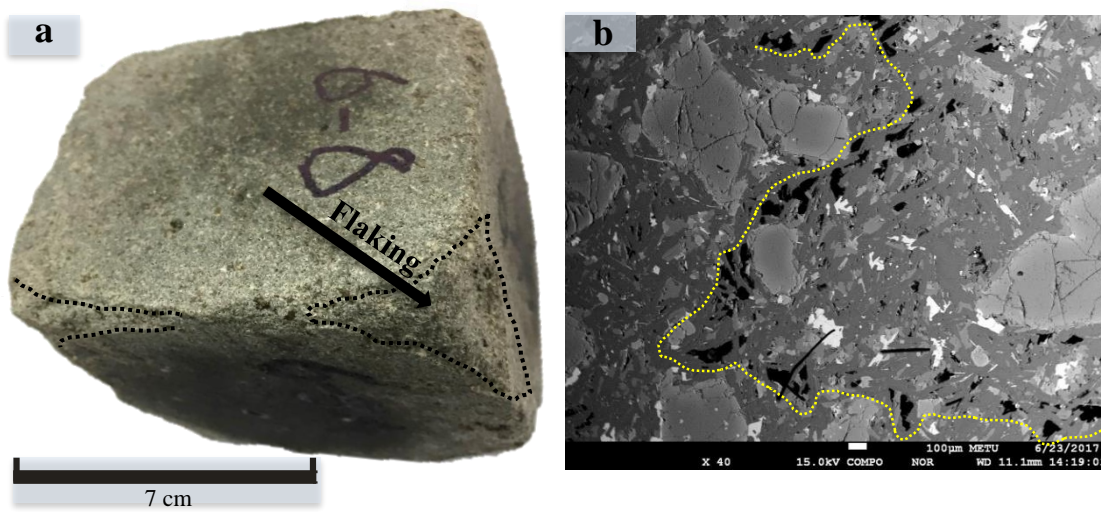


Figure 5.51 (a) An image displaying flaking pattern on a massive sample after the freezing-thawing test and (b) a back-scattered view of the flaked sample displaying micropore growth along the flow layer (the flaking and growing patterns are indicated by the dashed lines)

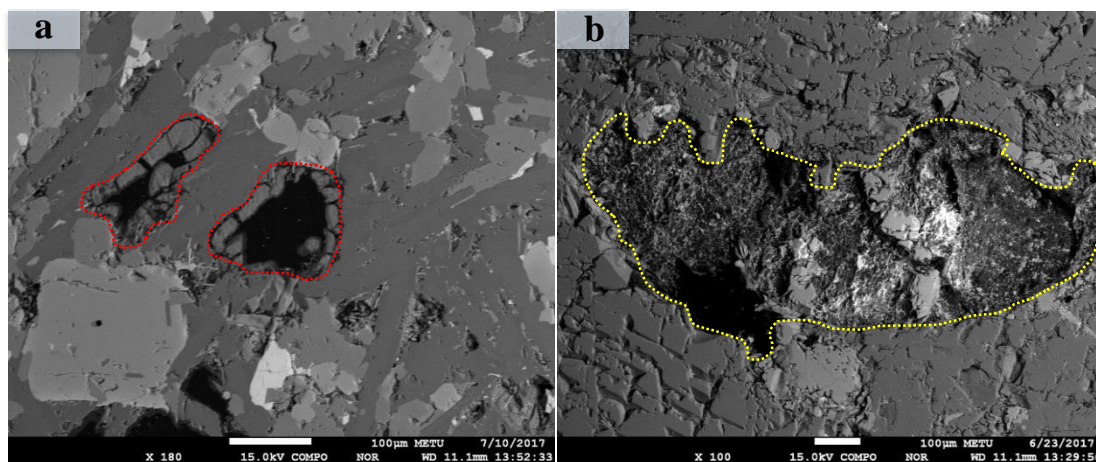


Figure 5.52 Back-scattered images indicating remnants of (a) the olivine and (b) the pyroxene crystals after the freezing thawing cycles (the olivine remnants are indicated by the reddish dotted lines; and pyroxene remnant is indicated by the yellowish dotted lines)

The effect of salt crystallization on microfracture development is also investigated. The structural and mostly intragranular microcracks are enlarged and became microfractures at the end of the salt crystallization test (Figure 5.53).

As in the massive sample used in the freezing-thawing test, micropore growth (mostly along the flow direction) and microfracture development around the vesicles are observed. The olivine grains continued to enlarge and deepen their microfractures in the salt crystallization test. Figure 5.54 shows the thin section and back-scattered view of an olivine grain in the massive sample. As it can be seen the microcrack widening and deepening is in progress. The vesicular sample is much more severely disintegrated by microcracks than it is by the freezing-thawing test. Unlike the other tests, spongy microfabric is observed on the rims of the pore edges of some vesicles (Figure 5.55). This sponge-like feel and appearance is observed on the surfaces of the vesicular cubic samples during the salt crystallization test as well. As they do after the freezing-thawing test, microcracks that originated from the edges of the vesicles progressively increase throughout the salt crystallization test. This is attributed to crystallization pressure generated by the salt crystals (Zehnder and Arnold, 1989; Scherer, 2002, 2004). Considering the overall microfracture development after the salt crystallization test, a chaotic microcrack network is observed, especially in the vesicular sample. The microcracks are mostly fresh, intragranular, transgranular, unstained, and present not only in the phenocrysts, but also in the groundmass. The microcracks do not have a specific direction. They run both parallel and perpendicular to the cleavage patterns and grain boundaries.

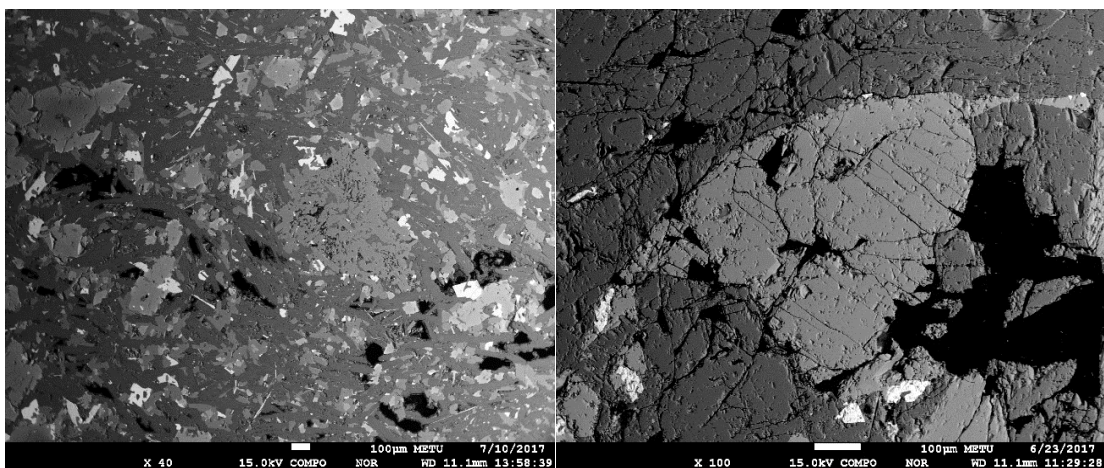


Figure 5.53 Back-scattered images displaying the microfracture morphology of the (left) massive and (right) vesicular basalt samples after the salt crystallization cycles

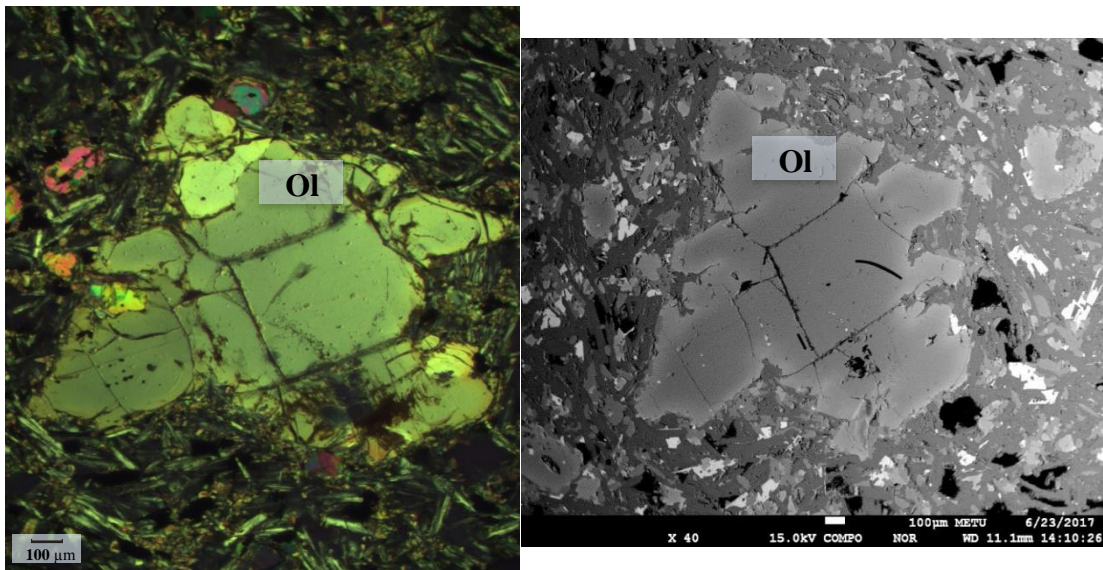


Figure 5.54 Photomicrograph and back-scattered views of an olivine mineral displaying weathering microcracks at the end of the salt crystallization test

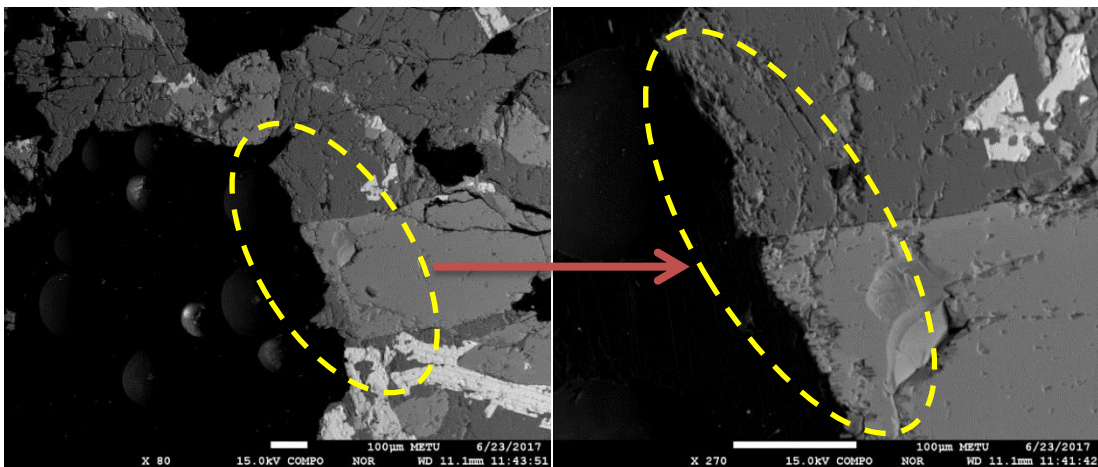


Figure 5.55 Back-scattered images showing spongy microfabrics on the pore-edge of a vesicular sample after the salt crystallization test (the sponge-like fabric is indicated by yellow dashed lines)

In order to assess the effect of natural weathering on the microfractures, a sample with scaling and flaking deterioration patterns was collected from the DCW and examined.

The groundmass and phenocrysts of this section are highly microfractured. The increase in the numbers of vesicles seems to increase the number of microcracks drastically (Figure 5.56). The section has three major microfracture sets. The microfracture sets are oriented nearly parallel to the elongated vesicles. Addition to these sets, there are some other microfractures in progress. Most of the intragranular microcracks are developed parallel to those microfracture sets, indicating the effect of vesicles in microcrack formation (Figure 5.57). Like the samples used in the accelerated weathering tests, the olivine crystals are intensively fractured by intragranular and transgranular microcracks (Figure 5.58). Unlike the other samples, some of the microfractures resulted in micro-detachments in the fabric of the weathered sample. Figure 5.59 shows a detached piece of fabric caused by microfracturing. These micro-detachments can be attributed to the specimen's scaling and flaking patterns. The overall microfracture development in the naturally weathered sample is more or less the same as those caused by the accelerated weathering tests. However, the effect of the microcracks is distinctly higher than that of the other samples.

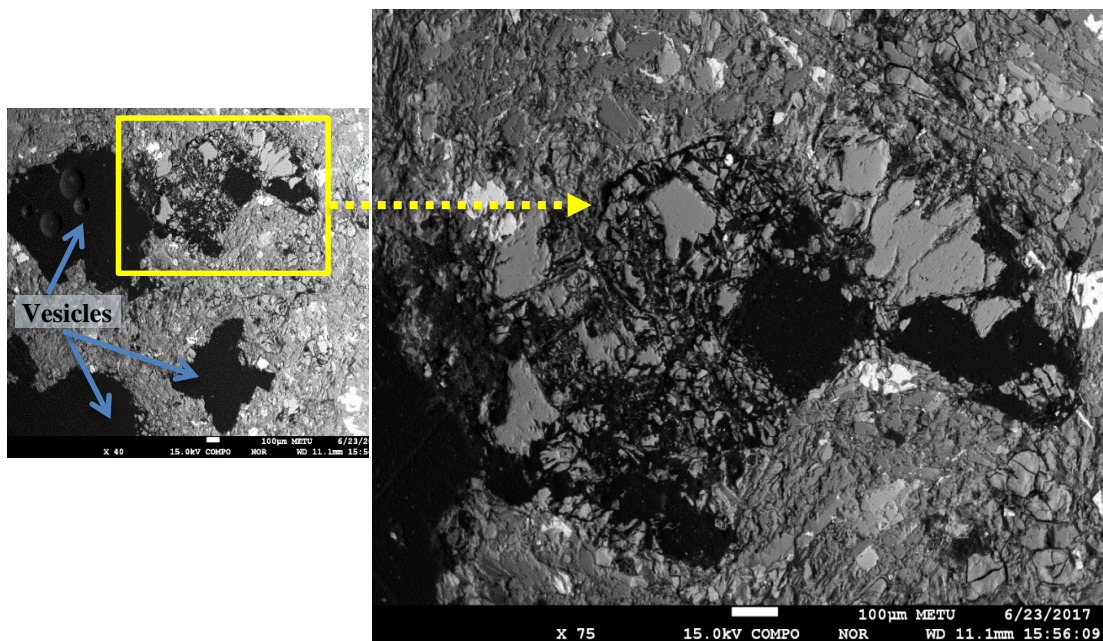


Figure 5.56 Back-scattered images showing vesicle-associated crack propagation in a naturally weathered basalt sample

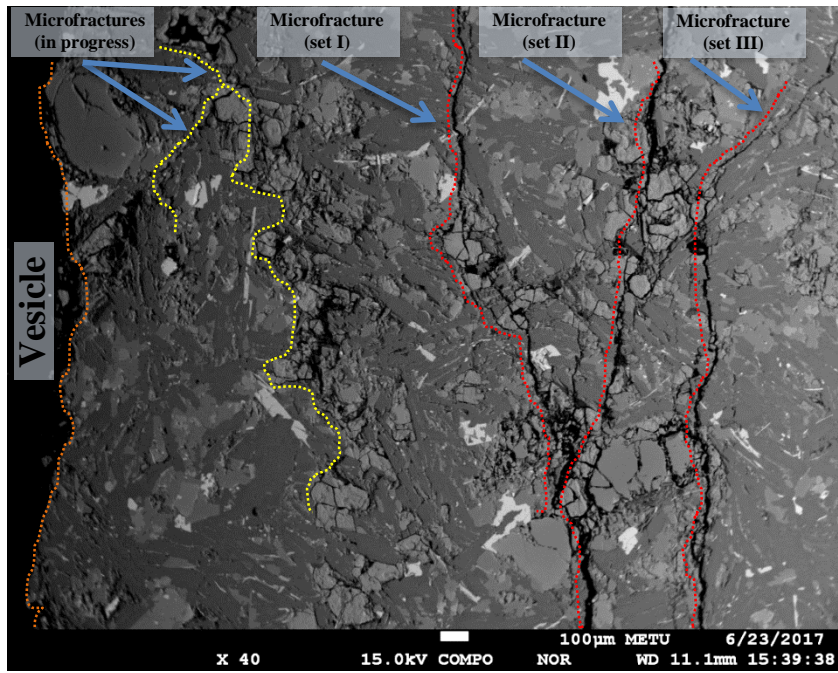


Figure 5.57 A back-scattered image of a naturally weathered basalt sample showing microfracture sets

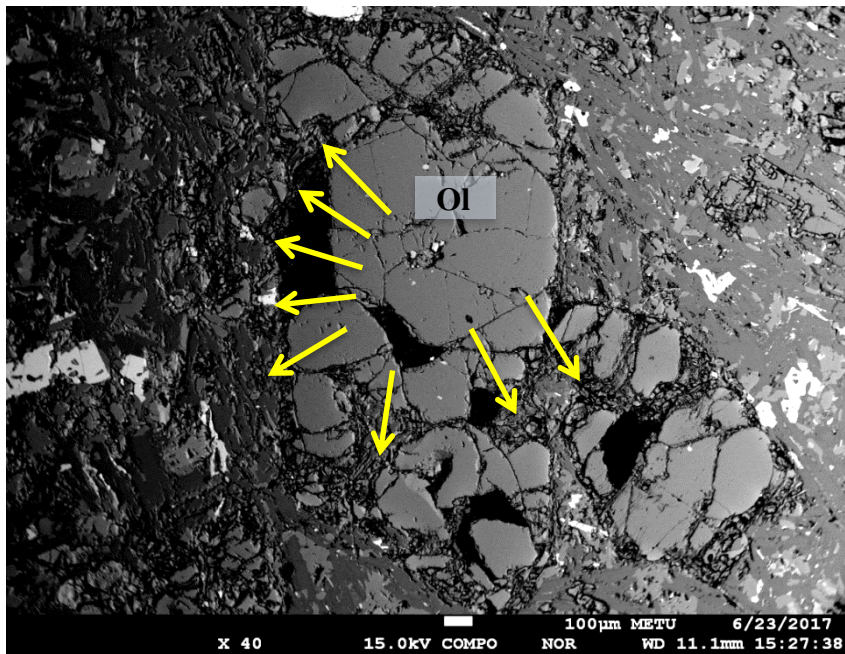


Figure 5.58 A back-scattered image displaying microfracture propagation along the rim of a naturally weathered olivine phenocryst (crack propagation is indicated by yellow arrows)

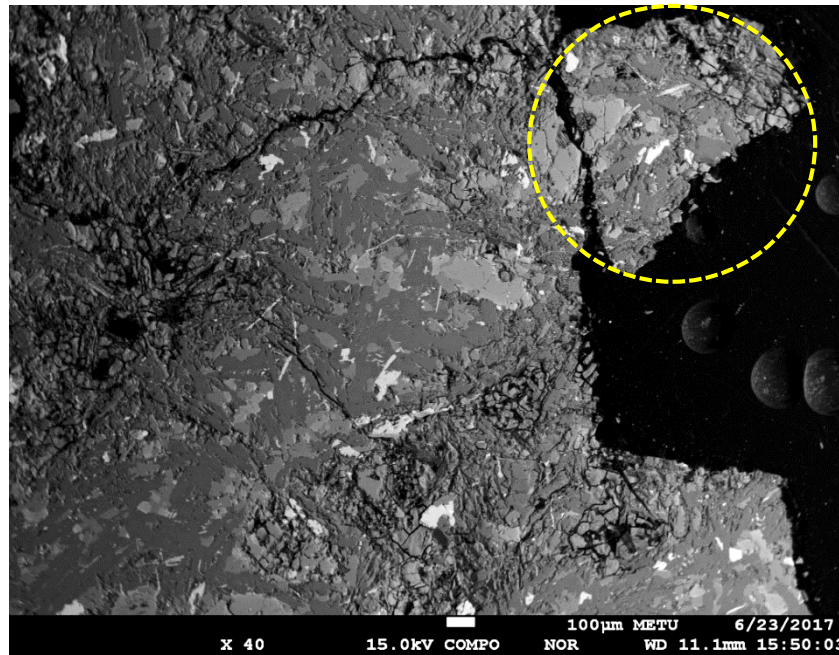


Figure 5.59 Back-scattered image of a naturally weathered basalt sample indicating a microfracture-associated detachment (the broken piece is indicated by the yellow dashed lines)

Overall, the microcrack morphology of the massive basalt samples differed significantly from that of vesicular samples. The crystal boundaries of olivine and pyroxene are the weakest zones for the microcrack formations. Considering the loss in mineral grains, crack propagation originated from the edge of vesicles, widening and deepening of microfractures and finally the increment in the number of intragranular and transgranular microfractures after the accelerated weathering tests.

5.5.1 Microfracture Counting

In order to quantify the number of microfractures and determine the effect of the accelerated weathering tests on their development, microfracture counting was performed. Two methods suggested were used in this study to quantify microfractures. The first method, suggested by Irfan and Dearman (1978), counts the number of microfractures along a selected profile length and is known as microfracture index (I_f).

The other method used for counting microfractures is proposed by Ündül and Tuğrul (2012).

It counts the number of microfractures within a defined area and is known as microfracture density (ρ_{mf}). The authors of these methods counted microfractures by examining thin sections under optical microscopy. Considering difficulties with measuring and possible misinterpretations in counting, optical microscopy has been considered not to be the optimal technique for microfracture counting. Therefore, the microfractures were counted using the back-scattered images obtained from the EPMA.

To measure the microfracture index and microfracture density, a total of nine (four massive, four vesicular and one weathered) basalt samples were used. Eight samples represented the initial and final cycles of the accelerated weathering tests performed in this study. Two sets of samples consisting four massive and four vesicular were prepared for investigation. A sample set comprised of one reference fresh sample, one sample from the final cycle (80) of the wetting-drying test, one sample from the final cycle (100) of the freezing-thawing test and one sample from the final cycle (50) of the salt crystallization test. In addition to these samples, a weathered sample collected from the DCW was also evaluated to compare the effects of artificial weathering and natural weathering. The samples were then prepared as polished sections and examined under optical microscopy to detect their most weathered zones. The polished sections were investigated using the back-scattered view obtained from the EPMA. Several back-scattered images of the samples were exported from the EPMA device during the investigations. The most appropriate and representative images were selected to be used in microfracture measurements. Based on the scale of the exported images, the back-scattered images were divided into 100 x 100 micrometer grid cells (Figures 5.60, 5.61 and 5.62). Afterwards, the microfractures per grid cells were manually counted for each sample, and the microfracture index and microfracture density were calculated separately for all nine samples.

The microfracture index and density values of the samples were determined using the following criteria: The microcracks, including hair-like, straight, branched, dendritic, tight, intragranular and transgranular were counted as microfracture. On the other hand, it is tried, as much as possible, to not count the structural microcracks including, cleavages, grain boundaries and twinning planes as microfracture. However, the widened structural microcracks were counted as microfracture. Any forms of voids were not counted as microfracture and were excluded from the total length or area of the sections in question.

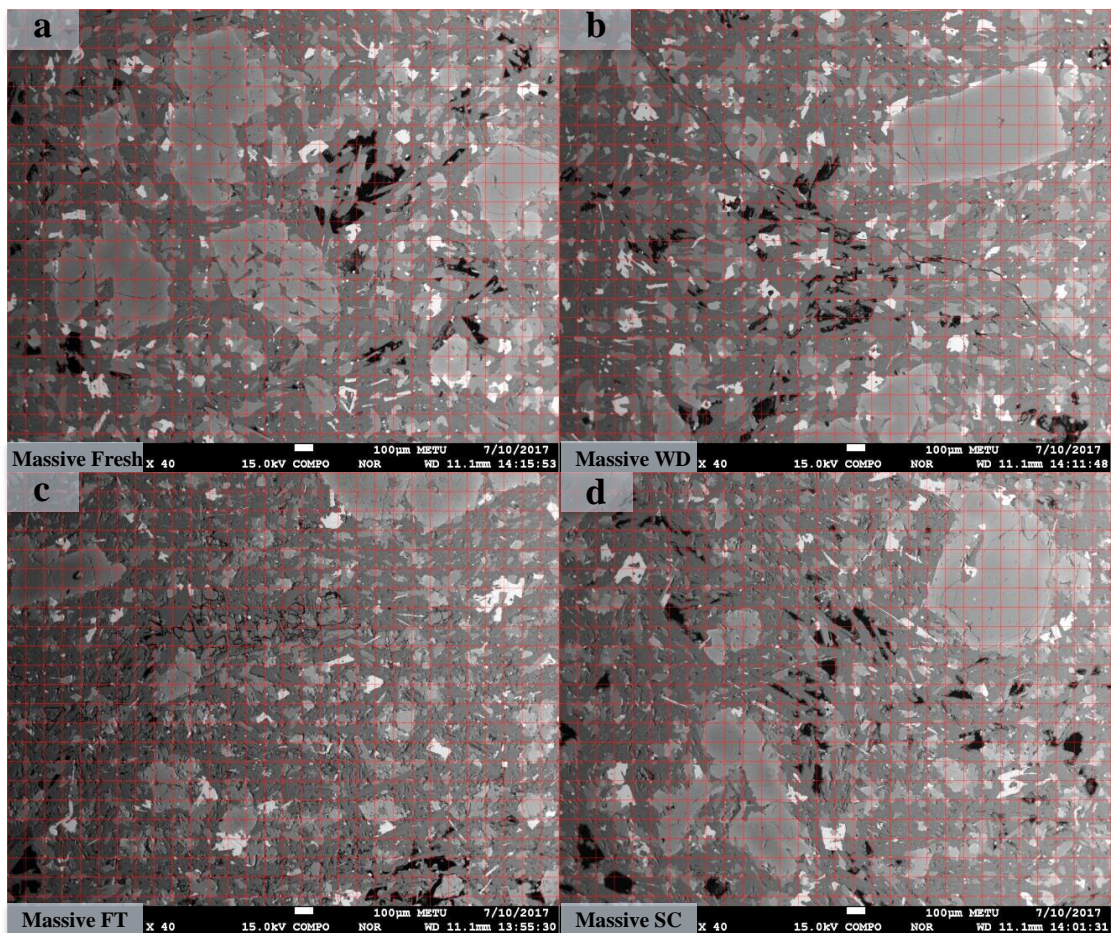


Figure 5.60 Gridded back-scattered images used in microfracture counting of massive basalts samples (WD: Wetting-Drying; FT: Freezing-Thawing; SC: Salt Crystallization)

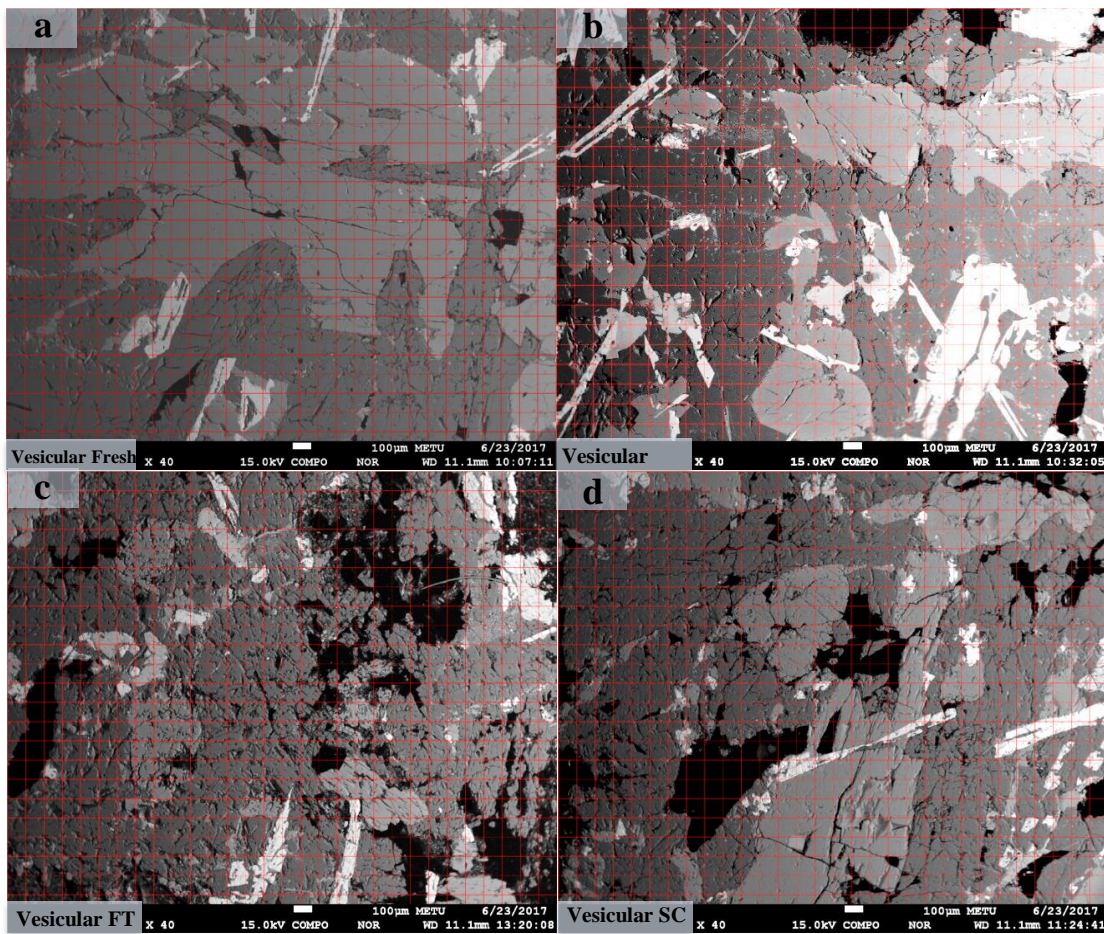


Figure 5.61 Gridded back-scattered images used in microfracture counting of vesicular basalts samples (WD: Wetting-Drying; FT: Freezing-Thawing; SC: Salt Crystallization)

In an area of 62.71 square millimeters, a total of 55,279 microfractures were counted, which indicates that the microfracture intensity of the samples increased with the destruction rate of the accelerated weathering tests. The histogram plots of the samples are shown in Figure 5.63. As the histograms show, the freezing-thawing and salt crystallization tests have almost an equal effect on microfracture development. This is true for both the massive and the vesicular samples. The wetting-drying test does not significantly increase the number of microfractures, especially in the massive samples. On the other hand, the microfracture development of the naturally weathered sample is more or less similar that of the samples used in accelerated weathering tests.

The overall results of this examination suggest that microfracture index and microfracture density are reliable methods for quantifying and correlating the degree of weathering on basalts.

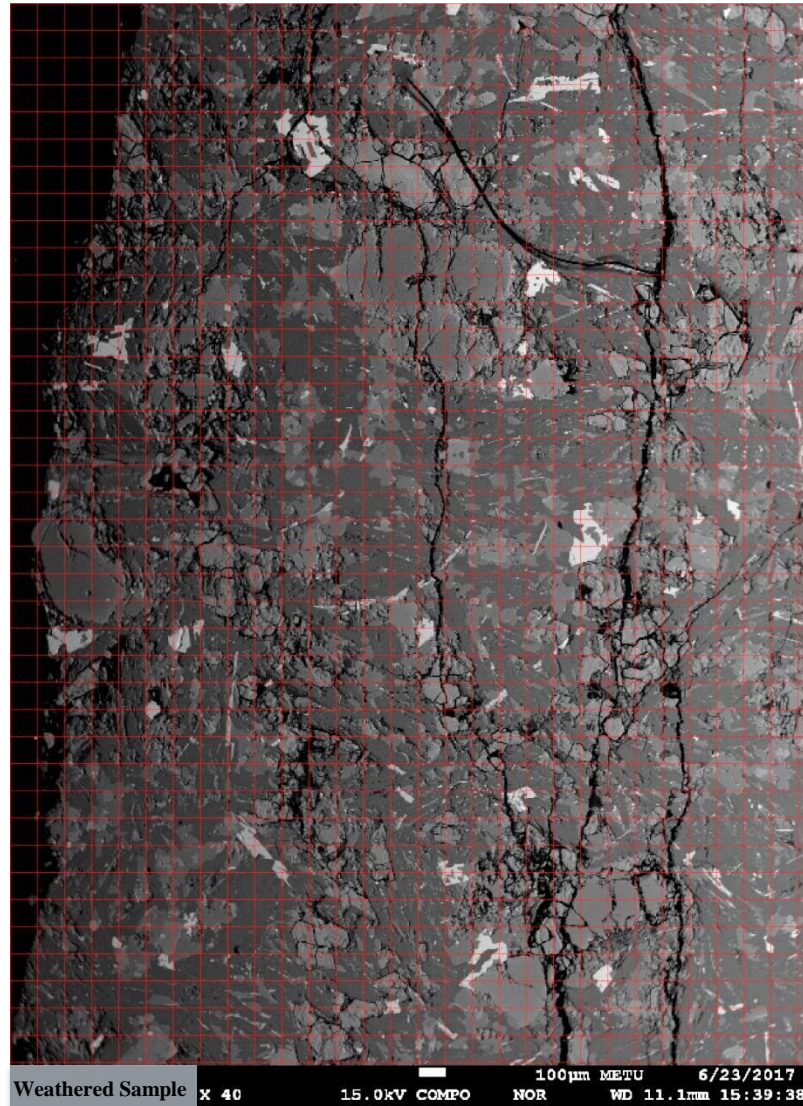


Figure 5.62 Gridded back-scattered image used in microfracture counting of a naturally weathered basalt sample

Table 5.10 Microfracture index of the massive, vesicular and naturally weathered basalt samples (WD: Wetting-Drying; FT: Freezing-Thawing; SC: Salt Crystallization)

Sample	Length of Line (millimeter)	# of Cracks	Microfracture Index (I_f)
Massive-Fresh	2.96	68	22.97
Massive-WD	2.96	78	26.35
Massive-FT	2.96	134	45.27
Massive-SC	2.96	140	47.30
Vesicular-Fresh	2.96	96	32.43
Vesicular-WD	2.96	110	37.16
Vesicular-FT	2.96	124	41.89
Vesicular-SC	2.96	112	37.84
Weathered Sample	2.96	108	36.49
SUM	26.64	970	327.70

Table 5.11 Microfracture density of the massive, vesicular and naturally weathered basalt samples (WD: Wetting-Drying; FT: Freezing-Thawing; SC: Salt Crystallization)

Sample	Final Area (millimeter ²)	Cracks	Microfracture Density (ρ_{mf})
Massive-Fresh	6.69	4563	6.82
Massive-WD	6.62	6808	10.28
Massive-FT	6.70	8229	12.29
Massive-SC	6.67	9567	14.34
Vesicular-Fresh	6.69	3218	4.81
Vesicular-WD	6.51	3343	5.14
Vesicular-FT	6.09	5754	9.46
Vesicular-SC	6.08	5863	9.65
Weathered Sample	10.67	7934	7.44
SUM	62.71	55279	80.22

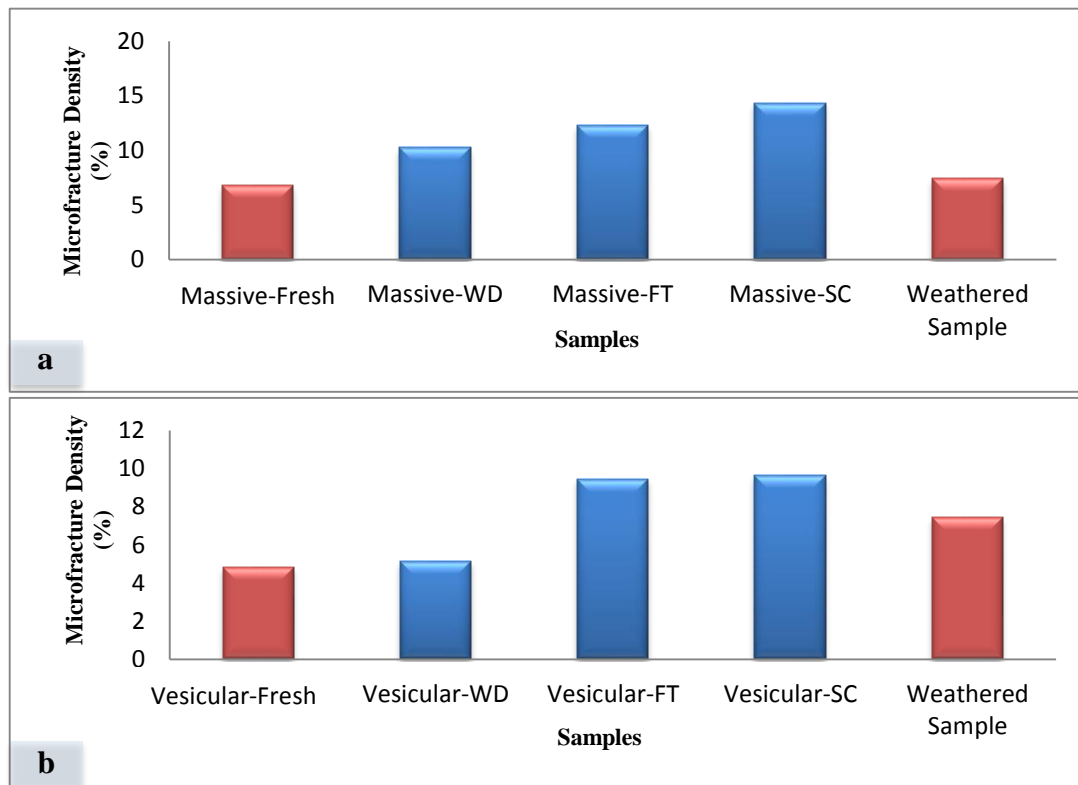


Figure 5.63 Histograms depicting the microfracture density of the examined samples (a: correlation of the massive and naturally weathered samples; b: correlation of the vesicular and naturally weathered samples; WD: Wetting-Drying; FT: Freezing-Thawing; SC: Salt Crystallization)

To produce thematic maps of microfracture density, the microfractures counted in each grid cell were converted into points in ArcGIS software. The thematic maps are produced to enhance the visualization of the microfracture density. The produced thematic maps for the massive, vesicular and weathered samples are shown in Figures 5.64, 5.65 and 5.66. The thematic maps of the massive and vesicular samples (Figures 5.64 and 5.65) reveal that the microfracture density of the massive samples is higher than the vesicular ones. This is strongly related to the density of the hair-like, tight and very short microcracks developed in the massive samples. Although the vesicular samples have also such microcracks, they are not distinct and clear as in the massive ones.

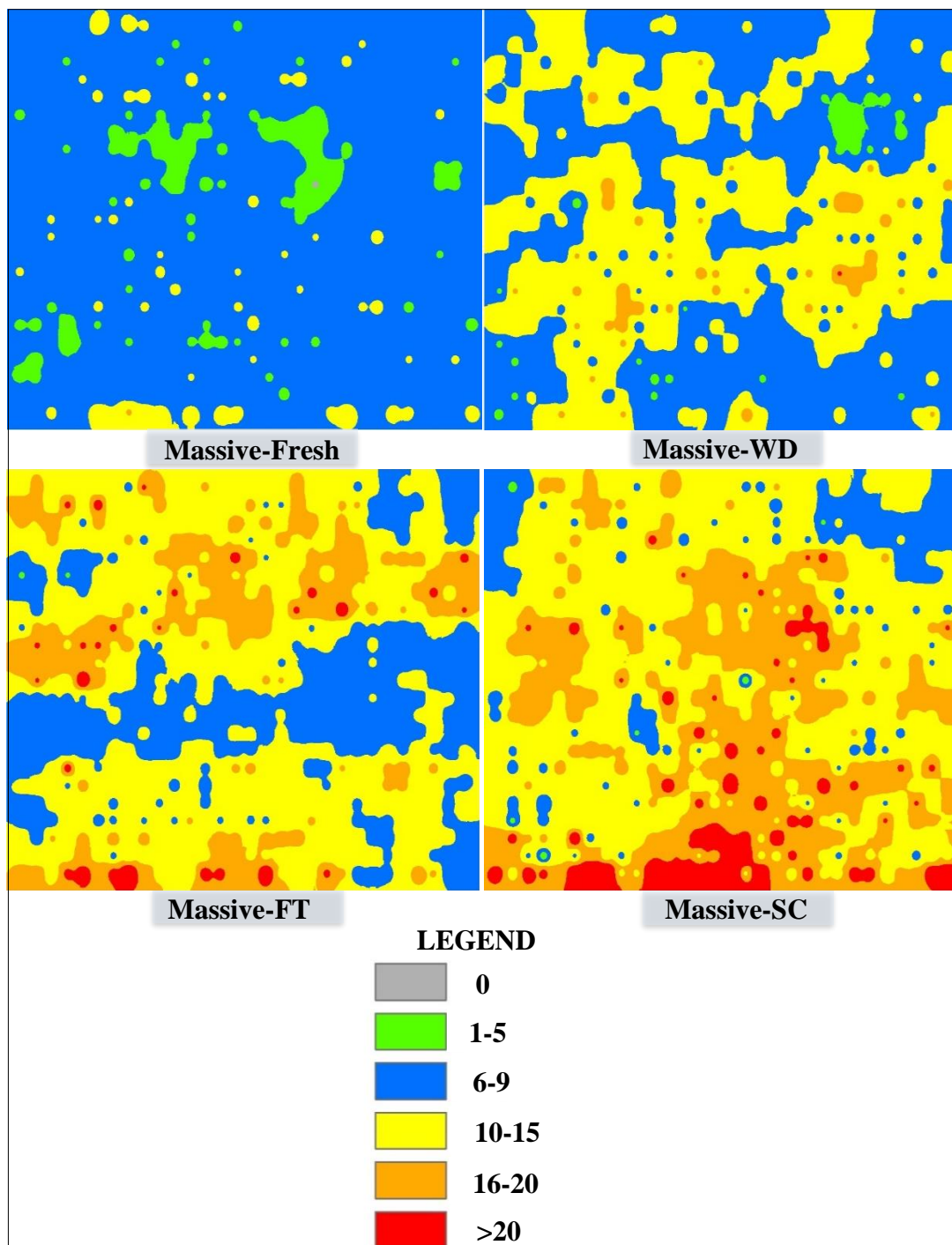


Figure 5.64 Thematic map of the microfracture density of the massive basalt samples (WD: Wetting-Drying; FT: Freezing-Thawing; SC: Salt Crystallization)

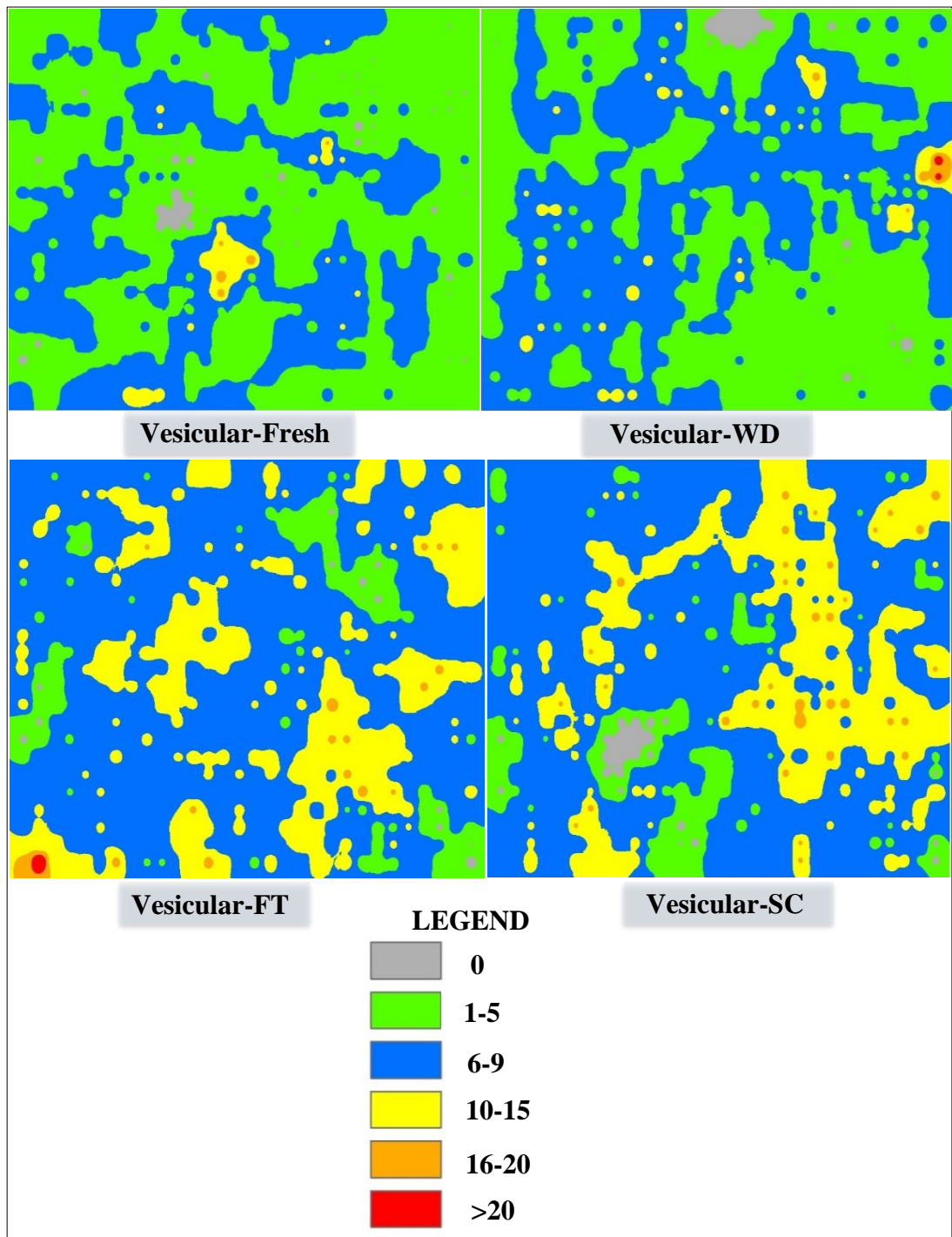


Figure 5.65 Thematic map of the microfracture density of the vesicular basalt samples (WD: Wetting-Drying; FT: Freezing-Thawing; SC: Salt Crystallization)

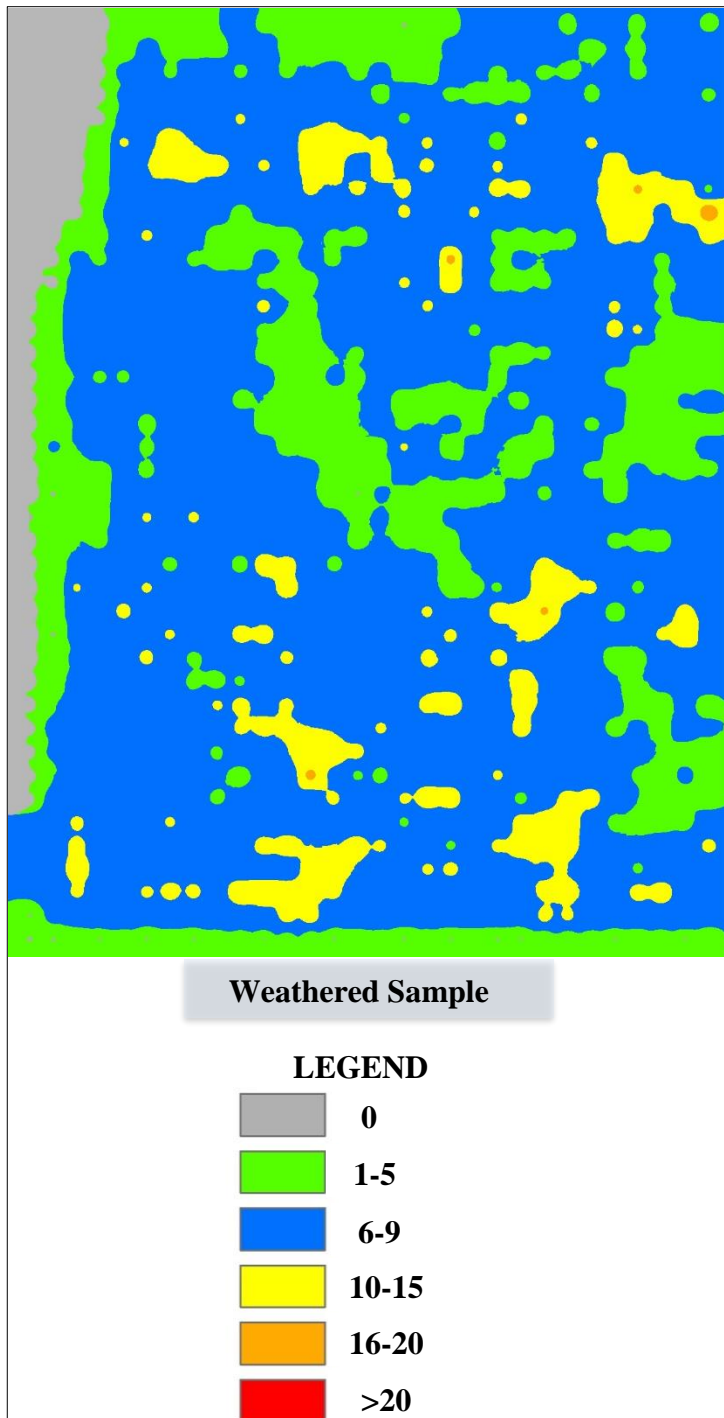


Figure 5.66 Thematic map of the microfracture density of a naturally weathered basalt sample

CHAPTER 6

DURABILITY ASSESSMENT

Durability is one of the most crucial parameters to be considered when employing a rock material for engineering purposes. The durability of a rock material can be defined as its ability to retain its original physical and mechanical properties while being exposed to weathering over an extensive period of time (Bell, 1980; Sims, 1991; Smith, 1999). There are several methods for assessing the durability of a rock material. This study assessed the durability of the basalts used in the DCW by average pore diameter, saturation coefficient and wet-to-dry strength ratio.

6.1 Average Pore Diameter

The response of stone to weathering is directly related to its average pore diameter. This parameter can be used to classify stone materials (Bell, 1993). Larson and Cady (1969) considered average pore size an important parameter for the assessment of stone durability because it reflects its frost susceptibility. The authors reported that the critical average pore diameter for frost damage appears to be about 5 μm , and that stones with larger average pore diameters can drain out the pore water. Therefore, stones with average pore diameters of less than 5 μm are susceptible to frost damage (Larson and Cady 1969; Topal and Doyuran, 1998).

The average pore diameter of the massive and vesicular basalt samples is determined using intrusion data from mercury porosimetry (MIP). The minimum, maximum and average pore diameters of the samples are shown in Table 6.1.

Table 6.1 Descriptive table for pore-size distribution of the massive and vesicular basalts after the MIP test

	Sample	Min. (μm)	Max. (μm)	Average (μm)
MASSIVE	1M-A	9.27	180.4	32.84
	1M-B	0.003891	204.1	23.31
	1M-C	4.168	176.3	26.06
	2M	0.0038	191.2	8.68
	4M	6.38	140.5	22.58
	6M	0.003892	197.3	3.82
VESICULAR	1V	5.728	184	24.66
	3V	5.229	173.2	23.28
	5V	0.13	130.4	15.76

The average pore diameter of the massive samples ranges from 3.82 to 32.84 μm , whereas the average pore diameter of the vesicular samples is between 15.76 and 24.66 μm . Considering all the measurements performed on 6 massive and 3 vesicular basalt samples, the average pore diameter of the massive and vesicular samples is calculated as 10.48 and 20.91 μm , respectively. The results suggest that most of the samples have an average pore diameter larger than the critical limit (i.e. 5 μm). This means that the absorbed water can freely drain out of the rock, making the basalt durable. However, the basalt blocks may locally be damaged where extremely small pores exist (as seen in pore-size distribution data). In general, considering the field observations and experimental studies, the average pore diameter is also found to be a useful parameter to assess the durability of the basalts.

6.2 Saturation Coefficient

The saturation coefficient of a rock material is the ratio between the water absorption by weight under atmospheric pressure and the water absorption by weight under vacuum pressure. The saturation coefficient is dimensionless and can be expressed as a decimal or as a percentage. It has been reported that a stone material with a very high saturation coefficient may not be immune to frost action (Schaffer, 1972; TSE, 1977; RILEM, 1980). Hence, this test can help to assess the resistance of stone to the freezing and thawing. Saturation coefficient values mostly lie between 0.4 and 0.95. Based on the empirical observations of the Hirschwald (1908), especially porous stones with a saturation coefficient greater than 0.8 (or 80%) are considered to be more susceptible to frost damage. However, since the critical porosity level of the stone was not defined in Hirschwald's study, and rocks generally have a saturation coefficient in different ranges, many researchers (e.g., Price, 1975; Ross and Butlin, 1989; Sims, 1991; Topal and Doyuran, 1998) have reported that this coefficient alone is not a reliable guide for evaluating the frost susceptibility and durability of rock material.

The saturation coefficients of the massive and vesicular basalt samples are determined using the complete immersion technique recommended by RILEM (1980). The details of the test results are shown in Appendix A: Tables A.23 and A.24.

The saturation coefficient of the massive basalts ranges between 0.18 and 0.68, with an average of 0.38. The saturation coefficient of the vesicular basalts is between 0.11 and 0.74, with an average of 0.52. All the basalt samples have saturation coefficients of less than 0.8, which means the samples should not be susceptible to frost damage; considering the field observations and experimental studies, frost damage has not dramatically affected the basalt samples. The results suggest that, saturation coefficient is also a useful method to assess the durability of the basalts.

6.3 Wet-to-dry Strength Ratio

The wet-to-dry strength ratio is another durability parameter, defined as the ratio between the strength of rock material in wet and dry conditions. Winkler (1986, 1993) suggested that the ratio between wet and dry strength values is a rapid and reliable method for classifying rock material in terms of durability. The method involves comparing the wet-to-dry strength ratio of modulus of rupture, tensile strength or uniaxial compressive strength.

In order to assess the wet-to-dry strength ratios of the massive and vesicular basalts, the averages of the saturated and dry uniaxial compressive strength values were used. The wet-to-dry strength ratios of the massive and vesicular basalts are determined to be 0.82 and 0.55, respectively. The wet and dry UCS values of the samples were plotted on the Winkler’s durability evaluation graph (Figure 6.1). According to the graph, the wet-to-dry strength ratio of the massive basalts falls into “very good to good” and “excellent” parts reflecting high durability; whereas the great majority of the of the vesicular samples fall into somewhere between “poor” and “fair” parts reflecting slightly less durability. Considering the field observations and laboratory performance of the massive and vesicular basalts, the wet-to-dry strength ratio should be considered a reliable guide for assessing their durability.

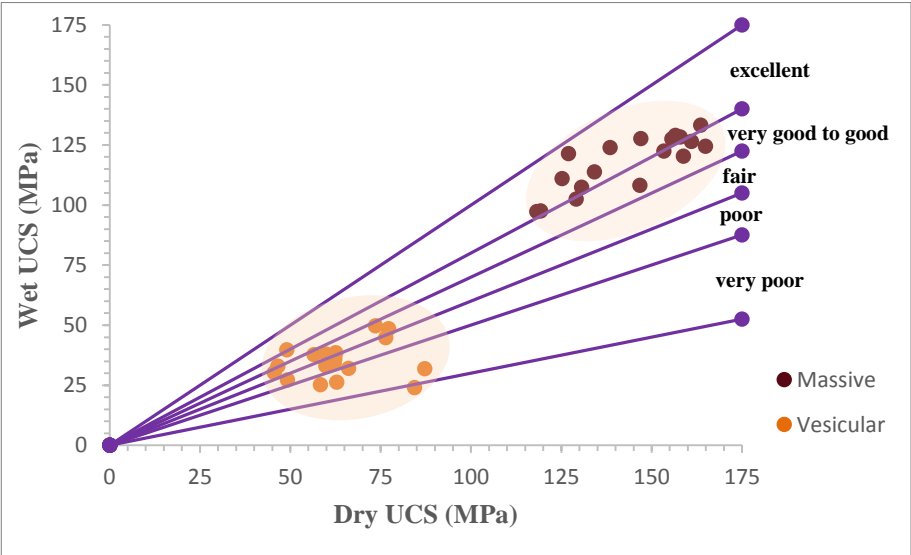


Figure 6.1 Durability assessment of the massive and vesicular basalt samples based on the wet-to-dry strength ratio proposed by Winkler (1986)

CHAPTER 7

DISCUSSION

In this chapter findings of the present study obtained from field and laboratory studies will be evaluated. It is an overview that offers a better understanding of the results.

7.1 Petrographic and Geochemical Properties of Fresh and Weathered Basalts

Previous studies and field surveys of the study area indicate that the locally available basalt material was originated from the lava eruptions of Karacadağ Volcano *ca.* 40 kilometers southwest of the city. Basalts with different types of textures were commonly used in the construction of the DCW. Although some of the basalts have amygdaloidal texture, most of the basalts employed in the DCW are classified as massive and vesicular.

The mineralogical and petrographic properties of the fresh and weathered basalts were determined by laboratory studies, including polarizing optical microscopy, back-scattered images (EPMA), SEM, EDX methylene blue adsorption, clay fraction and XRD.

For the optical microscopy investigations, more than forty thin and polished sections were prepared from the fresh and weathered basalt samples. Mineralogical and petrographic investigation of the fresh basalt samples revealed that, the samples consist predominantly of plagioclase, pyroxene and olivine. The minerals are set in the groundmass consisted of the same minerals.

Like the fresh samples, the thin sections of the weathered samples are also characterized by the presence of olivine, pyroxene and plagioclase minerals. The groundmass is also composed largely of plagioclase, olivine and pyroxene. Some opaque minerals are also detected in the groundmass. The thin section analyses of the weathered samples reveal different degrees of oxidation. The olivine and pyroxene crystals are discolored due to iron-oxide staining. Although primary minerals are conserved in most of the weathered samples, olivine phenocrysts are partly replaced by iddingsite which is the main secondary mineral in the weathered basalt samples. The iddingsite is mainly developed in the mineral boundaries and microfractures of the olivine crystals. The crystal boundaries (particularly of olivine and pyroxene) are the weakest zones for crack formations, and hence, for the secondary minerals.

The SEM analyses were performed to gather complementary information on surface morphology, microstructure and the chemical composition of the fresh massive and vesicular basalt samples. The SEM analyses of the fresh massive basalts reveal some formation of cleavages, honeycomb structure and calcite deposits. The SEM analyses of the vesicular basalt samples show that all the samples contained vesicles. Some secondary minerals and fibrous structures are also observed during the SEM analyses of the vesicular samples.

In order to quantify the presence and properties of clay minerals in the fresh basalt samples, the methylene blue adsorption test was performed. This test was performed on 8 fresh massive and vesicular basalt samples. The CECs of the fresh massive basalt samples range between 0.30 to 0.72 meq/100 g, with an average of 1.52 meq/100 g, and the fresh vesicular samples have CECs from 0.30 to 0.85 meq/100 g, with an average of 1.21 meq/100 g.

These CEC values are very low, which indicates an almost absence of clay in the bulk fresh samples. Similar to the fresh samples, the CECs of the weathered samples average around 1.3 meq/100 g. According to the test results of seven weathered samples, the CECs of the weathered basalt samples are also very low, indicating the absence of clay. Since the methylene blue adsorption test is not enough to quantify the abundance and type of the clay minerals, the samples were also examined for clay content and by XRD.

In an attempt to determine the content and type of the clay minerals, the fresh and weathered basalt samples were examined by the clay content measurements. Based on the results, the massive samples have a clay content ranging between 3.46 and 4.41 %, with an average of 4.20%. On the other hand, vesicular samples have a clay content between 3.61 and 5.68%, with an average of 4.48%. The clay fraction of the weathered samples is ranging from 3.2 to 6.22% with an average of 4.58%. The laboratory-determined clay content results indicate that most of the fresh and weathered samples have a clay content close to or below the detection limit (i.e., 5%) of the XRD. Four of the samples (two fresh and two weathered) with clay content near the detection limit were subjected to XRD analysis. The oriented samples were X-rayed in several conditions (e.g., air-dried, ethylene glycolated, heated at 300 and 550 °C). No peaks that can be attributed to clay content appeared in the X-ray patterns of the weathered samples. This suggests that the fresh and weathered samples do not contain any clay or contain a minor amount of the clay material which may control the engineering behavior of the basalts.

To examine the major and trace element characteristics of the fresh and weathered, eight fresh or relatively less altered and four weathered samples were selected for analysis after petrographic examination. The abundance of major oxides and trace elements was determined using ICP-MS. The relative content variations of the major elements of the fresh samples indicate that an abundance of SiO₂. The concentration of SiO₂ in the fresh basalt samples ranged from 46.33 to 49.73 wt%, with an average of 47.18 wt%. A relatively higher amount of oxides is observed in the Fe₂O₃, Al₂O₃, MgO, and CaO content.

Plotting the fresh samples on a total alkali-silica (TAS) diagram proposed by Le Bas et al. (1986) shows that most of the samples are basalt. There is only one sample falls the in the trachybasalt field with a 49.73 wt% of SiO₂. The plot also indicates that all the tested samples are characterized by alkaline composition. To understand the effect of chemical weathering and evaluate its state and depth, weathered samples were collected from a basalt block with spheroidal weathering. The outer part of the block was considered as weathered and the inner part as unweathered.

The major and trace element analyses of the collected samples do not significantly vary by depth. In comparison to the fresh samples, apart from a slight decrease in SiO₂ concentration, and a relative increase in loss on ignition (LoI), most of the major and trace elements conserved their initial tested values. However, since the increase in LoI is slightly larger than that of the raw samples, it can be inferred that enrichment of LoI is a good quantitative indicator of the basalts' chemical weathering depth. The results also suggest that, although chemical decomposition triggers the weathering of the basalts, most of the weathering processes are due to physical disintegration. This is also validated by almost absence of the clay minerals.

7.2 Index Properties of the Basalts

In order to determine the physical and mechanical properties of the massive and vesicular basalts, several laboratory tests for effective porosity, unit weight, water absorption under atmospheric and vacuum pressure, uniaxial compressive strength, indirect (Brazilian) tensile strength, sonic velocity, pore-size distribution, were conducted. Both the massive and vesicular basalt samples have medium porosity, with averages of 6.39% and 10.96%, respectively. The massive samples have a high dry unit weight with an average of 27.28 kN/m³, and the vesicular samples have a moderate dry unit weight with an average of 24.73 kN/m³. The water absorption by weight and water absorption by volume under atmospheric pressure of the massive basalt samples average around 0.89% and 2.46%, respectively. These average values are measured for the vesicular samples as 2.30% and 5.78%, respectively.

The average water absorption by weight and water absorption by volume under vacuum pressure of the massive basalt samples were measured as 2.30% and 6.39%, respectively. These average values were measured for the vesicular basalt samples as 4.35% and 10.96%, respectively. The uniaxial compressive strength (UCS) of the massive and vesicular basalts was measured both in dry and saturated conditions. The dry and saturated UCS of the massive basalt samples averaged 143.75 and 117.91 MPa, respectively. These values are measured for the vesicular basalt samples as 63.30 and 34.99 MPa, respectively.

Based on the dry UCS of the samples, the massive and vesicular basalts can be classified as very strong and strong, respectively. In order to determine the effect of water on the samples, the dry and saturated UCS values are compared. The results showed that saturation reduces the UCS of both massive and vesicular basalts by 17.98 and 44.72%, respectively. Thus, the water has a significant effect, especially on the UCS of the vesicular basalts. The tensile strength of the samples was investigated indirectly using the Brazilian test. The average indirect (Brazilian) tensile strength of the massive and vesicular basalts is measured as 16.60 and 8.76 MPa, respectively. It should be noted that the orientation of the cracks developed under the applied load may give some information on the isotropy of the material. During the indirect (Brazilian) tensile strength test, it is observed that most of the cracks on the surface of the specimens developed parallel to the initial crack at their centers. Considering the theory behind the indirect (Brazilian) tensile strength test (Markides et al., 2011; Li and Wong, 2013), one can assume that the isotropy of the fresh massive basalt samples tested in this study is very pronounced. However, due to weakness zones at the pore edges, isotropy is not well pronounced in some of the vesicular samples. The dry sonic velocity of the massive basalts ranges from 2123.05 to 5608.13 m/s, with an average of 4599.68 m/s, and the dry sonic velocity of the vesicular samples varies from 3306.67 to 5179.22 m/s, with an average of 4157.58 m/s. The sonic velocity of the saturated massive basalt samples is between 3510.40 and 5690.40 m/s. with an average of 4981.06 m/sec. The saturated sonic velocity of the vesicular basalt samples ranges from 3861.11 to 5401.53 m/s. with an average of 4609.15 m/s.

The massive and vesicular basalts are classified using the rock classification for sonic velocity proposed by Anon (1979) as having high sonic velocity in both the dry and saturated states.

The isotropy of the basalts was also evaluated through the current study. In order to check the isotropy, a total of 20 vesicular basalt samples showing distinct flow layers were investigated by measuring their UCS and sonic velocity. The samples were tested based on their flow directions (i.e., parallel and perpendicular to the flow direction). The average uniaxial compressive strengths of the samples that parallel and perpendicular to the flow direction are 79.10 and 51.26 MPa, respectively. The average dry sonic velocity of the samples that parallel and perpendicular to the flow direction are 4206.66 and 3754.79 m/s, respectively; whereas the average saturated sonic velocities of the samples that parallel and perpendicular to the flow direction are 4497.57 and 4081.62 m/s, respectively.

The results reveal that the measured strength and sonic velocity of the basalts which are parallel to the flow direction is larger than that perpendicular to the flow direction. Although the relatively higher strength values in parallel conditions are not expected (i.e., the highest strength is expected perpendicular to the flow direction), these results can be attributed to the presence of the incipient cracks and number of tested samples. Moreover, the results suggest that, the flow layers do not act as discontinuities and not exhibit a mineral lineation. Although some of the tested samples exhibit a slight anisotropy, such directional change in strength and sonic velocity cannot directly be attributed to the anisotropy of the material.

The pore-size distributions of the samples were determined by mercury intrusion porosimetry (MIP). The pore-size distribution of the massive basalt samples varies from 0.0038 to 180.4 μm and from 0.13 to 173.2 μm for the vesicular basalt samples. The results suggest although some of the samples have small pore ($< 5 \mu\text{m}$) most of the samples have pores larger than the 5 μm .

7.3 Classification of the Decay Forms

Several field surveys were conducted in the study area to characterize and monitor the type, degree and distribution of the weathering forms developed on the DCW. It is observed that there are numerous weathering forms of various sizes on the DCW, which are evidence of destruction and deterioration in progress. The weathering forms on the DCW are classified as cracks, detachments, material loss, discolorations, deposits and biological colonization. The deterioration patterns with detachment and loss of stone material are the most common forms on the DCW. The detachments generally take the form of blistering, delamination, disintegration, fragmentation and scaling. Blistering is common on the lower parts of the walls, and it is thought that blistering triggers new weathering forms as spalling, delamination and finally, loss of material. The delamination patterns on the DCW mostly develop parallel to the flow direction. There are also some rows of elongated vesicles on the delaminated surfaces. These weathering patterns are found mostly on the lower and middle parts of the masonry and towers, and are mostly associated with the improper placing of the basalt in the masonry. In other words, since the direction of flow layers is not properly oriented, delamination patterns developed on the basalt blocks. Disintegration of the DCW mostly takes the form of crumbling. This weathering type can develop in a spheroidal form as well. The DCW have also suffered from fragmentation, commonly in the form of splintering and chipping. Finally, as a form of detachment, scaling is another common form of weathering on the DCW. The thickness of the scaling on the DCW ranges from millimeters to centimeters, and most of it is in the form of flaking and contour scaling. There are also many visible signs of transitional detachment forms, especially blistering, crumbling and scaling. Material loss is another common weathering form on the DCW. Alveolization, erosion, mechanical damage and missing parts are the common forms of material loss on the DCW. Patterns of alveolization and coving (as a single alveole) are found on the DCW.

Those patterns commonly develop on the lower and middle parts of the masonry and towers. The causes of alveolization can be associated with salt crystallization and wind exposure. Erosion is another form of material loss on the DCW, which causes the loss

of the stone's original surface or edge of stones leading to smoothed forms. Erosion commonly takes the form of differential erosion, rounding and roughening. It can be observed not only on the stone blocks, but also on the iconic reliefs engraved on the towers. The DCW have suffered different kinds of mechanical damage. Material loss caused by mechanical damage takes the forms of impact damage, cuts, scratches and engraving, and pecking or keying. There are a variety of methods to shape and dress the surface of the rough stone blocks, including cladding, sandblasting, tumbling, pitching and broaching. These surface finishing techniques have been frequently used to make the stone appear ancient in recent efforts to restore the DCW (Figure 7.1). It should be borne in mind that some of the surface finishing treatments, especially those increase the roughness and irregularities of the basalt's surfaces, may not only alter the surface of the basalt blocks, but also accumulate exogenic materials and become a nest for micro-organisms (Figure 7.2).

The growth of higher plants is a deterioration problem that is frequently observed on sections of the DCW. Plants grow mostly in moist cracks, open joints and in the missing parts of the walls and towers. Their roots penetrate the walls, increase the amount of substrate and damage the material. Therefore, it is essential to seal or properly repair the open joints, cracks and missing parts to prevent further growth.

In addition to these common weathering forms, the DCW have suffered significantly from damages caused by human activities such as illegal housing, environmental pollution, painting, vibrations caused by traffic, fires, the dismantling of stone blocks and so forth.



Figure 7.1 Different surface finishes on the DCW

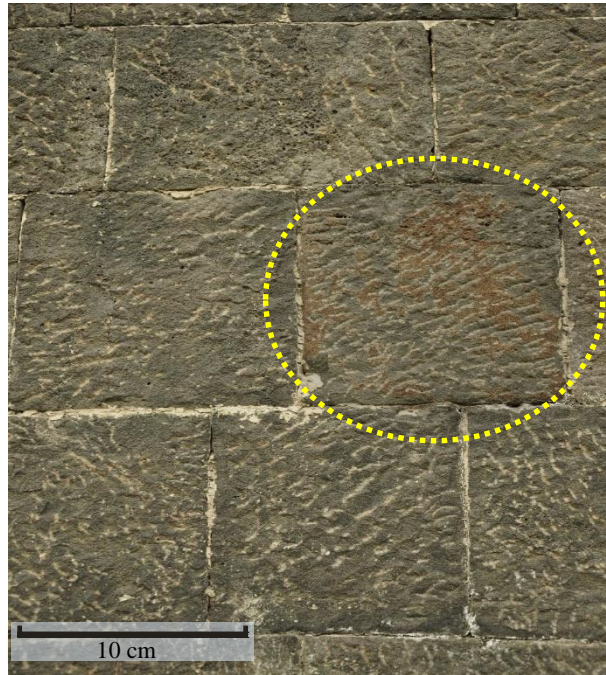


Figure 7.2 A surface finish that caused material loss and biological colonization on the surface of the basalt blocks (biological colonization is indicated by the dotted circle)

Based on the visual observations performed at the study area, the deterioration forms and their incidence for the massive and vesicular basalt are evaluated. The evaluation is carried out to correlate the incidence of the deterioration forms with the massive and vesicular basalts. Here, the relative incidence of each deterioration forms is rated from 0 (not observed) to 4 (very common). Table 7.1 shows the rating of the deterioration forms for the massive and vesicular basalts used in the construction of the DCW.

Based on the overall rating, the relative ratings of the deterioration forms, cracks, detachments, and discoloration and deposit have developed almost equally on the massive and vesicular basalts. It is also understood from the table of rating that, material loss is more common on the massive basalts, but it could be due to external factors (drainage problem, use of improper material, etc.) deteriorating the basalts. Finally, development of the biological colonization on the vesicular basalts is slightly higher than the massive basalts.

Table 7.1 Relative rating of the deterioration forms developed on the massive and vesicular basalts of the DCW

Main Groups	Sub-Groups	Rating*	
		Massive	Vesicular
CRACKS	Cracks	4	3
	Fractures	4	3
	Star cracks/Hair Cracks	1	1
	Craquele/Splitting	1	1
DETACHMENTS	Blistering	2	2
	Bursting	0	0
	Delamination	0	2
	Exfoliation	0	0
	Crumbling	3	2
	Granular Disintegration	0	0
	Splintering/Peeling	1	1
	Chipping	3	3
	Flaking/Scaling	4	3
MATERIAL LOSS	Alveolization	2	2
	Differential erosion	0	0
	Rounding	3	2
	Roughening	2	1
	Impact Damage	3	3
	Cut/ Scratch	3	2
	Abrasion	1	1
	Keying	3	1
	Micorkrast	0	0
	Missing Part/Gap	3	3
	Perforation/Pitting	0	0
DISCOLORATION AND DEPOSITS	Crusts	1	2
	Deposits	3	3
	Coloration	3	3
	Bleaching/Staining	3	2
	Moist Area	3	3
	Efflorescence	1	2
	Encrustation	0	0
	Film/Patina/ Glossy Aspect	0	0
	Graffiti	3	2
	Soiling	0	0
	Subflorescence	0	0
BIOLOGICAL COLONIZATION	Alga	1	2
	Lichen	1	3
	Moss	2	2
	Mould	0	0
	Plant	2	3

* (0: Not Observed; 1: Rare; 2: Occasional; 3: Common; 4: Very Common)

This study produced maps of the visual decay forms of the basalts used in the DCW. Two specific sections of the DCW were selected for mapping the visual decay forms. The first is a gate façade on the north section of the DCW. It was selected to document the deterioration of a recently restored section. The second is a tower façade on the south section of the DCW. It was selected to document the deterioration of a relatively original section. Recent restorations of the gate façade have triggered deterioration and caused new damages to the structure, most probably as a result of using of hard mortar and improper interventions. The weathering forms on the tower façade partially differ from those of the gate façade. Although formations of crust and alveolization are unusual weathering forms for the DCW, they are common on the lower part of the tower façade.

This can be attributed to the location of the tower on a steep slope facing the Tigris River, making it more vulnerable to moisture, salt, wind and solar exposure.

The surviving city walls have been subjected to numerous interventions throughout their long history, but preliminary research found very little documentation of these interventions. Most of the information about past interventions comes from inscriptions carved in different sections of the site and photographic records. The history, location, and techniques of the past interventions are essential information for conservation, especially when planning and applying new restoration projects. It is also important while assessing the service life of the material and classifying the decay forms. Although the field studies identified some traces of the past interventions by visual examination; here, it is important to point out that the studies of the type, extent and distribution of the weathering forms were conducted with a lack of information concerning past interventions and reuse of the material.

7.4 Accelerated Weathering Tests

In order to evaluate the physical deterioration and durability of the fresh massive and vesicular basalts, environmental conditions were artificially simulated in accelerated weathering tests such as wetting-drying, freezing-thawing and salt crystallization. The wetting-drying test was performed for 80 cycles, the freezing-thawing test was performed for 100 cycles, and the salt crystallization test was performed for 50 cycles. The effects of these tests were evaluated by visual examination, weight loss, effective porosity, dry and saturated unit weights, water absorptions under atmospheric pressure and under pressure, sonic velocity and uniaxial compressive strength. At the end of the wetting-drying tests, no remarkable change is observed in the dry unit weight of the massive and vesicular basalt samples. However, the porosity and water absorption of the samples increase greatly. Their sonic velocity and uniaxial compressive strength decrease throughout the cycles. The results indicate that wetting and drying has a more pronounced effect on the vesicular basalt samples. After the freezing-thawing cycles, no remarkable change in weight is observed for the massive basalt samples (0.74%); however, the vesicular basalt samples lost relatively more weight (3.06%). Considering the morphology of the samples, there are some signs of spalling and flaking at the edges of the massive basalt samples.

The vesicular basalt samples become lighter in color and grainy in feel and appearance during the freezing-thawing test cycles. As the freezing-thawing test cycles increase, so do the effective porosity and water absorption of the samples, but their sonic velocity and uniaxial compressive strength are reduced. The results show that the massive basalt samples have relatively good resistance to freezing and thawing. At the end of the salt crystallization test, there is no remarkable change in the weight of the massive and vesicular basalt samples. Nevertheless, the morphology of the massive and vesicular samples indicates different degrees of deterioration. The decay patterns in the massive samples commonly take the form of detachment and material loss (flaking, chipping, erosion and cavities). Due to crystallization pressure, some of the massive samples are broken through their primary cracks. Some of the vesicular samples are drastically damaged by the salt crystallization test.

Their deterioration patterns take the form of discoloration, flaking and efflorescence. As the cycle increases in number, especially at the end of cycle 10, some of the vesicular samples take on a highly rounded and globular shape. These samples then totally disintegrated at the end of the 16th cycle. As the salt crystallization test cycles increase, the effective porosity and water absorption of the massive and vesicular basalt samples increase progressively. The sonic velocity of the massive samples decreases throughout the test, while the sonic velocity of the vesicular samples increases. At the end of the salt crystallization test, the uniaxial compressive strengths of both the massive and vesicular samples are significantly reduced. Although the test has pronounced effects on the massive and vesicular basalt samples, the massive basalt samples have relatively good resistance to the salt attack.

Considering the variations of the physico-mechanical properties of the basalts, the salt crystallization test is found to affect both the massive and vesicular basalt samples most aggressively. Freezing and thawing has the next most effect on them, and wetting and drying has the least.

The durability tests have more or less effect on the physico-mechanical properties of the basalts. Of these parameters, unit weight is the least affected by the durability tests. The porosity, water absorption and UCS are the parameters most affected by the durability tests. Although sonic velocity shows some different trends, it tends to fall throughout the durability tests. Since the samples tested after the durability tests reveal different sonic velocities, such variations in the sonic velocity can be attributed to the basalts' heterogeneity due to different formation mechanisms.

These findings indicate that, except unit weight, all the other physico-mechanical properties are useful for assessing the deterioration of the massive and vesicular basalts. Nevertheless, since UCS and sonic velocity are better indicators of internal damage to rock material, future studies of basalt should use these parameters.

To check isotropy, the response of the basalts to accelerated weathering tests was evaluated in detail. Sonic velocity is a reliable parameter for checking the isotropy of rock material (Dearman et al., 1987).

During the evaluation, special attention was given to the sonic velocity of the samples that developed decay patterns during the weathering tests. Some of the massive and vesicular samples take on different forms of deterioration, especially during the freezing-thawing and salt crystallization test cycles. The sonic velocity of the cubic samples with decay patterns is compared with different pairs of their faces without significant decay patterns. There is a distinct change in the deteriorated faces of the samples. It was noticed that sonic travel time distinctly varies by change in direction (i.e., through the different faces of the cubic samples). Although the sonic velocity of the fresh massive and vesicular samples does not vary by direction, it does so significantly in some of the samples used in the accelerated weathering tests. Therefore, it can be stated that the variations in sonic velocity can be employed to outline decay and anisotropy in basalts.

7.5 Microfracture Properties of the Basalts

The microfracture properties of the basalt samples were evaluated by type, amount, orientation and density. Microfracture studies were carried out on nine basalt samples (one fresh massive and one fresh vesicular, three massive and three vesicular samples from the final cycles of the wetting-drying, freezing-thawing and salt crystallization tests, and finally, one naturally weathered basalt sample collected from the DCW). The microfracture studies show that the fresh samples have different forms of intragranular and transgranular structural microfractures. The orientation of the microfractures is commonly along the grain boundaries. The structural cracks are slightly widened after wetting-drying cycles. The olivine and pyroxene crystals, even those in the groundmass, are more susceptible to weathering than the plagioclases. Thus, most of the microfractures are developed along the grains of these susceptible crystals. It is also noted that the orientation of the microfractures may change in transitions from compositionally different mineral crystals. This was determined by following the propagation of a microfracture which changed its direction while passing from the olivine to the plagioclase crystal.

Most of the microfractures in the artificially and naturally weathered samples originate from the edges of the vesicles. As the distance of the crystal from the vesicles increases, the microfracture density falls rapidly and the reverse is also observed. Thus, it can be easily stated that the pore pressure in the vesicles, especially after the freezing-thawing cycles and salt crystallization, triggers microfracture development.

In order to visualize the influence of the accelerated weathering test on microfracture propagation, microfracture counting was carried out in this study, and 55,279 microfractures were counted for a total area of 62.71 square millimeters. These results show that the number of microfractures dramatically increases, especially at the end of the freezing-thawing and salt crystallization tests.

7.6 Assessment of Durability

The durability of the basalts was assessed using average pore diameter, saturation coefficient and wet-to-dry strength ratio. The average pore diameters of the massive and vesicular samples are calculated as 10.48 and 20.91 μm , respectively. The massive basalt samples have an average saturation coefficient of 0.38, and that of the vesicular basalt samples are 0.52. In order to evaluate their wet-to-dry strength ratio, the averages of the saturated and dry uniaxial compressive strength values are used, and the wet-to-dry strength ratios of massive and vesicular basalts are measured as 0.82 and 0.55, respectively.

Average pore diameters of the massive and vesicular basalt samples reveal that most of the samples have an average pore diameter larger than 5 μm . The results suggest that both massive and vesicular samples are durable. The saturation coefficients of the tested massive and vesicular basalt samples indicate that the samples do not dramatically affected by the frost damage. The wet-to-dry strength ratios of the samples in question reveal that water significantly reduces the uniaxial compressive strength of the basalts. The measured rate of this reduction in the vesicular samples is approximately 50% greater than that of the massive samples.

According to the classification of wet-to-dry strength ratios suggested by Winkler (1986, 1993), the massive basalt samples can be characterized as highly durable, and the vesicular basalt samples can be classified as slightly less durable.

It can be inferred from the durability assessment that, both massive and vesicular basalts are durable, however, the massive samples appear to be more durable than the vesicular ones.

Considering the laboratory performance of the massive and vesicular basalts and field observations, average pore diameter, saturation coefficient and wet-to-dry strength ratio are useful parameters to assess the durability of the basalts. Of these parameters, the wet-to-dry strength ratio should be considered a reliable guide for assessing the durability of basalt.

In reference to the laboratory studies performed within the scope of the present study, a summary of the results for the material properties of massive and vesicular basalt samples is presented in Table 7.2. As it indicates, the massive basalts have better properties than the vesicular basalts.

Table 7.2 Material properties of the massive and vesicular basalts based on the laboratory studies

Engineering Properties	Standards Used	# of Tested Samples (M/V)*	Test Results	
			Massive Mean \pm SD \dagger	Vesicular Mean \pm SD \dagger
Dry unit weight (kN/m³)	ISRM (1981)	130/130	27.28\pm0.70	24.73\pm0.56
Saturated unit weight (kN/m ³)	ISRM (1981)	130/130	27.91 \pm 0.69	25.80 \pm 0.54
Effective porosity (%)	ISRM (1981)	130/130	6.39\pm1.22	10.96\pm1.46
Water abs. by weight under atm. pressure (%)	RILEM (1980)	130/130	0.89 \pm 0.28	2.30 \pm 0.49
Water abs. by weight under vacuum pressure (%)	ISRM (1981)	130/130	2.30\pm0.45	4.35\pm0.62
(Dry) Uniaxial compressive strength (MPa)	ISRM (1981)	36/36	143.75 \pm 16.02	63.30 \pm 12.34
(Saturated) Uniaxial compressive strength (Mpa)	ISRM (1981)	36/36	117.91\pm11.34	34.99\pm7.47
(Dry) Indirect (Brazilian) tensile strength (MPa)	ISRM (1981)	10/10	16.60 \pm 1.27	8.76 \pm 2.35
Dry sonic velocity (m/s)	ISRM (1981)	130/130	4599.68\pm651.77	4157.58\pm369.60
Saturated sonic velocity (m/s)	ISRM (1981)	130/130	4981.06 \pm 322.02	4609.15 \pm 391.77
Cation exchange capacity (meq/100 g)	AFNOR (1980)	5/3	0.72\pm0.41	0.70\pm0.46
Microfracture Index (I _f) (Fresh sample)	Irfan and Dearman (1978)	1/1	23.99	32.43
Microfracture Index (I_f) (After wetting-drying test)	Irfan and Dearman (1978)	1/1	26.35	37.16
Microfracture Index (I _f) (After freezing-thawing test)	Irfan and Dearman (1978)	1/1	45.27	41.89
Microfracture Index (I_f) (After salt crystallization test)	Irfan and Dearman (1978)	1/1	47.29	46.28
Microfracture density (ρ_{mf}) (Fresh sample)	Ündül and Tuğrul (2012)	1/1	6.82	4.81
Microfracture density (ρ_{mf}) (After wetting-drying test)	Ündül and Tuğrul (2012)	1/1	10.28	5.14
Microfracture density (ρ_{mf}) (After freezing-thawing test)	Ündül and Tuğrul (2012)	1/1	12.29	9.46
Microfracture density (ρ_{mf}) (After salt crystallization test)	Ündül and Tuğrul (2012)	1/1	14.34	9.28
Average pore diameter (μ m) (MIP)	Washburn (1921)	6/3	10.48 \pm 27.27	20.91 \pm 31.29
Saturation coefficient	RILEM (1980)	130/130	0.38\pm0.09	0.5 \pm0.08
Wet/dry strength ratio (UCS)	Winkler (1986, 1993)	36/36	0.82	0.55

*: M/V: Massive/Vesicular; \dagger SD: Standard deviation

CHAPTER 8

CONCLUSIONS AND RECOMMENDATIONS

As a combination and reflection of influences of the various civilizations that have settled in the region, the Diyarbakır City Walls (DCW) are among the most gigantic surviving structures from ancient times. Basalts with two different types of textures were employed in the construction of the DCW. Although basalt is known as a long-lasting construction material it starts to deteriorate once it quarried and subjected to the environmental and structural stresses. Like numerous historical structures around the world, the DCW are also suffering from stone deterioration. A large variety of weathering patterns can be observed on the basalts used in the DCW. Thus, it is vital to investigate the causes of basalt deterioration and suggest proper materials and construction techniques to assist conservation studies.

In reference to this study, the following conclusions and recommendations are given:

- I. The basalts employed in the construction of the DCW are classified as massive and vesicular based on their texture.

- II. Mineralogical and petrographic investigation of the basalt samples reveal that, the both fresh and weathered samples consist predominantly of plagioclase, pyroxene, and olivine. The minerals are set in the groundmass consisted of the same minerals. Although the primary minerals are conserved in most of the weathered samples, the olivine and pyroxene crystals are discolored due to iron-oxide staining. Iddingsite, which is the main secondary mineral in the weathered basalt samples, is commonly observed in the olivine phenocrysts. It is understood from the geochemical studies that the fresh samples indicate abundance of SiO₂ concentration and characterize alkaline composition.
- III. Both the massive and vesicular basalt samples have medium porosity. While the massive samples have a high unit weight, the vesicular samples have a moderate unit weight. Based on the dry UCS of the samples, the massive and vesicular basalts can be classified as very strong and strong, respectively. The sonic velocity measurements of the fresh samples indicate that although some of the samples exhibit a slight anisotropy, most of the samples does not significantly vary by direction. The pore-size distribution of the massive basalt samples varies from 0.0038 to 180.4 μm and from 0.13 to 173.2 μm for the vesicular basalt samples.
- IV. Field studies show that there are numerous weathering forms of various sizes on the DCW, indicating that the destruction and deterioration of the basalt used in the DCW is in progress. Detachment and loss of stone material are the most common forms of deterioration patterns on the DCW. The delamination patterns are mostly associated with the stone facing. Since flow directions were not considered when placing the basalt blocks on the masonry walls, they have mainly delaminated in their flow directions.

Not all basalts are equally susceptible to flow layering, however, a special attention should be paid during placing on the wall particularly for the vesicular basalts that present a distinct flow layer.

- V. Material losses caused by mechanical damage were observed in a variety of forms. To make the basalt appear to be ancient, various surface finishing treatments have been applied in recent efforts to restore the DCW. It should be kept in mind that, since they cause material loss, accumulate exogenic materials and become a nest for micro-organisms, some of the surface finishing methods, particularly those that increase the roughness and irregularities of the basalt surfaces may activate degradation of the material. Therefore, stone finishes should not be used without assessing their chemical, physical and biological effects on the material.
- VI. The growth of higher plants is another common deterioration problem on the DCW. The plants grow mostly in cracks, open joints and where parts are missing. Since their roots penetrate the walls, they damage the material. Therefore, in order to prevent further growth, the open joints, cracks and missing parts should be sealed or repaired with proper materials and techniques compatible with the original stone and mortar
- VII. Based on the visual observations investigated at the study area, it can be stated that such deterioration forms as crack, detachment, and discoloration and deposit have developed almost equally on the massive and vesicular basalts. It is observed that material loss is more common on the massive basalts. Finally, it is visually examined that, development of the biological colonization on the vesicular basalts is slightly higher than the massive basalts.

VIII. In order to study the physical deterioration of the massive and vesicular basalts and to determine their durability, environmental conditions were artificially simulated in accelerated weathering tests such as the wetting-drying, freezing-thawing and salt crystallization. The variations in the index and mechanical parameters were determined for each of these tests. It is found that, except for unit weight, all the other physico-mechanical properties are useful for assessing the deterioration of the massive and vesicular basalts. Nevertheless, since UCS and sonic velocity give a better indication of the internal damage to the rock material, future studies of basalt should use these parameters. Of the accelerated weathering tests, salt crystallization affects the basalt most aggressively. Freezing and thawing has the next most effect, and wetting and drying has the least. Since the resistance of the basalts, especially to salt attack or crystallization pressure, is low, the use of any material that contains soluble salts should be avoided during restoration.

IX. To evaluate the depth of chemical weathering, samples were collected from a basalt block with spheroidal weathering. The results suggest that LoI is a good quantitative indicator of the basalts' chemical weathering depth. The analyses also found that, although chemical weathering affects the deterioration of the basalts, most of the weathering processes are controlled by the physical weathering. Here, it is important to remind that, due to the ongoing emergency conditions in the study area (e.g., conflict, and post-conflict situations) it is difficult to investigate and to sample the whole sections of the DCW. Therefore, due to the mentioned limitations of the site, a detailed and systematic sampling especially, for the chemical analyses and depth of weathering could not have been investigated.

- X. Durability assessment of the basalts reveals that both massive and vesicular basalts are durable and can be used as a construction material, especially for the restoration of the DCW. However, it should be noted that the massive samples appear to be more durable than the vesicular ones.
- XI. Considering the laboratory performance and field observations, average pore diameter, saturation coefficient and wet-to-dry strength ratio are useful parameters to assess the durability of the basalts.
- XII. The deterioration mechanism of the limestone, which is frequently used for decorative purposes; especially on the façades of some structures to produce an aesthetic contrast with the basalt, was beyond the scope of this study. Further studies must concentrate on the provenance and deterioration of the limestone. Additional studies may include:
- i. documentation of the past interventions,
 - ii. mapping of the materials and decay forms for whole sections of the DCW,
 - iii. effects of surface finishing on the material properties of the basalt,
 - iv. petrographic and physico-mechanical properties of the masonry mortars,
 - v. selection of the proper material and technique for sealing and repairing the cracks, open joints and missing parts,
 - vi. effects of pollution and vibration, mostly caused by dense traffic flow, on the structural instability and deterioration.

REFERENCES

- AFNOR (L'Association Francaise De Normalisation). (1980). Essai au Bleu de Methylene (pp. 18–592). AFNOR 80181, Paris La Defence.
- Aggitalis, G., Alivizatos, A., Stamoulis, D., and Stournaras, G. (1996). Correlating Uniaxial Compressive Strength with Schmidt Hardness, Point Load Index, Young's Modulus, and Mineralogy of Gabbros and Basalts (Northern Greece). *Bulletin of the International Association of Engineering Geology*, 54(1), 3–11.
- Aghamiri, R. R., and Schwartzman, D. W. (2002). Weathering Rates of Bedrock by Lichens: A Mini Watershed Study. *Chemical Geology*, 188(3), 249–259.
- Ahunbay, M. (2012). Early Phase of City Walls of Diyarbakir. In *Proceedings of the International Diyarbakir City Walls Symposium* (pp. 75–88). Diyarbakir: Diyarbakir Valiliği, Kültür Sanat Yayınları. (In Turkish with English abstract).
- Al-Harhi, A. A., Al-Amri, R. M., and Shehata, W. M. (1999). The Porosity and Engineering Properties of Vesicular Basalt in Saudi Arabia. *Engineering Geology*, 54(3), 313–320.
- Anon. (1979). Classification of Rocks and Soils for Engineering Geological Mapping, Part 1: Rock and Soil Materials. *Bulletin International Association of Engineering Geology*, 19, 364–371.
- Aomine, S., and Wada, K. (1962). Differential Weathering of Volcanic Ash and Pumice, Resulting in Formation of Hydrated Halloysite. *American Mineralogist*, 47, 1024–1048.
- Arger, J., Mitchell, J., and Westaway, R. W. (2000). Neogene and Quaternary Volcanism of Southeastern Turkey. *Geological Society, London, Special Publications*, 173(1), 459–487.
- Assenat, M. (2012). Diyarbakir City Walls: A Proposal Chronology. In *International Symposium of the City Walls of Diyarbakir* (pp. 53–65). Diyarbakir: Diyarbakir Valiliği, Kültür Sanat Yayınları.

- ASTM. (2013a). ASTM C88-13 Standard Test Method for Soundness of Aggregates by Use of Sodium Sulfate or Magnesium Sulfate. In *ASTM Standards, Volume 04.02*. West Conshohocken, PA: ASTM International.
- ASTM. (2013b). ASTM D7348-13 Standard Test Methods for Loss on Ignition (LoI) of Solid Combustion Residues. In *ASTM Standards, Volume 05.06*. West Conshohocken, PA.
- ASTM. (2017a). D5121–15 Standard Practice for Preparation of Rock Slabs for Durability Testing. In *ASTM Standards, Volume 04.08*. West Conshohocken, PA: ASTM International.
- ASTM. (2017b). D5240/D5240M-12(2013) Standard Test Method for Evaluation of Durability of Rock for Erosion Control Using Sodium Sulfate or Magnesium Sulfate. In *ASTM Standards, Volume 04.08*. West Conshohocken, PA: ASTM International.
- ASTM. (2017c). D5312/D5312M-12(2013) Standard Test Method for Evaluation of Durability of Rock for Erosion Control Under Freezing and Thawing Conditions. In *ASTM Standards, Volume 04.08*. West Conshohocken, PA: ASTM International.
- ASTM. (2017d). D5313/D5313M-12(2013) Standard Test Method for Evaluation of Durability of Rock for Erosion Control Under Wetting and Drying Conditions. In *ASTM Standards, Volume 04.08*. West Conshohocken, PA: ASTM International.
- Aşılı, A. (2010). Surlar, Diyarbakır. Retrieved April 3, 2017, from <https://goo.gl/RzHLUR>
- Atzeni, C., Pia, G., Sanna, U., and Spanu, N. (2008). A Fuzzy Model for Classifying Mechanical Properties of Vesicular Basalt Used in Prehistoric Buildings. *Ials Characterization*, 59(5), 606–612.
- Bağırşakçı, S., Akçay, A.E., Manav, E., Polat, C., Ay, Y., Kum, M., Akbulut, İ. and Özgür, İ.B. (1995). *Diyarbakır-Ergani ve Çınar Alanın Jeolojisi*. Ankara. (In Turkish).
- Balboni, E., Espinosa-Marzal, M., R., Doehne, E., and Scherer, G. W. (2011). Can Drying and Re-Wetting of Magnesium Sulfate Salts Lead to Damage of Stone? *Environmental Earth Sciences*, 63(7–8), 1463–1473.
- Baltali, S. H. (2007). *Architecture, Ritual Expression and Social Differentiation in Fourth Millennium North Mesopotamia*. University of Virginia. Unpublished Ph.D. Thesis.

- Banfield, J. F., Jones, B. F., and Veblen, D. R. (1991). An AEM-TEM Study of Weathering and Diagenesis, Abert Lake, Oregon: I. Weathering Reactions in the Volcanics. *Geochimica et Cosmochimica Acta*, 55(10), 2781–2793.
- Basham, I. R. (1974). Mineralogical changes associated with deep weathering of gabbro in Aberdeenshire. *Clay Minerals*, 10(3), 189–202.
- Bell, F. G. (1980). *Engineering Geology and Geotechnics. Engineering Geology and Geotechnics*.
- Bell, F. G. (1992). *Engineering Properties of Soils and Rocks* (3rd ed.). London: Butterworth-Heinemann.
- Bell, F. G. (1993). Durability of Carbonate Rock as Building Stone with Comments on Its Preservation. *Environmental Geology*, 21(4), 187–200.
- Bell, F. G. (2007). *Engineering Geology* (2nd ed.). Elsevier Ltd.
- Bell, F. G., and Coulthard, J. M. (1988). Stone Preservation with Illustrative Examples from the United Kingdom. In *The Engineering Geology of Ancient Works, Monuments and Historical Sites: Preservation and Protection* (Vol. 2, pp. 883–889). Athens: Greek National Group of IAEG.
- Bell, F. G., and Haskins, D. R. (1997). A Geotechnical Overview of Katse Dam and Transfer Tunnel, Lesotho, with A Note on Basalt Durability. *Engineering Geology*, 46(2), 175–198.
- Bell, F. G., Haskins, D. R., and Jermy, C. A. (2000). Basalt Durability and the Transfer Tunnel: Lesotho Highlands Water Project. In *ISRM International Symposium. International Society for Rock Mechanics*.
- Bell, G. (1924). *Amurath to Amurath*. (2nd ed.). Macmillan & Co Ltd.
- Bennett, P. C., Rogers, J. R., Choi, W. J., and Hiebert, F. K. (2001). Silicates, Silicate Weathering, and Microbial Ecology. *Geomicrobiology Journal*, 18(1), 3–19.
- Berchem, M., and Strzygowski, J. (1910). *Amida*. Heidelberg.
- Beysanoğlu, Ş. (2003). *Anıtları ve Kitabeleri ile Diyarbakır Tarihi*. Ankara: Neyir Matbaası. (In Turkish).
- Bilen, C. A., Erisis, S., Er, S., Yilmaz, M., Angi, S., and Tugrul, A. (2016). Deterioration Types of Stones Used in Suleymaniye Mosque (Istanbul, Turkey). In *IOP Conference Series: Earth and Environmental Science*.

- Blair, S. S. (2000). Decoration of city walls in the medieval Islamic world: The epigraphic message. In *City Walls: The Urban Enceinte in Global Perspective* (pp. 488–529).
- Borchardt, G. A., and Harward, M. E. (1971). Trace Element Correlation of Volcanic Ash Soils. *Soil Science Society of America Journal*, 35(4), 626–631.
- Borchardt, G. A., Harward, M. E., and Knox, E. G. (1971). Trace Element Concentration in Amorphous Clays of Volcanic Ash Soils in Oregon. *Clays and Clay Mineralogy*, 19, 375–382.
- Brace, W. F., Silver, E., Hadley, K., and Goetze, C. (1972). Cracks and Pores: A Closer Look. *Science*, 178, 162–164.
- Braidwood, L., and Braidwood, R. J. (1982). *Prehistoric Village Archaeology in Southeastern Turkey: The eighth millennium B.C. site at Çayönü*. British Archaeological Reports.
- Breasted, J. H. (1916). *Ancient Times: A History of the Early World*. Ginn and Company.
- Bridgland, D. R., Demir, T., Seyrek, A., Pringle, M., Westaway, R., Beck, A. R., Rowbotham, G., Yurtmen, S. (2007). Dating Quaternary Volcanism and Incision by the River Tigris at Diyarbakır, Southeast Turkey. *Journal of Quaternary Science*, 22(4), 387–393.
- Bristow, I. (1990). An Introduction to the Restoration, Conservation and Repair of Stone. In *Conservation of Building and Decorative Stone* (pp. 1–18).
- Bruinessen, M. V., and Boeschoten, H. (1988). *Evliya Çelebi in Diyarbakir: The relevant section of the Seyahatname Vol.1*. Brill Academic Publications.
- BSI. (2015). *Code of Practice for Ground Investigations*. British Standard Institution (BS 5930:2015), London, 328 p.
- Caner, E. N., and Türkmenoğlu, A. G. (1985). Deterioration of Basalts from a Hittite Archaeological Site, Karatepe, Turkey. In *Proceedings of the Vth International Congress on Deterioration and Conservation of Stone* (pp. 411–420). Lausanne: Presses Polytechniques Romandes.
- Carneiro, F. (1943). A New Method to Determine the Tensile Strength of Concrete. In *5th Meeting of the Brazilian Association for Technical Rules*.
- Carroll, D. (1970). *Clay Minerals: A Guide to Their X-ray Identification*. Colorado, USA: Geological Society of America, Special Publication No:126.

- Carroll, D. (2012). *Rock Weathering* (2nd ed.). Springer.
- Cawsey, D. C., and Mellon, P. (1983). A Review of Experimental Weathering of Basic Igneous Rocks. *Geological Society, London, Special Publications*, 11(1), 19–24.
- Chacon, M. A. (1999). *Architectural Stone: Fabrication, Installation, and Selection*. John Wiley and Sons.
- Charola, A. E. (2004). Stone Deterioration in Historic Buildings and Monuments. In *Proceedings of the 10th International Congress on Deterioration and Conservation of Stone*. Sweden: ICOMOS.
- Chen, J., Blume, H. P., and Beyer, L. (2000). Weathering of Rocks Induced by Lichen Colonization-A Review. *Catena*, 39(2), 121–146.
- Chesworth, W., Dejoux, J., and Larroque, P. (1981). The Weathering of Basalt and Relative Mobilities of the Major Elements at Belbex, France. *Geochimica et Cosmochimica Acta*, 45(7), 1235–1243.
- Colman, S. M. (1982). *Chemical Weathering of Basalts and Andesites*. U.S. Geological Survey, Professional Paper, 1246.
- Craig, D. C., and Loughnan, F. C. (1964). Chemical and Mineralogical Transformations Accompanying the Weathering of Basic Volcanic Rocks from New South Wales. *Soil Research*, 2(2), 218–234.
- Curl, J. S. (2003). *Oxford Dictionary of Architecture*. Oxford University Press.
- Dalkılıç, N., and Nabikoğlu, A. (2012). The Architectural Features of the Diyarbakır City Walls: A Report on Current Status and Issues of Conservation. *Mediterranean Archaeology and Archaeometry*, 12(2), 171–182.
- Dearman, W. R., Baynes, F. J., and Irfan, T. Y. (1978). Engineering Grading of Weathered Granite. *Engineering Geology*, 12, 345–374.
- Dearman, W. R., Turk, N., Irfan, Y., and Rowshanei, H. (1987). Detection of Rock Material Variation by Sonic Velocity Zoning. *Bulletin of Engineering Geology and the Environment*, 35(1), 3–8.
- DeLan, T., and QiaoLin, X. (2014). Mechanical Properties Research Base on Porous Basalt. *Electronic Journal of Geotechnical Engineering*, 19, 8295–8304.
- Dietler, M., and Herbich, I. (1998). Habitus, Techniques, Style: An Integrated Approach to the Social Understanding of Material Culture and Boundaries. *The Archaeology of Social Boundaries*, 232–263.

- Dinçer, I., Acar, A., Çobanoğlu, I., and Uras, Y. (2004). Correlation Between Schmidt Hardness, Uniaxial Compressive Strength and Young's Modulus for Andesites, Basalts and Tuffs. *Bulletin of Engineering Geology and the Environment*, 63(2), 141–148.
- DMM. (2014). *Nomination Dossier of the Diyarbakır Fortress and Hevsel Gardens Cultural Landscape for Inscription on the World Heritage List*. Diyarbakır Metropolitan Municipality, Diyarbakır.
- Doehne, E. (2002). Salt Weathering: A Selective Review. In *Natural Stone, Weathering Phenomena, Conservation Strategies and Case Studies* (Vol. 205, pp. 51–64). Geological Society of London, Special Publications.
- Dreesen, R., and Duser, M. (2004). Historical Building Stones in The Province of Limburg (NE Belgium): Role of Petrography in Provenance and Durability Assessment. *Materials Characterization*, 53(2), 273–287.
- Dumper, M., and Bruce, E. S. (Eds.). (2007). *Cities of the Middle East and North Africa: A Historical Encyclopedia*. ABC-CLIO.
- Duran, O., Şemşir, D., Sezgin, İ., and Perinçek, D. (1988). Güneydoğu Anadolu'da Midyat ve Silvan Gruplarının Stratigrafisi, Sedimentolojisi ve Petrol Potansiyeli. *TPJD Bülteni*, 1(2), 99–126. (In Turkish).
- Dursun, F. (2008). *Diyarbakır Kent Merkezindeki Zeminlerin Jeolojik ve Mühendislik Özelliklerinin İncelenmesi*. Dicle Üniversitesi, Unpublished M.Sc. Thesis (In Turkish with English abstract).
- Eggleton, R. A., Foudoulis, C., and Varkevisser, D. (1987). Weathering of Basalt; Changes in Rock Chemistry and Mineralogy. *Clays and Clay Minerals*, 35, 161–169.
- El-Gohary, M. A., and Al-Shorman, A. A. (2010). The Impact of the Climatic Conditions on the Decaying of Jordanian Basalt at Umm Qeis: Exfoliation as a Major Deterioration Symptom. *Mediterranean Archaeology and Archaeometry*, 10(1), 143–158.
- Ema, N. P., Buergo, M. A., and Bustamante, R. (2013). Effects of Conservation Interventions on the Archaeological Roman Site of Merida (Spain). Advance of Research. *Procedia Chemistry*, 8, 269–278.
- Endait, M., and Juneja, A. (2015). New Correlations Between Uniaxial Compressive Strength and Point Load Strength of Basalt. *International Journal of Geotechnical Engineering*, 9(4), 348–353.

- Engidasew, T. A., and Barbieri, G. (2014). Geo-engineering Evaluation of Termaber Basalt Rock Mass for Crushed Stone Aggregate and Building Stone from Central Ethiopia. *Journal of African Earth Sciences*, 99, 581–594.
- Ercan, T., Fujitani, T., Madsuda, J. I., Notsu, K., Tokel, S., and Uİ, T. (1990). Doğu ve Güneydoğu Anadolu Neojen-Kuvaterner Volkanitlerine İlişkin Yeni Jeokjmyasal, Radyometrik ve İzotopik Verilerin Yorumu. *Maden Tetkik ve Arama Dergisi*, 110, 143–164. (In Turkish with English abstract)
- Ercan, T., Şaroğlu, F., Turhan, N., Matsuda, J.I., Ui, T., Fujitani, T., Notsu, K., Bağırakçı, S., Aktimur, S., Can, B., Emre, Ö., Akçay, A.E., Manav, E., and Gürler, H. (1991). The Geology and Petrology of Karcadağ Volcanites. *Bulletin of Geological Congress of Turkey*, 6, 118–133.
- Etienne, S., and Dupont, J. (2002). Fungal Weathering of Basaltic Rocks in a Cold Oceanic Environment (Iceland): Comparison Between Experimental and Field Observations. *Earth Surface Processes and Landforms*, 27(7), 737–748.
- Fitzner, B. (1993). Porosity Properties and Weathering Behaviour of Natural Stones- methodology and Examples. In *2nd Course on the Stone Material in Monuments: Diagnosis and Conservation* (pp. 43–54). C.U.M. University School of Monument Conservation, Greece.
- Fitzner, B. (2004). Documentation and Evaluation of Stone Damage on Monuments. In *10th International Congress on Deterioration and Conservation of Stone* (pp. 677–690).
- Fitzner, B., and Heinrichs, K. (2001). Damage Diagnosis on Stone Monuments – Weathering Forms, Damage Categories and Damage Indices. *Acta-Universitatis Carolinae Geologica*, 1, 12–13.
- Fitzner, B., Heinrichs, K., and Kownatzki, R. (1992). Classification and Mapping of Weathering Forms. In *7th International Congress on Deterioration and Conservation of Stone* (pp. 957–968). Lisbon, Portugal.
- Fitzner, B., Heinrichs, K., and Kownatzki, R. (1995). Weathering forms-classification and mapping. In *Denkmalpflege und Naturwissenschaft, Natursteinkonservierung* (pp. 41–88). Berlin: Ernst and Sohn.
- Fitzner, B., Heinrichs, K., and Kownatzki, R. (1997). Weathering Forms at Natural Stone Monuments-Classification, Mapping and Evaluation. *International Journal for Restoration of Buildings and Monuments*, 3, 105–124.

- Fitzner, B., Heinrichs, K., La Bouchardiere, D., Bouchardiere, D. La, Galan, E., and Zezza, F. P. O. (2002). Damage Index for Stone Monuments. In *Proceedings of the 5th International Symposium on the Conservation of Monuments in the Mediterranean Basin* (pp. 315–326). Sevilla, Spain.
- Fitzner, B., and Kalde, M. (1991). Simulation of Frost-thaw Cycle and Salt Weathering: Nature Adapted Material Tests. In *International Symposium on The deterioration of Building Materials* (pp. 103–114). La Rochelle, France.
- Fookes, P. G., Gourley, C. S., and Ohikere, C. (1988). Rock Weathering in Engineering Time. *Quarterly Journal of Engineering Geology and Hydrogeology*, 21(1), 33–57.
- Fort, R., de Buergo, M. A., Perez-Monserrat, E. M., Gomez-Heras, M., Varas-Muriel, M. J., and Freire, D. M. (2013). Evolution in the use of natural building stone in Madrid, Spain. *Quarterly Journal of Engineering Geology and Hydrogeology*, 46(4), 421–429.
- Gabriel, A. (1933). Mardin ve Diyarbakir Vilâyetlerinde İcra Olunmuş Bir Arkeologya Seyahati Hakkında Rapor. *Türk Tarih, Arkeologya ve Etnografya Dergisi*, 1, 135–137. (In Turkish).
- Gabriel, A. (1940). *Voyages archéologiques dans la Turquie orientale*. Paris.
- Gabriel, A. (1993). *Diyarbakır Surları*. (K. Özsezgin, Ed.). Ankara: Diyarbakır Tanıtma, Kültür ve Yardımlaşma Vakfı Yayını. (In Turkish).
- Gabriel, A. (2014). *Şarki Türkiye’de Arkeolojik Geziler*. Dipnot Yayınları. (In Turkish).
- Galán, E., and Aparicio, P. (2009). An Approach to the Diagnostic Studies of Stone Degradation. *Letture Di Georisorse*, 2, 94–104.
- Garden, R. J. (1867). Description of Diarbekr. *Journal of the Royal Geographical Society of London*, 182–193.
- Gay, P., and LeMaitre, R. W. (1961). Some Observations on “iddingsite.” *The American Mineralogist*, 46, 92–111.
- Gierlichs, J. (2009). A victory monument in the name of Sultan Malik-Shah in Diyarbakır: Medieval figural reliefs used for political propaganda? *Islamic Art*, 6, 51–79.
- Glasmann, J. R., and Simonson, G. H. (1985). Alteration of Basalt in Soils of Western Oregon. *Soil Science Society of America Journal*, 49(1), 262–273.

- Goldich, S. S. (1938). A study in Rock-Weathering. *The Journal of Geology*, 46, 17–58.
- Gomes, R. L., and Rodrigues, J. E. (2007). Quality Ranking of Twelve Columnar Basalt Occurrences in the Northern Portion of the Paraná Basin—Brazil. *Engineering Geology*, 91(2), 265–278.
- González De Vallejo, L. I. Hijazo Ramiro, T., and Ferrer Gijón, M. (2008). Engineering Geological Properties of the Volcanic Rocks and Soils of the Canary Islands. *Soils and Rocks*, 31(1), 3–13.
- Gordon, S. J., and Dorn, R. I. (2005). Localized Weathering: Implications for Theoretical and Applied Studies. *The Professional Geographer*, 57(1), 28–43.
- Goudie, A., Cooke, R., and Evans, I. (1970). Experimental Investigation of Rock Weathering by Salt. *Area*, 2(4), 42–48.
- Government Gazette. (1937), 18.12.1937(3786). (In Turkish).
- Governorship of Diyarbakır. (2017). Surlar, Diyarbakır Valiliği Kültür Turizm Proje Birimi. Retrieved April 4, 2017, from <https://goo.gl/BeU3Vg>
- Graue, B., Siegesmund, S., and Middendorf, B. (2011). Quality Assessment of Replacement Stones for the Cologne Cathedral: Mineralogical and Petrophysical Requirements. *Environmental Earth Sciences*, 63(7–8), 1799–1822.
- Grimmer, A. E. (1984). *A Glossary of Historic Masonry Deterioration Problems and Preservation Treatments*. Washington: Department of the Interior National Park Service Preservation Assistance Division.
- Grissom, C. A. (1994). The Deterioration and Treatment of Volcanic Stone: A Review of the Literature. In *Lavas and Volcanic Tuffs: Proceedings of the International Meeting* (pp. 3–33). Easter Island, Chile: International Centre for the Study of the Preservation and the Restoration of Cultural Property.
- Güçhan, N. Ş., Ünay, A. İ., Böke, H., and Gökçe, F. (2005). Conservation Problems of Diyarbakır City Walls. *Metu Journal of the Faculty of Architecture*, 22(1), 27–55. (In Turkish with extended abstract in English).
- Gürocak, Z., and Kılıç, R. (2005). Effect of Weathering on the Geomechanical Properties of the Miocene Basalts in Malatya, Eastern Turkey. *Bulletin of Engineering Geology and the Environment*, 64(4), 373–381.
- Haksal, A. (1981). *Petrographie und Geochemie des Schildvulkans Karacadağ*. Hamburg University. Unpublished Ph.D. Thesis.

- Halifeoğlu, F. M. (2012). The Architectural Properties and Construction Technique of Diyarbakır City Walls. In *International Symposium of the City Walls of Diyarbakır* (pp. 115–129). Diyarbakır: Diyarbakır Valiliği, Kültür Sanat Yayınları. (In Turkish with English abstract).
- Hasançebi, N. (2016). Effect of Porosity on Uniaxial Compressive Strength of Basaltic Rock from Diyarbakır, Turkey. In *Rock Mechanics and Rock Engineering: From the Past to the Future* (pp. 337–340). CRC Press.
- Helmi, F. M. (1994). Study of the Deterioration of Volcanic Rocks from Egypt. In *Lavas and volcanic tuffs :proceedings of the international meeting, Easter Island, Chile, 25-31 October 1990* (pp. 53–61). ICCROM.
- Hendry, A. W., and Khalaf, F. M. (2001). *Masonry Wall Construction*. CRC Press.
- Hirschwald, J. (1908). *Die Prüfung der natürlichen Bausteine auf ihre Wetterbeständigkeit*. Berlin: Verlag von Wilhelm Ernst and Sohn.
- Hogg, I. V. (1975). *Fortress: A History of Military Defence*. St. Martin's Press.
- Honeyborne, D. B. (1998a). Weathering and Decay of Masonry. In *Conservation of Building and Decorative Stone* (pp. 153–184). Routledge.
- Honeyborne, D. B. (1998b). Weathering and Decay of Masonry in Conservation of Building and Decorative Stone. In *Conservation of Building and Decorative Stone* (2nd ed., pp. 153–178). Butterworth-Heinemann.
- Humphris, S. E., and Thompson, G. (1978). Hydrothermal Alteration of Oceanic Basalts by Seawater. *Geochimica et Cosmochimica Acta*, 42(1), 107–125.
- Hüsrev, N. (1950). *Sefername*. İstanbul: Milli Eğitim Basımevi. (In Turkish).
- ICOMOS. (2015). *A Bibliography on Stone Heritage*. International Council on Monuments and Sites, Documentation Centre.
- ICOMOS-ISCS. (2008). *Illustrated Glossary on Stone Deterioration Patterns*. (V. Verges-Belmin, Ed.). Paris: ICOMOS (International Council on Monuments and Sites) and ISCS (International Scientific Committee for Stone).
- Irfan, T. Y., and Dearman, W. R. (1978). The Engineering Petrography of a Weathered Granite in Cornwall, England. *Engineering Geology and Hydrogeology*, 11(3), 233–244.

- Ismail, B. (2004). Environmental Deterioration and Conservation of Monumental Basalt, Egypt. *Assiut University Bulletin for Environmental Researches*, 7(1), 153–171.
- ISRM. (1981). *Rock Characterization, Testing and Monitoring, International Society for Rock Mechanics Suggested Methods*. Oxford: Pergamon Press, 211 p.
- İçerler, A. (1981). *Diyarbakır-Karacadağ-Viransehir Petrol Aramaları Jeoelektrik Etüdü*. Ankara. (In Turkish).
- İmamoğlu, M. Ş. (1993). *Gölbasi (Adıyaman)- Pazarcık-Narlı (K.Maras) Arasındaki Sahada Doğu Anadolu Fayının Neotektonik İncelemesi*. Ankara Üniversitesi Unpublished Ph.D. Thesis (In Turkish with English abstract).
- İmamoğlu, M. Ş., and Çetin, E. (2007). Güneydoğu Anadolu Bölgesi ve Yakın Yöresinin Depremselliği. *Dicle Üniversitesi Ziya Gökalp Eğitim Fakültesi Dergisi*, 9, 93–103, (In Turkish with English abstract).
- İmamoğlu, M. Ş., Kavak, O., and Kaya, M. (2014). Diyarbakır İli Ergani İlçesi ve Çevresinin Jeolojik Özellikleri. In *Tüm Yönleriyle Ergani İlçesi, ve Turizm* (pp. 258–33), (In Turkish with English abstract).
- Jackson, M. L. (1979). *Soil Chemical Analysis-advanced Course* (2nd ed.). Madison, Wisconsin, USA.
- Jackson, T. A., and Keller, W. D. (1970). A Comparative Study of the Role of Lichens and “Inorganic” Processes in the Chemical Weathering of Recent Hawaiian Lava Flows. *American Journal of Science*, 269(5), 446–466.
- Jamshidi, A., Nikudel, M. R., and Khamehchiyan, M. (2013). Predicting the Long-Term Durability of Building Stones Against Freeze–Thaw Using a Decay Function Model. *Cold Regions Science and Technology*, 92, 29–36.
- Jones, D., Wilson, M. J., and Tait, J. M. (1980). Weathering of a Basalt by *Pertusaria Corallina*. *The Lichenologist*, 12(3), 277–290.
- Jongerden, J., and Verheij, J. (2012). *Social Relations in Ottoman Diyarbekir, 1870–1915*. Brill.
- Juling, H., Kirchner, D., Brüggerhoff, S., Linnow, K., Steiger, M., El Jarad, A., and Gülker, G. (2004). Salt Damage of Porous Materials: A Combined Theoretical and Experimental Approach. In *10th International Congress on Deterioration and Conservation of Stone* (pp. 187–194).

- Justo, J. L., Justo, E., Durand, P., and Azañón, J. M. (2006). The Foundation of a 40-storey Tower in Jointed Basalt. *International Journal of Rock Mechanics and Mining Sciences*, 43(2), 267–281.
- Karakuş, A., and Akatay, M. (2013). Determination of Basic Physical and Mechanical Properties of Basaltic Rocks from P-wave Velocity. *Nondestructive Testing and Evaluation*, 28(4), 342–353.
- Kaufmann, J. E., Kaufmann, H. W., and Jurga, R. M. (2004). *The Medieval Fortress: Castles, Forts, and Walled Cities of The Middle Ages*. Capo Press.
- Kelsall, P. C., Watters, R. J., and Franzone, J. G. (1986). Engineering Characterization of Fissured, Weathered Dolerite and Vesicular Basalt. In *The 27th US Symposium on Rock Mechanics (USRMS)* (pp. 77–84). American Rock Mechanics Association.
- Kılıç, A. M., Karakuş, A., and Keskin, M. Ö. (2003). Diyarbakir Yöresi Mermerlerinin Fiziko-Mekanik Özellikleri-Özgül Enerji İlişkisi. In *Türkiye IV. Mermer Sempozyumu (Mersem 2003) Bildiriler Kitabı* (pp. 159–171), (In Turkish with English abstract).
- Knöfel, D. K., Hoffman, D., and Snethlage, R. (1987). Physico-chemical Weathering Reactions as a Formulary for Time-lapsing Ageing Tests. *Materials and Structures*, 20, 127–145.
- Koçbay, A., and Kılıç, R. (2006). Engineering Geological Assessment of the Obruk Dam Site (Corum, Turkey). *Engineering Geology*, 87(3), 141–148.
- Korkanç, M., and Tuğrul, A. (2004). Evaluation of Selected Basalts from Niğde, Turkey, As Aource of Concrete Aggregate. *Engineering Geology*, 75(3), 291–307.
- Kranz, R. L. (1983). Microcracks in Rocks: A Review. *Tectonophysics*, 100, 449–480.
- Kuzucuoğlu, C., and Karadoğan, S. (2015). The Hevsel Gardens: Archives of Human Activities and of the Past and Present Evolution of the River Tigris at Diyarbakır. In M. Assénat (Ed.), *L'Hevsel à Amida-Diyarbakır: Études et Réhabilitation de Jardins Mésopotamiens*. İstanbul: Institut Français D'études Anatoliennes.
- Kühnel, R. A., Van der Gaast, S. J., Brych, J., Laan, G. J., and Kulnig, H. (1994). The Role of Clay Minerals in Durability of Rocks Observations on Basaltic Rocks. *Applied Clay Science*, 9(4), 225–237.

- La Iglesia, A., González, V., López-Acevedo, V., and Viedma, C. (1997). Salt Crystallization in Porous Construction Materials I Estimation of Crystallization Pressure. *Journal of Crystal Growth*, 117(1–2), 111–118.
- Larson, T. D., and Cady, P. D. (1969). *Identification of Frost-susceptible Particles in Concrete Aggregates. National Cooperative Research Program, Report 66.* Washington, D.C.: Highway Research Board.
- Le Bas, M. J., Le Maitre, R. W., Streckeisen, A., and Zanettin, B. (1986). A Chemical Classification of Volcanic Rocks Based on the Total Alkali-Silica Diagram. *Journal of Petrology*, 27(3), 745–750.
- Leyland, R. C., Verryn, S., and Momayez, M. (2015). Smectite Clay Identification and Quantification as an Indicator of Basic Igneous Rock Durability. *Bulletin of Engineering Geology and the Environment*, 74(3), 981–989.
- Li, D., and Wong, L. N. Y. (2013). The Brazilian Disc Test for Rock Mechanics Applications: Review and New Insights. *Rock Mechanics and Rock Engineering*, 46(2), 269–287.
- Loughnan, F. C. (1969). *Chemical Weathering of the Silicate Minerals.* New York: Elsevier.
- Lustrino, M., Keskin, M., Mattioli, M., Lebedev, V. A., Chugaev, A., Sharkov, E., and Kavak, O. (2010). Early Activity of the Largest Cenozoic Shield Volcano in the Circum-Mediterranean Area: Mt. Karacadağ, SE Turkey. *European Journal of Mineralogy*, 22(3), 343–362.
- Marcellinus, A. (1963). *The History.* (J. C. Rolfe, Ed.). Harvard University Press.
- Markides, C. F., Pазis, D. N., and Kourkoulis, S. K. (2011). Influence of Friction on the Stress Field of the Brazilian Tensile Test. *Rock Mechanics and Rock Engineering*, 44(1), 113–119.
- Meng, B. (1992). Moisture-transport-relevant Characterization of Pore Structure. In *7th International Congress on Deterioration and Conservation of Stone* (pp. 387–396). Portugal.
- MGM. (2017). Meteoroloji Genel Müdürlüğü. Retrieved March 27, 2016, from <https://goo.gl/51GYhD>
- Moore, D. M., and Reynolds, R. C. (1989). *X-ray Diffraction and the Identification and Analysis of Clay Minerals.* Oxford: Oxford University Press.

- Mustoe, G. E. (1982). The Origin of Honeycomb Weathering. *Ecological Society of America Bulletin*, 93(2), 108–115.
- Nabikođlu, A., and Dalkılıç, N. (2013). Diyarbakır Surlarının Günümüzdeki Durumuna Yeni Bir Bakış. *Restorasyon ve Konservasyon Çalışmaları Dergisi*, 15, 23–35, (In Turkish).
- Nesbitt, H. W., and Wilson, R. E. (1992). Recent Chemical Weathering of Basalts. *American Journal of Science*, 292(10), 740–777.
- Neuendorf, K. K. E., Mehl, J. P., and Jackson, J. A. (2005). *Glossary of Geology* (5th ed.). American Geological Institute.
- Nishiura, T., Ebisawa, T., Inoue, Y., Yamazaki, Y., Hamade, H., and Khayata, W. (1996). Conservation of a Newly Excavated Architectural Monument in Syria: Ain Dara Temple. *Studies in Conservation*, 41, 23–23.
- Notsu, K., Fujitani, T., Ui, T., Matsuda, J., and Ercan, T. (1995). Geochemical Features of Collision-related Volcanic Rocks in Central and Eastern Anatolia, Turkey. *Journal of Volcanology and Geothermal Research*, 64(3), 171–191.
- NUGBA. (2014). Newcastle University Gertrude Bell Archive. Retrieved December 16, 2016, from <https://goo.gl/rqP2wG>
- Odgers, D., and Henry, A. (2012). *English Heritage, Practical Building Conservation: Stone*. Ashgate Publishing, Ltd.
- Ollier, C. D. (1971). Causes of Spheroidal Weathering. *Earth-Science Reviews*, 7(3), 127–141.
- Osmançelebiođlu, R., Akbulut, İ., Abasıkeleş, G., Gürler, H., Üge, E., Karakaya, F., Keskin, M., and Şener, T. (2000). *Diyarbakır li (Merkez) Yerbilim Verilerinin Arazi Kullanımı Açısından Deđerlendirilmesi*. Ankara. (In Turkish).
- Özsan, A., and Akın, M. (2002). Engineering Geological Assessment of the Proposed Uruş Dam, Turkey. *Engineering Geology*, 66(3), 271–281.
- Parla, C. (2004). Osmanlı Öncesinde Diyarbakır: Kente Hakim Olanlar ve Bıraktıkları Fiziksel İzler. In *I. Uluslararası Ođuzlardan Osmalıya Diyarbakır Sempozyumu* (pp. 247–283). Diyarbakır. (In Turkish with English abstract).
- Parla, C. (2005). Diyarbakır Surlari ve Kent Tarihi. *Metu Journal of the Faculty of Architecture*, 22, 57–84, (In Turkish with English abstract).

- Parla, C. (2012). Revelations of Diyarbakır Walls. In *Proceedings of the International Diyarbakir City Walls Symposium* (pp. 21–51). Diyarbakir: Diyarbakır Valiliği, Kültür Sanat Yayınları. (In Turkish with English abstract).
- Pearce, J. A., Bender, J. F., De Long, S. E., Kidd, W. S. F., Low, P. J., Güner, Y., Saroğlu, F., Yılmaz, Y., Moorbatg, S., and Mitchell, J. G. (1990). Genesis of Collision Volcanism in Eastern Anatolia, Turkey. *Journal of Volcanology and Geothermal Research*, 44(1–2), 189–229.
- Perinçek, D., Günay, Y., and Kozlu, H. (1987). Doğu Anadolu Bölgesindeki Yanal Atımlı Faylar ile ilgili Yeni Gözlemler. In *Türkiye 7. Petrol Kongresi* (pp. 89–103), (In Turkish).
- Pollard, N. (2000). *Soldiers, Cities, and Civilians in Roman Syria*. University of Michigan Press.
- Pope, G. A., Meierding, T. C., and Paradise, T. (2002). Geomorphology's Role in the Study of Weathering of Cultural Stone. *Geomorphology*, 47, 211–225.
- Price, C. A. (1975). Testing Porous Building Stone. *Architects' Journal*, 162(33), 337–339.
- Price, C. A. (1987). The Evaluation of Stone Preservatives. In *Conservation of Historic Stone Buildings and Monuments* (pp. 329–340). Washington D.C.: National Research Council.
- Price, C. A., and Doehne, E. (2011). *Stone Conservation: An Overview of Current Research* (2nd ed.). Los Angeles: Getty Publications.
- Přikryl, R., Lokajíček, T., and Svobodová, J. Weishauptová, Z. (2003). Experimental Weathering of Marlstone from Přední Kopanina (Czech Republic): Historical Building Stone of Prague. *Building and Environment*, 38(9), 1163–1171.
- Rasmussen, C., Dahlgren, R. A., and Southard, R. J. (2010). Basalt Weathering and Pedogenesis Across an Environmental Gradient in the Southern Cascade Range, California, USA. *Geoderma*, 154(3), 473–485.
- RILEM. (1980). Recommended Tests to Measure the Deterioration of Stone and to Assess the Effectiveness of Treatment Methods: Commission 25-PEM. *Materials and Structures*, 13(75), 175–253.
- Robertson, E. C. (1987). Physical Properties of Building Stone. In *Conservation of Historic Stone Buildings and Monuments* (pp. 62–86). Washington D.C.: National Research Council.

- Rodriguez-Navarro, C. Doehne, E., and Sebastian, E. (1999). Origins of Honeycomb Weathering: The Role of Salts and Wind. *Geological Society of America Bulletin*, 111(8), 1250–1255.
- Rodriguez-Navarro, C., and Doehne, E. (1999). Salt Weathering: Influence of Evaporation Rate, Supersaturation and Crystallization Pattern. *Earth Surface Processes and Landforms*, 24(3), 191–209.
- Ross, K. D., and Butlin, R. N. (1989). *Durability Tests for Building Stone*. London: Building Research Establishment Report, 141.
- Rossi-Doria, P. R. (1985). Laboratory Tests on Artistic Stonework. *The Deterioration and Conservation of Stone, Studies and Documents on the Cultural Heritage*, 16, 235–242.
- Ruedrich, J., and Siegesmund, S. (2007). Salt and Ice Crystallisation in Porous Sandstones. *Environmental Geology*, 52(2), 225–249.
- Sanver, M. (1968). A Palaeomagnetic Study of Quaternary Volcanic Rocks from Turkey. *Phys. Earth Planet. Interiors*, 1, 403–421.
- Schaffer, R. J. (1972). *The Weathering of Natural Building Stones*. Department of Scientific and Industrial Research, Special Report No.18.
- Scheerer, S., Ortega-Morales, O., and Gaylarde, C. (2009). Microbial Deterioration of Stone Monuments-An Updated Overview. *Advances in Applied Microbiology*, 66, 97–139.
- Scherer, G. W. (2002). Factors Affecting Crystallization Pressure. In *International RILEM TC 186-ISA Workshop on Internal Sulfate Attack and Delayed Ettringite Formation* (pp. 139–154). Villars, Switzerland.
- Scherer, G. W. (2004). Stress from Crystallization of Salt. *Cement and Concrete Research*, 34(9), 1613–1624.
- Sear, F. (1998). *Roman Architecture*. Abingdon: Routledge.
- Sen, P. A., Temel, A., and Gourgau, A. (2004). Petrogenetic Modelling of Quaternary Post-Collisional Volcanism: A Case Study of Central and Eastern Anatolia. *Geological Magazine*, 141(1), 81–98.
- Sherwood, A. N. (2000). *Roman Architectural Influence in Provincia Asia: Augustus to Severus Alexander*. Princeton University. Unpublished Ph.D. Thesis.

- Siedel, H. (2010). Alveolar Weathering of Cretaceous Building Sandstones on Monuments in Saxony, Germany. *Geological Society, London, Special Publications*, 333(1), 11–23.
- Siedel, H. (2013). Magnesium Sulphate Salts on Monuments in Saxony (Germany): Regional Geological and Environmental Causes. *Environmental Earth Sciences*, 69(4), 1249–1261.
- Siedel, H., and Siegesmund. (2014). Characterization of Stone Deterioration on Buildings. In *Stone in Architecture* (pp. 349–414). Springer Berlin Heidelberg.
- Siegesmund, S., and Török, Á. (2011). Building Stones. In *Stone in Architecture* (pp. 11–95). Springer Berlin Heidelberg.
- Siegesmund, S., Weiss, T., and Vollbrecht, A. (2002). *Natural stone, weathering phenomena, conservation strategies and case studies. The Geological Society, London, Special Publications* (Vol. 205). Geological Society Special Publication.
- Sims, I. (1991). Quality and Durability of Stone for Construction. *Quarterly Journal of Engineering Geology and Hydrogeology*, 24(1), 67–73.
- Sleater, G. (1978). A Laboratory Test Program for Stone Preservations. In *International Symposium on the Deterioration and Protection of Stone Monuments* (p. 19). Paris.
- Smith, J. (1957). A Mineralogical Study of Weathering and Soil Formation from Olivine Basalt in Northern Ireland. *Journal of Soil Science*, 8(2), 225–239.
- Smith, K. L., Milnes, A. R., and Eggleton, R. A. (1987). Weathering of Basalt: Formation of Iddingsite. *Clays and Clay Minerals*, 35(6), 418–428.
- Smith, M. R. (1999). *Stone: Building Stone, Rock Fill and Armourstone in Construction. The Geological Society Engineering Geology Special Publication No: 16* (Smith, M.R). The Geological Society of London.
- Smith, W. W. (1962). Weathering of Some Scottish Basic Igneous Rocks with Reference to Soil Formation. *Journal of Soil Science*, 13(2), 202–215.
- Sourdel-Thomine, J. (1965). Diyar Bakr , Monuments. In *The Encyclopaedia of Islam* (pp. 346–347).
- Sowden, A. M. (1990). Inspection and Recording. In *The Maintenance of Brick and Stone Masonry Structures* (pp. 35–62). London: E and F.N Spon.

- Stanchits, S., Vinciguerra, S., and Dresen, G. (2006). Ultrasonic Velocities, Acoustic Emission Characteristics and Crack Damage of Basalt and Granite. *Pure and Applied Geophysics*, 163(5–6), 975–994.
- Steiger, M., Charola, A. E., and Sterflinger, K. (2011). Weathering and Deterioration. In *Stone in Architecture* (pp. 227–316). Springer Berlin Heidelberg.
- Steiger, M., Linnow, K., Juling, H., Gülker, G., Jarad, A. E., Brüggerhoff, S., and Kirchner, D. (2007). Hydration of MgSO₄.H₂O and Generation of Stress in Porous Materials. *Crystal Growth and Design*, 8(1), 336–343.
- Sumner, P. D., Hall, K. J., Van Rooy, J. L., and Meiklejohn, K. I. (2009). Rock Weathering on the Eastern Mountains of Southern Africa: Review and Insights from Case Studies. *Journal of African Earth Sciences*, 55(5), 236–244.
- Şaroğlu, F., and Emre, O. (1987). Karacadağ Volkanitlerinin Genel Özellikleri ve Güneydoğu Anadolu Otoktonundaki Yeri. In *Türkiye 7. Petrol Kongresi, Bildiriler Kitabı* (pp. 384–391). Turkish Association of Petroleum Geologists and Chamber of Turkish Petroleum Engineers.
- Tiller, K. G. (1958). The Geochemistry of Basaltic Materials and Australia Associated Soils of South-Eastern South Australia. *Journal of Soil Science*, 9(2), 225–241.
- Topal, T. (1996). The Use of Methylene Blue Adsorption Test to Assess the Clay Content of the Cappadocian Tuff. In *Proceedings of the Eight International Congress on the Deterioration and Conservation of Stone* (pp. 791–799). Berlin.
- Topal, T. (2002). Quantification of Weathering Depths in Slightly Weathered Tuffs. *Environmental Geology*, 42(6), 632–641.
- Topal, T., De Witte, E., and Dupas, M. (1998). Pore-size Distribution Characteristics and Durability of the Cappadocian Tuff. In *8th International Congress IAEG* (pp. 2931–2938). Vancouver.
- Topal, T., and Doyuran, V. (1998). Analyses of Deterioration of the Cappadocian Tuff, Turkey. *Environmental Geology*, 34(1), 5–20.
- Topal, T., and Sözmen, B. (2000). Freeze-Thaw Resistance of the Yazılıkaya Tuffs. In *9th International Congress on the Deterioration and Conservation of Stone* (pp. 275–281).
- Topal, T., and Sözmen, B. (2003). Deterioration Mechanisms of Tuffs in Midas Monument. *Engineering Geology*, 68(3–4), 201–223.

- Toprak, V. (2012). Geological and Morphological Characteristics of Diyarbakır City Walls. In *International Symposium of the City Walls of Diyarbakır* (pp. 139–147). Diyarbakır: Diyarbakır Valiliği, Kültür Sanat Yayınları. (In Turkish with English abstract)
- Torraca, G. (1982). Porous Building Materials-Materials Science for Architectural Conservation (2nd ed., p. 142). ICCROM.
- Török, Á., and Prikryl, R. (2010). Current Methods and Future Trends in Testing, Durability Analyses and Provenance Studies of Natural Stones Used in Historical Monuments. *Engineering Geology*, 115(3), 139–142.
- Trofimov, A. M., and Phillips, J. D. (1992). Theoretical and Methodological Premises of Geomorphological Forecasting. *Geomorphology*, 5(3–5), 203–211.
- TS 699. (1987). *Tabii Yapı Taşları Muayene Deney Metodları*. Türk Standartları Enstitüsü, Ankara, Turkey. (In Turkish)
- TSE. (1977). *TS2513 Doğal Yapı Taşları*. Türk Standartları Enstitüsü, Ankara, Turkey. (In Turkish).
- TSE. (1978). *Doğal Yapı Taşlarının Muayene ve Deney Metodları*. Türk Standartları Enstitüsü, Ankara, Turkey. (In Turkish).
- TSE. (2011). TS EN 12371: Determination of Frost Resistance. In *Natural Stone Test Methods*. (In Turkish).
- Tuğrul, A. (1995). *The Effects of Weathering on the Engineering Properties of Basalts in the Niksar Region*. İstanbul University, Unpublished Ph.D. Thesis (In Turkish with English abstract).
- Tuğrul, A. (2004). The Effect of Weathering on Pore Geometry and Compressive Strength of Selected Rock Types from Turkey. *Engineering Geology*, 75(3), 215–227.
- Tuğrul, A., and Gürpınar, O. (1997). A Proposed Weathering Classification for Basalts and Their Engineering Properties (Turkey). *Bulletin of Engineering Geology and the Environment*, 55(1), 139–149.
- Tuncer, O. C. (2012a). A Proposal for Diyarbakır Outer Fortress Walls. In *International Symposium of the City Walls of Diyarbakır* (pp. 213–241). Diyarbakır: Diyarbakır Valiliği, Kültür Sanat Yayınları. (In Turkish with English abstract)

- Tuncer, O. C. (2012b). *Diyarbakır Surları*. Diyarbakır Valiliği, Kültür Sanat Yayınları. (In Turkish).
- UNESCO. (2015). *Report of the Decisions Adopted by the World Heritage Committee at its 39th Session*. WHC-15/39.COM/19, Bonn.
- Ündül, Ö., and Tuğrul, A. (2012). The influence of weathering on the engineering properties of dunites. *Rock Mechanics and Rock Engineering*, 45(2), 225–239.
- Van Brakel, J., Modrý, S., and Svata, M. (1981). Mercury Porosimetry: State of the Art. *Powder Technology*, 29(1), 1–12.
- Vincente, M. A., Garcia-Talegon, J., Iñigo, A. C., Molina, E., and Rives, V. (1993). Weathering Mechanisms of Silicated Rocks in Continental Environments. In M. J. Thiel (Ed.), *Proceedings of the international RILEM/UNESCO congress, Conservation of stone and other materials*. (pp. 320–327). Paris.
- Vitruvius, P. (1960). *The Ten Books on Architecture*. (M. H. Morgan, Ed.). Dover Publications.
- Ward-Perkins, J. B. (1992). *Roman Imperial Architecture*. Yale University Press.
- Warke, P. A., Curran, J. M., Turkington, A. V., and Smith, B. J. (2003). Condition Assessment for Building Stone Conservation: A Staging System Approach. *Building and Environment*, 38(9), 1113–1123.
- Warke, P. A., McKinley, J., and Smith, B. J. (2006). Weathering of Building Stone: Approaches to Assessment. In *Fracture and Failure of Natural Building Stones Applications in the Restoration of Ancient Monuments* (pp. 313–327). Springer.
- Warscheid, T., and Braams, J. (2000). Biodeterioration of Stone: A Review. *International Biodeterioration and Biodegradation*, 46(4), 343–368.
- Washburn, E. W. (1921). Note on a Method of Determining the Distribution of Pore Sizes in a Porous Material. *Proceedings of the National Academy of Sciences*, 7, 115–116.
- Wedekind, W., Ruedrich, J., and Siegesmund, S. (2011). Natural Building Stones of Mexico-Tenochtitlán: Their Use, Weathering and Rock Properties at the Templo Mayor, Palace Heras Soto and the Metropolitan Cathedral. *Environmental Earth Sciences*, 63(7–8), 1787–1798.

- Weishauptová, Z., and Pfikryl, R. (2004). Porosimetric Studies in Rocks: Methods and Application for Weathered Building Stones. In *Dimension Stone. New Perspectives for a Traditional Building Material* (pp. 237–241). AA Balkema, Leiden.
- Westaway, R., Guillou, H., Seyrek, A., Demir, T., Bridgland, D., Scaillet, S., and Beck, A. (2009). Late Cenozoic Surface Uplift, Basaltic Volcanism, and Incision by the River Tigris Around Diyarbakır, SE Turkey. *International Journal of Earth Sciences*, 98(3), 601–625.
- Wilson, M. J. (2004). Weathering of the Primary Rock-forming Minerals: Processes, Products and Rates. *Clay Minerals*, 39(3), 233–266.
- Winkler, E. M. (1966). Important Agents of Weathering for Building and Monumental Stone. *Engineering Geology*, 1(5), 381–400.
- Winkler, E. M. (1986). A Durability Index for Stone. *Bulletin of the Association of Engineering Geologists*, 23, 344–347.
- Winkler, E. M. (1993). Discussion and Reply on “The Durability of Sandstone as a Building Stone, Especially in Urban Environments.” *Bulletin of the Association of Engineering Geologists*, 30, 99–101.
- Winkler, E. M. (1997). *Stone in Architecture: Properties, Durability*. New York: Springer-Verlag Berlin Heidelberg.
- Yaşar, E., and Erdoğan, Y. (2004). Estimation of Rock Physicomechanical Properties Using Hardness Methods. *Engineering Geology*, 71(3), 281–288.
- Yılmaz, E., and Duran, O. (1997). *Güneydoğu Anadolu Bölgesi Otokton ve Allohton Birimler Stratigrafisi Adlana Sözlüğü*. Ankara: TPAO Arastırma Merkezi Grubu Başkanlığı Eğitim Yayınları, No:31. (In Turkish).
- Yılmaz, Y. (1993). New Evidence and Model on the Evolution of the Southeast Anatolian Orogen. *Geological Society of America Bulletin*, 105(2), 251–271.
- Zalesskii, B. V. (1967). *Physical and Mechanical Properties of Rocks*. Academy of Sciences of the USSR. Institute of Geology of Ore Deposits, Petrography, Mineralogy and Geochemistry.
- Zehnder, K., and Arnold, A. (1989). Crystal Growth in Salt Efflorescence. *Journal of Crystal Growth*, 97(2), 513–521.

APPENDIX

A. LABORATORY TEST RESULTS OF THE FRESH BASALTS

Table A.1 Porosity and unit weight of the massive basalt samples

Sample No	M_{dry} (g.) (1)	M_{sat.} (g.) (2)	M_{sub.} (g.) (3)	V_v (cm ³) (2-1)	V (cm ³) (2-3)	Porosity (%) (n=V _v /V)	Dry Unit W. (kN/m ³)	Sat. Unit W. (kN/m ³)
1M-1	980.28	998.56	642.35	18.28	356.21	5.13	27.00	27.50
1M-2	1005.65	1022.39	661.30	16.74	361.09	4.64	27.32	27.78
1M-3	944.40	964.75	612.87	20.35	351.88	5.78	26.33	26.90
1M-4	918.44	943.48	596.50	25.04	346.98	7.22	25.97	26.67
1M-5	1000.79	1015.47	659.40	14.68	356.07	4.12	27.57	27.98
1M-6	916.90	942.67	596.10	25.77	346.57	7.44	25.95	26.68
1M-7	894.02	917.86	579.80	23.84	338.06	7.05	25.94	26.63
1M-8	933.18	952.70	603.90	19.52	348.80	5.60	26.25	26.79
1M-9	957.20	974.35	617.20	17.15	357.15	4.80	26.29	26.76
1M-10	1028.71	1042.51	675.07	13.80	367.44	3.76	27.46	27.83
1M-11	935.84	954.68	605.05	18.84	349.63	5.39	26.26	26.79
1M-12	933.96	954.53	605.35	20.57	349.18	5.89	26.24	26.82
1M-13	912.37	936.67	591.12	24.30	345.55	7.03	25.90	26.59
1M-14	912.52	935.09	590.10	22.57	344.99	6.54	25.95	26.59
1M-15	967.45	985.17	632.85	17.72	352.32	5.03	26.94	27.43
1M-16	978.22	993.77	636.15	15.55	357.62	4.35	26.83	27.26
1M-17	1000.04	1014.89	653.70	14.85	361.19	4.11	27.16	27.56
1M-18	911.28	928.88	585.90	17.60	342.98	5.13	26.06	26.57
1M-19	977.02	991.14	638.85	14.12	352.29	4.01	27.21	27.60
1M-20	960.28	977.81	625.35	17.53	352.46	4.97	26.73	27.22
1M-21	1000.87	1015.93	652.65	15.06	363.28	4.15	27.03	27.43
1M-22	989.56	1004.48	648.05	14.92	356.43	4.19	27.24	27.65

Table A.1 (continued)

Sample No	M _{dry} (g.) (1)	M _{sat.} (g.) (2)	M _{sub.} (g.) (3)	V _v (cm ³) (2-1)	V (cm ³) (2-3)	Porosity (%) (n=V _v /V)	Dry Unit W. (kN/m ³)	Sat. Unit W. (kN/m ³)
1M-23	985.39	1005.14	639.30	19.75	365.84	5.40	26.42	26.95
1M-24	992.71	1007.89	649.20	15.18	358.69	4.23	27.15	27.57
1M-25	620.45	637.65	402.95	17.20	234.70	7.33	25.93	26.65
1M-26	623.36	638.98	405.04	15.62	233.94	6.68	26.14	26.79
1M-27	679.88	695.56	449.98	15.68	245.58	6.38	27.16	27.79
1M-28	621.52	636.82	402.60	15.30	234.22	6.53	26.03	26.67
1M-29	691.01	706.27	456.40	15.26	249.87	6.11	27.13	27.73
1M-30	631.26	645.00	408.85	13.74	236.15	5.82	26.22	26.79
1M-31	669.63	683.32	442.85	13.69	240.47	5.69	27.32	27.88
1M-32	628.38	643.95	407.40	15.57	236.55	6.58	26.06	26.71
1M-33	619.45	635.05	402.05	15.60	233.00	6.70	26.08	26.74
1M-34	607.30	623.38	393.80	16.08	229.58	7.00	25.95	26.64
1M-35	966.70	983.13	633.55	16.43	349.58	4.70	27.13	27.59
1M-36	926.65	950.53	600.05	23.88	350.48	6.81	25.94	26.61
1M-37	919.85	941.35	595.12	21.50	346.23	6.21	26.06	26.67
1M-38	881.10	904.17	570.17	23.07	334.00	6.91	25.88	26.56
2M-1	1036.77	1053.72	695.16	16.95	358.56	4.73	28.37	28.83
2M-2	1006.06	1021.70	667.66	15.64	354.09	4.41	27.87	28.31
2M-3	1024.15	1041.54	684.91	17.39	356.63	4.88	28.17	28.65
2M-4	1039.30	1057.23	696.96	17.93	360.27	4.98	28.30	28.79
2M-5	976.20	994.31	647.27	18.11	347.04	5.22	27.59	28.11
2M-6	990.24	1008.15	663.31	17.91	344.84	5.19	28.17	28.68
2M-7	983.51	1001.23	653.51	17.72	347.72	5.10	27.75	28.25
2M-8	986.20	1005.74	657.66	19.54	348.08	5.61	27.79	28.34
2M-9	976.42	996.68	649.01	20.26	347.67	5.83	27.55	28.12
2M-10	990.10	1009.26	658.51	19.16	350.75	5.46	27.69	28.23
2M-11	1018.15	1036.17	679.68	18.02	356.49	5.05	28.02	28.51
2M-12	1012.50	1031.17	672.79	18.67	358.38	5.21	27.72	28.23
2M-13	972.04	990.67	645.06	18.63	345.61	5.39	27.59	28.12
2M-14	983.10	1002.32	654.76	19.22	347.56	5.53	27.75	28.29
2M-15	681.58	698.68	460.74	17.10	237.94	7.19	28.10	28.81
2M-16	656.37	675.73	441.21	19.36	234.52	8.26	27.46	28.27
2M-17	671.90	688.49	452.44	16.59	236.05	7.03	27.92	28.61
2M-18	665.37	682.61	449.94	17.24	232.67	7.41	28.05	28.78
2M-19	983.19	1002.16	656.06	18.97	346.10	5.48	27.87	28.41
2M-20	1016.90	1035.38	677.71	18.48	357.67	5.17	27.89	28.40
4M-1	1013.32	1030.90	678.50	17.58	352.40	4.99	28.21	28.70
4M-2	1035.50	1053.33	694.05	17.83	359.28	4.96	28.27	28.76

Table A.1 (continued)

Sample No	M _{dry} (g.) (1)	M _{sat.} (g.) (2)	M _{sub.} (g.) (3)	V _v (cm ³) (2-1)	V (cm ³) (2-3)	Porosity (%) (n=V _v /V)	Dry Unit W. (kN/m ³)	Sat. Unit W. (kN/m ³)
4M-3	982.25	998.69	656.96	16.44	341.73	4.81	28.20	28.67
4M-4	1042.27	1060.43	697.76	18.16	362.67	5.01	28.19	28.68
4M-5	977.79	996.55	652.10	18.76	344.45	5.45	27.85	28.38
4M-6	1031.74	1049.15	691.70	17.41	357.45	4.87	28.32	28.79
4M-7	1016.99	1034.46	681.06	17.47	353.40	4.94	28.23	28.72
4M-8	1021.96	1039.33	684.38	17.37	354.95	4.89	28.24	28.72
4M-9	1045.29	1063.52	698.93	18.23	364.59	5.00	28.13	28.62
4M-10	972.37	990.34	648.95	17.97	341.39	5.26	27.94	28.46
4M-11	1024.60	1042.24	686.10	17.64	356.14	4.95	28.22	28.71
4M-12	971.51	989.30	649.96	17.79	339.34	5.24	28.09	28.60
4M-13	708.05	724.74	480.18	16.69	244.56	6.82	28.40	29.07
4M-14	675.20	693.01	453.83	17.81	239.18	7.45	27.69	28.42
4M-15	630.63	647.12	426.08	16.49	221.04	7.46	27.99	28.72
4M-16	689.39	707.31	465.10	17.92	242.21	7.40	27.92	28.65
4M-17	730.07	747.03	493.76	16.96	253.27	6.70	28.28	28.93
4M-18	712.46	729.75	479.50	17.29	250.25	6.91	27.93	28.61
4M-19	702.06	719.72	475.48	17.66	244.24	7.23	28.20	28.91
4M-20	659.27	679.98	444.93	20.71	235.05	8.81	27.52	28.38
4M-21	691.37	707.59	465.60	16.22	241.99	6.70	28.03	28.68
4M-22	677.10	693.55	458.61	16.45	234.94	7.00	28.27	28.96
4M-23	697.14	714.85	470.46	17.71	244.39	7.25	27.98	28.69
4M-24	690.01	707.80	466.56	17.79	241.24	7.37	28.06	28.78
4M-25	645.80	662.49	436.61	16.69	225.88	7.39	28.05	28.77
4M-26	692.13	709.12	468.83	16.99	240.29	7.07	28.26	28.95
4M-27	669.91	688.27	452.83	18.36	235.44	7.80	27.91	28.68
4M-28	658.12	675.68	445.18	17.56	230.50	7.62	28.01	28.76
6M-1	968.65	988.28	636.47	19.63	351.81	5.58	27.01	27.56
6M-2	971.88	998.56	648.68	26.68	349.88	7.63	27.25	28.00
6M-3	978.57	1004.43	652.86	25.86	351.57	7.36	27.31	28.03
6M-4	969.95	995.14	647.03	25.19	348.11	7.24	27.33	28.04
6M-5	981.42	1007.51	654.78	26.09	352.73	7.40	27.29	28.02
6M-6	958.20	985.02	638.99	26.82	346.03	7.75	27.17	27.93
6M-7	979.47	1004.72	651.54	25.25	353.18	7.15	27.21	27.91
6M-8	967.27	993.15	644.67	25.88	348.48	7.43	27.23	27.96
6M-9	992.81	1018.79	662.03	25.98	356.76	7.28	27.30	28.01
6M-10	964.61	991.21	641.23	26.60	349.98	7.60	27.04	27.78

Table A.1 (continued)

Sample No	M_{dry} (g.) (1)	M_{sat.} (g.) (2)	M_{sub.} (g.) (3)	V_v (cm ³) (2-1)	V (cm ³) (2-3)	Porosity (%) (n=V _v /V)	Dry Unit W. (kN/m ³)	Sat. Unit W. (kN/m ³)
6M-11	980.96	1006.11	654.61	25.15	351.50	7.16	27.38	28.08
6M-12	971.30	996.63	647.54	25.33	349.09	7.26	27.30	28.01
6M-13	970.74	996.52	647.68	25.78	348.84	7.39	27.30	28.02
6M-14	949.11	975.44	625.99	26.33	349.45	7.53	26.64	27.38
6M-15	993.28	1018.70	662.21	25.42	356.49	7.13	27.33	28.03
6M-16	993.17	1019.45	662.36	26.28	357.09	7.36	27.28	28.01
6M-17	966.48	992.21	645.03	25.73	347.18	7.41	27.31	28.04
6M-18	971.64	997.30	648.03	25.66	349.27	7.35	27.29	28.01
6M-19	965.04	991.88	642.47	26.84	349.41	7.68	27.09	27.85
6M-20	965.09	989.56	635.99	24.47	353.57	6.92	26.78	27.46
6M-21	970.70	997.06	648.03	26.36	349.03	7.55	27.28	28.02
6M-22	987.77	1014.33	658.83	26.56	355.50	7.47	27.26	27.99
6M-23	967.02	992.02	642.79	25.00	349.23	7.16	27.16	27.87
6M-24	975.67	1002.04	650.86	26.37	351.18	7.51	27.25	27.99
6M-25	946.52	968.27	621.03	21.75	347.24	6.26	26.74	27.35
6M-26	923.00	948.24	616.98	25.24	331.26	7.62	27.33	28.08
6M-27	982.93	1008.90	656.16	25.97	352.74	7.36	27.34	28.06
6M-28	992.03	1017.31	660.78	25.28	356.53	7.09	27.30	27.99
6M-29	973.33	1000.07	648.86	26.74	351.21	7.61	27.19	27.93
6M-30	937.26	960.13	619.55	22.87	340.58	6.72	27.00	27.66
6M-31	957.02	986.54	637.54	29.52	349.00	8.46	26.90	27.73
6M-32	956.21	983.65	638.16	27.44	345.49	7.94	27.15	27.93
6M-33	942.99	969.99	627.93	27.00	342.06	7.89	27.04	27.82
6M-34	930.09	961.51	616.42	31.42	345.09	9.10	26.44	27.33
6M-35	962.39	988.78	642.49	26.39	346.29	7.62	27.26	28.01
6M-36	956.13	986.11	635.29	29.98	350.82	8.55	26.74	27.57
6M-37	937.52	962.53	618.46	25.01	344.07	7.27	26.73	27.44
6M-38	978.46	1004.02	653.11	25.56	350.91	7.28	27.35	28.07
6M-39	970.40	996.61	648.21	26.21	348.40	7.52	27.32	28.06
6M-40	965.48	992.51	643.36	27.03	349.15	7.74	27.13	27.89
6M-41	968.64	994.16	646.81	25.52	347.35	7.35	27.36	28.08
6M-42	968.28	988.19	641.84	19.91	346.35	5.75	27.43	27.99
6M-43	954.80	979.33	636.11	24.53	343.22	7.15	27.29	27.99
6M-44	962.70	988.09	641.98	25.39	346.11	7.34	27.29	28.01

Table A.2 Porosity and unit weight of the vesicular basalt samples

Sample No	M_{dry} (g.) (1)	M_{sat.} (g.) (2)	M_{sub.} (g.) (3)	V_v (cm ³) (2-1)	V (cm ³) (2-3)	Porosity (%) (n=V _v /V)	Dry Unit W. (kN/m ³)	Sat. Unit W. (kN/m ³)
1V-1	819.63	857.56	519.02	37.93	338.54	11.20	23.75	24.85
1V-2	857.92	885.71	540.00	27.79	345.71	8.04	24.34	25.13
1V-3	831.46	866.71	530.38	35.25	336.33	10.48	24.25	25.28
1V-4	850.41	883.11	541.47	32.70	341.64	9.57	24.42	25.36
1V-5	860.36	888.83	553.63	28.47	335.20	8.49	25.18	26.01
1V-6	842.95	873.61	535.06	30.66	338.55	9.06	24.43	25.31
1V-7	882.68	912.15	569.67	29.47	342.48	8.60	25.28	26.13
1V-8	844.42	875.78	536.63	31.36	339.15	9.25	24.43	25.33
1V-9	807.82	837.76	512.05	29.94	325.71	9.19	24.33	25.23
1V-10	845.30	880.11	539.23	34.81	340.88	10.21	24.33	25.33
1V-11	869.94	898.00	562.38	28.06	335.62	8.36	25.43	26.25
1V-12	832.74	871.75	527.25	39.01	344.50	11.32	23.71	24.82
1V-13	856.19	887.19	549.43	31.00	337.76	9.18	24.87	25.77
1V-14	787.49	827.50	495.35	40.01	332.15	12.05	23.26	24.44
1V-15	846.64	880.66	543.54	34.02	337.12	10.09	24.64	25.63
1V-16	875.86	904.30	559.02	28.44	345.28	8.24	24.88	25.69
1V-17	849.13	875.97	547.70	26.84	328.27	8.18	25.38	26.18
1V-18	841.46	873.38	538.13	31.92	335.25	9.52	24.62	25.56
1V-19	833.98	869.17	534.10	35.19	335.07	10.50	24.42	25.45
1V-20	855.96	885.87	552.30	29.91	333.57	8.97	25.17	26.05
1V-21	866.33	897.26	558.10	30.93	339.16	9.12	25.06	25.95
1V-22	813.74	849.10	511.30	35.36	337.80	10.47	23.63	24.66
1V-23	820.34	860.56	521.96	40.22	338.60	11.88	23.77	24.93
1V-24	844.13	877.94	540.10	33.81	337.84	10.01	24.51	25.49
1V-25	785.85	824.03	495.86	38.18	328.17	11.63	23.49	24.63
1V-26	807.25	835.25	510.65	28.00	324.60	8.63	24.40	25.24
1V-27	856.18	888.32	551.85	32.14	336.47	9.55	24.96	25.90
1V-28	847.74	881.65	536.02	33.91	345.63	9.81	24.06	25.02
1V-29	886.09	918.16	571.28	32.07	346.88	9.25	25.06	25.97
1V-30	832.66	861.03	523.80	28.37	337.23	8.41	24.22	25.05
1V-31	870.38	899.42	560.11	29.04	339.31	8.56	25.16	26.00
1V-32	816.59	845.22	507.44	28.63	337.78	8.48	23.72	24.55
1V-33	837.89	873.44	534.48	35.55	338.96	10.49	24.25	25.28
1V-34	829.94	858.72	529.19	28.78	329.53	8.73	24.71	25.56

Table A.2 (continued)

Sample No	M_{dry} (g.) (1)	M_{sat.} (g.) (2)	M_{sub.} (g.) (3)	V_v (cm ³) (2-1)	V (cm ³) (2-3)	Porosity (%) ($n=V_v/V$)	Dry Unit W. (kN/m ³)	Sat. Unit W. (kN/m ³)
1V-35	826.46	859.59	517.35	33.13	342.24	9.68	23.69	24.64
1V-36	815.62	851.05	512.10	35.43	338.95	10.45	23.61	24.63
1V-37	840.87	868.12	525.90	27.25	342.22	7.96	24.10	24.89
1V-38	834.97	867.22	529.10	32.25	338.12	9.54	24.23	25.16
1V-39	822.83	855.10	524.32	32.27	330.78	9.76	24.40	25.36
1V-40	864.45	892.96	557.05	28.51	335.91	8.49	25.25	26.08
1V-41	856.50	886.90	544.70	30.40	342.20	8.88	24.55	25.43
1V-42	839.75	874.72	536.25	34.97	338.47	10.33	24.34	25.35
1V-43	804.04	840.47	511.60	36.43	328.87	11.08	23.98	25.07
3V-1	889.25	923.68	579.73	34.43	343.95	10.01	25.36	26.34
3V-2	848.13	888.59	547.13	40.46	341.46	11.85	24.37	25.53
3V-3	863.53	896.08	559.21	32.55	336.87	9.66	25.15	26.09
3V-4	887.86	925.41	576.60	37.55	348.81	10.77	24.97	26.03
3V-5	821.55	867.67	529.38	46.12	338.29	13.63	23.82	25.16
3V-6	886.11	922.49	581.28	36.38	341.21	10.66	25.48	26.52
3V-7	886.38	924.58	578.63	38.20	345.95	11.04	25.13	26.22
3V-8	864.90	909.68	558.88	44.78	350.80	12.77	24.19	25.44
3V-9	886.69	924.39	579.53	37.70	344.86	10.93	25.22	26.30
3V-10	876.25	910.89	575.47	34.64	335.42	10.33	25.63	26.64
3V-11	855.44	896.94	555.28	41.50	341.66	12.15	24.56	25.75
3V-12	880.57	918.12	576.70	37.55	341.42	11.00	25.30	26.38
3V-13	890.67	930.18	582.41	39.51	347.77	11.36	25.12	26.24
3V-14	897.51	931.22	587.78	33.71	343.44	9.82	25.64	26.60
3V-15	893.35	929.54	583.38	36.19	346.16	10.45	25.32	26.34
3V-16	875.28	914.14	563.53	38.86	350.61	11.08	24.49	25.58
3V-17	872.12	910.83	569.06	38.71	341.77	11.33	25.03	26.14
3V-18	865.88	902.50	567.88	36.62	334.62	10.94	25.38	26.46
3V-19	881.97	917.83	574.27	35.86	343.56	10.44	25.18	26.21
3V-20	855.40	898.18	552.08	42.78	346.10	12.36	24.25	25.46
3V-21	907.53	945.94	595.68	38.41	350.26	10.97	25.42	26.49
3V-22	895.35	933.28	584.16	37.93	349.12	10.86	25.16	26.22
3V-23	892.42	932.04	583.08	39.62	348.96	11.35	25.09	26.20
3V-24	904.48	938.84	592.65	34.36	346.19	9.93	25.63	26.60
3V-25	903.62	942.74	591.25	39.12	351.49	11.13	25.22	26.31

Table A.2 (continued)

Sample No	M_{dry} (g.) (1)	M_{sat.} (g.) (2)	M_{sub.} (g.) (3)	V_v (cm ³) (2-1)	V (cm ³) (2-3)	Porosity (%) ($n=V_v/V$)	Dry Unit W. (kN/m ³)	Sat. Unit W. (kN/m ³)
3V-26	885.62	920.66	581.88	35.04	338.78	10.34	25.64	26.66
3V-27	870.45	913.01	568.27	42.56	344.74	12.35	24.77	25.98
3V-28	904.16	943.89	592.89	39.73	351.00	11.32	25.27	26.38
3V-29	883.28	921.50	577.63	38.22	343.87	11.11	25.20	26.29
3V-30	860.81	901.98	557.51	41.17	344.47	11.95	24.51	25.69
3V-31	860.17	900.56	560.18	40.39	340.38	11.87	24.79	25.95
3V-32	882.98	917.94	578.67	34.96	339.27	10.30	25.53	26.54
3V-33	878.56	918.05	577.18	39.49	340.87	11.59	25.28	26.42
3V-34	886.00	924.83	579.68	38.83	345.15	11.25	25.18	26.29
3V-35	888.26	925.47	580.88	37.21	344.59	10.80	25.29	26.35
3V-36	886.31	928.91	578.60	42.60	350.31	12.16	24.82	26.01
3V-37	837.25	878.72	544.58	41.47	334.14	12.41	24.58	25.80
3V-38	842.70	890.43	544.53	47.73	345.90	13.80	23.90	25.25
3V-39	859.43	896.50	564.80	37.07	331.70	11.18	25.42	26.51
3V-40	882.99	921.08	578.34	38.09	342.74	11.11	25.27	26.36
3V-41	812.49	854.08	524.28	41.59	329.80	12.61	24.17	25.40
3V-42	857.11	896.47	554.83	39.36	341.64	11.52	24.61	25.74
3V-43	900.49	934.91	586.28	34.42	348.63	9.87	25.34	26.31
5V-1	850.82	889.01	554.21	38.19	334.80	11.41	24.93	26.05
5V-2	832.36	873.97	562.21	41.61	311.76	13.35	26.19	27.50
5V-3	847.96	884.68	553.76	36.72	330.92	11.10	25.14	26.23
5V-4	858.54	903.46	557.31	44.92	346.15	12.98	24.33	25.60
5V-5	843.86	884.30	549.06	40.44	335.24	12.06	24.69	25.88
5V-6	850.36	889.63	553.54	39.27	336.09	11.68	24.82	25.97
5V-7	810.56	855.19	524.26	44.63	330.93	13.49	24.03	25.35
5V-8	854.78	893.77	557.10	38.99	336.67	11.58	24.91	26.04
5V-9	861.29	896.07	562.33	34.78	333.74	10.42	25.32	26.34
5V-10	847.14	884.23	551.46	37.09	332.77	11.15	24.97	26.07
5V-11	859.79	896.32	561.66	36.53	334.66	10.92	25.20	26.27
5V-12	817.07	859.83	528.86	42.76	330.97	12.92	24.22	25.49
5V-13	824.41	871.86	530.46	47.45	341.40	13.90	23.69	25.05
5V-14	860.18	895.58	562.01	35.40	333.57	10.61	25.30	26.34
5V-15	822.13	863.71	532.84	41.58	330.87	12.57	24.38	25.61
5V-16	839.68	880.44	540.11	40.76	340.33	11.98	24.20	25.38

Table A.2 (continued)

Sample No	M_{dry} (g.) (1)	M_{sat.} (g.) (2)	M_{sub.} (g.) (3)	V_v (cm ³) (2-1)	V (cm ³) (2-3)	Porosity (%) (n=V _v /V)	Dry Unit W. (kN/m ³)	Sat. Unit W. (kN/m ³)
5V-17	851.54	891.77	555.66	40.23	336.11	11.97	24.85	26.03
5V-18	846.80	882.57	552.14	35.77	330.43	10.83	25.14	26.20
5V-19	861.10	895.65	560.28	34.55	335.37	10.30	25.19	26.20
5V-20	863.68	898.87	564.89	35.19	333.98	10.54	25.37	26.40
5V-21	861.16	898.97	562.54	37.81	336.43	11.24	25.11	26.21
5V-22	842.64	886.79	545.46	44.15	341.33	12.93	24.22	25.49
5V-23	854.82	894.92	556.76	40.10	338.16	11.86	24.80	25.96
5V-24	824.88	870.74	532.86	45.86	337.88	13.57	23.95	25.28
5V-25	811.06	857.01	526.26	45.95	330.75	13.89	24.06	25.42
5V-26	862.87	897.82	563.26	34.95	334.56	10.45	25.30	26.33
5V-27	838.66	883.89	543.41	45.23	340.48	13.28	24.16	25.47
5V-28	855.93	896.51	558.51	40.58	338.00	12.01	24.84	26.02
5V-29	858.64	902.97	557.86	44.33	345.11	12.85	24.41	25.67
5V-30	859.44	900.52	558.58	41.08	341.94	12.01	24.66	25.84
5V-31	804.81	851.56	521.31	46.75	330.25	14.16	23.91	25.30
5V-32	851.30	892.15	556.31	40.85	335.84	12.16	24.87	26.06
5V-33	851.66	890.64	556.26	38.98	334.38	11.66	24.99	26.13
5V-34	838.20	880.67	546.56	42.47	334.11	12.71	24.61	25.86
5V-35	870.04	906.77	569.26	36.73	337.51	10.88	25.29	26.36
5V-36	854.47	893.78	559.06	39.31	334.72	11.74	25.04	26.19
5V-37	858.68	898.88	561.05	40.20	337.83	11.90	24.93	26.10
5V-38	858.11	896.18	560.76	38.07	335.42	11.35	25.10	26.21
5V-39	868.98	905.88	568.46	36.90	337.42	10.94	25.26	26.34
5V-40	850.58	889.53	555.86	38.95	333.67	11.67	25.01	26.15
5V-41	875.16	915.00	568.92	39.84	346.08	11.51	24.81	25.94
5V-42	817.36	864.72	531.26	47.36	333.46	14.20	24.05	25.44
5V-43	883.54	920.95	575.15	37.41	345.80	10.82	25.07	26.13
5V-44	851.66	897.36	552.36	45.70	345.00	13.25	24.22	25.52

Table A.3 Water absorption under atmospheric pressure data for the massive basalt samples

Sample No	M_{dry} (g.) (1)	M_{sat.} (g.) (2)	M_{sub.} (g.) (3)	Water abs. by weight (%) (2-1)/(1)	Water abs. by volume (%) (2-1)/(2-3)
1M-1	980.28	987.60	640.52	0.75	2.11
1M-2	1005.65	1012.15	659.38	0.65	1.84
1M-3	944.40	954.58	602.66	1.08	2.89
1M-4	918.44	930.86	583.62	1.35	3.58
1M-5	1000.79	1006.20	657.22	0.54	1.55
1M-6	916.90	929.99	583.32	1.43	3.78
1M-7	894.02	907.55	569.32	1.51	4.00
1M-8	933.18	942.23	593.38	0.97	2.59
1M-9	957.20	964.89	607.32	0.80	2.15
1M-10	1028.71	1032.12	672.95	0.33	0.95
1M-11	935.84	944.03	594.16	0.88	2.34
1M-12	933.96	944.30	595.16	1.11	2.96
1M-13	912.37	925.76	580.07	1.47	3.87
1M-14	912.52	924.41	579.13	1.30	3.44
1M-15	967.45	976.82	629.63	0.97	2.70
1M-16	978.22	983.74	633.35	0.56	1.58
1M-17	1000.04	1005.98	649.79	0.59	1.67
1M-18	911.28	921.69	578.87	1.14	3.04
1M-19	977.02	982.23	634.12	0.53	1.50
1M-20	960.28	970.84	621.57	1.10	3.02
1M-21	1000.87	1007.31	648.17	0.64	1.79
1M-22	989.56	995.38	642.08	0.59	1.65
1M-23	985.39	996.89	638.27	1.17	3.21
1M-24	992.71	999.21	646.80	0.65	1.84
1M-25	620.45	629.40	394.35	1.44	3.81
1M-26	623.36	631.80	397.65	1.35	3.60
1M-27	679.88	683.56	446.78	0.54	1.55
1M-28	621.52	629.68	395.10	1.31	3.48
1M-29	691.01	695.94	453.27	0.71	2.03
1M-30	631.26	638.57	402.18	1.16	3.09
1M-31	669.63	672.19	438.03	0.38	1.09
1M-32	628.38	636.25	399.53	1.25	3.32
1M-33	619.45	627.70	394.24	1.33	3.53
1M-34	607.30	617.00	387.10	1.60	4.22

Table A.3 (continued)

Sample No	M_{dry} (g.) (1)	M_{sat.} (g.) (2)	M_{sub.} (g.) (3)	Water abs. by weight (%) (2-1)/(1)	Water abs. by volume (%) (2-1)/(2-3)
1M-35	966.70	971.10	628.60	0.46	1.28
1M-36	926.65	939.14	588.38	1.35	3.56
1M-37	919.85	930.92	584.25	1.20	3.19
1M-38	881.10	895.64	561.51	1.65	4.35
2M-1	1036.77	1043.25	684.7	0.63	1.81
2M-2	1006.06	1016.77	656.87	1.06	2.98
2M-3	1024.15	1031.67	675.12	0.73	2.11
2M-4	1039.30	1047.02	686.85	0.74	2.14
2M-5	976.20	982.87	636.8	0.68	1.93
2M-6	990.24	998.16	653.45	0.80	2.30
2M-7	983.51	989.86	642.3	0.65	1.83
2M-8	986.20	995.07	647.13	0.90	2.55
2M-9	976.42	983.2	635.68	0.69	1.95
2M-10	990.10	997.47	647.18	0.74	2.10
2M-11	1018.15	1025.66	668.92	0.74	2.11
2M-12	1012.50	1019.83	661.5	0.72	2.05
2M-13	972.04	978.08	632.57	0.62	1.75
2M-14	983.10	991	643.52	0.80	2.27
2M-15	681.58	686.7	448.86	0.75	2.15
2M-16	656.37	663.37	428.9	1.07	2.99
2M-17	671.90	676.2	440.36	0.64	1.82
2M-18	665.37	670.6	438.16	0.79	2.25
2M-19	983.19	990.8	644.72	0.77	2.20
2M-20	1016.90	1024.31	666.58	0.73	2.07
4M-1	1013.32	1018.12	666.12	0.47	1.36
4M-2	1035.50	1040.8	681.6	0.51	1.48
4M-3	982.25	985.58	644.18	0.34	0.98
4M-4	1042.27	1047.71	685.5	0.52	1.50
4M-5	977.79	984.91	640.7	0.73	2.07
4M-6	1031.74	1036.24	678.88	0.44	1.26
4M-7	1016.99	1021.48	668.6	0.44	1.27
4M-8	1021.96	1026.48	671.84	0.44	1.27
4M-9	1045.29	1051.47	687.5	0.59	1.70
4M-10	972.37	978.32	637.32	0.61	1.74

Table A.3 (continued)

Sample No	M_{dry} (g.) (1)	M_{sat.} (g.) (2)	M_{sub.} (g.) (3)	Water abs. by weight (%) (2-1)/(1)	Water abs. by volume (%) (2-1)/(2-3)
4M-11	1024.60	1029.92	674.3	0.52	1.50
4M-12	971.51	976.6	637.6	0.52	1.50
4M-13	708.05	712.45	467.89	0.62	1.80
4M-14	675.20	679.89	441.08	0.69	1.96
4M-15	630.63	635.31	414.8	0.74	2.12
4M-16	689.39	693.46	452.45	0.59	1.69
4M-17	730.07	735.18	482.38	0.70	2.02
4M-18	712.46	718.34	468.7	0.83	2.36
4M-19	702.06	706.95	463.17	0.70	2.01
4M-20	659.27	664.8	430.07	0.84	2.36
4M-21	691.37	695.42	453.83	0.59	1.68
4M-22	677.10	681.62	447.32	0.67	1.93
4M-23	697.14	702.99	458.92	0.84	2.40
4M-24	690.01	695.74	454.87	0.83	2.38
4M-25	645.80	650.91	425.46	0.79	2.27
4M-26	692.13	697.21	457.51	0.73	2.12
4M-27	669.91	676.33	441.51	0.96	2.73
4M-28	658.12	663.4	433.12	0.80	2.29
6M-1	968.65	978.38	618.49	1.00	2.70
6M-2	971.88	983.05	625.36	1.15	3.12
6M-3	978.57	988.5	628.9	1.01	2.76
6M-4	969.95	978.88	623.07	0.92	2.51
6M-5	981.42	991.44	630.42	1.02	2.78
6M-6	958.20	969.74	615.44	1.20	3.26
6M-7	979.47	989.78	628.93	1.05	2.86
6M-8	967.27	976.55	620.23	0.96	2.60
6M-9	992.81	1000.89	636.5	0.81	2.22
6M-10	964.61	974.62	616.72	1.04	2.80
6M-11	980.96	988.71	629.3	0.79	2.16
6M-12	971.30	979.33	622.14	0.83	2.25
6M-13	970.74	980	623.09	0.95	2.59
6M-14	949.11	961.46	604.08	1.30	3.46
6M-15	993.28	1002.21	637.63	0.90	2.45
6M-16	993.17	1003.03	638.2	0.99	2.70

Table A.3 (continued)

Sample No	M_{dry} (g.) (1)	M_{sat.} (g.) (2)	M_{sub.} (g.) (3)	Water abs. by weight (%) (2-1)/(1)	Water abs. by volume (%) (2-1)/(2-3)
6M-17	966.48	975.14	620.02	0.90	2.44
6M-18	971.64	979.68	622.4	0.83	2.25
6M-19	965.04	975.5	618.2	1.08	2.93
6M-20	965.09	975.43	613.88	1.07	2.86
6M-21	970.70	980.52	623.64	1.01	2.75
6M-22	987.77	996.95	633.42	0.93	2.53
6M-23	967.02	976.13	618.9	0.94	2.55
6M-24	975.67	985.07	626.85	0.96	2.62
6M-25	946.52	957.21	602.12	1.13	3.01
6M-26	923.00	932.32	592.9	1.01	2.75
6M-27	982.93	992.7	632.07	0.99	2.71
6M-28	992.03	1000.91	636.37	0.90	2.44
6M-29	973.33	982.86	623.72	0.98	2.65
6M-30	937.26	946.68	597.83	1.01	2.70
6M-31	957.02	970.06	612.35	1.36	3.65
6M-32	956.21	967.63	613.97	1.19	3.23
6M-33	942.99	955.44	604.52	1.32	3.55
6M-34	930.09	941.97	588.9	1.28	3.36
6M-35	962.39	972.27	617.51	1.03	2.78
6M-36	956.13	968.72	609.83	1.32	3.51
6M-37	937.52	949.45	597.26	1.27	3.39
6M-38	978.46	988.36	628.96	1.01	2.75
6M-39	970.40	980.05	623.72	0.99	2.71
6M-40	965.48	976.71	619.53	1.16	3.14
6M-41	968.64	978.32	622.18	1.00	2.72
6M-42	968.28	976.69	622.07	0.87	2.37
6M-43	954.80	964.61	613.42	1.03	2.79
6M-44	962.70	971.98	617.85	0.96	2.62

Table A.4 Water absorption under atmospheric pressure data for the vesicular basalt samples

Sample No	M_{dry} (g.) (1)	M_{sat.} (g.) (2)	M_{sub.} (g.) (3)	Water abs. by weight (%) (2-1)/(1)	Water abs. by volume (%) (2-1)/(2-3)
1V-1	819.63	836.14	494.90	2.01	4.84
1V-2	857.92	873.54	526.59	1.82	4.50
1V-3	831.46	848.64	510.10	2.07	5.07
1V-4	850.41	869.62	524.42	2.26	5.56
1V-5	860.36	875.76	539.40	1.79	4.58
1V-6	842.95	857.75	519.45	1.76	4.37
1V-7	882.68	899.04	555.98	1.85	4.77
1V-8	844.42	860.81	519.64	1.94	4.80
1V-9	807.82	822.51	495.55	1.82	4.49
1V-10	845.30	863.28	521.74	2.13	5.26
1V-11	869.94	886.71	548.64	1.93	4.96
1V-12	832.74	848.89	503.23	1.94	4.67
1V-13	856.19	870.05	532.02	1.62	4.10
1V-14	787.49	802.33	471.68	1.88	4.49
1V-15	846.64	862.76	524.05	1.90	4.76
1V-16	875.86	891.20	544.75	1.75	4.43
1V-17	849.13	863.17	533.68	1.65	4.26
1V-18	841.46	856.68	520.95	1.81	4.53
1V-19	833.98	848.62	515.40	1.76	4.39
1V-20	855.96	869.92	535.76	1.63	4.18
1V-21	866.33	881.39	540.67	1.74	4.42
1V-22	813.74	828.23	489.99	1.78	4.28
1V-23	820.34	836.30	499.19	1.95	4.73
1V-24	844.13	858.44	520.23	1.70	4.23
1V-25	785.85	800.56	472.28	1.87	4.48
1V-26	807.25	819.87	493.72	1.56	3.87
1V-27	856.18	869.76	532.21	1.59	4.02
1V-28	847.74	862.46	513.50	1.74	4.22
1V-29	886.09	901.16	552.72	1.70	4.32
1V-30	832.66	845.46	507.23	1.54	3.78
1V-31	870.38	888.44	543.23	2.07	5.23
1V-32	816.59	829.06	491.30	1.53	3.69
1V-33	837.89	855.00	513.88	2.04	5.02
1V-34	829.94	843.41	515.13	1.62	4.10

Table A.4 (continued)

Sample No	M_{dry} (g.) (1)	M_{sat.} (g.) (2)	M_{sub.} (g.) (3)	Water abs. by weight (%) (2-1)/(1)	Water abs. by volume (%) (2-1)/(2-3)
1V-35	826.46	839.75	497.93	1.61	3.89
1V-36	815.62	831.34	491.20	1.93	4.62
1V-37	840.87	853.19	510.51	1.47	3.60
1V-38	834.97	848.46	510.18	1.62	3.99
1V-39	822.83	838.50	506.35	1.90	4.72
1V-40	864.45	878.63	541.52	1.64	4.21
1V-41	856.50	869.80	527.33	1.55	3.88
1V-42	839.75	854.96	515.51	1.81	4.48
1V-43	804.04	818.26	488.79	1.77	4.32
3V-1	889.25	911.97	570.57	2.55	6.65
3V-2	848.13	866.80	525.40	2.20	5.47
3V-3	863.53	883.28	549.99	2.29	5.93
3V-4	887.86	907.22	557.60	2.18	5.54
3V-5	821.55	842.53	503.24	2.55	6.18
3V-6	886.11	912.76	569.72	3.01	7.77
3V-7	886.38	904.63	558.36	2.06	5.27
3V-8	864.90	883.85	538.92	2.19	5.49
3V-9	886.69	905.65	560.00	2.14	5.49
3V-10	876.25	896.65	561.43	2.33	6.09
3V-11	855.44	875.55	532.86	2.35	5.87
3V-12	880.57	901.11	561.69	2.33	6.05
3V-13	890.67	914.14	565.72	2.64	6.74
3V-14	897.51	921.59	577.85	2.68	7.01
3V-15	893.35	915.11	568.40	2.44	6.28
3V-16	875.28	893.13	541.91	2.04	5.08
3V-17	872.12	892.85	551.05	2.38	6.06
3V-18	865.88	892.83	553.76	3.11	7.95
3V-19	881.97	902.28	558.93	2.30	5.92
3V-20	855.40	877.62	532.02	2.60	6.43
3V-21	907.53	934.71	584.60	2.99	7.76
3V-22	895.35	916.59	569.02	2.37	6.11
3V-23	892.42	915.20	568.01	2.55	6.56
3V-24	904.48	925.56	578.17	2.33	6.07
3V-25	903.62	925.37	574.36	2.41	6.20

Table A.4 (continued)

Sample No	M_{dry} (g.) (1)	M_{sat.} (g.) (2)	M_{sub.} (g.) (3)	Water abs. by weight (%) (2-1)/(1)	Water abs. by volume (%) (2-1)/(2-3)
3V-26	885.62	904.47	565.64	2.13	5.56
3V-27	870.45	891.96	548.04	2.47	6.25
3V-28	904.16	926.99	575.65	2.52	6.50
3V-29	883.28	904.10	559.40	2.36	6.04
3V-30	860.81	879.88	534.48	2.22	5.52
3V-31	860.17	879.13	538.64	2.20	5.57
3V-32	882.98	906.16	565.46	2.63	6.80
3V-33	878.56	902.39	560.95	2.71	6.98
3V-34	886.00	908.57	561.50	2.55	6.50
3V-35	888.26	909.08	564.70	2.34	6.05
3V-36	886.31	909.25	559.90	2.59	6.57
3V-37	837.25	862.92	532.67	3.07	7.77
3V-38	842.70	865.52	519.10	2.71	6.59
3V-39	859.43	882.78	548.33	2.72	6.98
3V-40	882.99	904.70	562.19	2.46	6.34
3V-41	812.49	831.79	502.07	2.38	5.85
3V-42	857.11	876.78	534.33	2.29	5.74
3V-43	900.49	917.67	568.10	1.91	4.91
5V-1	850.82	873.31	537.07	2.64	6.69
5V-2	832.36	853.83	552.40	2.58	7.12
5V-3	847.96	866.87	534.96	2.23	5.70
5V-4	858.54	863.54	536.86	0.58	1.53
5V-5	843.86	865.18	527.48	2.53	6.31
5V-6	850.36	873.58	535.70	2.73	6.87
5V-7	810.56	835.22	501.29	3.04	7.38
5V-8	854.78	874.70	537.19	2.33	5.90
5V-9	861.29	880.40	543.90	2.22	5.68
5V-10	847.14	870.50	535.46	2.76	6.97
5V-11	859.79	878.29	540.63	2.15	5.48
5V-12	817.07	842.13	508.03	3.07	7.50
5V-13	824.41	851.62	507.43	3.30	7.91
5V-14	860.18	877.92	542.41	2.06	5.29
5V-15	822.13	844.51	511.72	2.72	6.72
5V-16	839.68	868.24	525.28	3.40	8.33

Table A.4 (continued)

Sample No	M_{dry} (g.) (1)	M_{sat.} (g.) (2)	M_{sub.} (g.) (3)	Water abs. by weight (%) (2-1)/(1)	Water abs. by volume (%) (2-1)/(2-3)
5V-17	851.54	874.26	537.12	2.67	6.74
5V-18	846.80	867.98	536.58	2.50	6.39
5V-19	861.10	884.04	546.62	2.66	6.80
5V-20	863.68	883.12	545.80	2.25	5.76
5V-21	861.16	884.48	546.18	2.71	6.89
5V-22	842.64	865.64	522.10	2.73	6.69
5V-23	854.82	878.55	539.40	2.78	7.00
5V-24	824.88	853.12	511.85	3.42	8.27
5V-25	811.06	835.04	502.10	2.96	7.20
5V-26	862.87	885.54	548.94	2.63	6.73
5V-27	838.66	866.27	524.10	3.29	8.07
5V-28	855.93	875.50	536.70	2.29	5.78
5V-29	858.64	882.25	535.25	2.75	6.80
5V-30	859.44	880.63	537.82	2.47	6.18
5V-31	804.81	830.17	498.65	3.15	7.65
5V-32	851.30	872.87	535.53	2.53	6.39
5V-33	851.66	875.73	540.70	2.83	7.18
5V-34	838.20	862.89	527.80	2.95	7.37
5V-35	870.04	889.72	550.60	2.26	5.80
5V-36	854.47	874.50	539.25	2.34	5.97
5V-37	858.68	883.74	544.53	2.92	7.39
5V-38	858.11	878.62	541.25	2.39	6.08
5V-39	868.98	888.35	548.90	2.23	5.71
5V-40	850.58	873.94	538.65	2.75	6.97
5V-41	875.16	898.46	550.79	2.66	6.70
5V-42	817.36	843.49	508.50	3.20	7.80
5V-43	883.54	904.52	558.57	2.37	6.06
5V-44	851.66	881.72	535.14	3.53	8.67

Table A.5 Water absorption under vacuum pressure data for the massive basalt samples

Sample No	M_{dry} (g.) (1)	M_{sat.} (g.) (2)	M_{sub.} (g.) (3)	Water abs. by weight (%) (2-1)/(1)	Water abs. by volume (%) (2-1)/(2-3)
1M-1	980.28	998.56	642.35	1.86	5.13
1M-2	1005.65	1022.39	661.30	1.66	4.64
1M-3	944.40	964.75	612.87	2.15	5.78
1M-4	918.44	943.48	596.50	2.73	7.22
1M-5	1000.79	1015.47	659.40	1.47	4.12
1M-6	916.90	942.67	596.10	2.81	7.44
1M-7	894.02	917.86	579.80	2.67	7.05
1M-8	933.18	952.70	603.90	2.09	5.60
1M-9	957.20	974.35	617.20	1.79	4.80
1M-10	1028.71	1042.51	675.07	1.34	3.76
1M-11	935.84	954.68	605.05	2.01	5.39
1M-12	933.96	954.53	605.35	2.20	5.89
1M-13	912.37	936.67	591.12	2.66	7.03
1M-14	912.52	935.09	590.10	2.47	6.54
1M-15	967.45	985.17	632.85	1.83	5.03
1M-16	978.22	993.77	636.15	1.59	4.35
1M-17	1000.04	1014.89	653.70	1.48	4.11
1M-18	911.28	928.88	585.90	1.93	5.13
1M-19	977.02	991.14	638.85	1.45	4.01
1M-20	960.28	977.81	625.35	1.83	4.97
1M-21	1000.87	1015.93	652.65	1.50	4.15
1M-22	989.56	1004.48	648.05	1.51	4.19
1M-23	985.39	1005.14	639.30	2.00	5.40
1M-24	992.71	1007.89	649.20	1.53	4.23
1M-25	620.45	637.65	402.95	2.77	7.33
1M-26	623.36	638.98	405.04	2.51	6.68
1M-27	679.88	695.56	449.98	2.31	6.38
1M-28	621.52	636.82	402.60	2.46	6.53
1M-29	691.01	706.27	456.40	2.21	6.11
1M-30	631.26	645.00	408.85	2.18	5.82
1M-31	669.63	683.32	442.85	2.04	5.69
1M-32	628.38	643.95	407.40	2.48	6.58
1M-33	619.45	635.05	402.05	2.52	6.70
1M-34	607.30	623.38	393.80	2.65	7.00

Table A.5 (continued)

Sample No	M_{dry} (g.) (1)	M_{sat.} (g.) (2)	M_{sub.} (g.) (3)	Water abs. by weight (%) (2-1)/(1)	Water abs. by volume (%) (2-1)/(2-3)
1M-35	966.70	983.13	633.55	1.70	4.70
1M-36	926.65	950.53	600.05	2.58	6.81
1M-37	919.85	941.35	595.12	2.34	6.21
1M-38	881.10	904.17	570.17	2.62	6.91
2M-1	1036.77	1053.72	695.16	1.63	4.73
2M-2	1006.06	1021.70	667.66	1.55	4.42
2M-3	1024.15	1041.54	684.91	1.70	4.88
2M-4	1039.30	1057.23	696.96	1.73	4.98
2M-5	976.20	994.31	647.27	1.86	5.22
2M-6	990.24	1008.15	663.31	1.81	5.19
2M-7	983.51	1001.23	653.51	1.80	5.10
2M-8	986.20	1005.74	657.66	1.98	5.61
2M-9	976.42	996.68	649.01	2.07	5.83
2M-10	990.10	1009.26	658.51	1.94	5.46
2M-11	1018.15	1036.17	679.68	1.77	5.05
2M-12	1012.50	1031.17	672.79	1.84	5.21
2M-13	972.04	990.67	645.06	1.92	5.39
2M-14	983.10	1002.32	654.76	1.96	5.53
2M-15	681.58	698.68	460.74	2.51	7.19
2M-16	656.37	675.73	441.21	2.95	8.26
2M-17	671.90	688.49	452.44	2.47	7.03
2M-18	665.37	682.61	449.94	2.59	7.41
2M-19	983.19	1002.16	656.06	1.93	5.48
2M-20	1016.90	1035.38	677.71	1.82	5.17
4M-1	1013.32	1030.90	678.50	1.73	4.99
4M-2	1035.50	1053.33	694.05	1.72	4.96
4M-3	982.25	998.69	656.96	1.67	4.81
4M-4	1042.27	1060.43	697.76	1.74	5.01
4M-5	977.79	996.55	652.10	1.92	5.45
4M-6	1031.74	1049.15	691.70	1.69	4.87
4M-7	1016.99	1034.46	681.06	1.72	4.94
4M-8	1021.96	1039.33	684.38	1.70	4.89
4M-9	1045.29	1063.52	698.93	1.74	5.00
4M-10	972.37	990.34	648.95	1.85	5.26

Table A.5 (continued)

Sample No	M_{dry} (g.) (1)	M_{sat.} (g.) (2)	M_{sub.} (g.) (3)	Water abs. by weight (%) (2-1)/(1)	Water abs. by volume (%) (2-1)/(2-3)
4M-11	1024.60	1042.24	686.10	1.72	4.95
4M-12	971.51	989.30	649.96	1.83	5.24
4M-13	708.05	724.74	480.18	2.36	6.82
4M-14	675.20	693.01	453.83	2.64	7.45
4M-15	630.63	647.12	426.08	2.61	7.46
4M-16	689.39	707.31	465.10	2.60	7.40
4M-17	730.07	747.03	493.76	2.32	6.70
4M-18	712.46	729.75	479.50	2.43	6.91
4M-19	702.06	719.72	475.48	2.52	7.23
4M-20	659.27	679.98	444.93	3.14	8.81
4M-21	691.37	707.59	465.60	2.35	6.70
4M-22	677.10	693.55	458.61	2.43	7.00
4M-23	697.14	714.85	470.46	2.54	7.25
4M-24	690.01	707.80	466.56	2.58	7.37
4M-25	645.80	662.49	436.61	2.58	7.39
4M-26	692.13	709.12	468.83	2.45	7.07
4M-27	669.91	688.27	452.83	2.74	7.80
4M-28	658.12	675.68	445.18	2.67	7.62
6M-1	968.65	988.28	636.47	2.03	5.58
6M-2	971.88	998.56	648.68	2.75	7.63
6M-3	978.57	1004.43	652.86	2.64	7.36
6M-4	969.95	995.14	647.03	2.60	7.24
6M-5	981.42	1007.51	654.78	2.66	7.40
6M-6	958.20	985.02	638.99	2.80	7.75
6M-7	979.47	1004.72	651.54	2.58	7.15
6M-8	967.27	993.15	644.67	2.68	7.43
6M-9	992.81	1018.79	662.03	2.62	7.28
6M-10	964.61	991.21	641.23	2.76	7.60
6M-11	980.96	1006.11	654.61	2.56	7.16
6M-12	971.30	996.63	647.54	2.61	7.26
6M-13	970.74	996.52	647.68	2.66	7.39
6M-14	949.11	975.44	625.99	2.77	7.53
6M-15	993.28	1018.70	662.21	2.56	7.13
6M-16	993.17	1019.45	662.36	2.65	7.36

Table A.5 (continued)

Sample No	M_{dry} (g.) (1)	M_{sat.} (g.) (2)	M_{sub.} (g.) (3)	Water abs. by weight (%) (2-1)/(1)	Water abs. by volume (%) (2-1)/(2-3)
6M-17	966.48	992.21	645.03	2.66	7.41
6M-18	971.64	997.30	648.03	2.64	7.35
6M-19	965.04	991.88	642.47	2.78	7.68
6M-20	965.09	989.56	635.99	2.54	6.92
6M-21	970.70	997.06	648.03	2.72	7.55
6M-22	987.77	1014.33	658.83	2.69	7.47
6M-23	967.02	992.02	642.79	2.59	7.16
6M-24	975.67	1002.04	650.86	2.70	7.51
6M-25	946.52	968.27	621.03	2.30	6.26
6M-26	923.00	948.24	616.98	2.73	7.62
6M-27	982.93	1008.90	656.16	2.64	7.36
6M-28	992.03	1017.31	660.78	2.55	7.09
6M-29	973.33	1000.07	648.86	2.75	7.61
6M-30	937.26	960.13	619.55	2.44	6.72
6M-31	957.02	986.54	637.54	3.08	8.46
6M-32	956.21	983.65	638.16	2.87	7.94
6M-33	942.99	969.99	627.93	2.86	7.89
6M-34	930.09	961.51	616.42	3.38	9.10
6M-35	962.39	988.78	642.49	2.74	7.62
6M-36	956.13	986.11	635.29	3.14	8.55
6M-37	937.52	962.53	618.46	2.67	7.27
6M-38	978.46	1004.02	653.11	2.61	7.28
6M-39	970.40	996.61	648.21	2.70	7.52
6M-40	965.48	992.51	643.36	2.80	7.74
6M-41	968.64	994.16	646.81	2.63	7.35
6M-42	968.28	988.19	641.84	2.06	5.75
6M-43	954.80	979.33	636.11	2.57	7.15
6M-44	962.70	988.09	641.98	2.64	7.34

Table A.6 Water absorption under vacuum pressure data for the vesicular basalt samples

Sample No	M_{dry} (g.) (1)	M_{sat.} (g.) (2)	M_{sub.} (g.) (3)	Water abs. by weight (%) (2-1)/(1)	Water abs. by volume (%) (2-1)/(2-3)
1V-1	819.63	857.56	519.02	4.63	11.20
1V-2	857.92	885.71	540.00	3.24	8.04
1V-3	831.46	866.71	530.38	4.24	10.48
1V-4	850.41	883.11	541.47	3.85	9.57
1V-5	860.36	888.83	553.63	3.31	8.49
1V-6	842.95	873.61	535.06	3.64	9.06
1V-7	882.68	912.15	569.67	3.34	8.60
1V-8	844.42	875.78	536.63	3.71	9.25
1V-9	807.82	837.76	512.05	3.71	9.19
1V-10	845.30	880.11	539.23	4.12	10.21
1V-11	869.94	898.00	562.38	3.23	8.36
1V-12	832.74	871.75	527.25	4.68	11.32
1V-13	856.19	887.19	549.43	3.62	9.18
1V-14	787.49	827.50	495.35	5.08	12.05
1V-15	846.64	880.66	543.54	4.02	10.09
1V-16	875.86	904.30	559.02	3.25	8.24
1V-17	849.13	875.97	547.70	3.16	8.18
1V-18	841.46	873.38	538.13	3.79	9.52
1V-19	833.98	869.17	534.10	4.22	10.50
1V-20	855.96	885.87	552.30	3.49	8.97
1V-21	866.33	897.26	558.10	3.57	9.12
1V-22	813.74	849.10	511.30	4.35	10.47
1V-23	820.34	860.56	521.96	4.90	11.88
1V-24	844.13	877.94	540.10	4.01	10.01
1V-25	785.85	824.03	495.86	4.86	11.63
1V-26	807.25	835.25	510.65	3.47	8.63
1V-27	856.18	888.32	551.85	3.75	9.55
1V-28	847.74	881.65	536.02	4.00	9.81
1V-29	886.09	918.16	571.28	3.62	9.25
1V-30	832.66	861.03	523.80	3.41	8.41
1V-31	870.38	899.42	560.11	3.34	8.56
1V-32	816.59	845.22	507.44	3.51	8.48
1V-33	837.89	873.44	534.48	4.24	10.49
1V-34	829.94	858.72	529.19	3.47	8.73

Table A.6 (continued)

Sample No	M_{dry} (g.) (1)	M_{sat.} (g.) (2)	M_{sub.} (g.) (3)	Water abs. by weight (%) (2-1)/(1)	Water abs. by volume (%) (2-1)/(2-3)
1V-35	826.46	859.59	517.35	4.01	9.68
1V-36	815.62	851.05	512.10	4.34	10.45
1V-37	840.87	868.12	525.90	3.24	7.96
1V-38	834.97	867.22	529.10	3.86	9.54
1V-39	822.83	855.10	524.32	3.92	9.76
1V-40	864.45	892.96	557.05	3.30	8.49
1V-41	856.50	886.90	544.70	3.55	8.88
1V-42	839.75	874.72	536.25	4.16	10.33
1V-43	804.04	840.47	511.60	4.53	11.08
3V-1	889.25	923.68	579.73	3.87	10.01
3V-2	848.13	888.59	547.13	4.77	11.85
3V-3	863.53	896.08	559.21	3.77	9.66
3V-4	887.86	925.41	576.60	4.23	10.77
3V-5	821.55	867.67	529.38	5.61	13.63
3V-6	886.11	922.49	581.28	4.11	10.66
3V-7	886.38	924.58	578.63	4.31	11.04
3V-8	864.90	909.68	558.88	5.18	12.77
3V-9	886.69	924.39	579.53	4.25	10.93
3V-10	876.25	910.89	575.47	3.95	10.33
3V-11	855.44	896.94	555.28	4.85	12.15
3V-12	880.57	918.12	576.70	4.26	11.00
3V-13	890.67	930.18	582.41	4.44	11.36
3V-14	897.51	931.22	587.78	3.76	9.82
3V-15	893.35	929.54	583.38	4.05	10.45
3V-16	875.28	914.14	563.53	4.44	11.08
3V-17	872.12	910.83	569.06	4.44	11.33
3V-18	865.88	902.50	567.88	4.23	10.94
3V-19	881.97	917.83	574.27	4.07	10.44
3V-20	855.40	898.18	552.08	5.00	12.36
3V-21	907.53	945.94	595.68	4.23	10.97
3V-22	895.35	933.28	584.16	4.24	10.86
3V-23	892.42	932.04	583.08	4.44	11.35
3V-24	904.48	938.84	592.65	3.80	9.93
3V-25	903.62	942.74	591.25	4.33	11.13

Table A.6 (continued)

Sample No	M_{dry} (g.) (1)	M_{sat.} (g.) (2)	M_{sub.} (g.) (3)	Water abs. by weight (%) (2-1)/(1)	Water abs. by volume (%) (2-1)/(2-3)
3V-26	885.62	920.66	581.88	3.96	10.34
3V-27	870.45	913.01	568.27	4.89	12.35
3V-28	904.16	943.89	592.89	4.39	11.32
3V-29	883.28	921.50	577.63	4.33	11.11
3V-30	860.81	901.98	557.51	4.78	11.95
3V-31	860.17	900.56	560.18	4.70	11.87
3V-32	882.98	917.94	578.67	3.96	10.30
3V-33	878.56	918.05	577.18	4.49	11.59
3V-34	886.00	924.83	579.68	4.38	11.25
3V-35	888.26	925.47	580.88	4.19	10.80
3V-36	886.31	928.91	578.60	4.81	12.16
3V-37	837.25	878.72	544.58	4.95	12.41
3V-38	842.70	890.43	544.53	5.66	13.80
3V-39	859.43	896.50	564.80	4.31	11.18
3V-40	882.99	921.08	578.34	4.31	11.11
3V-41	812.49	854.08	524.28	5.12	12.61
3V-42	857.11	896.47	554.83	4.59	11.52
3V-43	900.49	934.91	586.28	3.82	9.87
5V-1	850.82	889.01	554.21	4.49	11.41
5V-2	832.36	873.97	562.21	5.00	13.35
5V-3	847.96	884.68	553.76	4.33	11.10
5V-4	858.54	903.46	557.31	5.23	12.98
5V-5	843.86	884.30	549.06	4.79	12.06
5V-6	850.36	889.63	553.54	4.62	11.68
5V-7	810.56	855.19	524.26	5.51	13.49
5V-8	854.78	893.77	557.10	4.56	11.58
5V-9	861.29	896.07	562.33	4.04	10.42
5V-10	847.14	884.23	551.46	4.38	11.15
5V-11	859.79	896.32	561.66	4.25	10.92
5V-12	817.07	859.83	528.86	5.23	12.92
5V-13	824.41	871.86	530.46	5.76	13.90
5V-14	860.18	895.58	562.01	4.12	10.61
5V-15	822.13	863.71	532.84	5.06	12.57
5V-16	839.68	880.44	540.11	4.85	11.98

Table A.6 (continued)

Sample No	M_{dry} (g.) (1)	M_{sat.} (g.) (2)	M_{sub.} (g.) (3)	Water abs. by weight (%) (2-1)/(1)	Water abs. by volume (%) (2-1)/(2-3)
5V-17	851.54	891.77	555.66	4.72	11.97
5V-18	846.80	882.57	552.14	4.22	10.83
5V-19	861.10	895.65	560.28	4.01	10.30
5V-20	863.68	898.87	564.89	4.07	10.54
5V-21	861.16	898.97	562.54	4.39	11.24
5V-22	842.64	886.79	545.46	5.24	12.93
5V-23	854.82	894.92	556.76	4.69	11.86
5V-24	824.88	870.74	532.86	5.56	13.57
5V-25	811.06	857.01	526.26	5.67	13.89
5V-26	862.87	897.82	563.26	4.05	10.45
5V-27	838.66	883.89	543.41	5.39	13.28
5V-28	855.93	896.51	558.51	4.74	12.01
5V-29	858.64	902.97	557.86	5.16	12.85
5V-30	859.44	900.52	558.58	4.78	12.01
5V-31	804.81	851.56	521.31	5.81	14.16
5V-32	851.30	892.15	556.31	4.80	12.16
5V-33	851.66	890.64	556.26	4.58	11.66
5V-34	838.20	880.67	546.56	5.07	12.71
5V-35	870.04	906.77	569.26	4.22	10.88
5V-36	854.47	893.78	559.06	4.60	11.74
5V-37	858.68	898.88	561.05	4.68	11.90
5V-38	858.11	896.18	560.76	4.44	11.35
5V-39	868.98	905.88	568.46	4.25	10.94
5V-40	850.58	889.53	555.86	4.58	11.67
5V-41	875.16	915.00	568.92	4.55	11.51
5V-42	817.36	864.72	531.26	5.79	14.20
5V-43	883.54	920.95	575.15	4.23	10.82
5V-44	851.66	897.36	552.36	5.37	13.25

Table A.7 Uniaxial compressive strength of the dry massive basalt samples

Sample No	Area (cm²)	Failure Load (Kgf)	Uniaxial Compressive Strength (MPa)
1M-U1	48.28	62536.48	127.01
1M-U2	51.79	73143.36	138.51
1M-U3	48.36	81324.78	164.92
1M-U4	49.45	63127.35	125.19
1M-U5	52.19	71365.06	134.11
1M-U6	50.78	79438.35	153.40
1M-U7	49.65	66098.35	130.56
2M-U1	51.34	81438.34	155.56
2M-U2	48.76	77836.98	156.53
2M-U3	49.62	74387.56	147.02
2M-U4	50.53	81347.36	157.88
4M-U1	48.36	79409.42	161.03
4M-U2	49.22	82098.39	163.57
4M-U3	50.14	81187.35	158.79
6M-U1	51.15	67340.38	129.11
6M-U2	49.55	59735.71	118.23
6M-U3	50.21	75134.28	146.75
6M-U4	50.36	61243.09	119.26

Table A.8 Uniaxial compressive strength of the saturated massive basalt samples

Sample No	Area (cm²)	Failure Load (Kgf)	Uniaxial Compressive Strength (MPa)
1M-U8	47.28	1237.98	121.40
1M-U9	49.17	1263.49	123.91
1M-U10	48.35	1269.19	124.46
1M-U11	51.24	1131.58	110.97
1M-U12	49.85	1160.43	113.80
1M-U13	49.1	1248.11	122.40
1M-U14	50.47	1094.74	107.36
2M-U5	48.74	1300.00	127.49
2M-U6	51.24	1315.35	128.99
2M-U7	50.38	1301.16	127.60
2M-U8	49.23	1307.89	128.26
4M-U4	51.41	1289.21	126.43
4M-U5	47.98	1358.75	133.25
4M-U6	48.36	1227.41	120.37
6M-U7	50.96	1045.49	102.53
6M-U8	50.21	992.08	97.29
6M-U9	48.78	1103.81	108.25
6M-U10	51.52	995.24	97.60

Table A.9 Uniaxial compressive strength of the dry vesicular basalt samples

Sample No	Area (cm²)	Failure Load (Kgf)	Uniaxial Compressive Strength (MPa)
1V-U1	49.73	38735.07	76.38
1V-U2	48.55	36421.98	73.57
1V-U3	51.06	40182.31	77.17
3V-U1	51.27	44127.35	84.40
3V-U2	51.79	46065.06	87.23
3V-U3	49.55	24873.91	49.23
3V-U4	50.17	25084.28	49.03
3V-U5	52.02	24185.87	45.59
3V-U6	50.20	23805.65	46.50
3V-U7	50.03	32045.35	62.81
3V-U8	49.87	31815.19	62.56
5V-U1	50.45	30762.09	59.80
5V-U2	49.66	31571.99	62.35
5V-U3	50.41	29976.05	58.31
5V-U4	49.05	33048.75	66.07
5V-U5	49.36	28451.24	56.53
5V-U6	50.62	32048.94	62.09
5V-U7	50.03	30517.37	59.82

Table A.10 Uniaxial compressive strength of the saturated vesicular basalt samples

Sample No	Area (cm²)	Failure Load (Kgf)	Uniaxial Compressive Strength (MPa)
1V-U4	47.36	21631.20	44.79
1V-U5	50.37	25554.32	49.75
1V-U6	49.35	24394.18	48.48
3V-U8	49.86	12226.20	24.05
3V-U9	50.99	16545.65	31.82
3V-U10	50.15	13899.53	27.18
3V-U11	50.71	20551.60	39.74
3V-U12	51.25	15811.77	30.26
3V-U13	51.95	17435.17	32.91
3V-U14	50.17	13479.83	26.35
3V-U15	50.31	19764.38	38.53
5V-U8	49.23	16587.58	33.04
5V-U9	51.01	18718.74	35.99
5V-U10	49.36	12675.89	25.18
5V-U11	50.62	16523.21	32.01
5V-U12	50.03	19226.44	37.69
5V-U13	50.21	17434.32	34.05
5V-U14	49.21	19045.52	37.95

Table A.11 Tensile strength of the massive basalt samples

Sample No	Diameter (mm) (1)	Thickness (mm) (2)	Failure Load (kN) (3)	Tensile Strength $[(0.636) \times (3)] / [(1) \times (2)] \times 1000$ (MPa)
1M-1	54.8	30.05	37.78	14.59
1M-2	55.01	33.45	51.03	17.63
2M-1	55.04	33.75	49.63	16.99
2M-2	55.01	35.85	54.35	17.52
2M-3	54.9	35.14	47.29	15.59
4M-1	55.06	32.54	52.18	18.52
4M-2	54.84	34.28	50.64	17.13
6M-1	55.01	34.85	52.25	17.33
6M-2	54.97	36.45	48.91	15.52
6M-3	55.02	32.17	42.36	15.22

Table A.12 Tensile strength of the vesicular basalt samples

Sample No	Diameter (mm) (1)	Thickness (mm) (2)	Failure Load (kN) (3)	Tensile Strength $[(0.636) \times (3)] / [(1) \times (2)] \times 1000$ (MPa)
1V-1	55.14	38.51	34.87	10.44
1V-2	54.85	32.48	33.94	12.12
1V-3	55.01	34.29	29.81	10.05
1V-4	54.84	36.17	33.47	10.73
1V-5	55.03	33.94	32.61	11.10
5V-1	55.5	37.09	24.87	7.68
5V-2	55.05	31.55	17.19	6.29
5V-3	55.07	36.41	21.85	6.93
5V-4	54.92	32.28	18.94	6.79
5V-5	55.03	35.05	16.81	5.54

Table A.13 Sonic velocity measurements of the dry massive basalt samples

Sample No	Length I	Length II	Length III	Tp1 (mic.s)	Tp2 (mic.s)	Tp3 (mic.s)	Vpd1 (m/s)	Vpd2 (m/s)	Vpd3 (m/s)
1M-1	70.32	70.12	71.23	16.10	14.70	16.30	4367.70	4770.07	4369.94
1M-2	70.12	70.67	72.48	15.50	15.40	18.70	4523.87	4588.96	3875.94
1M-3	71.55	70.65	70.76	16.40	15.90	16.90	4362.80	4443.40	4186.98
1M-4	70.44	71.20	70.33	16.30	16.90	17.10	4321.47	4213.02	4112.87
1M-5	71.02	70.74	70.49	14.40	14.70	15.30	4931.94	4812.24	4607.19
1M-6	69.85	71.43	70.15	14.10	14.40	14.60	4953.90	4960.42	4804.79
1M-7	69.88	70.29	70.61	18.00	15.30	20.10	3882.22	4594.12	3512.94
1M-8	70.50	71.32	71.39	15.40	18.00	15.50	4577.92	3962.22	4605.81
1M-9	69.80	73.75	71.27	15.40	21.60	14.00	4532.47	3414.35	5090.71
1M-10	70.50	70.38	73.38	13.80	16.10	23.40	5108.70	4371.43	3135.90
1M-11	70.32	71.36	70.95	14.80	14.00	14.30	4751.35	5097.14	4961.54
1M-12	70.71	70.71	70.77	15.10	21.00	18.90	4682.78	3367.14	3744.44
1M-13	70.45	71.77	70.84	15.60	17.00	19.40	4516.03	4221.76	3651.55
1M-14	70.62	70.70	70.50	16.30	15.50	18.00	4332.52	4561.29	3916.67
1M-15	70.70	69.70	72.26	16.80	25.00	17.70	4208.33	2788.00	4082.49
1M-16	71.58	70.23	70.91	16.20	17.10	15.20	4418.52	4107.02	4665.13
1M-17	70.84	72.15	70.18	15.00	27.40	17.50	4722.67	2633.21	4010.29
1M-18	69.52	71.45	70.92	14.80	15.00	15.70	4697.30	4763.33	4517.20
1M-19	71.68	69.76	70.52	15.20	16.00	15.30	4715.79	4360.00	4609.15
1M-20	70.85	68.54	72.80	17.60	19.40	21.60	4025.57	3532.99	3370.37
1M-21	70.90	70.57	73.28	16.10	20.70	18.30	4403.73	3409.18	4004.37
1M-22	69.04	70.64	73.20	14.80	14.90	19.80	4664.86	4740.94	3696.97
1M-23	70.91	70.33	73.06	33.40	27.70	22.70	2123.05	2538.99	3218.50
1M-24	70.70	72.02	70.40	18.60	16.00	15.40	3801.08	4501.25	4571.43
1M-25	61.53	62.80	61.93	13.50	14.90	16.50	4557.78	4214.77	3753.33
1M-26	62.01	62.80	62.75	14.40	15.90	14.70	4306.25	3949.69	4268.71
1M-27	62.58	62.62	62.11	15.00	16.40	15.10	4172.00	3818.29	4113.25
1M-28	61.20	61.82	63.30	13.80	21.70	15.30	4434.78	2848.85	4137.25
1M-29	63.44	62.95	63.09	12.80	23.80	13.80	4956.25	2644.96	4571.74
1M-30	62.18	61.95	62.84	14.00	17.00	14.70	4441.43	3644.12	4274.83
1M-31	61.99	61.07	62.55	23.70	16.30	20.90	2615.61	3746.63	2992.82
1M-32	61.91	61.81	62.86	13.20	13.80	13.30	4690.15	4478.99	4726.32
1M-33	61.62	62.98	62.70	13.80	15.00	18.90	4465.22	4198.67	3317.46
1M-34	61.80	60.40	62.75	15.80	15.10	18.20	3911.39	4000.00	3447.80

Table A.13 (continued)

Sample No	Length I	Length II	Length III	Tp1 (mic.s)	Tp2 (mic.s)	Tp3 (mic.s)	Vpd1 (m/s)	Vpd2 (m/s)	Vpd3 (m/s)
1M-35	70.06	68.48	71.28	19.40	17.10	30.00	3611.34	4004.68	2376.00
1M-36	70.62	71.55	70.50	14.60	15.40	16.00	4836.99	4646.10	4406.25
1M-37	70.82	70.72	70.96	16.40	16.80	17.80	4318.29	4209.52	3986.52
1M-38	70.61	69.27	69.90	17.00	15.90	19.60	4153.53	4356.60	3566.33
2M-1	70.46	71.13	73.02	24.00	13.40	16.10	2935.83	5308.21	4535.40
2M-2	70.02	71.71	73.13	32.00	17.40	17.30	2188.13	4121.26	4227.17
2M-3	70.26	71.69	72.70	28.50	15.00	15.80	2465.26	4779.33	4601.27
2M-4	73.10	70.96	69.94	14.00	16.80	15.40	5221.43	4223.81	4541.56
2M-5	70.59	71.67	70.13	14.30	14.70	22.90	4936.36	4875.51	3062.45
2M-6	70.86	70.29	70.47	21.10	14.30	22.90	3358.29	4915.38	3077.29
2M-7	70.08	71.17	70.30	13.80	14.50	15.80	5078.26	4908.28	4449.37
2M-8	71.03	69.93	72.34	15.40	15.40	15.40	4612.34	4540.91	4697.40
2M-9	71.30	70.20	70.65	14.00	14.00	21.10	5092.86	5014.29	3348.34
2M-10	70.68	70.55	72.00	15.40	14.30	14.80	4589.61	4933.57	4864.86
2M-11	69.91	70.58	73.00	15.90	14.60	23.50	4396.86	4834.25	3106.38
2M-12	70.36	71.31	73.03	18.60	15.70	15.30	3782.80	4542.04	4773.20
2M-13	70.72	70.67	70.04	15.80	14.50	15.40	4475.95	4873.79	4548.05
2M-14	70.29	71.25	70.48	18.60	14.80	14.30	3779.03	4814.19	4928.67
2M-15	62.35	62.40	61.92	16.90	15.10	13.50	3689.35	4132.45	4586.67
2M-16	62.94	62.23	61.16	13.10	17.50	15.80	4804.58	3556.00	3870.89
2M-17	62.54	61.36	62.79	23.60	12.60	22.40	2650.00	4869.84	2803.13
2M-18	62.91	61.32	62.24	18.90	16.50	17.90	3328.57	3716.36	3477.09
2M-19	70.56	70.42	71.09	16.40	23.00	14.50	4302.44	3061.74	4902.76
2M-20	70.22	70.62	73.49	25.00	15.10	14.70	2808.80	4676.82	4999.32
4M-1	68.98	73.49	70.20	12.30	14.00	13.30	5608.13	5249.29	5278.20
4M-2	74.30	70.04	69.72	14.80	13.10	12.70	5020.27	5346.56	5489.76
4M-3	70.15	70.22	70.22	13.20	12.90	12.70	5314.39	5443.41	5529.13
4M-4	70.56	70.80	74.47	13.40	12.90	13.80	5265.67	5488.37	5396.38
4M-5	70.09	71.33	70.65	14.30	13.80	14.80	4901.40	5168.84	4773.65
4M-6	70.12	69.36	74.97	12.90	13.30	14.50	5435.66	5215.04	5170.34
4M-7	73.13	70.77	70.20	13.30	12.90	12.80	5498.50	5486.05	5484.38
4M-8	70.52	73.20	69.90	13.40	13.80	12.90	5262.69	5304.35	5418.60
4M-9	74.80	70.11	70.80	14.60	13.00	12.70	5123.29	5393.08	5574.80
4M-10	69.78	71.34	70.22	14.40	13.50	13.80	4845.83	5284.44	5088.41

Table A.13 (continued)

Sample No	Length I	Length II	Length III	Tp1 (mic.s)	Tp2 (mic.s)	Tp3 (mic.s)	Vpd1 (m/s)	Vpd2 (m/s)	Vpd3 (m/s)
4M-11	74.11	70.00	70.00	13.90	12.70	13.40	5331.65	5511.81	5223.88
4M-12	71.87	70.42	70.72	13.00	12.80	14.80	5528.46	5501.56	4778.38
4M-13	62.43	63.18	62.58	12.10	11.80	11.60	5159.50	5354.24	5394.83
4M-14	62.83	62.19	62.52	12.60	11.70	12.30	4986.51	5315.38	5082.93
4M-15	62.96	59.15	60.70	15.20	11.80	12.70	4142.11	5012.71	4779.53
4M-16	62.05	62.58	63.11	11.40	12.00	12.50	5442.98	5215.00	5048.80
4M-17	66.25	62.93	62.54	12.50	12.50	12.10	5300.00	5034.40	5168.60
4M-18	62.21	63.24	66.15	11.90	13.70	12.40	5227.73	4616.06	5334.68
4M-19	64.73	61.45	62.76	11.90	16.40	11.30	5439.50	3746.95	5553.98
4M-20	62.35	61.27	62.23	13.40	12.30	13.60	4652.99	4981.30	4575.74
4M-21	62.39	63.18	62.34	11.60	12.20	11.90	5378.45	5178.69	5238.66
4M-22	60.34	62.39	63.10	11.30	12.10	12.50	5339.82	5156.20	5048.00
4M-23	63.87	63.33	63.03	14.10	12.10	12.60	4529.79	5233.88	5002.38
4M-24	63.19	61.70	64.19	16.50	11.60	12.50	3829.70	5318.97	5135.20
4M-25	60.87	61.92	61.76	11.40	11.20	13.50	5339.47	5528.57	4574.81
4M-26	62.33	64.56	61.30	11.70	11.80	11.00	5327.35	5471.19	5572.73
4M-27	64.66	61.88	61.87	15.00	13.50	13.50	4310.67	4583.70	4582.96
4M-28	62.15	60.16	62.94	12.90	15.10	11.50	4817.83	3984.11	5473.04
6M-1	70.09	73.24	70.95	14.90	15.10	14.20	4704.03	4850.33	4996.48
6M-2	72.19	70.92	70.59	15.00	14.60	14.50	4812.67	4857.53	4868.28
6M-3	71.10	70.97	72.05	14.40	15.10	15.20	4937.50	4700.00	4740.13
6M-4	73.37	70.95	68.82	15.00	14.60	14.20	4891.33	4859.59	4846.48
6M-5	70.01	72.75	70.86	14.30	15.90	14.70	4895.80	4575.47	4820.41
6M-6	70.74	72.35	70.16	14.50	16.00	14.20	4878.62	4521.88	4940.85
6M-7	71.00	73.25	71.05	15.00	15.30	14.40	4733.33	4787.58	4934.03
6M-8	72.44	71.10	69.97	16.00	14.30	14.10	4527.50	4972.03	4962.41
6M-9	71.01	73.35	70.88	15.00	15.50	14.70	4734.00	4732.26	4821.77
6M-10	72.34	70.88	71.08	15.40	14.40	14.40	4697.40	4922.22	4936.11
6M-11	73.42	71.18	70.44	15.60	14.90	14.10	4706.41	4777.18	4995.74
6M-12	70.95	72.22	70.45	14.60	15.10	13.40	4859.59	4782.78	5257.46
6M-13	70.60	71.18	70.80	15.20	16.80	14.40	4644.74	4236.90	4916.67
6M-14	72.07	70.74	70.84	15.40	16.30	14.80	4679.87	4339.88	4786.49
6M-15	73.21	70.90	70.90	15.60	15.90	14.50	4692.95	4459.12	4889.66
6M-16	70.90	71.03	73.36	14.60	14.70	15.00	4856.16	4831.97	4890.67

Table A.13 (continued)

Sample No	Length I	Length II	Length III	Tp1 (mic.s)	Tp2 (mic.s)	Tp3 (mic.s)	Vpd1 (m/s)	Vpd2 (m/s)	Vpd3 (m/s)
6M-17	70.42	69.28	70.45	14.50	14.10	14.60	4856.55	4913.48	4825.34
6M-18	70.93	72.33	70.70	14.70	14.70	14.20	4825.17	4920.41	4978.87
6M-19	72.00	70.74	71.40	14.80	14.40	14.30	4864.86	4912.50	4993.01
6M-20	73.03	70.87	70.38	15.20	15.30	14.60	4804.61	4632.03	4820.55
6M-21	73.29	69.43	73.38	15.30	13.80	14.10	4790.20	5031.16	5204.26
6M-22	73.25	70.87	73.36	14.50	14.60	15.30	5051.72	4854.11	4794.77
6M-23	72.11	70.58	70.85	15.00	14.30	14.30	4807.33	4935.66	4954.55
6M-24	71.09	70.80	72.32	14.40	14.40	15.30	4936.81	4916.67	4726.80
6M-25	70.57	71.03	72.29	14.80	14.60	15.30	4768.24	4865.07	4724.84
6M-26	70.67	67.00	66.43	13.90	13.70	15.90	5084.17	4890.51	4177.99
6M-27	70.68	71.17	71.07	14.90	14.80	15.00	4743.62	4808.78	4738.00
6M-28	71.03	71.07	73.11	14.60	14.60	15.80	4865.07	4867.81	4627.22
6M-29	71.09	71.43	72.15	14.50	14.50	14.90	4902.76	4926.21	4842.28
6M-30	70.54	70.34	72.76	14.70	14.40	14.30	4798.64	4884.72	5088.11
6M-31	70.67	72.67	71.08	15.10	15.00	14.50	4680.13	4844.67	4902.07
6M-32	70.75	72.62	70.49	14.60	15.10	14.00	4845.89	4809.27	5035.00
6M-33	71.72	69.95	72.11	14.50	14.50	15.10	4946.21	4824.14	4775.50
6M-34	70.70	72.55	70.64	14.20	15.50	14.70	4978.87	4680.65	4805.44
6M-35	70.44	70.78	72.52	14.40	14.50	15.20	4891.67	4881.38	4771.05
6M-36	70.77	72.41	71.28	15.00	15.10	13.80	4718.00	4795.36	5165.22
6M-37	71.02	73.08	69.66	15.10	15.40	13.30	4703.31	4745.45	5237.59
6M-38	72.02	71.11	71.04	14.80	15.00	14.10	4866.22	4740.67	5038.30
6M-39	70.95	73.32	69.24	14.70	15.30	14.90	4826.53	4792.16	4646.98
6M-40	71.39	72.40	70.93	14.30	15.10	14.70	4992.31	4794.70	4825.17
6M-41	72.22	70.75	72.19	14.90	14.30	15.00	4846.98	4947.55	4812.67
6M-42	72.60	70.22	70.91	15.00	15.60	13.50	4840.00	4501.28	5252.59
6M-43	71.01	72.15	69.34	14.40	15.00	13.60	4931.25	4810.00	5098.53
6M-44	71.14	69.05	73.28	14.30	14.30	15.50	4974.83	4828.67	4727.74

Table A.14 Sonic velocity measurements of the saturated massive basalts

Sample No	Length I	Length II	Length III	Tp1 (mic.s)	Tp2 (mic.s)	Tp3 (mic.s)	Vpd1 (m/s)	Vpd2 (m/s)	Vpd3 (m/s)
1M-1	70.32	70.12	71.23	14.70	14.50	15.80	4783.67	4835.86	4508.23
1M-2	70.12	70.67	72.48	14.50	13.30	16.90	4835.86	5313.53	4288.76
1M-3	71.55	70.65	70.76	14.40	14.50	15.50	4968.75	4872.41	4565.16
1M-4	70.44	71.20	70.33	14.90	14.60	14.50	4727.52	4876.71	4850.34
1M-5	71.02	70.74	70.49	13.20	13.10	13.20	5380.30	5400.00	5340.15
1M-6	69.85	71.43	70.15	14.10	14.10	14.20	4953.90	5065.96	4940.14
1M-7	69.88	70.29	70.61	15.20	14.30	15.20	4597.37	4915.38	4645.39
1M-8	70.50	71.32	71.39	13.40	14.00	14.00	5261.19	5094.29	5099.29
1M-9	69.80	73.75	71.27	14.50	15.70	13.60	4813.79	4697.45	5240.44
1M-10	70.50	70.38	73.38	12.60	13.00	13.50	5595.24	5413.85	5435.56
1M-11	70.32	71.36	70.95	13.60	14.00	14.20	5170.59	5097.14	4996.48
1M-12	70.71	70.71	70.77	13.70	16.00	14.40	5161.31	4419.38	4914.58
1M-13	70.45	71.77	70.84	14.00	15.00	16.00	5032.14	4784.67	4427.50
1M-14	70.62	70.70	70.50	14.40	13.90	14.20	4904.17	5086.33	4964.79
1M-15	70.70	69.70	72.26	13.80	14.10	14.40	5123.19	4943.26	5018.06
1M-16	71.58	70.23	70.91	15.40	13.70	16.00	4648.05	5126.28	4431.88
1M-17	70.84	72.15	70.18	15.70	17.10	15.60	4512.10	4219.30	4498.72
1M-18	69.52	71.45	70.92	14.60	14.40	13.80	4761.64	4961.81	5139.13
1M-19	71.68	69.76	70.52	14.70	13.60	13.40	4876.19	5129.41	5262.69
1M-20	70.85	68.54	72.80	15.70	15.80	14.50	4512.74	4337.97	5020.69
1M-21	70.90	70.57	73.28	14.30	14.40	15.50	4958.04	4900.69	4727.74
1M-22	69.04	70.64	73.20	14.30	13.70	16.40	4827.97	5156.20	4463.41
1M-23	70.91	70.33	73.06	20.20	17.20	18.00	3510.40	4088.95	4058.89
1M-24	70.70	72.02	70.40	15.20	14.60	13.50	4651.32	4932.88	5214.81
1M-25	61.53	62.80	61.93	12.00	12.60	12.40	5127.50	4984.13	4994.35
1M-26	62.01	62.80	62.75	12.10	12.50	12.30	5124.79	5024.00	5101.63
1M-27	62.58	62.62	62.11	12.80	12.00	12.10	4889.06	5218.33	5133.06
1M-28	61.20	61.82	63.30	13.00	15.10	12.30	4707.69	4094.04	5146.34
1M-29	63.44	62.95	63.09	14.10	12.50	14.00	4499.29	5036.00	4506.43
1M-30	62.18	61.95	62.84	12.30	13.20	12.70	5055.28	4693.18	4948.03
1M-31	61.99	61.07	62.55	12.20	11.30	14.90	5081.15	5404.42	4197.99
1M-32	61.91	61.81	62.86	12.30	12.40	12.40	5033.33	4984.68	5069.35
1M-33	61.62	62.98	62.70	12.70	13.00	13.50	4851.97	4844.62	4644.44
1M-34	61.80	60.40	62.75	12.80	11.80	12.80	4828.13	5118.64	4902.34

Table A.14 (continued)

Sample No	Length I	Length II	Length III	Tp1 (mic.s)	Tp2 (mic.s)	Tp3 (mic.s)	Vpd1 (m/s)	Vpd2 (m/s)	Vpd3 (m/s)
1M-35	70.06	68.48	71.28	14.00	15.90	16.40	5004.29	4306.92	4346.34
1M-36	70.62	71.55	70.50	14.50	14.50	13.90	4870.34	4934.48	5071.94
1M-37	70.82	70.72	70.96	15.40	14.90	16.00	4598.70	4746.31	4435.00
1M-38	70.61	69.27	69.90	14.60	13.60	14.40	4836.30	5093.38	4854.17
2M-1	70.46	71.13	73.02	15.10	12.50	13.10	4666.23	5690.40	5574.05
2M-2	70.02	71.71	73.13	14.50	13.80	13.80	4828.97	5196.38	5299.28
2M-3	70.26	71.69	72.70	18.10	16.00	13.60	3881.77	4480.63	5345.59
2M-4	73.10	70.96	69.94	13.40	15.00	12.80	5455.22	4730.67	5464.06
2M-5	70.59	71.67	70.13	13.90	13.80	14.80	5078.42	5193.48	4738.51
2M-6	70.86	70.29	70.47	15.00	12.80	14.70	4724.00	5491.41	4793.88
2M-7	70.08	71.17	70.30	13.90	14.40	14.50	5041.73	4942.36	4848.28
2M-8	71.03	69.93	72.34	13.80	13.00	13.70	5147.10	5379.23	5280.29
2M-9	71.30	70.20	70.65	13.40	12.90	15.50	5320.90	5441.86	4558.06
2M-10	70.68	70.55	72.00	14.60	13.20	13.40	4841.10	5344.70	5373.13
2M-11	69.91	70.58	73.00	14.60	12.90	14.80	4788.36	5471.32	4932.43
2M-12	70.36	71.31	73.03	14.40	13.00	13.60	4886.11	5485.38	5369.85
2M-13	70.72	70.67	70.04	13.90	14.20	13.10	5087.77	4976.76	5346.56
2M-14	70.29	71.25	70.48	15.50	13.70	13.40	4534.84	5200.73	5259.70
2M-15	62.35	62.40	61.92	12.20	12.70	12.10	5110.66	4913.39	5117.36
2M-16	62.94	62.23	61.16	12.10	12.80	12.60	5201.65	4861.72	4853.97
2M-17	62.54	61.36	62.79	16.10	14.00	12.30	3884.47	4382.86	5104.88
2M-18	62.91	61.32	62.24	13.40	12.90	13.40	4694.78	4753.49	4644.78
2M-19	70.56	70.42	71.09	13.50	15.90	13.50	5226.67	4428.93	5265.93
2M-20	70.22	70.62	73.49	13.00	12.80	13.60	5401.54	5517.19	5403.68
4M-1	68.98	73.49	70.20	12.50	13.80	14.00	5518.40	5325.36	5014.29
4M-2	74.30	70.04	69.72	14.50	13.60	13.00	5124.14	5150.00	5363.08
4M-3	70.15	70.22	70.22	13.20	13.40	12.60	5314.39	5240.30	5573.02
4M-4	70.56	70.80	74.47	13.20	12.70	14.50	5345.45	5574.80	5135.86
4M-5	70.09	71.33	70.65	14.90	13.80	15.90	4704.03	5168.84	4443.40
4M-6	70.12	69.36	74.97	13.40	12.60	14.50	5232.84	5504.76	5170.34
4M-7	73.13	70.77	70.20	13.20	13.30	13.00	5540.15	5321.05	5400.00
4M-8	70.52	73.20	69.90	13.60	14.60	13.00	5185.29	5013.70	5376.92
4M-9	74.80	70.11	70.80	14.10	12.80	13.10	5304.96	5477.34	5404.58
4M-10	69.78	71.34	70.22	14.10	13.60	13.40	4948.94	5245.59	5240.30

Table A.14 (continued)

Sample No	Length I	Length II	Length III	Tp1 (mic.s)	Tp2 (mic.s)	Tp3 (mic.s)	Vpd1 (m/s)	Vpd2 (m/s)	Vpd3 (m/s)
4M-11	74.11	70.00	70.00	14.00	12.90	13.00	5293.57	5426.36	5384.62
4M-12	71.87	70.42	70.72	13.00	13.00	13.50	5528.46	5416.92	5238.52
4M-13	62.43	63.18	62.58	12.00	11.70	11.10	5202.50	5400.00	5637.84
4M-14	62.83	62.19	62.52	13.50	11.50	11.70	4654.07	5407.83	5343.59
4M-15	62.96	59.15	60.70	13.60	11.60	11.90	4629.41	5099.14	5100.84
4M-16	62.05	62.58	63.11	11.30	12.00	14.00	5491.15	5215.00	4507.86
4M-17	66.25	62.93	62.54	12.00	11.60	12.10	5520.83	5425.00	5168.60
4M-18	62.21	63.24	66.15	11.50	14.10	12.50	5409.57	4485.11	5292.00
4M-19	64.73	61.45	62.76	11.80	16.20	11.20	5485.59	3793.21	5603.57
4M-20	62.35	61.27	62.23	12.70	11.70	14.20	4909.45	5236.75	4382.39
4M-21	62.39	63.18	62.34	11.30	11.60	12.00	5521.24	5446.55	5195.00
4M-22	60.34	62.39	63.10	11.20	12.00	12.00	5387.50	5199.17	5258.33
4M-23	63.87	63.33	63.03	12.40	11.90	12.50	5150.81	5321.85	5042.40
4M-24	63.19	61.70	64.19	12.30	11.20	11.90	5137.40	5508.93	5394.12
4M-25	60.87	61.92	61.76	11.50	11.20	13.40	5293.04	5528.57	4608.96
4M-26	62.33	64.56	61.30	11.60	12.10	11.00	5373.28	5335.54	5572.73
4M-27	64.66	61.88	61.87	13.10	12.70	12.60	4935.88	4872.44	4910.32
4M-28	62.15	60.16	62.94	12.00	14.50	11.30	5179.17	4148.97	5569.91
6M-1	70.09	73.24	70.95	14.90	15.20	14.50	4704.03	4818.42	4893.10
6M-2	72.19	70.92	70.59	14.70	14.20	14.30	4910.88	4994.37	4936.36
6M-3	71.10	70.97	72.05	14.40	14.10	14.90	4937.50	5033.33	4835.57
6M-4	73.37	70.95	68.82	15.10	14.50	14.10	4858.94	4893.10	4880.85
6M-5	70.01	72.75	70.86	14.20	15.00	14.60	4930.28	4850.00	4853.42
6M-6	70.74	72.35	70.16	14.20	14.90	14.00	4981.69	4855.70	5011.43
6M-7	71.00	73.25	71.05	14.90	15.10	14.40	4765.10	4850.99	4934.03
6M-8	72.44	71.10	69.97	13.80	13.90	13.90	5249.28	5115.11	5033.81
6M-9	71.01	73.35	70.88	14.50	15.20	14.20	4897.24	4825.66	4991.55
6M-10	72.34	70.88	71.08	14.80	14.60	15.10	4887.84	4854.79	4707.28
6M-11	73.42	71.18	70.44	15.10	14.40	15.00	4862.25	4943.06	4696.00
6M-12	70.95	72.22	70.45	14.80	14.50	14.20	4793.92	4980.69	4961.27
6M-13	70.60	71.18	70.80	14.90	14.30	14.20	4738.26	4977.62	4985.92
6M-14	72.07	70.74	70.84	15.40	15.10	14.70	4679.87	4684.77	4819.05
6M-15	73.21	70.90	70.90	15.60	14.50	14.20	4692.95	4889.66	4992.96
6M-16	70.90	71.03	73.36	14.20	14.40	15.00	4992.96	4932.64	4890.67

Table A.14 (continued)

Sample No	Length I	Length II	Length III	Tp1 (mic.s)	Tp2 (mic.s)	Tp3 (mic.s)	Vpd1 (m/s)	Vpd2 (m/s)	Vpd3 (m/s)
6M-17	70.42	69.28	70.45	14.50	14.10	15.60	4856.55	4913.48	4516.03
6M-18	70.93	72.33	70.70	14.30	14.60	14.10	4960.14	4954.11	5014.18
6M-19	72.00	70.74	71.40	14.70	14.30	14.20	4897.96	4946.85	5028.17
6M-20	73.03	70.87	70.38	15.10	15.30	14.50	4836.42	4632.03	4853.79
6M-21	73.29	69.43	73.38	14.90	13.90	14.40	4918.79	4994.96	5095.83
6M-22	73.25	70.87	73.36	14.10	14.30	15.10	5195.04	4955.94	4858.28
6M-23	72.11	70.58	70.85	14.90	14.40	14.50	4839.60	4901.39	4886.21
6M-24	71.09	70.80	72.32	14.50	14.20	14.90	4902.76	4985.92	4853.69
6M-25	70.57	71.03	72.29	14.80	14.60	15.10	4768.24	4865.07	4787.42
6M-26	70.67	67.00	66.43	13.90	13.40	14.70	5084.17	5000.00	4519.05
6M-27	70.68	71.17	71.07	14.30	14.60	14.20	4942.66	4874.66	5004.93
6M-28	71.03	71.07	73.11	14.30	14.70	15.40	4967.13	4834.69	4747.40
6M-29	71.09	71.43	72.15	14.30	14.10	14.70	4971.33	5065.96	4908.16
6M-30	70.54	70.34	72.76	14.20	14.40	14.40	4967.61	4884.72	5052.78
6M-31	70.67	72.67	71.08	14.70	15.10	14.50	4807.48	4812.58	4902.07
6M-32	70.75	72.62	70.49	14.40	14.60	14.00	4913.19	4973.97	5035.00
6M-33	71.72	69.95	72.11	14.40	14.10	14.70	4980.56	4960.99	4905.44
6M-34	70.70	72.55	70.64	14.20	14.90	14.70	4978.87	4869.13	4805.44
6M-35	70.44	70.78	72.52	14.40	14.40	15.00	4891.67	4915.28	4834.67
6M-36	70.77	72.41	71.28	13.80	15.10	14.50	5128.26	4795.36	4915.86
6M-37	71.02	73.08	69.66	15.20	15.40	14.10	4672.37	4745.45	4940.43
6M-38	72.02	71.11	71.04	14.70	14.20	14.30	4899.32	5007.75	4967.83
6M-39	70.95	73.32	69.24	14.50	14.90	14.50	4893.10	4920.81	4775.17
6M-40	71.39	72.40	70.93	13.90	14.50	14.50	5135.97	4993.10	4891.72
6M-41	72.22	70.75	72.19	14.80	14.30	15.00	4879.73	4947.55	4812.67
6M-42	72.60	70.22	70.91	14.30	13.80	13.80	5076.92	5088.41	5138.41
6M-43	71.01	72.15	69.34	13.80	14.80	14.10	5145.65	4875.00	4917.73
6M-44	71.14	69.05	73.28	13.30	13.20	14.10	5348.87	5231.06	5197.16

Table A.15 Sonic velocity measurements of the dry vesicular basalt samples

Sample No	Length I	Length II	Length III	Tp1 (mic.s)	Tp2 (mic.s)	Tp3 (mic.s)	Vpd1 (m/s)	Vpd2 (m/s)	Vpd3 (m/s)
1V-1	71.10	71.33	70.00	17.80	15.90	15.40	3994.38	4486.16	4545.45
1V-2	71.60	70.61	70.73	17.20	16.90	14.90	4162.79	4178.11	4746.98
1V-3	70.59	70.90	70.83	15.50	15.80	15.10	4554.19	4487.34	4690.73
1V-4	70.41	72.53	69.46	15.60	17.70	16.00	4513.46	4097.74	4341.25
1V-5	70.91	70.50	69.50	15.20	15.70	16.50	4665.13	4490.45	4212.12
1V-6	70.39	70.84	69.92	16.00	15.60	19.20	4399.38	4541.03	3641.67
1V-7	69.81	71.17	70.64	13.90	16.90	15.80	5022.30	4211.24	4470.89
1V-8	70.73	72.04	69.84	14.90	16.10	14.50	4746.98	4474.53	4816.55
1V-9	68.60	69.53	70.74	19.00	17.30	18.80	3610.53	4019.08	3762.77
1V-10	71.86	70.21	69.55	19.40	20.10	16.20	3704.12	3493.03	4293.21
1V-11	70.54	69.50	70.73	15.60	15.10	16.60	4521.79	4602.65	4260.84
1V-12	70.82	69.71	72.44	19.00	15.50	17.80	3727.37	4497.42	4069.66
1V-13	70.69	71.18	70.98	13.90	15.80	16.80	5085.61	4505.06	4225.00
1V-14	70.40	69.81	70.69	16.40	15.60	17.60	4292.68	4475.00	4016.48
1V-15	71.61	70.53	69.76	16.40	16.30	16.70	4366.46	4326.99	4177.25
1V-16	69.53	70.47	72.81	13.60	15.70	16.70	5112.50	4488.54	4359.88
1V-17	69.17	69.87	70.61	14.80	15.00	14.50	4673.65	4658.00	4869.66
1V-18	70.36	71.30	70.76	15.80	16.60	15.80	4453.16	4295.18	4478.48
1V-19	71.79	70.11	69.91	15.50	14.60	16.00	4631.61	4802.05	4369.38
1V-20	70.31	69.96	70.37	15.60	15.10	16.90	4507.05	4633.11	4163.91
1V-21	70.37	69.76	71.16	16.40	16.50	17.90	4290.85	4227.88	3975.42
1V-22	70.51	72.29	69.73	14.40	17.20	17.20	4896.53	4202.91	4054.07
1V-23	70.71	70.60	70.75	15.80	16.00	16.70	4475.32	4412.50	4236.53
1V-24	70.44	69.58	72.27	15.20	15.30	16.40	4634.21	4547.71	4406.71
1V-25	70.55	70.62	69.75	15.90	17.40	15.80	4437.11	4058.62	4414.56
1V-26	71.35	68.20	70.16	14.90	15.00	17.70	4788.59	4546.67	3963.84
1V-27	71.33	70.03	71.14	15.40	15.90	16.10	4631.82	4404.40	4418.63
1V-28	70.67	70.73	72.74	16.20	16.60	17.10	4362.35	4260.84	4253.80
1V-29	70.71	73.26	69.51	15.90	17.00	18.00	4447.17	4309.41	3861.67
1V-30	71.40	69.85	70.70	16.40	15.90	17.80	4353.66	4393.08	3971.91
1V-31	70.45	70.58	71.19	14.00	15.90	16.50	5032.14	4438.99	4314.55
1V-32	71.42	70.66	70.70	15.40	16.70	18.20	4637.66	4231.14	3884.62
1V-33	70.42	69.76	72.17	15.10	17.50	20.20	4663.58	3986.29	3572.77
1V-34	70.90	70.89	68.22	16.50	14.50	15.30	4296.97	4888.97	4458.82

Table A.15 (continued)

Sample No	Length I	Length II	Length III	Tp1 (mic.s)	Tp2 (mic.s)	Tp3 (mic.s)	Vpd1 (m/s)	Vpd2 (m/s)	Vpd3 (m/s)
1V-35	70.14	72.68	71.48	17.90	15.70	16.20	3918.44	4629.30	4412.35
1V-36	72.19	69.94	70.46	17.00	18.20	17.70	4246.47	3842.86	3980.79
1V-37	70.94	71.63	70.99	15.70	16.80	15.70	4518.47	4263.69	4521.66
1V-38	72.07	70.56	70.03	14.60	14.50	16.20	4936.30	4866.21	4322.84
1V-39	70.34	69.66	70.38	15.30	16.60	17.60	4597.39	4196.39	3998.86
1V-40	71.45	69.70	70.48	14.60	16.00	14.80	4893.84	4356.25	4762.16
1V-41	70.60	72.50	70.40	15.80	15.90	15.80	4468.35	4559.75	4455.70
1V-42	70.75	70.57	70.26	16.20	14.50	16.40	4367.28	4866.90	4284.15
1V-43	70.20	71.10	70.55	15.50	15.80	16.90	4529.03	4500.00	4174.56
3V-1	70.77	71.12	71.36	17.50	14.80	16.00	4044.00	4805.41	4460.00
3V-2	70.66	70.55	71.24	17.60	15.40	16.10	4014.77	4581.17	4424.84
3V-3	70.49	70.87	72.48	16.40	16.40	16.00	4298.17	4321.34	4530.00
3V-4	71.00	70.74	72.39	16.80	15.00	16.60	4226.19	4716.00	4360.84
3V-5	70.42	70.98	70.87	18.00	16.00	16.00	3912.22	4436.25	4429.38
3V-6	70.93	70.97	75.92	17.50	19.60	20.60	4053.14	3620.92	3685.44
3V-7	70.77	70.82	72.14	14.90	16.10	18.10	4749.66	4398.76	3985.64
3V-8	70.83	71.82	70.84	15.70	15.70	15.30	4511.46	4574.52	4630.07
3V-9	71.22	70.53	71.83	16.40	15.00	15.90	4342.68	4702.00	4517.61
3V-10	69.87	70.64	79.76	15.40	16.50	15.40	4537.01	4281.21	5179.22
3V-11	71.16	70.93	72.34	17.80	16.60	17.20	3997.75	4272.89	4205.81
3V-12	70.55	70.75	72.56	21.00	14.60	15.80	3359.52	4845.89	4592.41
3V-13	70.69	72.72	70.83	17.80	16.10	16.00	3971.35	4516.77	4426.88
3V-14	71.34	71.09	71.27	19.40	17.60	16.30	3677.32	4039.20	4372.39
3V-15	70.55	70.73	72.43	17.80	18.40	16.10	3963.48	3844.02	4498.76
3V-16	73.02	70.92	70.58	16.10	16.20	16.50	4535.40	4377.78	4277.58
3V-17	70.82	70.86	72.04	18.40	17.40	18.30	3848.91	4072.41	3936.61
3V-18	70.53	72.72	70.92	18.40	17.50	15.70	3833.15	4155.43	4517.20
3V-19	70.80	71.95	70.57	16.45	15.80	14.40	4303.95	4553.80	4900.69
3V-20	70.61	72.03	70.96	17.10	16.50	16.10	4129.24	4365.45	4407.45
3V-21	72.95	70.48	70.92	16.40	16.40	18.40	4448.17	4297.56	3854.35
3V-22	70.65	72.64	71.08	18.40	16.30	16.30	3839.67	4456.44	4360.74
3V-23	70.71	70.98	72.07	16.90	16.10	16.70	4184.02	4408.70	4315.57
3V-24	71.02	73.45	70.45	16.90	16.40	15.30	4202.37	4478.66	4604.58
3V-25	70.85	70.65	72.15	15.40	17.40	16.40	4600.65	4060.34	4399.39

Table A.15 (continued)

Sample No	Length I	Length II	Length III	Tp1 (mic.s)	Tp2 (mic.s)	Tp3 (mic.s)	Vpd1 (m/s)	Vpd2 (m/s)	Vpd3 (m/s)
3V-26	70.37	69.93	71.55	18.30	16.00	16.10	3845.36	4370.63	4444.10
3V-27	71.49	71.04	71.22	15.50	16.40	16.30	4612.26	4331.71	4369.33
3V-28	72.62	70.91	71.04	16.30	17.60	16.30	4455.21	4028.98	4358.28
3V-29	70.54	71.04	71.31	15.60	15.40	15.40	4521.79	4612.99	4630.52
3V-30	71.94	70.06	70.88	17.30	18.10	16.20	4158.38	3870.72	4375.31
3V-31	71.03	70.42	70.83	16.30	19.00	18.40	4357.67	3706.32	3849.46
3V-32	69.44	70.96	73.02	16.90	17.40	16.20	4108.88	4078.16	4507.41
3V-33	70.89	71.06	70.76	17.80	16.60	15.60	3982.58	4280.72	4535.90
3V-34	70.42	71.03	72.76	19.10	17.00	16.80	3686.91	4178.24	4330.95
3V-35	71.37	71.89	71.07	18.80	16.50	14.60	3796.28	4356.97	4867.81
3V-36	71.26	72.15	71.08	16.70	17.70	16.60	4267.07	4076.27	4281.93
3V-37	70.91	71.44	72.40	19.00	15.40	16.30	3732.11	4638.96	4441.72
3V-38	70.09	70.71	71.45	16.50	18.10	16.40	4247.88	3906.63	4356.71
3V-39	69.00	71.00	70.97	15.40	17.80	15.90	4480.52	3988.76	4463.52
3V-40	70.71	71.20	70.30	16.40	16.80	17.30	4311.59	4238.10	4063.58
3V-41	70.45	69.61	70.19	16.70	15.90	17.60	4218.56	4377.99	3988.07
3V-42	70.42	71.90	70.94	20.50	16.50	16.40	3435.12	4357.58	4325.61
3V-43	70.87	71.67	70.58	17.10	17.20	15.80	4144.44	4166.86	4467.09
5V-1	71.01	70.67	69.40	17.30	18.10	17.10	4104.62	3904.42	4058.48
5V-2	70.70	69.40	70.69	18.50	18.30	18.40	3821.62	3792.35	3841.85
5V-3	69.60	71.10	70.11	17.30	17.20	16.70	4023.12	4133.72	4198.20
5V-4	71.27	71.15	71.07	18.30	18.10	17.90	3894.54	3930.94	3970.39
5V-5	69.45	71.25	70.70	17.10	19.40	18.10	4061.40	3672.68	3906.08
5V-6	70.84	70.98	69.40	19.40	19.50	18.30	3651.55	3640.00	3792.35
5V-7	70.82	70.92	69.40	19.50	19.50	19.30	3631.79	3636.92	3595.85
5V-8	70.84	70.92	69.42	17.20	20.50	16.60	4118.60	3459.51	4181.93
5V-9	69.40	70.77	70.94	18.00	17.00	17.10	3855.56	4162.94	4148.54
5V-10	70.84	69.24	70.79	18.10	18.00	18.00	3913.81	3846.67	3932.78
5V-11	70.86	69.46	70.76	18.00	17.90	17.20	3936.67	3880.45	4113.95
5V-12	70.83	70.80	69.50	19.30	18.70	18.60	3669.95	3786.10	3736.56
5V-13	71.13	70.96	71.03	18.80	17.90	18.80	3783.51	3964.25	3778.19
5V-14	69.42	71.17	70.88	17.30	16.90	17.80	4012.72	4211.24	3982.02
5V-15	71.05	70.69	69.44	19.90	19.40	21.00	3570.35	3643.81	3306.67
5V-16	70.47	71.65	71.27	20.10	19.40	19.90	3505.97	3693.30	3581.41

Table A.15 (continued)

Sample No	Length I	Length II	Length III	Tp1 (mic.s)	Tp2 (mic.s)	Tp3 (mic.s)	Vpd1 (m/s)	Vpd2 (m/s)	Vpd3 (m/s)
5V-17	71.05	71.26	69.55	19.50	18.90	19.10	3643.59	3770.37	3641.36
5V-18	71.51	71.02	69.40	19.60	19.40	18.50	3648.47	3660.82	3751.35
5V-19	71.49	69.55	70.98	17.40	17.50	18.50	4108.62	3974.29	3836.76
5V-20	71.18	70.86	70.70	17.00	17.90	17.50	4187.06	3958.66	4040.00
5V-21	70.99	69.70	70.72	18.10	18.50	18.30	3922.10	3767.57	3864.48
5V-22	71.20	71.04	71.23	19.00	18.40	18.90	3747.37	3860.87	3768.78
5V-23	69.71	71.17	70.93	18.10	19.10	19.00	3851.38	3726.18	3733.16
5V-24	71.06	70.54	71.02	20.10	19.50	19.50	3535.32	3617.44	3642.05
5V-25	70.79	70.80	70.24	19.80	18.90	18.50	3575.25	3746.03	3796.76
5V-26	70.88	70.98	69.54	18.30	18.80	17.50	3873.22	3775.53	3973.71
5V-27	71.14	71.07	70.12	20.10	20.20	19.70	3539.30	3518.32	3559.39
5V-28	71.13	70.21	71.05	17.80	16.50	17.90	3996.07	4255.15	3969.27
5V-29	71.02	71.15	70.94	19.50	19.20	19.20	3642.05	3705.73	3694.79
5V-30	71.19	71.02	71.40	18.30	17.90	18.90	3890.16	3967.60	3777.78
5V-31	71.02	70.95	69.52	19.50	20.00	19.40	3642.05	3547.50	3583.51
5V-32	70.95	69.42	71.09	17.90	17.60	17.80	3963.69	3944.32	3993.82
5V-33	71.04	71.34	69.23	18.90	19.80	17.80	3758.73	3603.03	3889.33
5V-34	69.21	70.91	70.93	19.70	19.70	19.80	3513.20	3599.49	3582.32
5V-35	69.41	71.03	71.03	17.10	17.60	17.10	4059.06	4035.80	4153.80
5V-36	69.36	70.92	70.79	17.80	19.00	18.80	3896.63	3732.63	3765.43
5V-37	71.10	69.61	70.88	19.20	18.10	17.90	3703.13	3845.86	3959.78
5V-38	70.85	70.85	69.35	18.10	17.20	17.20	3914.36	4119.19	4031.98
5V-39	71.17	71.07	69.90	18.00	17.40	16.60	3953.89	4084.48	4210.84
5V-40	70.75	69.48	70.55	18.40	18.50	18.70	3845.11	3755.68	3772.73
5V-41	71.23	71.22	70.86	17.90	18.80	17.70	3979.33	3788.30	4003.39
5V-42	69.31	70.82	70.72	19.40	20.10	18.40	3572.68	3523.38	3843.48
5V-43	71.09	70.91	70.59	18.90	17.60	19.60	3761.38	4028.98	3601.53
5V-44	71.15	70.72	70.59	19.30	19.00	19.80	3686.53	3722.11	3565.15

Table A.16 Sonic velocity measurements of the saturated vesicular basalt samples

Sample No	Length I	Length II	Length III	Tp1 (mic.s)	Tp2 (mic.s)	Tp3 (mic.s)	Vpd1 (m/s)	Vpd2 (m/s)	Vpd3 (m/s)
1V-1	71.10	71.33	70.00	14.00	14.20	14.50	5078.57	5023.24	4827.59
1V-2	71.60	70.61	70.73	14.40	13.70	13.30	4972.22	5154.01	5318.05
1V-3	70.59	70.90	70.83	13.60	13.80	13.30	5190.44	5137.68	5325.56
1V-4	70.41	72.53	69.46	14.40	14.50	14.50	4889.58	5002.07	4790.34
1V-5	70.91	70.50	69.50	14.40	14.70	15.90	4924.31	4795.92	4371.07
1V-6	70.39	70.84	69.92	14.30	13.60	13.70	4922.38	5208.82	5103.65
1V-7	69.81	71.17	70.64	13.20	14.60	13.30	5288.64	4874.66	5311.28
1V-8	70.73	72.04	69.84	14.10	14.00	13.50	5016.31	5145.71	5173.33
1V-9	68.60	69.53	70.74	14.40	13.90	14.20	4763.89	5002.16	4981.69
1V-10	71.86	70.21	69.55	13.80	14.20	13.50	5207.25	4944.37	5151.85
1V-11	70.54	69.50	70.73	13.80	14.20	15.20	5111.59	4894.37	4653.29
1V-12	70.82	69.71	72.44	14.20	13.40	14.40	4987.32	5202.24	5030.56
1V-13	70.69	71.18	70.98	13.10	13.80	13.20	5396.18	5157.97	5377.27
1V-14	70.40	69.81	70.69	14.20	13.60	13.90	4957.75	5133.09	5085.61
1V-15	71.61	70.53	69.76	14.20	13.70	13.00	5042.96	5148.18	5366.15
1V-16	69.53	70.47	72.81	13.00	13.70	14.70	5348.46	5143.80	4953.06
1V-17	69.17	69.87	70.61	13.30	13.90	13.60	5200.75	5026.62	5191.91
1V-18	70.36	71.30	70.76	13.60	14.30	13.10	5173.53	4986.01	5401.53
1V-19	71.79	70.11	69.91	14.40	13.80	13.50	4985.42	5080.43	5178.52
1V-20	70.31	69.96	70.37	14.20	14.20	13.60	4951.41	4926.76	5174.26
1V-21	70.37	69.76	71.16	13.40	13.40	14.10	5251.49	5205.97	5046.81
1V-22	70.51	72.29	69.73	14.60	15.10	13.50	4829.45	4787.42	5165.19
1V-23	70.71	70.60	70.75	14.90	14.10	14.00	4745.64	5007.09	5053.57
1V-24	70.44	69.58	72.27	13.70	14.10	14.10	5141.61	4934.75	5125.53
1V-25	70.55	70.62	69.75	14.40	14.70	13.90	4899.31	4804.08	5017.99
1V-26	71.35	68.20	70.16	14.30	13.70	15.70	4989.51	4978.10	4468.79
1V-27	71.33	70.03	71.14	14.10	13.00	13.40	5058.87	5386.92	5308.96
1V-28	70.67	70.73	72.74	13.40	14.30	14.40	5273.88	4946.15	5051.39
1V-29	70.71	73.26	69.51	13.70	14.80	12.90	5161.31	4950.00	5388.37
1V-30	71.40	69.85	70.70	14.50	13.20	14.20	4924.14	5291.67	4978.87
1V-31	70.45	70.58	71.19	14.20	13.80	13.60	4961.27	5114.49	5234.56
1V-32	71.42	70.66	70.70	14.30	14.00	14.10	4994.41	5047.14	5014.18
1V-33	70.42	69.76	72.17	14.10	13.20	13.90	4994.33	5284.85	5192.09
1V-34	70.90	70.89	68.22	13.40	13.70	14.40	5291.04	5174.45	4737.50

Table A.16 (continued)

Sample No	Length I	Length II	Length III	Tp1 (mic.s)	Tp2 (mic.s)	Tp3 (mic.s)	Vpd1 (m/s)	Vpd2 (m/s)	Vpd3 (m/s)
1V-35	70.14	72.68	71.48	14.20	14.20	13.70	4939.44	5118.31	5217.52
1V-36	72.19	69.94	70.46	15.50	13.80	14.00	4657.42	5068.12	5032.86
1V-37	70.94	71.63	70.99	13.70	14.30	13.80	5178.10	5009.09	5144.20
1V-38	72.07	70.56	70.03	14.40	15.00	13.30	5004.86	4704.00	5265.41
1V-39	70.34	69.66	70.38	13.60	14.50	14.20	5172.06	4804.14	4956.34
1V-40	71.45	69.70	70.48	13.70	14.00	13.40	5215.33	4978.57	5259.70
1V-41	70.60	72.50	70.40	13.60	14.60	13.40	5191.18	4965.75	5253.73
1V-42	70.75	70.57	70.26	14.20	14.00	13.90	4982.39	5040.71	5054.68
1V-43	70.20	71.10	70.55	13.70	14.00	14.00	5124.09	5078.57	5039.29
3V-1	70.77	71.12	71.36	16.40	14.90	14.90	4315.24	4773.15	4789.26
3V-2	70.66	70.55	71.24	17.20	15.30	15.60	4108.14	4611.11	4566.67
3V-3	70.49	70.87	72.48	15.90	15.40	15.70	4433.33	4601.95	4616.56
3V-4	71.00	70.74	72.39	16.50	14.90	16.00	4303.03	4747.65	4524.38
3V-5	70.42	70.98	70.87	17.20	16.40	15.80	4094.19	4328.05	4485.44
3V-6	70.93	70.97	75.92	15.90	17.20	16.80	4461.01	4126.16	4519.05
3V-7	70.77	70.82	72.14	14.60	15.00	16.20	4847.26	4721.33	4453.09
3V-8	70.83	71.82	70.84	15.60	15.50	15.60	4540.38	4633.55	4541.03
3V-9	71.22	70.53	71.83	14.60	15.50	15.40	4878.08	4550.32	4664.29
3V-10	69.87	70.64	79.76	14.50	16.00	15.00	4818.62	4415.00	5317.33
3V-11	71.16	70.93	72.34	16.40	15.40	15.40	4339.02	4605.84	4697.40
3V-12	70.55	70.75	72.56	17.40	14.40	15.40	4054.60	4913.19	4711.69
3V-13	70.69	72.72	70.83	17.00	16.60	15.00	4158.24	4380.72	4722.00
3V-14	71.34	71.09	71.27	17.50	16.10	15.60	4076.57	4415.53	4568.59
3V-15	70.55	70.73	72.43	14.70	15.30	15.00	4799.32	4622.88	4828.67
3V-16	73.02	70.92	70.58	15.70	15.90	16.10	4650.96	4460.38	4383.85
3V-17	70.82	70.86	72.04	17.10	15.40	17.10	4141.52	4601.30	4212.87
3V-18	70.53	72.72	70.92	16.30	16.40	16.90	4326.99	4434.15	4196.45
3V-19	70.80	71.95	70.57	14.80	15.10	14.90	4783.78	4764.90	4736.24
3V-20	70.61	72.03	70.96	16.90	15.80	16.30	4178.11	4558.86	4353.37
3V-21	72.95	70.48	70.92	15.40	15.00	17.50	4737.01	4698.67	4052.57
3V-22	70.65	72.64	71.08	16.40	15.40	15.30	4307.93	4716.88	4645.75
3V-23	70.71	70.98	72.07	15.40	15.40	15.90	4591.56	4609.09	4532.70
3V-24	71.02	73.45	70.45	15.50	15.00	14.50	4581.94	4896.67	4858.62
3V-25	70.85	70.65	72.15	15.70	17.30	15.30	4512.74	4083.82	4715.69

Table A.16 (continued)

Sample No	Length I	Length II	Length III	Tp1 (mic.s)	Tp2 (mic.s)	Tp3 (mic.s)	Vpd1 (m/s)	Vpd2 (m/s)	Vpd3 (m/s)
3V-26	70.37	69.93	71.55	17.10	16.00	15.50	4115.20	4370.63	4616.13
3V-27	71.49	71.04	71.22	15.40	15.40	15.70	4642.21	4612.99	4536.31
3V-28	72.62	70.91	71.04	16.00	16.40	15.80	4538.75	4323.78	4496.20
3V-29	70.54	71.04	71.31	15.70	15.30	15.70	4492.99	4643.14	4542.04
3V-30	71.94	70.06	70.88	16.20	17.50	16.10	4440.74	4003.43	4402.48
3V-31	71.03	70.42	70.83	16.10	17.40	16.40	4411.80	4047.13	4318.90
3V-32	69.44	70.96	73.02	14.50	17.20	16.10	4788.97	4125.58	4535.40
3V-33	70.89	71.06	70.76	16.70	15.80	15.10	4244.91	4497.47	4686.09
3V-34	70.42	71.03	72.76	17.00	16.00	15.70	4142.35	4439.38	4634.39
3V-35	71.37	71.89	71.07	16.30	15.40	14.60	4378.53	4668.18	4867.81
3V-36	71.26	72.15	71.08	16.00	17.00	15.90	4453.75	4244.12	4470.44
3V-37	70.91	71.44	72.40	17.70	15.60	15.40	4006.21	4579.49	4701.30
3V-38	70.09	70.71	71.45	15.60	16.60	17.00	4492.95	4259.64	4202.94
3V-39	69.00	71.00	70.97	14.20	17.70	15.60	4859.15	4011.30	4549.36
3V-40	70.71	71.20	70.30	15.10	16.40	16.30	4682.78	4341.46	4312.88
3V-41	70.45	69.61	70.19	16.40	16.60	16.30	4295.73	4193.37	4306.13
3V-42	70.42	71.90	70.94	17.80	15.10	15.30	3956.18	4761.59	4636.60
3V-43	70.87	71.67	70.58	16.10	15.80	15.00	4401.86	4536.08	4705.33
5V-1	71.01	70.67	69.40	15.80	16.00	15.60	4494.30	4416.88	4448.72
5V-2	70.70	69.40	70.69	16.40	16.40	17.10	4310.98	4231.71	4133.92
5V-3	69.60	71.10	70.11	17.10	15.50	15.20	4070.18	4587.10	4612.50
5V-4	71.27	71.15	71.07	16.80	16.00	16.30	4242.26	4446.88	4360.12
5V-5	69.45	71.25	70.70	15.90	16.40	16.30	4367.92	4344.51	4337.42
5V-6	70.84	70.98	69.40	16.60	16.70	16.10	4267.47	4250.30	4310.56
5V-7	70.82	70.92	69.40	17.80	17.60	17.30	3978.65	4029.55	4011.56
5V-8	70.84	70.92	69.42	16.00	16.10	15.60	4427.50	4404.97	4450.00
5V-9	69.40	70.77	70.94	16.40	15.90	15.80	4231.71	4450.94	4489.87
5V-10	70.84	69.24	70.79	16.70	16.30	16.90	4241.92	4247.85	4188.76
5V-11	70.86	69.46	70.76	16.10	16.00	15.90	4401.24	4341.25	4450.31
5V-12	70.83	70.80	69.50	17.50	18.10	18.00	4047.43	3911.60	3861.11
5V-13	71.13	70.96	71.03	18.00	17.20	16.40	3951.67	4125.58	4331.10
5V-14	69.42	71.17	70.88	15.40	15.60	15.70	4507.79	4562.18	4514.65
5V-15	71.05	70.69	69.44	17.80	17.60	17.90	3991.57	4016.48	3879.33
5V-16	70.47	71.65	71.27	15.40	15.80	13.20	4575.97	4534.81	5399.24

Table A.16 (continued)

Sample No	Length I	Length II	Length III	Tp1 (mic.s)	Tp2 (mic.s)	Tp3 (mic.s)	Vpd1 (m/s)	Vpd2 (m/s)	Vpd3 (m/s)
5V-17	71.05	71.26	69.55	17.20	16.80	16.20	4130.81	4241.67	4293.21
5V-18	71.51	71.02	69.40	16.90	16.30	16.30	4231.36	4357.06	4257.67
5V-19	71.49	69.55	70.98	16.30	16.60	16.80	4385.89	4189.76	4225.00
5V-20	71.18	70.86	70.70	16.20	16.20	15.40	4393.83	4374.07	4590.91
5V-21	70.99	69.70	70.72	16.60	16.20	15.90	4276.51	4302.47	4447.80
5V-22	71.20	71.04	71.23	16.40	16.20	16.90	4341.46	4385.19	4214.79
5V-23	69.71	71.17	70.93	16.40	16.80	15.50	4250.61	4236.31	4576.13
5V-24	71.06	70.54	71.02	16.40	16.80	16.30	4332.93	4198.81	4357.06
5V-25	70.79	70.80	70.24	17.40	16.90	16.70	4068.39	4189.35	4205.99
5V-26	70.88	70.98	69.54	15.80	16.30	16.20	4486.08	4354.60	4292.59
5V-27	71.14	71.07	70.12	17.40	17.90	16.20	4088.51	3970.39	4328.40
5V-28	71.13	70.21	71.05	15.40	16.70	15.60	4618.83	4204.19	4554.49
5V-29	71.02	71.15	70.94	17.20	18.40	15.70	4129.07	3866.85	4518.47
5V-30	71.19	71.02	71.40	16.40	15.80	15.60	4340.85	4494.94	4576.92
5V-31	71.02	70.95	69.52	17.00	17.80	15.40	4177.65	3985.96	4514.29
5V-32	70.95	69.42	71.09	16.60	16.80	16.60	4274.10	4132.14	4282.53
5V-33	71.04	71.34	69.23	16.40	16.40	15.80	4331.71	4350.00	4381.65
5V-34	69.21	70.91	70.93	16.40	17.60	17.80	4220.12	4028.98	3984.83
5V-35	69.41	71.03	71.03	15.40	15.80	15.90	4507.14	4495.57	4467.30
5V-36	69.36	70.92	70.79	16.20	16.70	16.70	4281.48	4246.71	4238.92
5V-37	71.10	69.61	70.88	17.20	16.80	16.00	4133.72	4143.45	4430.00
5V-38	70.85	70.85	69.35	16.10	16.30	16.80	4400.62	4346.63	4127.98
5V-39	71.17	71.07	69.90	16.10	15.90	15.40	4420.50	4469.81	4538.96
5V-40	70.75	69.48	70.55	17.80	17.10	16.30	3974.72	4063.16	4328.22
5V-41	71.23	71.22	70.86	17.20	17.50	17.30	4141.28	4069.71	4095.95
5V-42	69.31	70.82	70.72	17.40	17.80	17.80	3983.33	3978.65	3973.03
5V-43	71.09	70.91	70.59	16.90	16.80	16.30	4206.51	4220.83	4330.67
5V-44	71.15	70.72	70.59	17.60	17.00	17.40	4042.61	4160.00	4056.90

Table A.17 Uniaxial compressive strength of the vesicular basalt samples for isotropy measurements (parallel to the flow direction)

Sample No	Area (cm²)	Failure Load (Kgf)	Uniaxial Compressive Strength (MPa)
I-1	49.45	41235.20	81.78
I-2	51.17	47365.27	90.78
I-3	52.25	40393.18	75.82
I-4	51.58	32869.20	62.50
I-5	49.86	34764.70	68.37
I-6	49.96	57385.20	112.64
I-7	48.95	37692.50	75.51
I-8	50.17	48314.60	94.44
I-9	49.89	31219.80	61.37
I-10	50.25	34745.50	67.81

Table A.18 Uniaxial compressive strength of the vesicular basalt samples for isotropy measurements (perpendicular to the flow direction)

Sample No	Area (cm²)	Failure Load (Kgf)	Uniaxial Compressive Strength (MPa)
I-11	50.71	27618.40	53.41
I-12	49.83	26176.90	51.52
I-13	54.55	28768.20	51.72
I-14	51.00	27683.40	53.23
I-15	49.76	20318.20	40.04
I-16	49.74	28812.50	56.81
I-17	49.79	29849.30	58.79
I-18	51.33	26318.70	50.29
I-19	50.69	21792.40	42.16
I-20	49.82	27745.50	54.62

Table A.19 Dry sonic velocity of the vesicular basalt samples for isotropy measurements (parallel to the flow direction)

Sample No	Length	Tp (mic.sec)	Vpd (m/s)
I-1	70.66	19.9	3550.75
I-2	70.91	15.3	4634.64
I-3	69.3	16.3	4251.53
I-4	71.01	15.9	4466.03
I-5	70.9	15.3	4633.98
I-6	71.45	16.3	4383.43
I-7	70.9	17.6	4028.40
I-8	70.69	18.8	3760.10
I-9	69.37	18.1	3832.59
I-10	70.14	15.5	4525.16

Table A.20 Dry sonic velocity of the vesicular basalt samples for isotropy measurements (perpendicular to the flow direction)

Sample No	Length	Tp (mic.sec)	Vpd (m/s)
I-11	70.5	20.3	3472.90
I-12	72.39	17.7	4089.83
I-13	70.78	19.9	3556.78
I-14	70.81	18.9	3746.56
I-15	70.62	18.8	3756.38
I-16	69.27	18	3848.33
I-17	69.4	16.9	4106.50
I-18	70.71	18.8	3760.10
I-19	70.61	18.1	3832.59
I-20	70.18	15.5	4525.16

Table A.21 Saturated sonic velocity of the vesicular basalt samples for isotropy measurements (parallel to the flow direction)

Sample No	Length	Tp (mic.sec)	Vpd (m/s)
I-1	70.66	17.20	4108.14
I-2	70.91	14.70	4823.81
I-3	69.3	14.40	4812.50
I-4	71.01	15.30	4641.18
I-5	70.9	14.70	4823.13
I-6	71.45	15.90	4493.71
I-7	70.9	17.20	4122.09
I-8	70.69	16.80	4207.74
I-9	69.37	16.50	4204.24
I-10	70.14	14.80	4739.19

Table A.22 Saturated sonic velocity of the vesicular basalt samples for isotropy measurements (perpendicular to the flow direction)

Sample No	Length	Tp (mic.sec)	Vpd (m/s)
I-11	70.50	17.10	4122.81
I-12	72.39	15.80	4581.65
I-13	70.78	19.20	3686.46
I-14	70.81	18.20	3890.66
I-15	70.62	17.50	4035.43
I-16	69.27	16.30	4249.69
I-17	69.4	17.00	4082.35
I-18	70.71	16.90	4184.02
I-19	70.61	17.50	4034.86
I-20	70.18	17.80	3942.70

Table A.23 Saturation coefficient of the massive basalt samples

Sample No	Water abs. by weight (under atm. pres.)	Water abs. by weight (under vacuum pres.)	Saturation Coefficient
	(%) (1)	(%) (2)	(S) (1)/(2)
1M-1	0.75	1.86	0.40
1M-2	0.65	1.66	0.39
1M-3	1.08	2.15	0.50
1M-4	1.35	2.73	0.50
1M-5	0.54	1.47	0.37
1M-6	1.43	2.81	0.51
1M-7	1.51	2.67	0.57
1M-8	0.97	2.09	0.46
1M-9	0.80	1.79	0.45
1M-10	0.33	1.34	0.25
1M-11	0.88	2.01	0.43
1M-12	1.11	2.20	0.50
1M-13	1.47	2.66	0.55
1M-14	1.30	2.47	0.53
1M-15	0.97	1.83	0.53
1M-16	0.56	1.59	0.35
1M-17	0.59	1.48	0.40
1M-18	1.14	1.93	0.59
1M-19	0.53	1.45	0.37
1M-20	1.10	1.83	0.60
1M-21	0.64	1.50	0.43
1M-22	0.59	1.51	0.39
1M-23	1.17	2.00	0.58
1M-24	0.65	1.53	0.43
1M-25	1.44	2.77	0.52
1M-26	1.35	2.51	0.54
1M-27	0.54	2.31	0.23
1M-28	1.31	2.46	0.53
1M-29	0.71	2.21	0.32
1M-30	1.16	2.18	0.53
1M-31	0.38	2.04	0.19
1M-32	1.25	2.48	0.51
1M-33	1.33	2.52	0.53
1M-34	1.60	2.65	0.60

Table A.23 (continued)

Sample No	Water abs. by weight (under atm. pres.)	Water abs. by weight (under vacuum pres.)	Saturation Coefficient
	(%) (1)	(%) (2)	(S) (1)/(2)
1M-35	0.46	1.70	0.27
1M-36	1.35	2.58	0.52
1M-37	1.20	2.34	0.51
1M-38	1.65	2.62	0.63
2M-1	0.63	1.63	0.38
2M-2	1.06	1.55	0.68
2M-3	0.73	1.70	0.43
2M-4	0.74	1.73	0.43
2M-5	0.68	1.86	0.37
2M-6	0.80	1.81	0.44
2M-7	0.65	1.80	0.36
2M-8	0.90	1.98	0.45
2M-9	0.69	2.07	0.33
2M-10	0.74	1.94	0.38
2M-11	0.74	1.77	0.42
2M-12	0.72	1.84	0.39
2M-13	0.62	1.92	0.32
2M-14	0.80	1.96	0.41
2M-15	0.75	2.51	0.30
2M-16	1.07	2.95	0.36
2M-17	0.64	2.47	0.26
2M-18	0.79	2.59	0.30
2M-19	0.77	1.93	0.40
2M-20	0.73	1.82	0.40
4M-1	0.47	1.73	0.27
4M-2	0.51	1.72	0.30
4M-3	0.34	1.67	0.20
4M-4	0.52	1.74	0.30
4M-5	0.73	1.92	0.38
4M-6	0.44	1.69	0.26
4M-7	0.44	1.72	0.26
4M-8	0.44	1.70	0.26
4M-9	0.59	1.74	0.34
4M-10	0.61	1.85	0.33

Table A.23 (continued)

Sample No	Water abs. by weight (under atm. pres.)	Water abs. by weight (under vacuum pres.)	Saturation Coefficient
	(%) (1)	(%) (2)	(S) (1)/(2)
4M-11	0.52	1.72	0.30
4M-12	0.52	1.83	0.29
4M-13	0.62	2.36	0.26
4M-14	0.69	2.64	0.26
4M-15	0.74	2.61	0.28
4M-16	0.59	2.60	0.23
4M-17	0.70	2.32	0.30
4M-18	0.83	2.43	0.34
4M-19	0.70	2.52	0.28
4M-20	0.84	3.14	0.27
4M-21	0.59	2.35	0.25
4M-22	0.67	2.43	0.27
4M-23	0.84	2.54	0.33
4M-24	0.83	2.58	0.32
4M-25	0.79	2.58	0.31
4M-26	0.73	2.45	0.30
4M-27	0.96	2.74	0.35
4M-28	0.80	2.67	0.30
6M-1	1.00	2.03	0.50
6M-2	1.15	2.75	0.42
6M-3	1.01	2.64	0.38
6M-4	0.92	2.60	0.35
6M-5	1.02	2.66	0.38
6M-6	1.20	2.80	0.43
6M-7	1.05	2.58	0.41
6M-8	0.96	2.68	0.36
6M-9	0.81	2.62	0.31
6M-10	1.04	2.76	0.38
6M-11	0.79	2.56	0.31
6M-12	0.83	2.61	0.32
6M-13	0.95	2.66	0.36
6M-14	1.30	2.77	0.47
6M-15	0.90	2.56	0.35
6M-16	0.99	2.65	0.38

Table A.23 (continued)

Sample No	Water abs. by weight	Water abs. by weight	Saturation
	(under atm. pres.)	(under vacuum pres.)	Coefficient
	(%) (1)	(%) (2)	(S) (1)/(2)
6M-17	0.90	2.66	0.34
6M-18	0.83	2.64	0.31
6M-19	1.08	2.78	0.39
6M-20	1.07	2.54	0.42
6M-21	1.01	2.72	0.37
6M-22	0.93	2.69	0.35
6M-23	0.94	2.59	0.36
6M-24	0.96	2.70	0.36
6M-25	1.13	2.30	0.49
6M-26	1.01	2.73	0.37
6M-27	0.99	2.64	0.38
6M-28	0.90	2.55	0.35
6M-29	0.98	2.75	0.36
6M-30	1.01	2.44	0.41
6M-31	1.36	3.08	0.44
6M-32	1.19	2.87	0.42
6M-33	1.32	2.86	0.46
6M-34	1.28	3.38	0.38
6M-35	1.03	2.74	0.37
6M-36	1.32	3.14	0.42
6M-37	1.27	2.67	0.48
6M-38	1.01	2.61	0.39
6M-39	0.99	2.70	0.37
6M-40	1.16	2.80	0.42
6M-41	1.00	2.63	0.38
6M-42	0.87	2.06	0.42
6M-43	1.03	2.57	0.40
6M-44	0.96	2.64	0.37

Table A.24 Saturation coefficient of the vesicular basalt samples

Sample No	Water abs. by weight (under atm. pres.)	Water abs. by weight (under vacuum pres.)	Saturation Coefficient
	(%) (1)	(%) (2)	(S) (1)/(2)
1V-1	2.01	4.63	0.44
1V-2	1.82	3.24	0.56
1V-3	2.07	4.24	0.49
1V-4	2.26	3.85	0.59
1V-5	1.79	3.31	0.54
1V-6	1.76	3.64	0.48
1V-7	1.85	3.34	0.56
1V-8	1.94	3.71	0.52
1V-9	1.82	3.71	0.49
1V-10	2.13	4.12	0.52
1V-11	1.93	3.23	0.60
1V-12	1.94	4.68	0.41
1V-13	1.62	3.62	0.45
1V-14	1.88	5.08	0.37
1V-15	1.90	4.02	0.47
1V-16	1.75	3.25	0.54
1V-17	1.65	3.16	0.52
1V-18	1.81	3.79	0.48
1V-19	1.76	4.22	0.42
1V-20	1.63	3.49	0.47
1V-21	1.74	3.57	0.49
1V-22	1.78	4.35	0.41
1V-23	1.95	4.90	0.40
1V-24	1.70	4.01	0.42
1V-25	1.87	4.86	0.39
1V-26	1.56	3.47	0.45
1V-27	1.59	3.75	0.42
1V-28	1.74	4.00	0.43
1V-29	1.70	3.62	0.47
1V-30	1.54	3.41	0.45
1V-31	2.07	3.34	0.62
1V-32	1.53	3.51	0.44
1V-33	2.04	4.24	0.48
1V-34	1.62	3.47	0.47

Table A.24 (continued)

Sample No	Water abs. by weight (under atm. pres.)	Water abs. by weight (under vacuum pres.)	Saturation Coefficient
	(%) (1)	(%) (2)	(S) (1)/(2)
1V-35	1.61	4.01	0.40
1V-36	1.93	4.34	0.44
1V-37	1.47	3.24	0.45
1V-38	1.62	3.86	0.42
1V-39	1.90	3.92	0.49
1V-40	1.64	3.30	0.50
1V-41	1.55	3.55	0.44
1V-42	1.81	4.16	0.43
1V-43	1.77	4.53	0.39
3V-1	2.55	3.87	0.66
3V-2	2.20	4.77	0.46
3V-3	2.29	3.77	0.61
3V-4	2.18	4.23	0.52
3V-5	2.55	5.61	0.45
3V-6	3.01	4.11	0.73
3V-7	2.06	4.31	0.48
3V-8	2.19	5.18	0.42
3V-9	2.14	4.25	0.50
3V-10	2.33	3.95	0.59
3V-11	2.35	4.85	0.48
3V-12	2.33	4.26	0.55
3V-13	2.64	4.44	0.59
3V-14	2.68	3.76	0.71
3V-15	2.44	4.05	0.60
3V-16	2.04	4.44	0.46
3V-17	2.38	4.44	0.54
3V-18	3.11	4.23	0.74
3V-19	2.30	4.07	0.57
3V-20	2.60	5.00	0.52
3V-21	2.99	4.23	0.71
3V-22	2.37	4.24	0.56
3V-23	2.55	4.44	0.57
3V-24	2.33	3.80	0.61
3V-25	2.41	4.33	0.56

Table A.24 (continued)

Sample No	Water abs. by weight (under atm. pres.)	Water abs. by weight (under vacuum pres.)	Saturation Coefficient
	(%) (1)	(%) (2)	(S) (1)/(2)
3V-26	2.13	3.96	0.54
3V-27	2.47	4.89	0.51
3V-28	2.52	4.39	0.57
3V-29	2.36	4.33	0.54
3V-30	2.22	4.78	0.46
3V-31	2.20	4.70	0.47
3V-32	2.63	3.96	0.66
3V-33	2.71	4.49	0.60
3V-34	2.55	4.38	0.58
3V-35	2.34	4.19	0.56
3V-36	2.59	4.81	0.54
3V-37	3.07	4.95	0.62
3V-38	2.71	5.66	0.48
3V-39	2.72	4.31	0.63
3V-40	2.46	4.31	0.57
3V-41	2.38	5.12	0.46
3V-42	2.29	4.59	0.50
3V-43	1.91	3.82	0.50
5V-1	2.64	4.49	0.59
5V-2	2.58	5.00	0.52
5V-3	2.23	4.33	0.51
5V-4	0.58	5.23	0.11
5V-5	2.53	4.79	0.53
5V-6	2.73	4.62	0.59
5V-7	3.04	5.51	0.55
5V-8	2.33	4.56	0.51
5V-9	2.22	4.04	0.55
5V-10	2.76	4.38	0.63
5V-11	2.15	4.25	0.51
5V-12	3.07	5.23	0.59
5V-13	3.30	5.76	0.57
5V-14	2.06	4.12	0.50
5V-15	2.72	5.06	0.54
5V-16	3.40	4.85	0.70

Table A.24 (continued)

Sample No	Water abs. by weight (under atm. pres.) (%) (1)	Water abs. by weight (under vacuum pres.) (%) (2)	Saturation Coefficient (S) (1)/(2)
5V-17	2.67	4.72	0.56
5V-18	2.50	4.22	0.59
5V-19	2.66	4.01	0.66
5V-20	2.25	4.07	0.55
5V-21	2.71	4.39	0.62
5V-22	2.73	5.24	0.52
5V-23	2.78	4.69	0.59
5V-24	3.42	5.56	0.62
5V-25	2.96	5.67	0.52
5V-26	2.63	4.05	0.65
5V-27	3.29	5.39	0.61
5V-28	2.29	4.74	0.48
5V-29	2.75	5.16	0.53
5V-30	2.47	4.78	0.52
5V-31	3.15	5.81	0.54
5V-32	2.53	4.80	0.53
5V-33	2.83	4.58	0.62
5V-34	2.95	5.07	0.58
5V-35	2.26	4.22	0.54
5V-36	2.34	4.60	0.51
5V-37	2.92	4.68	0.62
5V-38	2.39	4.44	0.54
5V-39	2.23	4.25	0.52
5V-40	2.75	4.58	0.60
5V-41	2.66	4.55	0.58
5V-42	3.20	5.79	0.55
5V-43	2.37	4.23	0.56
5V-44	3.53	5.37	0.66